



January 2017

# Optimal Control Of Induction Machines To Minimize Transient Energy Losses

Siby Jose Plathottam

Follow this and additional works at: <https://commons.und.edu/theses>

---

## Recommended Citation

Plathottam, Siby Jose, "Optimal Control Of Induction Machines To Minimize Transient Energy Losses" (2017). *Theses and Dissertations*. 2313.

<https://commons.und.edu/theses/2313>

This Dissertation is brought to you for free and open access by the Theses, Dissertations, and Senior Projects at UND Scholarly Commons. It has been accepted for inclusion in Theses and Dissertations by an authorized administrator of UND Scholarly Commons. For more information, please contact [zeinebyousif@library.und.edu](mailto:zeinebyousif@library.und.edu).

OPTIMAL CONTROL OF INDUCTION MACHINES TO MINIMIZE TRANSIENT  
ENERGY LOSSES

by

Siby Jose Plathottam

Bachelor of Technology, Mahatma Gandhi University, 2007

Master of Technology, National Institute of Technology Calicut, 2011

A Dissertation

Submitted to the Graduate Faculty

of the

University of North Dakota

in partial fulfillment of the requirements

for the degree of

Doctor of Philosophy

Grand Forks, North Dakota

December

2017

Copyright 2017 Siby Jose Plathottam

This dissertation, submitted by Siby Jose Plathottam in partial fulfillment of the requirements for the Degree of Doctor of Philosophy from the University of North Dakota, has been read by the Faculty Advisory Committee under whom the work has been done and is hereby approved.

---

Hossein Salehfar, Chairperson

---

Prakash Ranganathan, Committee Member

---

John Collings, Committee Member

---

Marcellin Zahui, Committee Member

---

Mohammed Khavanin, Member at Large

This dissertation is being submitted by the appointed advisory committee as having met all of the requirements of the School of Graduate Studies at the University of North Dakota and is hereby approved.

---

Grant McGimpsey

Dean of the School of Graduate Studies

## PERMISSION

Title           Optimal Control of Induction Machines to Minimize Transient Energy Losses  
Department   Electrical Engineering  
Degree         Doctor of Philosophy

In presenting this dissertation in partial fulfillment of the requirements for a graduate degree from the University of North Dakota, I agree that the library of this University shall make it freely available for inspection. I further agree that permission for extensive copying for scholarly purposes may be granted by the professor who supervised my dissertation work or, in his absence, by the Chairperson of the department or the dean of the School of Graduate Studies. It is understood that any copying or publication or other use of this dissertation or part thereof for financial gain shall not be allowed without my written permission. It is also understood that due recognition shall be given to me and to the University of North Dakota in any scholarly use which may be made of any material in my dissertation.

Siby Jose Plathottam

8<sup>th</sup> November 2017

## TABLE OF CONTENTS

LIST OF FIGURES.....	ix
LIST OF TABLES.....	xiii
ABBREVIATIONS.....	xiv
SYMBOLS.....	xv
ACKNOWLEDGMENTS.....	xvi
ABSTRACT.....	xvii
CHAPTER	
1 INTRODUCTION.....	1
1.1 Key Ingredients in dynamic optimization problems .....	3
1.2 Statement of the Problem .....	4
1.3 Organization of the manuscript.....	4
1.4 Summary .....	5
2 INTRODUCTION TO OPTIMAL CONTROL AND PONTRYAGIN'S MINIMUM PRINCIPLE.....	7
2.1 Dynamic Optimization .....	7
2.2 Optimal Control.....	8
2.3 Pontryagin's Minimum Principle.....	9
2.4 Summary .....	11
3 ELECTROMECHANICAL ENERGY CONVERSION .....	13
3.1 Features of Electric Machines .....	13
3.2 Energy efficiency in electric machines .....	16
3.3 Maximizing Energy Efficiency .....	17
3.4 Importance of Transient Energy Efficiency in Induction Machines .....	18
3.5 Summary .....	19
4 INDUCTION MACHINES.....	20
4.1 Induction Machine Operation.....	20
4.2 Induction Machine Drives.....	23
4.3 Induction Machine Power Flow and Power/Energy Losses.....	24
4.4 Induction Machine Dynamics .....	28
4.5 Mathematical Modelling of Induction Machines .....	31

4.6	Current Fed Model of The Induction Machine .....	33
4.7	Detailed Problem Statement.....	35
4.8	Summary .....	35
5	LITERATURE SURVEY .....	36
5.1	History of Optimal Control .....	36
5.2	Literature on transient energy loss minimization in IM's .....	38
5.3	Contributions of this Dissertation .....	45
5.4	Summary .....	46
6	OPTIMAL CONTROL OF DC MOTOR .....	47
6.1	PMDC Motor Model and Cost Functional.....	47
6.2	Necessary Conditions using Pontryagin's Minimum Principle .....	48
6.3	Summary .....	50
7	NECESSARY CONDITIONS FOR OPTIMAL CONTROL IN INDUCTION MACHINE .....	51
7.1	Rotor Field Oriented IM Model .....	51
7.2	Analysis of the IM Model .....	52
7.2.1	Regime I.....	55
7.2.2	Regime II .....	56
7.2.3	Regime III .....	56
7.2.4	Rotor speed corresponding to Regime I and Regime II.....	57
7.3	Energy Loss Functions .....	57
7.3.1	Power loss in terms of rotor d-axis flux at steady state .....	58
7.3.2	Mechanical Power output .....	59
7.4	Optimal Flux at Steady State.....	59
7.5	Cost Functional .....	61
7.5.1	Reasoning behind setting terminal values of flux, rotor speed, and torque .....	62
7.6	Deriving the necessary conditions for optimal control .....	63
7.7	Summary .....	65
8	NUMERICAL SOLUTION OF INDUCTION MACHINE OPTIMAL CONTROL PROBLEM .....	67
8.1	Modified Conjugate Gradient Method .....	67
8.2	Numerical Solution Example – Scenario 1 .....	71
8.2.1	Scenario 1 - Optimal .....	71
8.2.2	Scenario 1 - Baseline .....	81
8.2.3	Comparison of the optimal trajectories vs Regime I trajectories.....	87

8.2.4	Comparing energy efficiency for optimal and Regime I in scenario 1 .....	88
8.3	Numerical Solution - Scenario 2 .....	89
8.3.1	Scenario 2 - Optimal .....	89
8.3.2	Scenario 2 - Baseline .....	95
8.3.3	Comparison of the optimal trajectories vs Regime I trajectories.....	98
8.3.4	Comparing Energy Efficiencies .....	98
8.4	Summary .....	99
9	ANALYTICAL EXPRESSIONS FOR IM OPTIMAL CONTROL TRAJECTORIES .....	101
9.1	Prototype Expression for Optimal Rotor d-axis Flux.....	102
9.1.1	Regime I rotor flux trajectory expression .....	103
9.1.2	Expressing the conic polynomial trajectory in terms of rotor flux values	103
9.2	Prototype expression for Optimal Stator q-axis Current.....	104
9.2.1	Regime I q-axis current trajectory .....	105
9.2.2	Expressing conic trajectory parameters in terms of stator d-axis current.	105
9.3	Assumptions to Prove Optimality .....	106
9.4	Energy Costs and Rotor Angle Displacement for Regime I Trajectories .....	109
9.5	Expressions for Optimal Rotor Flux, Current, and Transient Energy Loss .....	110
9.6	Stator q-axis Current and Transient Energy Losses for Trajectory A.....	111
9.7	Stator q-axis Current Energy Loss for Trajectory B .....	113
9.8	Determining the Optimal Flux ratio $x$ .....	114
9.9	Evaluating Improvement in Energy Efficiency using Analytical expressions.	118
9.10	Sensitivity of Energy Efficiency to Parameters .....	122
9.11	Practicality of using Analytical Expressions in Real-Time Control .....	126
9.12	Summary .....	127
10	EMULATING OPTIMAL CONTROL OF IM USING ARTIFICIAL NEURAL NETWORKS.....	128
10.1	Neural Network Basics.....	128
10.2	Using Neural Networks as Controllers.....	131
10.3	Training the ANN to Emulate Optimal Control Trajectories.....	133
10.4	Incorporating ANN into an IM drive control system.....	138
10.5	Performance of the ANN Optimal Control .....	141
10.6	Summary .....	144
11	REAL-TIME SIMULATION RESULTS USING ANN OPTIMAL CONTROL SYSTEM AND FINITE ELEMENT MODEL OF IM.....	145



11.1	Experimental Results for IM Field-oriented Control (FOC).....	145
11.2	ANN controller deployed on real-time controller hardware .....	149
11.3	IM Finite Element Model and Co-simulation using Simulink and Maxwell... ..	149
11.4	Results .....	151
11.5	Summary on Comparing Performances for the Drive Cycle .....	156
11.6	Summary .....	157
12	CONCLUSION AND FURTHER WORK.....	158
12.1	Further work.....	159
	REFERENCES .....	160
	APPENDICES.....	165

## LIST OF FIGURES

Figure 2.1. Visualizaing the minimum principle .....	10
Figure 4.1. Induction machine cross sectional diagram.....	21
Figure 4.2. IM Electric Drive Schematic .....	24
Figure 4.3. Power flows in an induction machine .....	25
Figure 4.4. Relative magnitude of Power flows in an induction machine .....	25
Figure 4.5. Transients in input phase voltage waveforms of an induction machine.....	29
Figure 4.6. Transients and steady states in rotor speed of IM corresponding to voltage transients .....	30
Figure 4.7. Transients & steady states in energy input to IM corresponding to voltage transients .....	30
Figure 4.8. Visualizing change in reference frame .....	31
Figure 4.9. Concept of Current Fed IM Model .....	34
Figure 5.1. Relationship between optimal control and other technical areas .....	36
Figure 5.2. Optimal Control through history .....	37
Figure 5.3. Dynamic optimization in Induction Machines Literature .....	39
Figure 5.4. Dynamic optimization in Induction Machines in Literature .....	43
Figure 5.5. Different techniques used to generate the optimal control trajectories of IM .....	43
Figure 8.1. Applying the modified CG algorithm to find numerical solution of optimal trajectories.....	70
Figure 8.2. Trajectory for rotor d-axis flux (Scenario 1- optimal).....	73
Figure 8.3. Trajectory for rotor speed (Scenario 1 - optimal).....	73
Figure 8.4. Trajectory for q-axis current (Scenario 1- optimal). .....	74
Figure 8.5. Trajectory for d-axis current (Scenario 1- optimal). .....	74
Figure 8.6. Trajectory of co-state 1 (Scenario 1 - optimal). .....	75
Figure 8.7. Trajectory of co-state 2 (Scenario 1 - optimal). .....	75
Figure 8.8. Electromagnetic torque trajectory (Scenario 1 - optimal). .....	76
Figure 8.9. Mechanical power corresponding to the rotor speed and torque trajectories (Scenario 1 -optimal). .....	76
Figure 8.10. Hamiltonian function value during transient (Scenario 1 - optimal).....	77
Figure 8.11. Stator Ohmic power losses in IM (Scenario 1 - optimal).....	78

Figure 8.12. Rotor Ohmic power losses in IM (Scenario 1 - optimal). .....	78
Figure 8.13. Stator core power losses in IM (Scenario 1 - optimal). .....	79
Figure 8.14. Total power losses in IM (Scenario 1 - optimal). .....	79
Figure 8.15. Change in the value of the energy loss cost function over iterations (Scenario 1 - optimal). .....	80
Figure 8.16. Change in the value of the gradient norm over iterations (Scenario 1 – optimal) .....	80
Figure 8.17. Trajectory of rotor d-axis flux (Scenario 1 – baseline) .....	82
Figure 8.18. Trajectory of rotor speed (Scenario 1 – baseline) .....	82
Figure 8.19. Trajectory of stator q-axis current (Scenario 1 – baseline). .....	83
Figure 8.20. Trajectory of stator d-axis current (Scenario 1 – baseline). .....	83
Figure 8.21. Electromagnetic torque produced during transient (Scenario 1 – baseline). .....	84
Figure 8.22. Mechanical power produced during transient (Scenario 1 - baseline). .....	84
Figure 8.23. Hamiltonian function value (Scenario 1 - baseline). .....	85
Figure 8.24. Stator Ohmic power losses in IM (Scenario 1 - baseline). .....	85
Figure 8.25. Rotor Ohmic power losses in IM (Scenario 1 -baseline). .....	86
Figure 8.26. Core power losses in IM (Scenario 1 -baseline). .....	86
Figure 8.27. Total power losses in IM (Scenario 1 -base case) .....	87
Figure 8.28. Trajectory for rotor d-axis flux (Scenario 2 - optimal).....	90
Figure 8.29. Trajectory for rotor speed (Scenario 2 - optimal).....	90
Figure 8.30. Trajectory for q-axis current (Scenario 2- optimal). .....	91
Figure 8.31. Trajectory for d-axis current (Scenario 2- optimal). .....	91
Figure 8.32. Electromagnetic torque trajectory (Scenario 2 - optimal) .....	92
Figure 8.33. Mechanical power corresponding to rotor speed and torque trajectory (Scenario 1 - optimal). .....	92
Figure 8.34. Total power losses in IM (Scenario 2 - optimal). .....	93
Figure 8.35. Change in value of energy loss cost function over iterations (Scenario 2 - optimal) .....	94
Figure 8.36. Change in value of gradient norm over iterations (Scenario 2 - optimal) ....	94
Figure 8.37. Trajectory of d-axis rotor flux (Scenario 2 – baseline) .....	95
Figure 8.38. Trajectory of rotor speed (Scenario 2 – baseline) .....	96
Figure 8.39. Trajectory of electromagnetic torque (Scenario 2 – baseline).....	96
Figure 8.40. Mechanical power produced during transient (Scenario 2 - baseline). .....	97
Figure 8.41. Total power losses in IM (Scenario 2 - baseline) .....	97
Figure 9.1. Illustration of flux trajectories for baseline (Regime 1) and optimal .....	104

Figure 9.2. Illustrating stator q-axis current for baseline (Regime 1) and optimal.....	106
Figure 9.3. Sensitivity of optimal ratio $x$ to the initial flux and moment of inertia.....	116
Figure 9.4. Sensitivity of optimal $x$ to the initial flux and change in speed .....	117
Figure 9.5. Sensitivity of optimal $x$ to the initial flux and rotor time constant.....	117
Figure 9.6. Comparison of rotor d-axis flux trajectories .....	119
Figure 9.7. Comparison of rotor speed trajectories.....	120
Figure 9.8. Comparison of electromagnetic torque trajectories.....	120
Figure 9.9. Comparison of power losses.....	121
Figure 9.10. Sensitivity of transient energy efficiency to initial flux, and change in rotor speed .....	123
Figure 9.11. Sensitivity of energy efficiency to initial rotor flux and moment of inertia.....	124
Figure 9.12. Sensitivity of energy efficiency to initial rotor flux and rotor time constant .....	125
Figure 10.1. Structure of an Artificial Neuron.....	129
Figure 10.2. Neurons arranged in layers to create a neural network .....	130
Figure 10.3. Template training an ANN as a controller .....	132
Figure 10.4. Operations in the ANN emulating the IM optimal control solution.....	134
Figure 10.5. TensorFlow computational graph implementing the ANN of the IM Optimal control problem.....	136
Figure 10.6. Change in the mean square error of training and validation data set during ANN training using Levenberg-Marquardt algorithm in MATLAB .....	137
Figure 10.7. Change in the mean square error of training and validation data set during training using ADAM algorithm in TensorFlow .....	137
Figure 10.8. Template trained ANN block as a part of the IM drive control system .....	139
Figure 10.9. Supervisory logic to implement the ANN based IM optimal controller ....	140
Figure 10.10. ANN output emulating solution of IM optimal control problem .....	142
Figure 10.11. Input from supervisory logic to ANN during real time simulation. ....	143
Figure 10.12. Output from ANN during real- time simulation.....	143
Figure 11.1. IM experimental hardware setup .....	145
Figure 11.2. IM, 3ph Inverter, and connector hardware .....	146
Figure 11.3. dSPACE controller board and ControlDesk UI.....	146
Figure 11.4. Speed and power input. ....	147
Figure 11.5. Rotor flux and d-axis current corresponding to change in rotor speed. ....	147
Figure 11.6. Change in rotor flux for change in d-axis current. ....	148
Figure 11.7. Quarter section of IM FEM model simulated in ANSYS Maxwell .....	150
Figure 11.8. Co-simulation using Simulink, ANSYS SImplorer, and Maxwell.....	151

Figure 11.9. IM rotor speed profile corresponding to drive cycle. ....	153
Figure 11.10. IM electromagnetic torque trajectories for given drive cycle .....	153
Figure 11.11. IM rotor d-axis flux trajectories for given drive cycle .....	154
Figure 11.12. Comparing measured stator d-axis current for drive cycle .....	154
Figure 11.13. Comparing stator q-axis current for drive cycle.....	155
Figure 11.14. Comparing IM energy losses during drive cycle.....	156
Figure 11.15. Comparing mechanical energy output at shaft during drive cycle. ....	156

## LIST OF TABLES

Table 3.1. Comparison of electric machine types.....	14
Table 3.2 Potential energy savings in Tesla EV's.....	19
Table 5.1. Comparing literature on transient energy loss minimization in induction machines .....	44
Table 6.1. Comparing optimal control and non-optimal control in PMDC Motor.....	50
Table 8.1. Scenarios for testing IM optimal control problem using Type I IM.....	72
Table 8.2. Comparing total energy cost for scenario 1 .....	88
Table 8.3. Scenarios for testing IM optimal control problem using Type II IM .....	89
Table 8.4. Comparing total energy cost for scenario 2 .....	98
Table 9.1. Optimal x for different scenarios. ....	119
Table 9.2. Comparing energy efficiency for optimal and Regime I (baseline) cases. ....	122
Table 10.1. Selecting input-output features for ANN to emulate the optimal control trajectory. ....	134
Table 11.1. Comparing performance parameters over the drive cycles for all regimes .	157

## ABBREVIATIONS

OC: Optimal Control  
AC: Alternating Current  
DC: Direct Current  
IM: Induction Machine/Motor  
SQIM: Squirrel Cage Induction Machine/Motor  
PMDC: Permanent Magnet Direct Current  
FO: Field Oriented  
FOC: Field Oriented Control  
ODE: Ordinary Differential Equation  
q-axis: Quadrature Axis  
d-axis: Direct Axis  
TPBVP: Two Point Boundary Value Problem  
CG: Conjugate Gradient  
ANN: Artificial Neural Network  
FOC: Field Oriented Control  
PID: Proportional-Integral-Derivative  
AI: Artificial Intelligence  
ANN: Artificial Neural Network  
FE: Finite Element

## SYMBOLS

$N_r, \omega_r$ : Rotor speed in electrical radians/s

$N_s$ : Synchronous speed in rotations per minute

$T_e$ : Electromagnetic torque/moment (Nm)

$T_L$ : Load torque/moment (Nm)

$R_s$ : Stator winding resistance (ohm)

$R_r$ : Rotor winding resistance (ohm)

$L_{lr}$ : Stator leakage inductance (H)

$L_{ls}$ : Rotor leakage inductance (H)

$L_m$ : Mutual inductance (H)

$p$ : Number of poles in stator

$V, v$ : Voltage (V)

$i$ : Current (A)

$i_{qs}$ : Stator q-axis current (A)

$i_{ds}$ : Stator d-axis current (A)

$\Psi$ : Magnetic flux (Wb)

$\Psi_{dr}$ : Rotor d-axis magnetic flux (A)

$\lambda$ : Co-state in Hamiltonian function

$x$ : Ratio of rotor flux value at vertex of conic section to initial rotor flux value



## ACKNOWLEDGEMENTS

I want to thank God for the blessings showered upon me during the last four years. I want to thank my mother and father whose love, support, and prayers that allowed me to reach where I am today. I would like to especially thank my advisor Dr. Hossein Salehfar for guidance, feedback, and freedom he provided while pursuing my research. I would also like to thank Dr. Prakash Ranganathan for his feedback and opportunities he provided for collaborative research. Special thanks to Dr. John Collings for the insightful questions on the research work. I would also like to thank the committee members Dr. Marcellin Zahui and Dr. Mohammed Khavanin for their feedback during the presentations. I am grateful for the opportunity and financial support provided to me by the Electrical Engineering Department during my Ph.D. program. I also take this opportunity to acknowledge the financial support received from ND EPSCoR and NSF through the 2015-17 Doctoral Dissertation Award. I want to thank the Dr. John Mihelich, Department Chair and Dr. Sima Noghianian, Graduate Program Director along with the previous faculty who occupied these positions for their support during my degree program. Finally, I want to thank my wife Rosy, for the love and understanding she gave me without which I couldn't have completed my dissertation.

To my grandmother Ethamma George,  
I wouldn't be what I am without your love and sacrifice!

## ABSTRACT

Induction machines are electromechanical energy conversion devices comprised of a stator and a rotor. Torque is generated due to the interaction between the rotating magnetic field from the stator, and the current induced in the rotor conductors. Their speed and torque output can be precisely controlled by manipulating the magnitude, frequency, and phase of the three input sinusoidal voltage waveforms. Their ruggedness, low cost, and high efficiency have made them ubiquitous component of nearly every industrial application. Thus, even a small improvement in their energy efficient tend to give a large amount of electrical energy savings over the lifetime of the machine. Hence, increasing energy efficiency (reducing energy losses) in induction machines is a constrained optimization problem that has attracted attention from researchers.

The energy conversion efficiency of induction machines depends on both the speed-torque operating point, as well as the input voltage waveform. It also depends on whether the machine is in the transient or steady state. Maximizing energy efficiency during steady state is a Static Optimization problem, that has been extensively studied, with commercial solutions available. On the other hand, improving energy efficiency during transients is a Dynamic Optimization problem that is sparsely studied. This dissertation exclusively focuses on improving energy efficiency during transients.

This dissertation treats the transient energy loss minimization problem as an optimal control problem which consists of a dynamic model of the machine, and a cost functional.

The rotor field oriented current fed model of the induction machine is selected as the dynamic model. The rotor speed and rotor d-axis flux are the state variables in the dynamic model. The stator currents referred to as d-and q-axis currents are the control inputs. A cost functional is proposed that assigns a cost to both the energy losses in the induction machine, as well as the deviations from desired speed-torque-magnetic flux setpoints. Using Pontryagin's minimum principle, a set of necessary conditions that must be satisfied by the optimal control trajectories are derived. The conditions are in the form a two-point boundary value problem, that can be solved numerically. The conjugate gradient method that was modified using the Hestenes-Stiefel formula was used to obtain the numerical solution of both the control and state trajectories.

Using the distinctive shape of the numerical trajectories as inspiration, analytical expressions were derived for the state, and control trajectories. It was shown that the trajectory could be fully described by finding the solution of a one-dimensional optimization problem. The sensitivity of both the optimal trajectory and the optimal energy efficiency to different induction machine parameters were analyzed.

A non-iterative solution that can use feedback for generating optimal control trajectories in real time was explored. It was found that an artificial neural network could be trained using the numerical solutions and made to emulate the optimal control trajectories with a high degree of accuracy. Hence a neural network along with a supervisory logic was implemented and used in a real-time simulation to control the Finite Element Method model of the induction machine. The results were compared with three other control regimes and the optimal control system was found to have the highest energy efficiency for the same drive cycle.

## 1 INTRODUCTION

“For since the fabric of the universe is most perfect and the work of a most wise Creator, nothing at all takes place in the universe in which some rule of maximum or minimum does not appear.” Leonhard Euler.

The concept that Euler tries to convey through this quote, made nearly 300 years ago, hasn't lost any of its relevance. In Engineering, we find the application of this concept when finding ways to improve upon existing systems so that a performance goal is maximized or minimized. The procedure and method by which the extremum of a performance goal is found may be broadly classified under the term 'Optimization'. It is also known as 'Operations Research' in the field of management. Engineering optimization problems can be broadly divided into two categories:

a) System design is optimized:

Here the system being built is optimized so that a performance goal is minimized (or maximized). The solutions for these types of problems are in the form of scalar values.

A few examples are:

- 1) An electric motor may be designed to give the maximum torque for a given input voltage.
- 2) Designing a Proportional-Integral-Derivative (PID) controller used in a process control loop to minimize the system settling time.

The problem discussed in this dissertation does not belong to this category.

b) System operation is optimized:

Here we take an existing system and modify its operation to minimize (or maximize) some performance goal. This class of problems may be separated into two, depending upon whether the system is in a steady state or in a transient state.

In steady state optimization problems, the solutions are only applicable when the system has reached steady state. The solutions are in the form of a scalar value or an algebraic relationship. A few examples are:

- 1) Finding the right combination of pressure and temperature that would maximize the yield of a desirable product in a chemical reactor.
- 2) Finding electric current required by the motors in a heating, ventilation, and air-conditioning (HVAC) system to maintain the desired air flow and maximize energy efficiency.

The problem addressed in this dissertation does not belong to the category of steady state optimization problems.

There exists a niche of engineering problems where optimization cannot wait for the steady state. This is either because the system spends much of its operating time in transient states or because optimization cannot ignore the transient conditions of the system. These problems may be broadly called Dynamic Optimization Problems. The solutions are in the form of a function with respect to (w.r.t.) time (or some other continuous variable) or vector containing values specific to a time instant. A few examples are:

- 1) Finding the optimal thrust vector to be supplied by the engines of a jet plane so that it can make a turn in the minimum time.
- 2) Finding optimal thrust vector to be supplied by a space probe in interplanetary missions to minimize fuel consumption.
- 3) Finding the optimal route to be taken by a traveling salesman.

The engineering problem addressed in this dissertation is a dynamic optimization problem.

### 1.1 Key Ingredients in dynamic optimization problems

The solution of any engineering optimization problem involves three key ingredients, namely:

1. system model,
2. cost function, and
3. optimization algorithm.

The cost function, also referred to as the objective function, gives a scalar value which provides a means to compare how much the system has improved against a baseline. In the dynamic optimization problem of this dissertation, we use a cost functional, i.e., a function of a function which still provides a scalar value. In this dissertation, the cost functional measures the energy losses in an induction machine.

The solution to engineering optimization problems are intimately linked with key features of the system being optimized. A system model defines the relationship between its constituent variables and parameters. In static optimization problems, a system of algebraic equations may be enough to properly define the model. However, in dynamic

optimization problems the changes w.r.t. time must be considered, and hence the model is usually defined by a system of ordinary differential equations. In this work, the system model is based on that of a current fed induction machine.

Once the system model and the cost function are determined, solving the problem requires an optimization algorithm. The same optimization problem may be solved by different optimization algorithms, i.e. optimization algorithms are not problem specific. However, some algorithms may perform better than others for specific problems. Many optimization algorithms have been developed through modification of certain core concepts. In case of dynamic optimization problems, optimization algorithms may be classified under either calculus of variations or optimal control theory.

## 1.2 Statement of the Problem

The main objective of this dissertation is to develop a control law to minimize energy losses in an induction machine during transients. This is a sparsely researched topic, compared to the problem of minimizing energy losses during steady-state operation. For this purpose, Pontryagin's minimum principle from optimal control theory, and a modified conjugate gradient algorithm are used to obtain a numerical solution to the problem under study. An analytical closed-form solution is proposed based on observations from the numerical solution. Finally, Neural Networks are used to generate the optimal solution to the problem in a real-time scenario.

## 1.3 Organization of the manuscript

Since this manuscript explores several concepts from multiple technical fields, the first three chapters provide a brief background on each. An introduction to the optimal control method to be used is given in Chapter 2. The importance of electromechanical energy



conversion efficiency, as a performance index, is discussed in Chapter 3. Mathematical models of induction machines, as well as the various energy losses within those machines, are presented and discussed in Chapter 4. A literature survey is provided in Chapter 5 that collates all the related research over the past 40 years for the problem being investigated in this dissertation. Chapter 6 solves the optimal control problem for a DC motor which is a simplified version of the main optimization problem being investigated for AC induction motors. Chapter 7 defines the optimal control problem for induction machines and derives the necessary conditions for optimal control using Pontryagin's minimum principle. Chapter 8 presents the numerical solution of the necessary conditions (from the previous chapter) using the modified conjugate gradient optimization algorithm. Solutions for two types of induction machines for different operating conditions are presented. Chapter 9 derives analytical expressions for the optimal control law, state trajectories, and the energy losses due to them which is applicable for any induction machine. Chapter 10 presents the concept of using of neural networks in generating the optimal control trajectories for an accelerating induction machine in a real-time environment. Using the control system developed in Chapter 10, Chapter 11 presents the real-time optimization simulation results using a Finite Element Model (FEM). And finally, Chapter 12 provides conclusions and some suggestions for future work.

#### 1.4 Summary

This chapter introduced the general concept of dynamic optimization problems from the point of view of an engineering optimization problem. A few examples were provided to differentiate static and dynamic optimization problems. The list of all key concepts that will be utilized in this dissertation was presented. The statement of the problem under

investigation was provided to give a broad overview of the content of this dissertation document. Finally, a one-line overview of each of the succeeding chapters was provided.

## 2 INTRODUCTION TO OPTIMAL CONTROL AND PONTRYAGIN'S MINIMUM PRINCIPLE

Dynamic optimization is fundamentally an applied mathematical problem. Hence, a background on some of the fundamental concepts of optimal control theory that have been used in this work are provided in this chapter. A significant amount of literature exists on optimal control theory with a varying degree of mathematical complexity. But [1] and [2] provide excellent relevant references with some practical examples.

### 2.1 Dynamic Optimization

A Dynamic optimization problem for a continuous system may be defined as follows. If we have a dynamic system defined by the ordinary differential state equation,

$$\dot{x} = g(x, t) \tag{2.1.1}$$

and a cost functional,

$$J = \int_{t_0}^{t_f} f(x(t), t) dt \tag{2.1.2}$$

where, depending on the system being modelled,  $x(t)$  may represent a single state variable or a system of state variables. In (2.1.2)  $t_f$  and  $t_0$  are the start and the end points of a horizon in time during which we are interested in optimizing the given dynamic system.  $J$  represents the total energy cost incurred by the IM over the time horizon of interest. It is called a cost functional (instead of a cost function), because it the function of a function.  $f(x(t), t)$  represents the cost value at a single time instant in the horizon of interest. A

Dynamic optimization method requires one to find an optimal state trajectory  $x^*(t)$  such that:

$$J_{\min} = \int_{t_0}^{t_f} f(x^*(t), t) dt \quad (2.1.3)$$

In other words, one needs to find a function describing  $x^*(t)$  during the time horizon  $t_0$  to  $t_f$ , that minimizes (or maximizes) the cost functional  $J$ . The mathematical technique that provides a means to find  $x^*(t)$  is called Calculus of Variations.

## 2.2 Optimal Control

It must be noted that dynamic optimization only tells us what the optimal state trajectory looks like. It does not tell us how to cause the state variable follow this optimal trajectory. To gain insight into this issue, one must consider the fact that change in the state variables of a dynamic system need not be dependent only on the current state of the system. The system can be influenced in two ways: a) The parameters of the system change, b) Disturbances may enter the system from outside. The disturbances affecting the system may be controllable or uncontrollable. The controlled disturbances are referred to as control variables or control inputs and are represented by  $u(t)$ . The state equation in (2.1.1) may then be rewritten as (2.2.1). As stated earlier, a cost is also be assigned to the control trajectory by a cost function or functional. It is also desirable that the state variables in the system attain certain terminal values at the end of the transient time. This can be incorporated into the cost functional using a terminal cost function  $\phi(x(t_f))$ . Hence the cost functional (2.1.2) can be rewritten as (2.2.2).

$$\dot{x} = g(x(t), u(t), t) \quad (2.2.1)$$

$$J = \phi(x(t_f)) + \int_{t_0}^{t_f} f(x(t), u(t), t) dt \quad (2.2.2)$$

If the system is fully controllable, the control variable can manipulate all the state variables. Hence, the problem of finding the optimal state variable  $x^*(t)$  may be converted into a problem of finding the optimal control variable  $u^*(t)$  instead. In other words, we find a trajectory for the control variable  $u^*(t)$  that causes the state variable  $x(t)$  to follow the optimal state trajectory as well as minimize the cost functional. This is known as the optimal control problem.

### 2.3 Pontryagin's Minimum Principle

Pontryagin's minimum principle allows us to derive a set of necessary conditions that must be satisfied by the optimal control variable  $u^*(t)$ . To derive the required necessary conditions, first the state equation (2.2.1) and the cost function inside the integral of (2.2.2) are combined to form what is known as the Hamiltonian function (also called Hamiltonian) as shown in (2.3.1). Note that the terminal constraints are not included in the Hamiltonian directly.

$$H(x, u, \lambda, t) = g(x(t), u(t), t) \lambda(t) + f(x, u, t) \quad (2.3.1)$$

In (2.3.1)  $\lambda$  is called the co-state and each state equation is multiplied by a corresponding co-state  $\lambda$ . According to the minimum principle, for the trajectory of control input  $u(t)$  to be optimum, it must minimize the Hamiltonian for all  $t \in [t_0; t_f]$ . This may be expressed by (2.3.2). A visualization of the how the Hamiltonian for an optimal control differs from that of a non-optimal control is provided using Figure. 2.1.

$$H(x^*(t), u^*(t), \lambda^*(t), t) \leq H(x(t), u(t), \lambda(t), t) \quad (2.3.2)$$

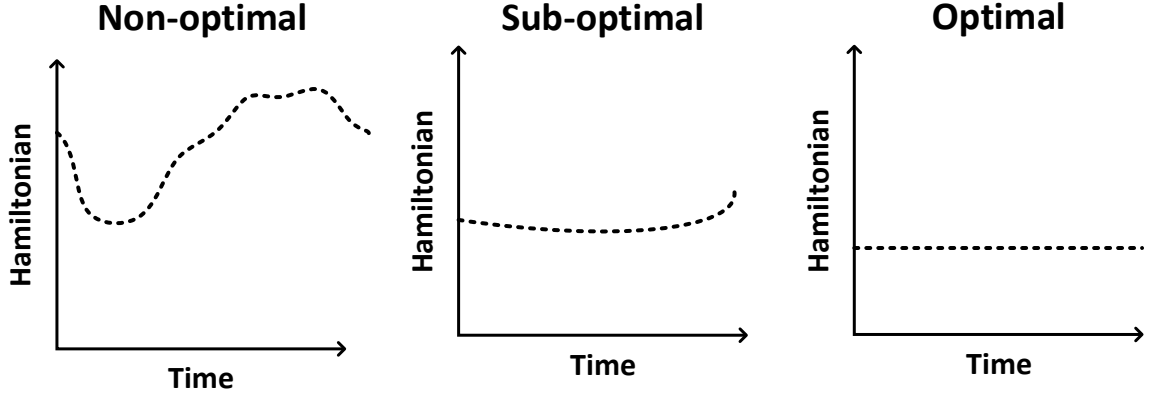


Figure 2.1. Visualizing the minimum principle

The minimum principle given in (2.3.2) is for control inputs  $u(t)$  that have constraints (are bounded). However, this principle can also be applied for unconstrained control inputs. Hence, we have the condition that the partial derivative of the Hamiltonian w.r.t.  $u(t)$  should be equal to zero given by (2.3.3). Also, to guarantee that  $u^*(t)$  indeed minimizes the Hamiltonian, the second variation of the Hamiltonian w.r.t.  $u(t)$  should be greater than zero as shown in (2.3.4).

$$\frac{\partial H(x^*(t), u^*(t), \lambda^*(t), t)}{\partial u} = 0 \quad (2.3.3)$$

$$\frac{\partial^2 H(x^*(t), u^*(t), \lambda^*(t), t)}{\partial u^2} > 0 \quad (2.3.4)$$

In addition to the above optimality condition, the state equation (2.3.5) must also be satisfied. Note that the state equation (2.3.5) would turn out to be the same as the state equation in (2.2.1). The dynamics of the co-state  $\lambda$  can be found through the co-state equation given by (2.3.6).

$$\frac{dx}{dt} = \frac{\partial H(x^*(t), u^*(t), \lambda^*(t), t)}{\partial \lambda} \quad (2.3.5)$$

$$\frac{d\lambda}{dt} = -\frac{\partial H(x^*(t), u^*(t), \lambda^*(t), t)}{\partial x} \quad (2.3.6)$$

The terminal cost function  $\phi(x(t_f))$  can be introduced into the solution process by using the transversality condition to calculate the boundary condition for the co-states  $\lambda$  as given by (2.3.7).

$$\lambda(t_f) = \frac{\partial \phi(x(t_f))}{\partial x} \quad (2.3.7)$$

To reiterate, using the minimum principle of optimal control theory, finding the optimal control  $u^*(t)$  during the time  $t_0$  to  $t_f$  becomes just a problem of finding the corresponding control variable  $u(t)$  that minimizes (or maximizes) the Hamiltonian. For simple systems this may be possible through visual inspection of the Hamiltonian as has been demonstrated in [1]. However, for non-linear multi-state systems solutions based on visual inspection is not a feasible exercise. Only numerical methods can be used in such cases. Finally, an important property of the Hamiltonian that must be kept in mind is as follows. If the Hamiltonian is not an explicit function of time, then its value is constant at all points on the optimal trajectory given by (2.3.8).

$$H(x^*(t), u^*(t), \lambda^*(t)) = c_1 \quad (2.3.8)$$

## 2.4 Summary

This chapter discussed the Dynamic Optimization based on optimal control concepts and how it differs from optimization solutions based on Calculus of variations. A brief

overview of the state equations and cost functional was provided. The use of Optimal Control theory was discussed. Finally, Pontryagin's Minimum Principle and the associated necessary conditions were explained.



### 3 ELECTROMECHANICAL ENERGY CONVERSION

Human society takes for granted its ability to harness and utilize mechanical power from sources other than what is available from our bodies. Whether it be in mundane applications like an automobile or remarkable feat like drilling tunnels under the ocean, this concept has been one of the cornerstones of human civilization. Humanity's first source of mechanical power were domesticated animals, and they continued to be the primary sources of energy until the advent of the steam turbine in the 1<sup>st</sup> half of the 19<sup>th</sup> century. However, it was the concept of electromechanical energy conversion using electric motors and generators (collectively referred to as electric machines) that brought about a paradigm shift. Before the advent of electric machines, mechanical power could only be transmitted using couplings, gears, belts, or fluids (compressed air, oil), limiting the maximum distance between the power source and the application. But electric machines enabled mechanical power to be available on demand with the throw of a switch, with electrical power being supplied through metal conductors. Suffice it to say that electric machines revolutionized human society in unforeseen ways.

#### 3.1 Features of Electric Machines

Electric machines can be broadly divided into two types, namely machines that work on Direct Current (DC), and machines that work on Alternating Current (AC). Within these two types of machines, there are further classifications. However, all electric machines share certain common features irrespective of their type and their widespread acceptability.

The common features are:

- a) Rotary motion: Electric machines produce mechanical power in the form of smooth rotational motion which may be measured in terms of angular velocity, and torque (moment of force). Comparatively, steam engines produce a reciprocating motion which must be converted to a rotary motion through additional components.
- b) High efficiency: The conversion efficiency from electrical energy to mechanical energy and vice versa is usually in the range of 80 to 95% at the rated power of the machine. Comparatively, the maximum efficiency of a diesel engine is only about 35%.
- c) Controllability: By controlling the magnitude and/or the frequency of the electric current of electric machines it is possible to precisely regulate or throttle the speed/torque output of an electric machine.
- d) Ruggedness: There are very few moving parts in an electric machine resulting in less wear and tear, low maintenance, and machine lifetime's exceeding 30 years.

There are significant differences among the electric machines. A graphical overview of different motor types can be found in [3]. Table 3.1 lists the relative differences among the most common types of electric machines, and their common application areas.

*Table 3.1. Comparison of electric machine types.*

Type	Permanent Magnet DC Motor	AC Induction	AC Synchronous	Stepper Motor
Maximum power rating	Medium	High	High	Low
Starting torque capability	High	Medium	Medium	High
Efficiency	Medium	Medium	High	Medium
Maintenance	High	Very Low	Low	Medium

Capital Cost	Low	Low	High	Medium
Operating complexity	Low	Low	Medium	High
Speed control complexity	Low	Medium	Medium	High
Application	Drones, robotics, cooling fans, toys, and engine starters	Industry+ commercial, electric cars, wind turbine generators	Power generation, electric cars, wind turbine generators	Robotics, actuators

Note that there are a few other distinct electric machine types like switched reluctance machine and DC series motor which have not been listed in Table 3.1. It can be noted from Table 3.1 that certain machine types have found a niche in certain applications. One example is the permanent magnet DC motors which are exclusively used in toys and drones, and the stepper motors in robotics. Another important fact that must be pointed out is that two types of electrical machine account for nearly 100 % of the mechanical and electric power generated in the world. All the conventional power generation plants exclusively use AC Synchronous generators. The power ratings of these machines range from a few kilowatts (kW) in case of portable generator sets (gensets) to more than 600 Megawatts (MW) in case of steam turbine generators in electric power plants. Conversely, nearly 70% of the power generated by the AC Synchronous machines are consumed by the AC Induction motors to produce mechanical power in industrial, commercial, and domestic application. They can be found in everything from refrigerators, and air conditioning systems to industrial conveyors, and electric cars.

The design of an optimal control system for the AC Induction machine is the focus of this dissertation report.

### 3.2 Energy efficiency in electric machines

A consequence of the Second law of Thermodynamics is that conversion of energy from one form of energy to another is not 100% efficient. Electro-mechanical energy conversion systems are no exception. A fraction of electrical/mechanical power input is wasted as heat in electric machines. Depending on the measurements available, the energy efficiency of an electric machine may be calculated in two ways. If the electrical machine is motoring, i.e. converting electrical energy into mechanical energy, the efficiency is calculated using (3.2.1) or (3.2.2). In case the machine is generating power, i.e. converting mechanical energy into electrical energy, the energy efficiency may be calculated using (3.2.3) or (3.2.4).

$$\eta_{mot} = \frac{E_{out}^{mech}}{E_{in}^{elect}} \quad (3.2.1)$$

$$\eta_{mot} = \frac{E_{out}}{E_{out} + E_{loss}} \quad (3.2.2)$$

$$\eta_{mot} = \frac{E_{out}^{elect}}{E_{in}^{mech}} \quad (3.2.3)$$

$$\eta_{gen} = \frac{E_{in} - E_{loss}}{E_{in}} \quad (3.2.4)$$

where  $E_{out}$  is the mechanical energy output,  $E_{in}$  is the electrical energy input, and  $E_{loss}$  is the energy losses in the machine over a time interval.

Electro-mechanical energy conversion systems, i.e. electric machines, are considerably more efficient than the thermochemical–mechanical or mechanical–mechanical energy conversion systems. Electric machines outnumber other energy conversion systems, both in quantity and operating time, and hence even small power losses add up over time to

become significant energy losses. Conversely, even a couple of percentage points of improvement in energy efficiency of electric machines can lead to large energy savings over time. Energy efficiency of an electric machine (or any other energy conversion device) is not a static quantity. It is a function of state variables, input variables, and external disturbances related to the machine. Energy efficiency of an electric machine can take any value from zero to a maximum theoretical efficiency (below 100%). Also, it is highly dependent on the speed-torque output from the machine.

### 3.3 Maximizing Energy Efficiency

Improving the efficiency (or reducing losses) of an electro-mechanical energy conversion system is ultimately an engineering optimization problem, consisting of a cost function to be minimized (or maximized) and a set of constraints. This problem can be approached using all three methodologies mentioned in Chapter I. These are discussed as follows:

- a) Optimize design parameters: Select electric machine parameters like resistance, inductance, number of windings, grade of steel used in the stator/rotor, type of metal used in windings, etc. to obtain maximum energy efficiency at a specific speed-torque operating point (usually the rated speed and torque operating point).
- b) Optimize operation during steady state: Modify state variables of the electric machine like electro-magnetic flux or stator electric current after it has reached a steady state, and maximize the efficiency at its present speed and torque operating point.
- c) Optimize operation during transients: Modify state variables of the electric machine like electro-magnetic flux or stator electric current while it is accelerating or

decelerating to a new speed-torque operating point in such a way that its efficiency during those transitions is maximized.

It is easy to observe how (a) above fundamentally differs from (b) and (c) in terms of the engineering work involved. However, from the point of view of an optimization algorithm, (a) and (b) are static optimization problems and would use similar techniques to solve. On the other hand, (c) is a dynamic optimization problem and would need a considerably different approach. As mentioned in Chapter I, this dissertation is about dynamic optimization as it exclusively focuses on optimizing induction machine operation during transients (acceleration and deceleration). Since the dynamics governing the operation of each electric machine is different, dynamic optimization problems and their solutions for different electric machines will be distinct. This work focuses entirely on the problem of improving the efficiency (or reducing energy losses) of the induction machine during its acceleration and deceleration (transient) states.

### 3.4 Importance of Transient Energy Efficiency in Induction Machines

In most IM applications, the operating points (rotor speed and torque) remain constant for most of its operating time (also referred to as duty cycle). For example, the rotor speed may change once every hour on average in a refrigerator application. This means that only a small fraction of the IM's duty cycle is in transient state. For this reason, improving transient energy efficiency will have only a marginal impact on the overall energy efficiency and hence has never received much interest from researchers. But in recent years IM's have found application in electric vehicles (EV) [4], wind turbine generators [5], and fly wheel energy storage [6]. In these applications, for a significant fraction of the operating time, the IM is in a transient state because the operating point changes rapidly. In case of

EV's, this is apparent from the US EPA sample drive schedules for vehicles that can be found in [7]. Hence while the objective of this thesis is applicable to IM's in all applications, the best results would be obtained in applications with frequent speed transients.

A simple illustration of the potential electrical energy savings in EV's is given here. Assume that a 2% improvement in drive cycle energy efficiency is achieved by using transient loss minimization algorithms within the EV drive train control software. This would translate to a 2% decrease in the specific energy consumptions (kWh per mile). The resulting energy savings for different Tesla models are shown in Table 3.1. Note that Tesla exclusive uses IM's in all their EV models. The number of Tesla vehicles on road around the world was about 200,000 in 2017 [8]. However, it is expected to reach 1 million vehicles in a couple of years and keep increasing for the near future [9]. Hence even a 2% improvement can lead to saving of millions of units of electrical energy.

*Table 3.2 Potential energy savings in Tesla EV's*

Model	EPA range (Miles)	Battery capacity (kWh)	Specific energy per mile (kWh/mile)	2% Energy Saving (kWh/mile)	Energy Saving for 100000 miles (kWh)
Tesla Model S 75D	259	75	0.306	0.0061	579
Tesla Model X 75D	237	75	0.32	0.0063	633
Tesla Model 3	215	60*	0.233	0.0047	558

### 3.5 Summary

This chapter discussed the importance of electro-mechanical energy conversion using electric machines. It specifically highlighted the importance of induction machines. The concept of energy conversion efficiency was discussed. Different levels at which the electric machine operation can be optimized to maximize its energy conversion efficiency were described.

## 4 INDUCTION MACHINES

The invention of the first practical induction machine (IM) can be attributed to Nikola Tesla in 1887 and Galileo Ferraris in 1885 (both working independently). The operating principle of an induction machine was first explained by Tesla in his paper “*A New System for Alternating Current Motors and Transformers*”. However, it was Michael Dolivo-Dobrowolsky who perfected the design of Tesla and Ferraris and invented the most common type of induction machine being used today, namely the 3-phase Squirrel Cage induction machine (SQIM). This design has been optimized over the last 100 years and has been the subject of many volumes of research [10], [11]. A brief explanation of the IM operation is provided below for completeness.

### 4.1 Induction Machine Operation

It is known that when electric current flows through a closed loop wire, a magnetic field is established that surrounds the current carrying loop of wire. Now, when a magnetic field and a conductor moving at relative speeds w.r.t. each other intersect, a voltage (also referred to as the electromotive force (emf)) is induced across the conductor (Faraday’s law of induction). If the conductor is short circuited, i.e. forms a loop, the induced emf causes a current to flow through it. The direction of this current is in such a way that the magnetic field it produces will be in the opposition to the magnetic field that caused it in the first place (Lenz’s law). If the magnetic field is moving and the metal conductor is stationary (as in the case of an IM), the induced current interacts with the magnetic field



(Lorentz's force law) to produce a force that acts on the conductor and causes the conductor to move in the direction of the magnetic field.

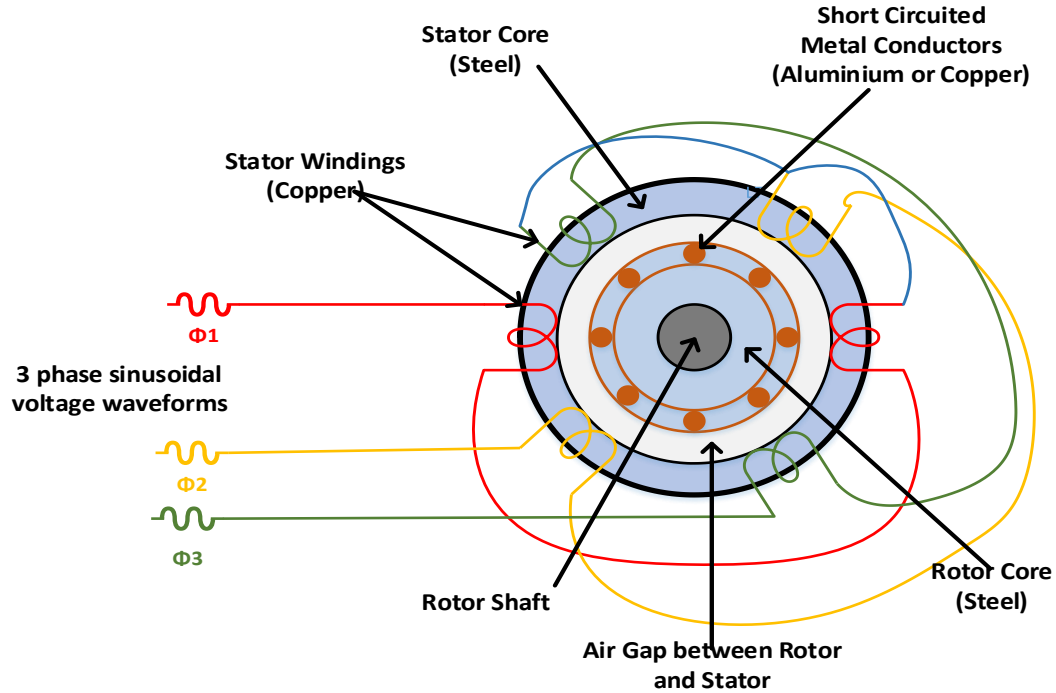


Figure 4.1. Induction machine cross section diagram.

An IM has primarily two major components as illustrated in Figure 4.1, namely the stator and the rotor. The stator consists of three coils of insulated copper wires and are physically displaced by 120 degrees on the stator. This three-coil arrangement is known as the stator winding. The terminals of each of the three stator windings are supplied with a sinusoidal voltage waveform. The three sinusoidal voltage waveforms are themselves phase displaced from each other by 120 degrees and when applied to the stator windings will produce a rotating magnetic field (RMF). The RMF links with the rotor conductors through the air gap (a clearance between the rotor and the stator). The rotor core consists of insulated metal discs called laminations fixed around a shaft that is free to rotate about its axis. Embedded with these laminations are short-circuited metal conductors. The current

induced in the rotor interacts with the RMF to produce a torque that causes the rotor structure to spin and catch up with the RMF, thereby reducing the relative speed between them. Hence, all the energy transfer that occurs between the stator and rotor is through the electromagnetic linkage through the air gap. The speed at which the RMF rotates is known as the synchronous speed,  $N_{synchron}$  and is given by (4.1.1), if measured in revolutions per minute (RPM).

$$N_{sync} = \frac{120f}{p} \quad (4.1.1)$$

where  $f$  is the frequency of the sinusoidal voltage waveforms being supplied to the stator windings, and  $p$  is the number of stator magnetic poles that result from stator windings.

The rotor speed,  $N_r$ , can never reach the synchronous speed of the stator magnetic field. If  $N_r$  were to become equal to  $N_{sync}$  then the relative speed between the stator magnetic field and the rotor conductors would become zero thereby preventing emf from being induced (Faraday's law), current from flowing (Lenz's law), and consequently torque becoming zero. The relative difference between rotor speed and the RMF's synchronous speed is known as the slip of the machine and is calculated using (4.1.2). More importantly, slip is a measure of the magnitude of current that flows in the rotor conductors, as well as the amount of electro-magnetic torque that is being produced. The value of slip typically varies from 0.1% to 5%.

$$s = \frac{N_{sync} - N_r}{N_{sync}} \quad (4.1.2)$$

## 4.2 Induction Machine Drives

In many industrial applications precision control of speed and torque is necessary, i.e. the machine's speed is expected to change depending upon the need of the application at that time. An old example is the HVAC systems in buildings, while electric cars are a new example. Speed control over a limited range is possible through the use of gears, however, these would add complexity and energy losses to the system. From (4.1.1) and (4.1.2), speed control is possible by changing the frequency of the stator's sinusoidal voltage waveform. However, changing the supply frequency is not a trivial task, and for this reason, DC motors were the favored machines for such speed control applications until the latter half of the 20<sup>th</sup> century.

However, the advances in power electronics technology made it possible to have precise control over the magnitude, frequency, and phase of the voltage waveform supplied to the stator of the IM even at high current and voltage levels for a reasonable price and complexity. The power electronic devices that convert DC waveforms to sinusoidal AC waveforms required by AC machines are called 3-phase inverters. A simple description for these are: circuits comprised of on/off electronic switches which can be controlled independently with one side connected to a DC voltage source and other side connected to the AC machine. The switches are functionally like a normal mechanical switch except that they can be turned on and off thousands of times every second continuously with minimal power losses. Also, these switches can carry very large currents without damage if sufficient heat dissipation is provided. Through operating the switches in a precise and specific sequence and duty cycles, the desired voltage waveforms with the desired frequency can be generated. The inverter, IM, and the software algorithms are collectively

referred to as the IM drive. References like [12] discuss IM and other electric drives in detail. The schematic of a generic IM electric drive system is shown in Figure 4.2.

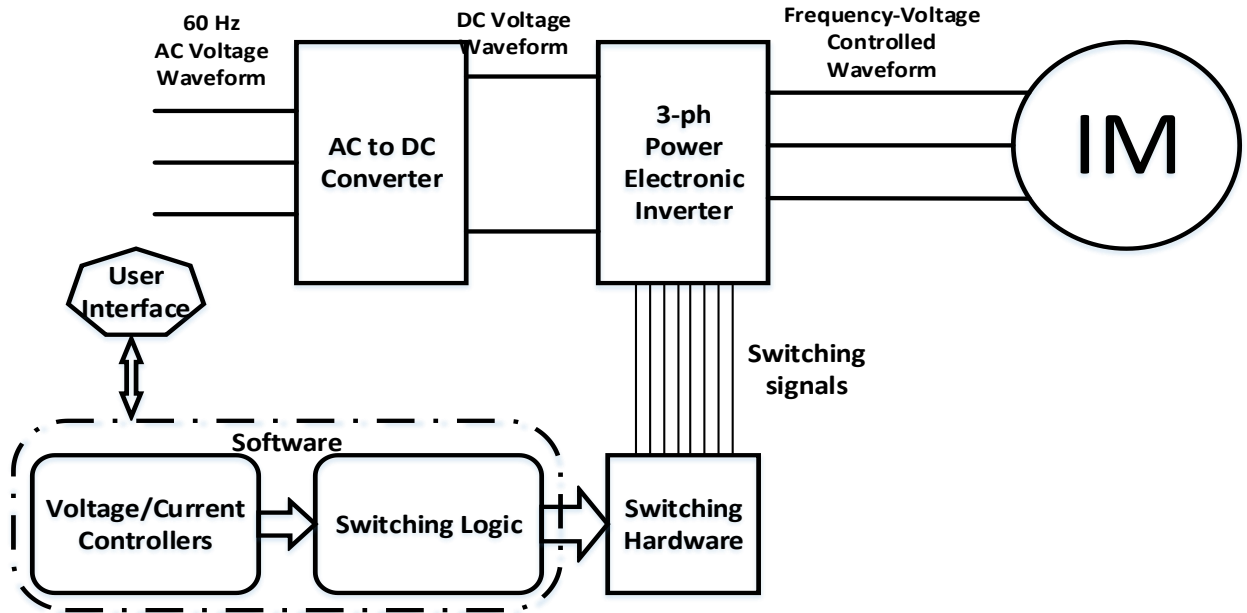


Figure 4.2. IM Electric Drive Schematic

#### 4.3 Induction Machine Power Flow and Power/Energy Losses

A graphical illustration of the power flows and relative differences in magnitude between power/energy losses in an induction machine are given in Figure. 4.3 and Figure. 4.4, respectively.

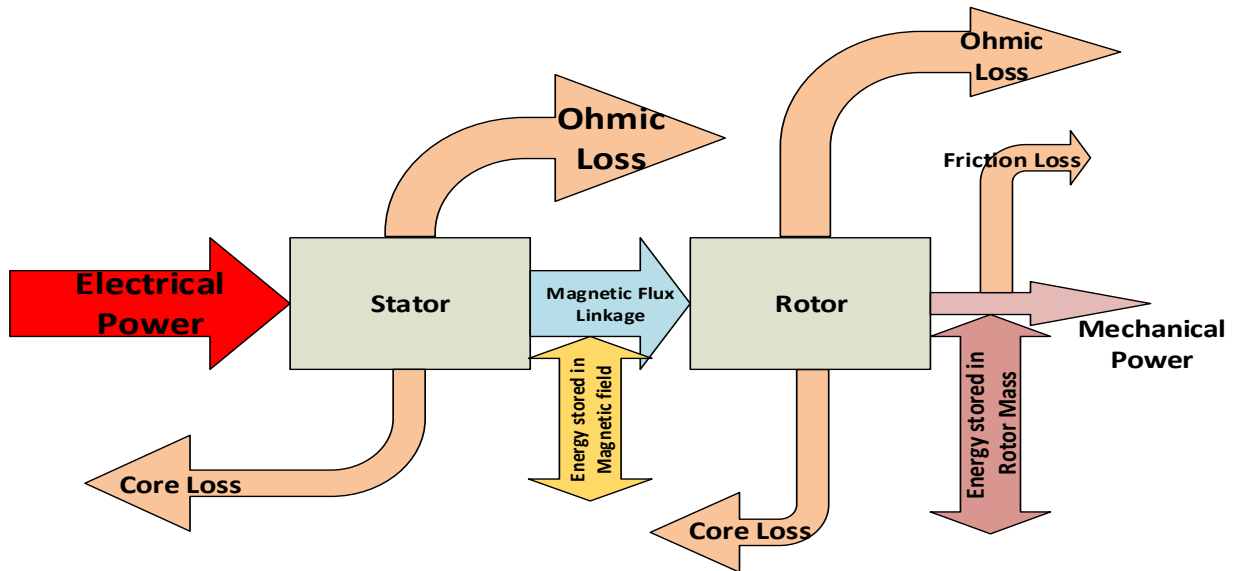


Figure 4.3. Power flows in an induction machine

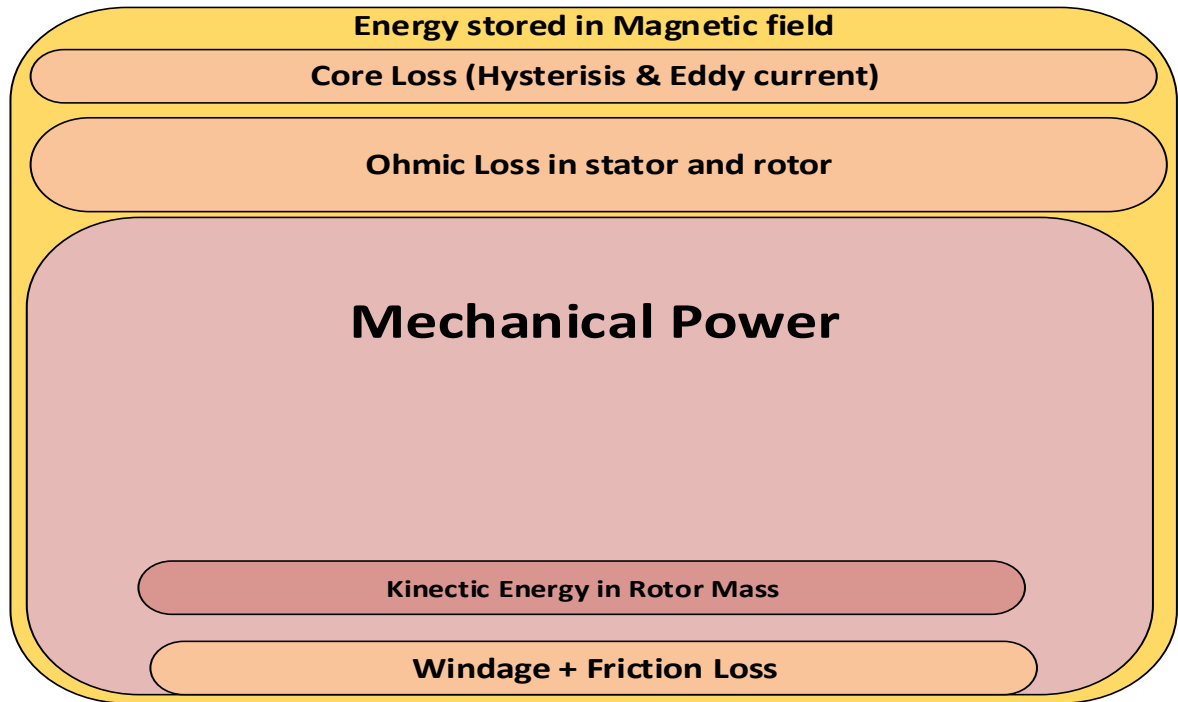


Figure 4.4. Relative magnitude of Power flows in an induction machine

Electrical power that the source supplies to an IM is transformed in three ways.

- 1) Mechanical power: Most of the input electric power is transformed into output mechanical power at the rotor. This output mechanical power is a function of the torque of the load connected to the motor shaft and the rotor speed. It can be expressed as

(4.3.1). A small fraction of the mechanical power is lost due to friction in the bearings that support the rotor shaft. Another fraction is lost due to drag offered by air due to the rotation of the shaft. These losses are functions of the rotor speed (4.3.2). Another fraction of the output mechanical power is stored as kinetic energy (4.3.3) in the rotating mass of the rotor. Note that transfer of power to the rotor mass occurs only when rotor speed is increasing. If the rotor speed were to decrease, the kinetic energy is released as the mechanical output of the rotor. No energy is transferred to the rotor mass when rotor speed reaches steady state.

$$P_{mech} = T_L \omega_r \quad (4.3.1)$$

$$P_{friction/windage} = f(\omega_r) \quad (4.3.2)$$

$$E_{stored} = \frac{1}{2} J \omega_r^2 \quad (4.3.3)$$

In the above equations  $T_L$  is the load torque on the rotor shaft,  $\omega_r$  is the rotor mechanical speed, and  $J$  is the moment of inertia of the rotor mass.

Every speed-torque operating point has a corresponding mechanical power output. Hence these are hard constraints for the energy efficiency optimization problem. Since the friction and windage losses are fixed for a specific speed-torque operating point, these are considered as uncontrollable energy losses and not part of the optimization problem.

- 2) Ohmic losses: When an electric current passes through any type of conductor heat is generated which can be expressed as (4.3.4). In case of an IM, Ohmic losses occur when current flows through the stator windings and the short-circuited rotor conductors.

$$P_{ohmic} = i^2 R \quad (4.3.4)$$

where  $i$  is the current flowing through the conductors, and  $R$  is the resistance of the conductors.

Since electric current is a controllable input to the IM, Ohmic losses can be considered as controllable losses and part of the optimization problem to maximize energy efficiency.

- 3) Electromagnetic flux: As explained earlier, a rotating magnetic field is produced due to the sinusoidal currents flowing through the stator windings. The magnetic flux flows through the stator core, air-gap, and rotor core. Some of the input electrical energy is stored in the magnetic field. The amount of energy stored is a function of the current flowing through the stator windings. The flow of magnetic flux through the metal that constitutes the core of the stator and the rotor also results in two types of energy losses: eddy current losses and hysteresis losses. These losses are expressed by (4.3.5) and (4.3.6), respectively. These losses are collectively referred to as core or iron losses.

$$P_{eddy} = K_e K_f B_m^2 f^2 \quad (4.3.5)$$

$$P_{hysteresis} = K_h B_m^{1.6} f \quad (4.3.6)$$

where  $B_m$  and  $f$  are the peak magnetic flux and the frequency at which the magnetic poles change on the stator, respectively.  $B_m$  is proportional to the magnitude of the sinusoidal voltage waveform, while  $f$  is equal to the frequency of the same.  $K_e$ ,  $K_f$ , and  $K_h$  are constants related to the type, volume, and the shape of material used to construct the stator and rotor cores.

Since the functions describing core losses have two degrees of freedom, the core losses can be considered as controllable losses and hence part of the optimization problem.

#### 4.4 Induction Machine Dynamics

Like all dynamical systems, the operating cycle of an IM can be separated into transient and steady state phases. An induction machine is said to be in steady state if its rotor speed, electromagnetic torque, magnitude of the voltage and current waveforms, and peak magnetic flux remain constant. The IM can be induced into a transient phase from steady state in two ways as listed below:

- a) Change in the frequency or the magnitude of input sinusoidal voltage waveforms.
- b) Change in the load torque on the shaft.

Transients can also be caused due to short circuits or open circuits in the stator or rotor windings. These are outside the scope of this dissertation, and hence not discussed.

The most common transient that occurs in IM is when the machine accelerates or decelerates from its current speed to a higher or lower speed, respectively. As with other dynamical systems, transients in IM can lead to two possibilities.

- a) IM achieves a new steady state operating point.

The simplest example of this is an IM increasing its rotor speed to a new operating point in response to a change in input voltage magnitude and frequency.

- b) IM becomes unstable which may lead to stalling, over speeding, or overheating.



The most common example of instability is when the load torque on the IM is suddenly increased to a value that is beyond its maximum torque rating. This results in the net torque becoming negative, and the machine coming to a stop (stalling).

Figure 4.5. Illustrates a transient in the input phase voltages of an IM. It can be observed that the magnitude and frequency of the voltage waveforms for all three phases change at 0.5s, 1s, and 2s. The transient phase that follows is highlighted using the circles.

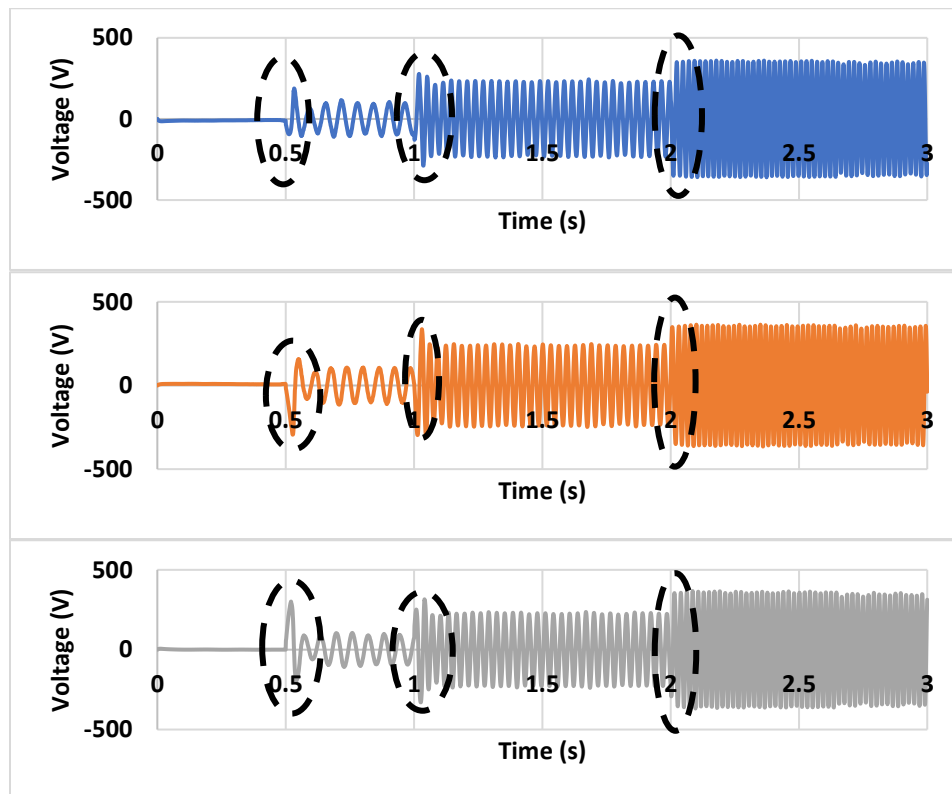


Figure 4.5. Transients in input phase voltage waveforms of an induction machine.

The change in input voltage corresponds to a change in the rotor speed as shown in Figure 4.6. A steady state phase follows each of the transients. There is a difference in the magnitude of the power/energy that is consumed by the IM during transients and steady states. This is illustrated in Figure 4.7. by plotting the cumulative energy input into the IM during the above transients.

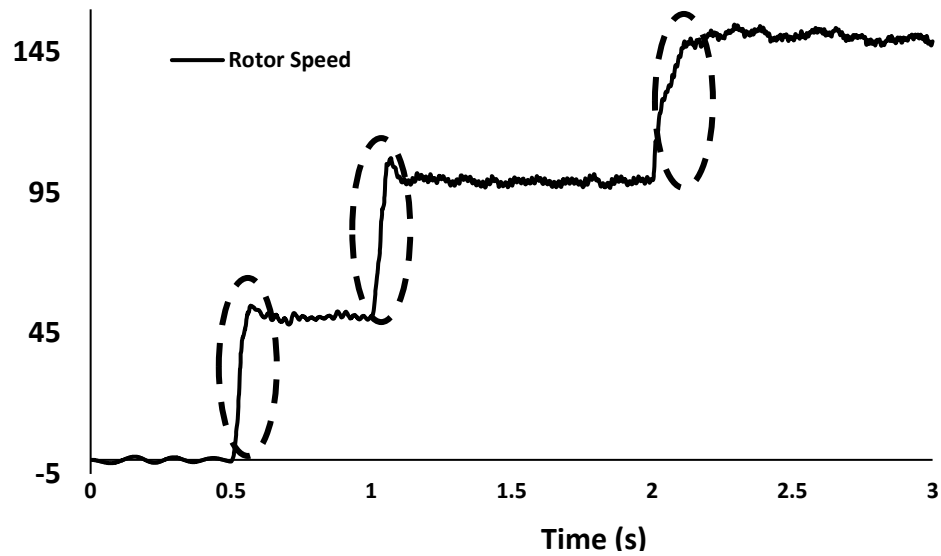


Figure 4.6. Transients and steady states in rotor speed of IM corresponding to voltage transients

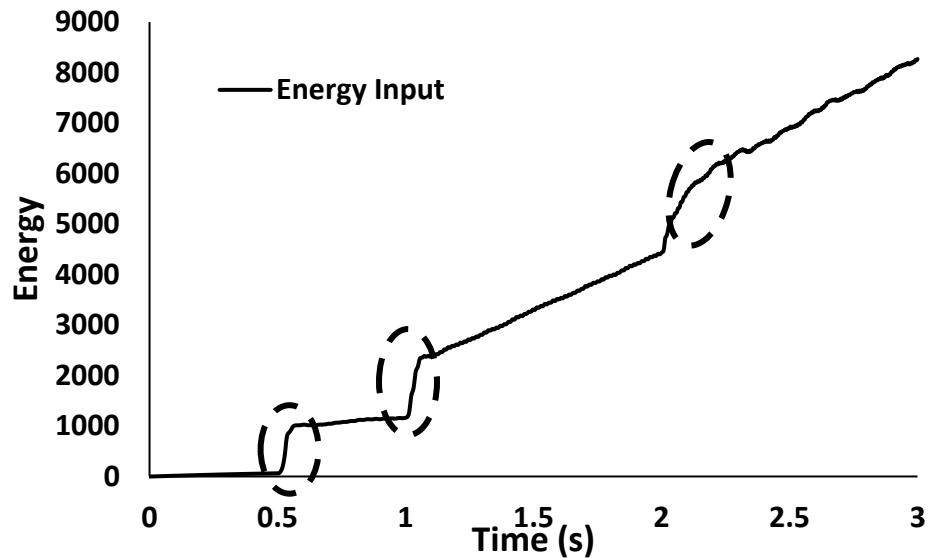


Figure 4.7. Transients & steady states in energy input to IM corresponding to voltage transients

Most of the input energy consumed during transients is used to accelerate the IM to its new speed-torque operating point while the rest is consumed by the energy losses that were described earlier. Details on how the dynamics of the IM affect the energy input and the energy losses will be explained in the Methodology section of this dissertation.

#### 4.5 Mathematical Modelling of Induction Machines

The dynamics of an IM can be described through a system of ordinary differential equations (ODE's). In one approach, the model is built around treating the three-phase variables as they are. That is, there is no transformation of the variables. In such an approach, there will be 3 variables representing the current, voltage, and the magnetic flux linkage of each phase of the IM. Also, the mutual inductance of the IM, which is a coefficient in the ODE's, would be a function of the rotor speed. Hence, we arrive at a time variant model of the IM consisting of 3 input variables, 7 state variables, and 6 dependent variables.

Fortunately, there is a second approach that can yield a significantly simpler model without losing accuracy of the model. This involves transforming the three a, b, and c phase variables into two d and q phase variables by projecting them onto the orthogonal d- and q-axes of a rotating reference frame [13]. Apart from reducing the number of variables, the transformation of variables also results in the mutual inductance becoming independent of the rotor speed, i.e. it becomes a constant. The transformation from 3 phase variables to 2 phase variables is called Park's transform. The speed of the rotating reference frame can be arbitrarily chosen, and the properties of the IM model varies accordingly. The concept is illustrated in Figure 4.8.

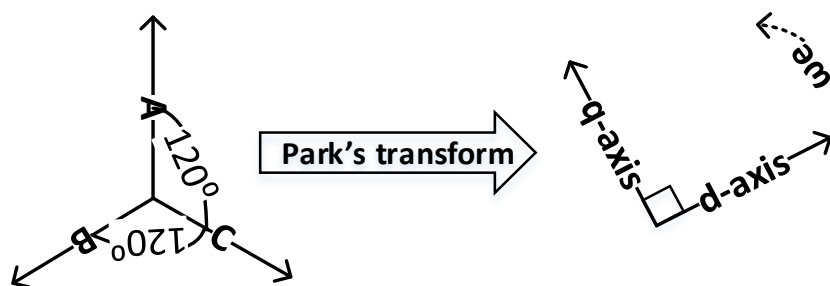


Figure 4.8. Visualizing change in reference frame

In this dissertation, the reference frame speed is chosen to be equal to the frequency of the input voltage waveforms of the stator. Using magnetic flux linkages as the state variables, the transformation of variables results in an ODE model of the IM as given by (4.5.1) to (4.5.5) [14], [15].

$$\frac{d\psi_{ds}}{dt} = v_{ds} - R_s i_{ds} + \omega_{sync} \psi_{qs} \quad (4.5.1)$$

$$\frac{d\psi_{qs}}{dt} = v_{qs} - R_s i_{qs} - \omega_{sync} \psi_{ds} \quad (4.5.2)$$

$$\frac{d\psi_{dr}}{dt} = v_{dr} - R_r i_{dr} + (\omega_{sync} - \omega_r) \psi_{qr} \quad (4.5.3)$$

$$\frac{d\psi_{qr}}{dt} = v_{qr} - R_r i_{qr} - (\omega_{sync} - \omega_r) \psi_{dr} \quad (4.5.4)$$

$$\frac{d\omega_r}{dt} = \left( \frac{p}{2} \right) \left( \frac{\frac{p}{2} (\psi_{qr} i_{dr} - \psi_{dr} i_{qr}) - T_L}{J} \right) = \left( \frac{p}{2} \right) \left( \frac{\frac{pL_m}{2L_r} (\psi_{dr} i_{qs} - \psi_{qr} i_{ds}) - T_L}{J} \right) \quad (4.5.5)$$

where  $\Psi_{ds}$  and  $\Psi_{qs}$  are the stator flux linkages along the new d-axis and q-axis, respectively.  $\Psi_{dr}$  and  $\Psi_{qr}$  are the rotor flux linkages along d-axis and q-axis, respectively.  $i_{ds}$  and  $i_{qs}$  are the stator currents along d-axis and q-axis, respectively.  $i_{dr}$  and  $i_{qr}$  are the rotor currents along d-axis and q-axis, respectively.  $v_{ds}$  and  $v_{qs}$  are the stator input voltage along d-axis and q-axis, respectively.  $v_{dr}$  and  $v_{qr}$  are the rotor input voltage along d-axis and q-axis, respectively.  $R_s$  and  $R_r$  are the resistances of the stator and rotor windings, respectively.  $\omega_{sync}$  is the frequency of the source voltage waveforms at the stator and  $\omega_r$  is the rotor speed.  $T_L$  is the load torque on the rotor (torque in opposition

to rotation of the rotor) while  $J$  is the moment of inertia of the rotor. Finally,  $p$  denotes the number of magnetic poles due to the stator windings.

In most IM's the rotor windings are short circuited, hence  $v_{qr} = v_{dr} = 0$ . The rotor currents can be expressed as functions of stator currents, and the rotor flux linkages can be expressed through the algebraic relationships given by (4.5.6) to (4.5.9) [15].

$$i_{dr} = \frac{\psi_{ds} - L_s i_{ds}}{L_m} \quad (4.5.6)$$

$$i_{qr} = \frac{\psi_{qs} - L_s i_{qs}}{L_m} \quad (4.5.7)$$

$$i_{dr} = \frac{\psi_{dr} - L_m i_{ds}}{L_r} \quad (4.5.8)$$

$$i_{qr} = \frac{\psi_{qr} - L_m i_{qs}}{L_r} \quad (4.5.9)$$

where  $L_s$  is the stator inductance,  $L_r$  is the rotor inductance, and  $L_m$  is the mutual inductance.

#### 4.6 Current Fed Model of The Induction Machine

The mathematical model in section 4.5 used stator input voltages as control inputs and hence it is known as the voltage fed model. It is also possible to use stator input currents as the control inputs and obtain a smaller model of the IM. Using currents as inputs imply that the dynamics between stator flux and stator voltages can be neglected. It is assumed that there are current controllers with very fast settling times between the IM and the input voltage source that control the input voltage. Hence the dynamics of the IM only depend on the reference to the current controller. This concept is illustrated in Figure 4.9.

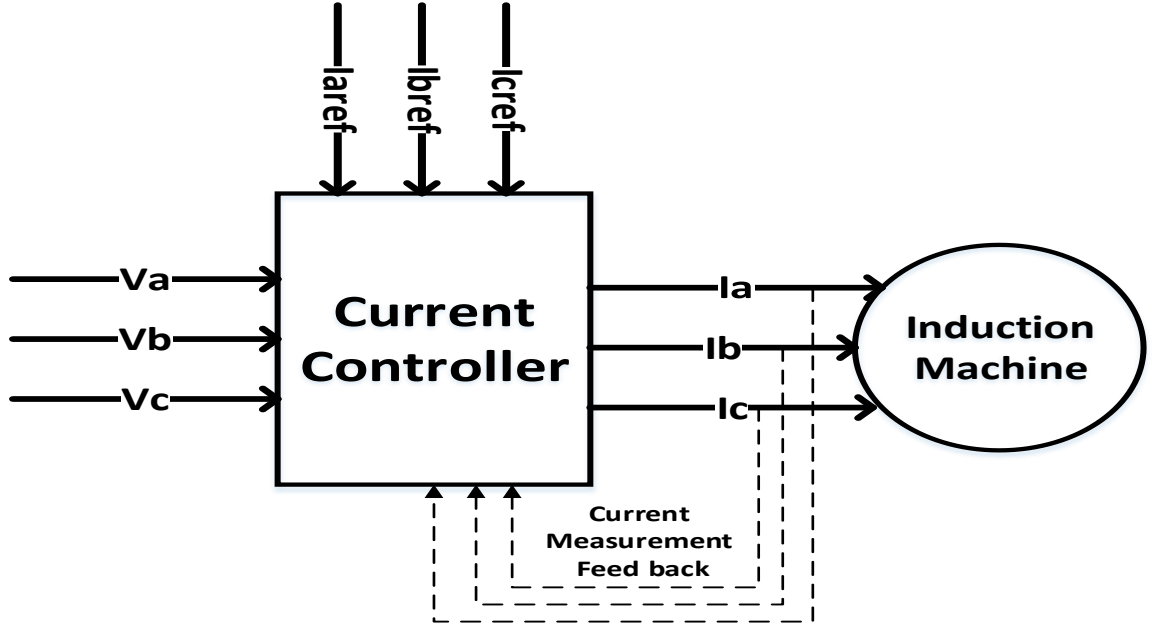


Figure 4.9. Concept of Current Fed IM Model

Using stator current as an input to the model removes the need for ODE's involving stator flux variables, i.e. (4.5.1) and (4.5.2). Substituting the equations for rotor currents, (4.5.8) and (4.5.9) in (4.5.3) to (4.5.5) results in an IM model having 3 state variables as shown in (4.6.1) to (4.6.3).

$$\frac{d\psi_{dr}}{dt} = -R_r \left( \frac{\psi_{dr} - L_m i_{ds}}{L_r} \right) + (\omega_{sync} - \omega_r) \psi_{qr} \quad (4.6.1)$$

$$\frac{d\psi_{qr}}{dt} = R_r \left( \frac{\psi_{qr} - L_m i_{qs}}{L_r} \right) - (\omega_{sync} - \omega_r) \psi_{dr} \quad (4.6.2)$$

$$\frac{d\omega_r}{dt} = \left( \frac{p}{2} \right) \left( \frac{\frac{p}{2} \left( \psi_{qr} \left( \frac{\psi_{dr} - L_m i_{ds}}{L_r} \right) - \psi_{dr} \left( \frac{\psi_{qr} - L_m i_{qs}}{L_r} \right) \right) - T_L}{J} \right) \quad (4.6.3)$$

The above model will be further simplified later in this work and used in the IM optimal control problem.

#### 4.7 Detailed Problem Statement

There is a significant scope for improving the energy efficiency of an IM during both steady state and transient phases. Algorithms for minimizing energy losses during steady state are already available in commercial IM drives, whereas transient energy loss minimization algorithms are not. As such, the contribution and the objective of this work is to find an optimal control law that minimizes the Ohmic and iron energy losses inside an IM during the transient phases of operation without compromising the performance of the machine in terms of its output mechanical power. A secondary contribution and objective of this work is to determine the sensitivity of the control law to the operating conditions of the IM. Additionally, the tertiary objective is that the designed control law must be in a form that allows it to be incorporated into the existing IM drive control algorithms.

#### 4.8 Summary

This chapter briefly explained the operation of, the power flow through, and the various power losses within an IM. The transient phase of the machine was discussed. The ODE representation of the IM model was given. Finally, a more detailed overview of the research problem that is addressed in this work was provided.

## 5 LITERATURE SURVEY

Optimal control is a fascinating optimization technique and its development history, which began about 300 years ago, is equally fascinating. Its relationship to mathematics, engineering, and computer science is illustrated in Figure 5.1.

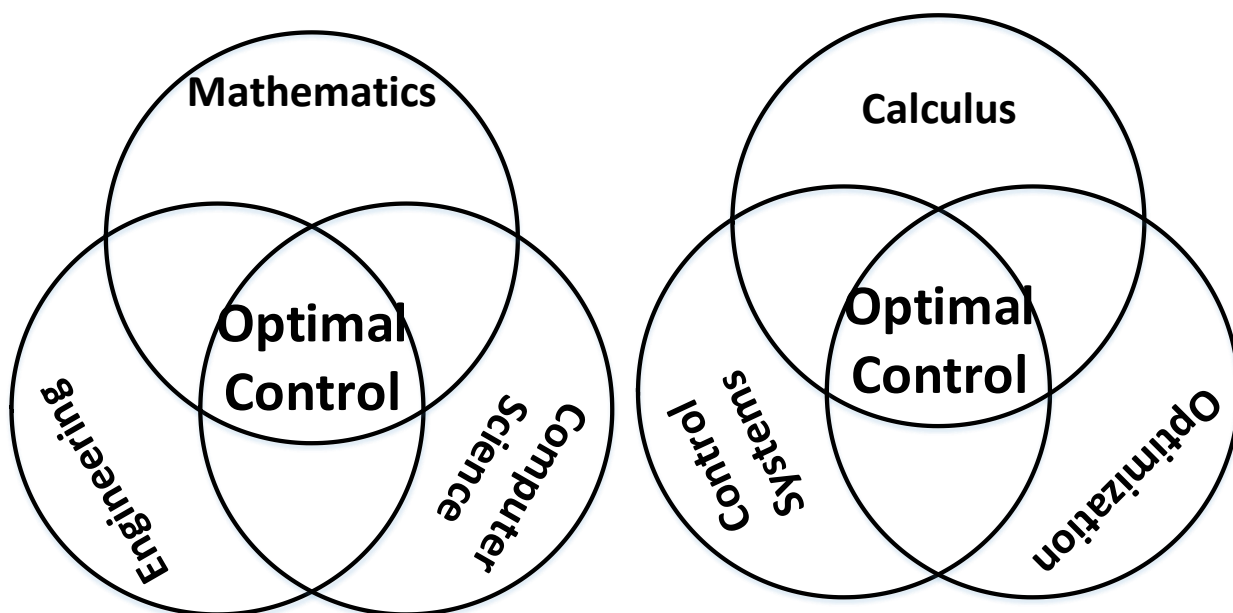


*Figure 5.1. Relationship between optimal control and other technical areas*

### 5.1 History of Optimal Control

The excellent historical overview provided by Sussmann et al. in [16] describes the inception of optimal control theory through a mathematical challenge put forward by Johann Bernoulli in 1696 in the form of the Brachystochrone problem. The authors of [16] also present their solution to the said problem using the optimal control approach and showed how it was superior to the Calculus of Variations solution. A few other notable works chronicling the history of optimal control are [17], [18], and [19]. The development



of the Euler-Lagrange equation was a key discovery in the advancement of Calculus of Variations. However, it was the efforts of two cold war era mathematicians, Lev Pontryagin in the Soviet Union and Richard Bellman in the US that established optimal control theory as a new field in applied mathematics and distinguished it from Calculus of Variations.

A timeline has been created illustrating the major developments in the field by extracting relevant information from the above-mentioned references and shown in Figure 5.2.

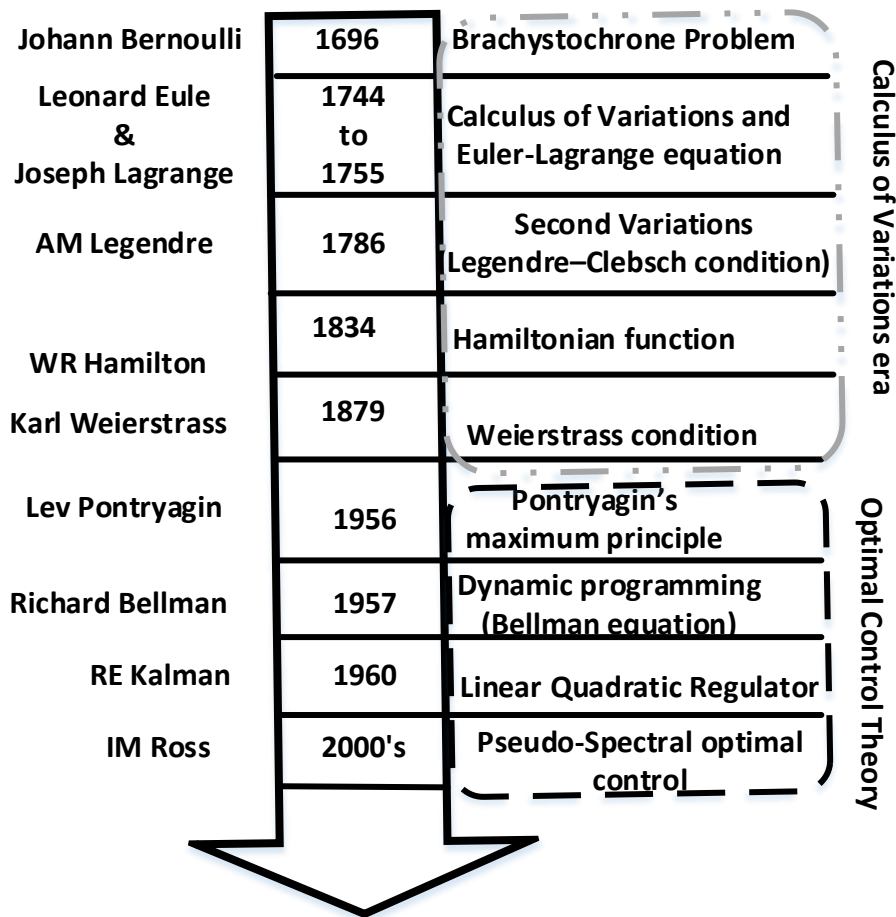


Figure 5.2. Optimal Control through history

Pontryagin's discovery of the Maximum principle paved the way for control engineers to solve optimal control problems involving continuous variables in a more intuitive way compared to using Calculus of Variations. Bellman was responsible for the development

of dynamic programming, which made it possible to solve piecewise optimal control problems [20]. The development of the Linear Quadratic Regulator by Kalman using the minimum principle enabled practically implementable optimal controllers for linear systems [21], [22].

The work of this dissertation uses Pontryagin's maximum principle to define a set of necessary conditions and use them to develop an optimal control law for minimizing transient energy losses in an accelerating IM.

## 5.2 Literature on Transient Energy Loss Minimization in IM's

The problems involving optimizing the IM operation during steady state in real time is a heavily researched topic compared to optimizing during transient states. An excellent survey of the various techniques used for IM steady state optimization over the past 15 years is given in [23].

There have been several researchers who have attempted to solve the research problem of optimizing IM operation during transients, but there has yet to be a survey that chronicles their efforts. This section will provide a brief outline on the efforts of all the researchers over the last 40 years who have worked on this research problem. A chronological illustration is provided in Figure. 5.3. Note that the survey includes papers from both conferences and journals.

1968	Petrov [24]
1984	Figalli [25]
1988	Sangwongwanich [29,30], Lorenz [26]
1990	Murata [33]
1991	Sangwongwanich [31-32]
1992	Lorenz [27,28]
1999	De Wit [34]
2002	Rodriguez [35]
2006	Gonzalez [36]
2007	Inoue [38]
2008	Botan [37]
2009	Gaicenau [42]
2010	Rosu [43], Ali [45]
2011	Inoue [39]
2012	Inoue [40]
2013	Stumper [46,47], Gaiceanu [44], Inoue [41]
2015	Plathottam [49]
2016	Weis[48], Plathottam [50], Borisevich [51]

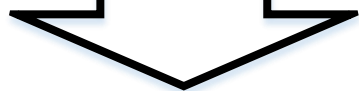


*Figure 5.3. Dynamic optimization in Induction Machines Literature*

The concept of using optimal control theory in electric machine control applications can be traced back to the work of a Soviet engineer named Petrov in [24]. He developed control trajectories for DC series motor, DC permanent magnet motor, and the induction motor using optimal control principles. However, he only considered stator transient Ohmic losses, used a very simple model, and used control variables that made it impractical to implement with modern power electronic drives. The work by Figalli in [25] during early 1980's was the first to use Bellman's equation to develop an optimal control law for frequency of the IM with objective to reduce speed error and control effort. The subject did not receive much attention until the early 1990's. The work by Lorenz in [26]–[28]

again proposed to use Bellman's equations from Dynamic programming to solve the transient energy loss problem, considering both stator and rotor Ohmic losses as well as core losses. This was also the first work to use d- & q-axis currents as control inputs in the transient energy loss minimization problem. This solution was compatible with power electronic drives using the Field Oriented Control algorithm. However, the Bellman equations resulted in the need to solve partial differential equations to compute the optimal control trajectories. Hence, trajectories were computed offline and stored as a lookup table on the controller. This technique could only be used if all possible load torque values and speed reference values encountered in the IM duty cycle were available before hand, thereby limiting its practical use. During the same period Sangwongwanich used Pontryagin's minimum principle to develop a control law for the IM that minimized the time taken to increase its rotor speed [29]–[32]. It used the angle between d- and q-axis currents as the control input. However, energy losses were not considered in this work, i.e. it was purely a minimum time solution. Another work that used optimal control principles without considering transient energy losses was by Murata in [33]. The linear quadratic regulator was used for speed control with stator currents as the control inputs.

In the late 1990's the work by De Wit in [34] used the Euler-Lagrange equation to derive a set of necessary conditions to be satisfied by the optimal rotor flux trajectory in a field oriented control of an induction machine. Stator and rotor Ohmic losses were considered in the cost function. This work treated the problem like a Calculus of Variations problem rather than an optimal control one. However, unlike the earlier works, they gave no simulation or hardware results to show the feasibility of their optimal rotor flux trajectory solutions.

During the early 2000's the work by Rodriquez in [35] and Gonzalez in [36] used Pontryagin's minimum principle for obtaining the maximum torque per current input. However, their cost functional didn't have any power loss terms or terminal costs. Hence, they could find an equation for the optimal d- and q-axis current trajectories (as control inputs). The parameter's in their analytical equation took on different values for different initial and final conditions. Hence, they had to be computed offline and stored in a lookup table in the controller. The work by Botan in [37] also used the minimum principle, a cost function with stator and rotor Ohmic losses, and the stator d- and q-axis currents as control inputs. However, the fact that they considered only the rotor speed dynamics makes the validity of their optimal trajectory debatable. The work by Inoue in [38] used the Euler-Lagrange equation to find the optimal torque trajectory that maximizes regenerative power. In early 2010 the same concept was used again by the same authors in [39]–[41] for minimizing stator and rotor Ohmic losses during transients. During the same time period, the work by Gaiceanu and Rosu in [42]–[44] used a linear quadratic regulator for speed control and for minimizing the stator Ohmic losses. They calculated the optimal trajectory of the stator q-axis current online using the Matrix Riccati Differential Equation (MRDE). This is a good approach for practical implementation except that only the Ohmic losses due to stator q-axis current are considered. Another work that used the Bellman equation to minimize stator and rotor Ohmic losses was by Ali in [45]. Unlike the work by Lorenz, Ali found the optimal flux trajectory as an offline solution, instead of the optimal stator current, and then fitted a polynomial curve to reproduce the optimal flux trajectory during real-time operations. However, this method was not generalized to be applicable for an arbitrary IM.

The recent related works in this area (other than the work of the author of this dissertation) are by Stumper [46], [47] in 2013 and Weis [48] in 2016, both of which extended De Wit's work. Stumper's work used the Euler-Lagrange equation to come-up with a predetermined torque trajectory to find the optimal rotor d-axis flux trajectory that minimized Ohmic and eddy current losses during torque transients. The distinguishing feature of Stumper's work was the development of a closed form equation for the optimal rotor d-axis flux trajectory which took the shape of a first order lag. However, the problem with this optimal trajectory was that it assumed speed was constant during the torque transients. Hence, it was not optimal for an IM that is accelerating from one speed to another. The next work in this area was by the author of this dissertation in [49] and [50] in 2015 and 2016, respectively. Weis [48] extended the work of Stumper but did not assume speed was constant during transients. He found that the optimal rotor flux trajectory in an accelerating IM could be described by a conic section. Concurrently, the same conclusion was arrived at by the author of this dissertation in [50]. Since both Stumper and Weis treated it as a Calculus of variation problem, they found the optimal state trajectory instead of the optimal control trajectory. The latest work in this area just before the writing of this dissertation was by Borisevich [51]. He set up an optimal control problem to minimize stator and rotor ohmic losses, but only considered the flux dynamics since he assumed a predetermined trajectory for the electromagnetic torque (like Stumper). Borisevich also derived some necessary conditions using Pontryagin's minimum principle but did not solve them numerically. Instead, using some simplifications he was able to express the stator d-axis current in terms of the q-axis current (which was known due to the pre-determined torque trajectory). However, no analysis was done on the shape of these trajectories.

The literature surveyed has been classified into four groups depending on the mathematical technique used as illustrated in Figure 5.4. The different techniques used to generate the optimal control trajectories of IM in real time are illustrated in Figure 5.5. The dynamic models, cost functions, and control inputs that have been used in the surveyed literature are tabulated in Table 5.1.

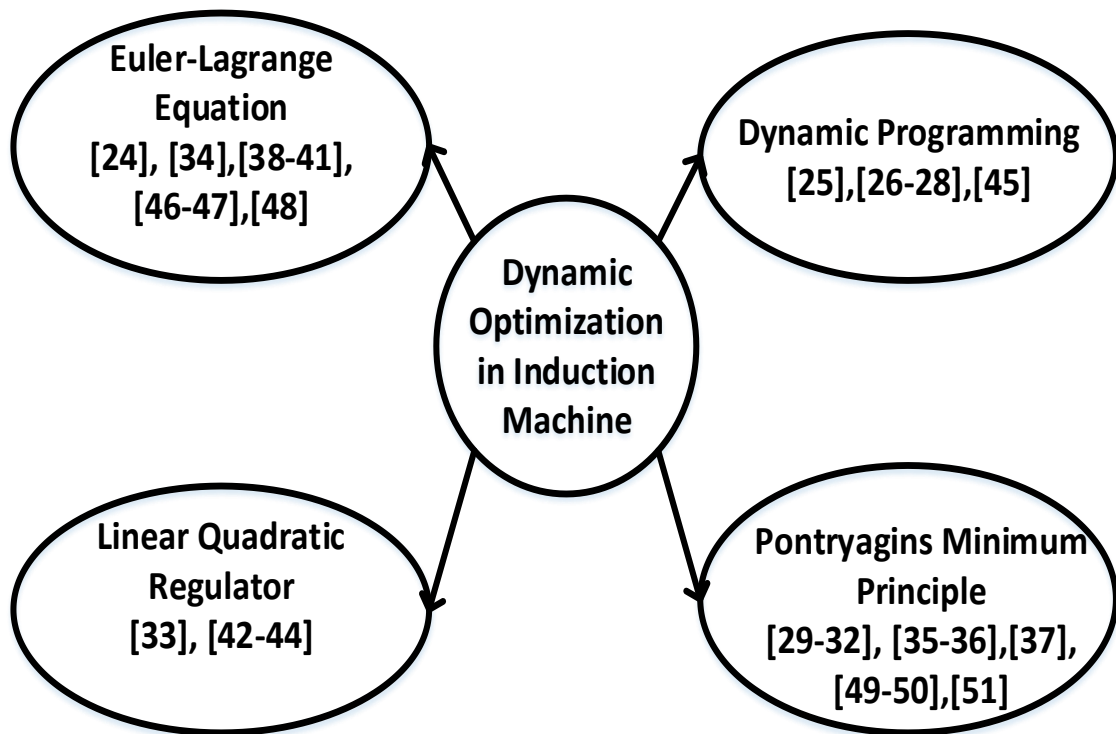


Figure 5.4. Dynamic optimization in Induction Machines in Literature

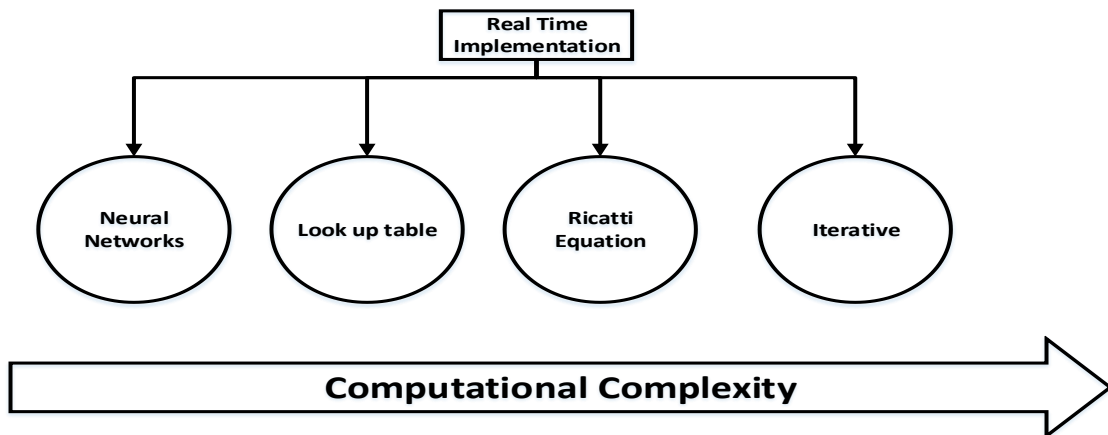


Figure 5.5. Different techniques used to generate the optimal control trajectories of IM

Table 5.1. Comparing literature on transient energy loss minimization in induction machines

Reference	Energy cost	Operating point cost	State variable	Control input	Solution
Petrov	Rotor Ohmic loss	None	Stator flux, rotor speed	Frequency, Voltage	NA
Lorenz	Stator + rotor Ohmic, eddy current + hysteresis losses	None	Rotor d-axis flux, Rotor speed	Stator d- and q-axis current	Look up table
Sangwongwanich	None	Minimum time	Rotor d-axis flux, Rotor speed	Phase angle of stator current vector	Algebraic equation
De Wit	Stator + rotor Ohmic losses, Stored magnetic energy	None	Rotor d- and q-axis flux	Stator d- and q-axis currents	NA
Rodriguez, Gonzalez	Stator Ohmic losses	Minimum time	Rotor magnetizing current, rotor speed	Stator d- and q-axis currents	Algebraic equation
Inoue	Regenerative braking power	None	Rotor speed	Optimal torque	Algebraic equation
Botan	Stator + rotor Ohmic losses,	None	Rotor speed	Stator d- and q-axis currents	Algebraic equation
Ali	Stator + rotor Ohmic losses	None	Rotor d- and q-axis flux, Rotor speed	Stator d- and q-axis currents	Polynomial
Gaiceanu	Stator Ohmic losses (q-axis current)	Speed error	Rotor speed	Stator q-axis current	Riccati
Stumper	Stator + rotor Ohmic losses, Eddy current losses	None	Rotor d-axis flux	Rotor d-axis flux	Iterative



Plathottam	Stator + rotor Ohmic losses, Eddy current losses	Speed error, load torque error	Rotor d-axis flux, Rotor speed	Stator d-axis current, rotor q-axis current	ANN
Weis	Stator + rotor Ohmic losses, Eddy current losses	None	Rotor d-axis flux	Rotor d-axis flux	Iterative

### 5.3 Contributions of this Dissertation

The distinguishing features which differentiate the work in this dissertation from previous works are listed below:

1. This work showed that it was possible to numerically solve an IM optimal control incorporating both transient energy losses (stator ohmic, rotor ohmic, and eddy current) and steady state error (rotor speed, rotor flux, electromagnetic torque). Consequently, it was possible to minimize the energy losses as well as bring the IM to its new speed-torque operating point in a specified amount of time. This is a straightforward approach compared to earlier works. Also, this work considered both the non-linear flux and speed dynamics while formulating the IM optimal control problem. In contrast, many of the other works neglected either the flux dynamics or the speed dynamics or used linearized models while formulating the optimal control problem.
2. This work is the first to generate real-time optimal trajectories for stator currents using neural networks. Many works used lookup tables for entire optimal trajectories corresponding to specific initial and final conditions. Other works used open loop control laws that took different parameters depending upon the operating point of the IM.

3. This work was one of the first to propose a conic trajectory for rotor d-axis flux during IM acceleration/deceleration (Weis et al. concurrently arrived at the same conclusion). Additionally, it discovered that the optimal q-axis current could take either a conic trajectory or a constant value trajectory. The prototype trajectories were fully described in the form of analytic expression that are applicable to a generic field oriented induction machine. These expressions made it possible to perform a sensitivity analysis of energy efficiency during transient which has not been done in literature before.

#### 5.4 Summary

The history of optimal control was briefly discussed and important contributions by various mathematicians over the time were presented. All the publicly available literature on transient loss minimization in induction machines were discussed. In solving the problem, it was evident from historical developments that primarily four methodologies were used and that the Euler-Lagrange equation was the most popular. The most used control inputs were stator currents or d-axis rotor flux. Stator and rotor Ohmic losses were considered by almost all researchers. Finally, the contributions of this dissertation to the existing literature were listed.

## 6 OPTIMAL CONTROL OF DC MOTOR

To set the stage for the work of this dissertation, instead of first tackling the transient energy loss minimization problem for an IM, a similar problem for the Permanent Magnet DC (PMDC) motor is presented. Using Pontryagin's minimum principle, the necessary conditions for an optimal trajectory are derived, from which an analytical expression for the optimal armature current is developed.

### 6.1 PMDC Motor Model and Cost Functional

The current fed model for the permanent magnet DC motor (PMDC) is given by state equation (6.1.1) and has rotor speed as the state variable and armature current as the control variable.

$$\frac{d\omega_r}{dt} = \frac{k i_a - T_L}{J}, \omega_r(t_0) = \omega_r^{t_0} \quad (6.1.1)$$

For simplicity, in what follows we assume  $T_L = t_0 = \omega_r^{t_0} = 0$  and  $k_1 = \frac{k}{J}$  and  $k_2 = \frac{k_1}{R_a}$ .

The value of armature current  $i_a$  that would accelerate the machine to a reference speed,  $\omega_r^{ref}$  in time  $t_f$  can be calculated by (6.1.2).

$$i_a = \frac{\omega_r^{ref}}{t_f k_1} \quad (6.1.2)$$

However, the goal here is to minimize Ohmic losses for the DC motor during the transient period. A functional is defined in (6.1.3) that puts a cost on both the Ohmic losses

due to the armature resistance, and the deviation from the reference rotor speed at the end of the transient time interval. A weight  $w_1$  is assigned to the speed deviation.

$$J = w_1 \left( \omega_r^{ref} - \omega_r(t_f) \right)^2 + \int_{t_0}^{t_f} i_a^2(t) R_a dt \quad (6.1.3)$$

## 6.2 Necessary Conditions using Pontryagin's Minimum Principle

Applying the Hamiltonian in (2.3.1) to (6.1.1) and (6.1.3) a new Hamiltonian is created as in (6.2.1) from which the co-state equation (6.2.2) is then derived. The co-state equation can be integrated to obtain (6.2.3).

$$H(\omega_r, i_a) = \left( \frac{k i_a(t)}{J} \right) \lambda(t) + i_a^2(t) R_a \quad (6.2.1)$$

$$\frac{d\lambda}{dt} = -\frac{\partial H}{\partial \omega_r} = 0 \quad (6.2.2)$$

$$\lambda(t) = c_1 \quad (6.2.3)$$

Using the transversality condition and the terminal cost function, the following boundary condition for the co-state is found.

$$\lambda(t_f) = \frac{\partial \left( \omega_r^{ref} - \omega_r(t_f) \right)^2 w_1}{\partial \omega_r} = -2w_1 \left( \omega_r^{ref} - \omega_r(t_f) \right) \quad (6.2.4)$$

The optimal armature current  $i_a^*(t)$  should also satisfy the optimal control equation (6.2.5). The control input (armature current) can then be expressed in terms of the co-state as in (6.2.6). Note that if we substitute (6.2.3) and (6.2.6) back into the Hamiltonian (6.2.1), it's value becomes a constant during the transient as expected (see (2.3.6)).

$$\frac{\partial H(\omega_r, i_a)}{\partial i_a} = k_1 \lambda(t) + 2R_a i_a(t) = 0 \quad (6.2.5)$$

$$i_a(t) = -\left(\frac{k_2}{2}\right)\lambda(t) = -\left(\frac{k_2}{2}\right)c_1 \quad (6.2.6)$$

Integrate the state equation (6.1.1) and substitute (6.2.6) into that to express the rotor speed in terms of the co-state as shown in (6.2.7). Similarly, the terminal rotor speed can be expressed using (6.2.8).

$$\omega_r(t) = k_1 i_a(t) = -\left(\frac{k_1 k_2}{2}\right)c_1 t \quad (6.2.7)$$

$$\omega_r(t_f) = -\left(\frac{k_1 k_2}{2}\right)c_1 t_f \quad (6.2.8)$$

Using (6.2.3), (6.2.4), and (6.2.8) it is possible to obtain the condition (6.2.9), which can be solved to find the co-state  $c_1$  as in (6.2.10).

$$-2w_1 \left( \omega_r^{ref} + \left(\frac{k_1 k_2}{2}\right)c_1 t_f \right) = c_1 \quad (6.2.9)$$

$$c_1 = \frac{-2w_1 \omega_r^{ref}}{1 + w_1 k_1 k_2 t_f} \quad (6.2.10)$$

$c_1$  can now be substituted into (6.2.6) to find the value of the optimal current trajectory (6.2.11) and the terminal rotor speed corresponding to that trajectory (6.2.12).

$$i_a(t) = \frac{w_1 k_2 \omega_r^{ref}}{1 + w_1 k_1 k_2 t_f} \quad (6.2.11)$$

$$\omega_r(t_f) = \frac{w_1 k_1 k_2 \omega_r^{ref}}{1 + w_1 k_1 k_2 t_f} t_f \quad (6.2.12)$$

Finally, by substituting (6.2.11) and (6.2.12) into the cost function (6.1.3) we get the optimal cost (6.2.13). If instead the sub-optimal value of current, as given by (6.1.2), had been used, then the cost function would have been as given in (6.2.14).

$$J_{opt} = \frac{w_1 (\omega_r^{ref})^2}{(1 + k_1 k_2 w_1 t_f)} \quad (6.2.13)$$

$$J_{non-opt} = \left( \frac{\omega_r^{ref}}{t_f k_1} \right)^2 R_a t_f = \frac{(\omega_r^{ref})^2}{t_f k_1 k_2} \quad (6.2.14)$$

$J_{opt}$  will always be smaller than  $J_{non-opt}$ , and as  $w_1$  tends to infinity,  $J_{opt} = J_{non-opt}$ . The above proposed optimal control solution was tested using the DC motor specifications given in Appendix I. Table 6.1 gives the optimal current, energy cost, and current for different speed deviation weights. For comparison, Table 6.1 also gives the cost if the DC motor was accelerated using the sub-optimal current calculated through (6.1.2). As expected, these results show that the value of the optimized objective function is always smaller than that of the sub-optimal control. Also, as  $w_1$  increases the optimal current converges to the same value as that of the non-optimal control.

*Table 6.1. Comparing optimal control and non-optimal control in PMDC Motor*

Weight ( $w_1$ )	Current (A)	Energy cost (J)	Terminal speed (rad/s)	Speed Deviation (rad/s)	Objective function
Optimal control					
1	15.78947	498	94.73	5.26	526.31
2.5	16.30435	531	97.82	2.17	543.47
100	16.65741	554.938786	99.94	0.055525	555.24
Non- optimal control					
NA	16.67	555.55	100	0	555.55

The derivation of the optimal control trajectory for PMDC was an illustration of how solutions for even simple optimal control problems are neither intuitive nor trivial.

### 6.3 Summary

This chapter presented the application of Pontryagin's minimum principle for finding the optimal control law for the armature current to accelerate a PMDC motor.

## 7 NECESSARY CONDITIONS FOR OPTIMAL CONTROL IN INDUCTION MACHINE

This chapter presents the optimal control problem formulation for IM transient loss minimization purposes. First, the rotor field oriented model is presented and sub-optimal control trajectories are analyzed. The power losses are expressed in terms of the variables in the model. Finally, the minimum principle is applied to derive the necessary conditions.

### 7.1 Rotor Field Oriented IM Model

The current fed model of the IM in section 4.6 can be further simplified if we assume that the entire rotor flux vector lies on the d-axis of the rotating frame of reference. This can be accomplished by manipulating the electrical frequency using (7.1.1). [15] provides a detailed explanation of the reasoning behind it. Note that this concept is used in almost all commercially available IM drives for achieving high precision speed control [52].

$$\omega_{sync}(t) = \omega_r(t) + \frac{R_r L_m}{L_r \psi_{dr}(t)} i_{qs}(t) \quad (7.1.1)$$

With the above manipulation, the rotor flux along the q-axis of transformation would be  $\Psi_{qr} = 0$ , and  $\frac{d\Psi_{qr}}{dt} = 0$ . Hence equations (4.6.1) to (4.6.3) may be rewritten as (7.1.2) to (7.1.4). It can be noted that in a rotor field oriented IM the stator currents are decoupled from each other i.e. if we try to change one it will not affect the other. This allows us to have a simple control scheme to independently control rotor flux and electromagnetic torque.

$$\frac{d\psi_{dr}}{dt} = \left( \frac{R_r}{L_r} \right) (L_m i_{ds}(t) - \psi_{dr}(t)) \quad (7.1.2)$$

$$\frac{d\omega_r}{dt} = \left( \frac{p}{2} \right) \left( \frac{\left( \frac{pL_m}{2L_r} \right) i_{qs}(t) \psi_{dr}(t) - T_L}{J} \right) \quad (7.1.3)$$

$$\omega_r(t_0) = \omega_r^0, \psi_{dr}(t_0) = \psi_{dr}^0 \quad (7.1.4)$$

where  $\psi_{dr}^0$  is the initial value of the rotor flux along the d-axis and  $\omega_r^0$  is the initial rotor speed.

In (7.1.4),  $\omega_r$  corresponds to the rotor speed in electrical radians per second, also referred to as the electrical speed. Rotor speed can also be expressed in terms of the mechanical radians per second as shown in (7.1.5), which is referred to as the mechanical speed of the machine. Speed encoders used for measuring the rotor speed measure the mechanical speed. The mechanical power output at the rotor shaft is calculated using this mechanical speed.

$$\omega_m = 2 \frac{\omega_r}{p} \quad (7.1.5)$$

From here onward all the expressions for rotor speed will be written in terms of the mechanical speed.

## 7.2 Analysis of the IM Model

This section discusses the different trajectories that can be taken by state and control variables of the rotor field oriented current fed IM model when it is accelerating from one operating point to another.



Using Newton's 2nd law, it is possible to calculate the torque required to increase (or decrease) the speed of a rotating body from one operating point to another as given by (7.2.1). After reaching steady state, the torque required for maintaining the steady state speed is equal to the load torque (7.2.2).

$$T_{accel} = J \frac{d\omega}{dt} + T_L \quad (7.2.1)$$

$$T_{steady} = T_L \quad (7.2.2)$$

where  $\frac{d\omega}{dt}$  is the acceleration of the rotor.

It is obvious that  $|T_{accel}| > |T_{steady}|$  in most scenarios, which means that the torque produced by the IM during transients should be much higher than what is required at steady state. The ideal case would be for the IM torque to transition instantaneously from  $T_{accel}$  to  $T_{steady}$  at the end of the transient time interval. However, this does not happen in practice, and torque transients result in rotor speeds overshooting the desired steady state reference speed. The constraint on the electromagnetic torque may be expressed using (7.2.3). Also from (7.1.3) the expression for electromagnetic torque can be separated and written as in (7.2.4).

$$T_e = \begin{cases} T_{accel}, & t \leq t_{transient} \\ T_{steady}, & t > t_{transient} \end{cases} \quad (7.2.3)$$

$$T_e = \left( \frac{pL_m}{2L_r} \right) i_{qs}(t) \psi_{dr}(t) \quad (7.2.4)$$

It can be observed that  $T_e$  can be manipulated by changing the q-axis stator current  $i_{qs}$ , while keeping the d-axis rotor flux  $\Psi_{dr}$  constant or vice versa. There is also the possibility of changing both current and flux at the same time.

However, rotor flux cannot be changed instantaneously. For a step change in d-axis stator current  $i_{ds}$ , the state equation for rotor flux (7.1.2) can be solved to get (7.2.5). It can be observed that the rotor flux has a first order response with a time constant  $\tau_r$ . This means that using only rotor flux to manipulate torque production would result in a slower speed response. Additionally, from (7.2.5), the value of rotor flux at steady state is equal to  $L_m i_{ds}$ . The mutual inductance  $L_m$  can take a magnitude in the range of  $10^{-3}$  to  $10^{-1}$ . Hence the range of values through which flux can be manipulated is much smaller than what is possible with q-axis current. Hence, changing  $T_e$  and consequently the rotor speed, requires that, in addition to the rotor flux,  $i_{qs}$  is also changed. This means that the rotor flux  $\Psi_{dr}$  need not be constant during the accelerating and/or decelerating periods.

$$\psi_{dr}(t) = L_m i_{ds} - (L_m i_{ds} - \psi_{dr}^0) e^{-\frac{t}{\tau_r}} \quad (7.2.5)$$

where,  $\tau_r = \frac{L_r}{R_r}$ .

We can identify four feasible regimes for the control trajectories.

- 1) Regime I: Constant electromagnetic torque  $T_e$  and constant acceleration  $\frac{d\omega}{dt}$ . In this case the rotor flux  $\Psi_{dr}$  remains constant. A step change is made in the q-axis stator current  $i_{qs}$  at the start of the accelerating period followed by a step change at the end of the accelerating period.

- 2) Regime II: Constant  $T_e$  and constant  $\frac{d\omega}{dt} \cdot \Psi_{dr}$  changes due to a step change in  $i_{qs}$ .  
 $i_{qs}$  changes w.r.t.  $\Psi_{dr}$  in order to maintain  $T_e$  constant.
- 3) Regime III: Time variant  $T_e$ , time variant  $\frac{d\omega}{dt} \cdot \Psi_{dr}$  remains constant,  $i_{qs}$  changes depending on  $\frac{d\omega}{dt}$ .
- 4) Regime IV: Time variant  $T_e$ , time variant  $\frac{d\omega}{dt}$ . Both  $\Psi_{dr}$  and  $i_{qs}$  change.

The first, second, and third regimes are discussed in the following sections. Regime IV is the optimal control regime that will be obtained from derivations in Section 7.6 and Chapter 11 of the dissertation. Regime IV will be implemented in real time using the work in Chapter 10 of this document. The following sections of this chapter discuss details of the first, second, and third regimes of the control trajectories.

### 7.2.1 Regime I

The d-axis and q-axis stator current trajectories may be expressed using (7.2.1.1) and (7.2.1.2), respectively. Here the change in reference speed is a step function. There is no change in rotor flux  $\Psi_{dr}$  since there is no change in d-axis current as shown in (7.2.1.3). This regime approximates the behavior of PI speed control loops used in most IM drives.

$$i_{ds}(t) = i_{ds}^a, \quad \text{for all } t \quad (7.2.1.1)$$

$$i_{qs}(t) = \begin{cases} \frac{T_{accel}}{pk\Psi_{dr}^a}, & t_0 < t \leq t_f \\ \frac{T_{steady}}{pk\Psi_{dr}^a}, & t > t_f \end{cases} \quad (7.2.1.2)$$

$$\Psi_{dr}(t) = \Psi_{dr}^a, \quad \text{for all } t \quad (7.2.1.3)$$

where  $\Psi_{dr}^a$  is the rated steady state rotor flux while  $i_{ds}^a$  is the stator d-axis current required to produce this flux.

### 7.2.2 Regime II

The d-axis and q-axis stator current trajectories may be expressed using (7.2.2.1) and (7.2.2.2), respectively. Here the change in reference speed and rotor flux is a step function.

The change in rotor flux corresponding to change in d-axis current is given by (7.2.2.3).

$$i_{ds}(t) = \begin{cases} i_{ds}^a, & t < t_0 \\ i_{ds}^b, & t \geq t_0 \end{cases} \quad (7.2.2.1)$$

$$i_{qs}(t) = \begin{cases} \frac{T_{accel}}{pk\psi_{dr}(t)}, & t_0 \leq t \leq t_f \\ \frac{T_{steady}}{pk\psi_{dr}(t)}, & t > t_f \end{cases} \quad (7.2.2.2)$$

$$\psi_{dr}(t) = L_m i_{ds}^b - (L_m i_{ds}^b - \Psi_{dr}^a) e^{\frac{-t}{\tau_r}}, \quad t > t_0 \quad (7.2.2.3)$$

where  $\Psi_{dr}^a$  is the steady state rotor flux at the start of transient time and  $i_{ds}^b$  is the stator d-axis current required to establish a new steady state rotor flux.

### 7.2.3 Regime III

In Regime I and Regime II the change in reference speed is assumed to be a step function while in Regime III a ramp function as described by (7.2.3.1) is used instead. This regime approximates the behavior of practical electric drives more closely.

$$\omega_{ref} = \begin{cases} \omega_0 + kt, & t \leq t_{tf} \\ \omega_{ref}^{tf}, & t > t_{tf} \end{cases} \quad (7.2.3.1)$$

#### 7.2.4 Rotor speed corresponding to Regime I and Regime II

In both Regime I, and Regime II the electromagnetic torque generated during transients is constant, and hence acceleration is constant. The rotor speed may be expressed as a ramp function (7.2.4.1) with a constant coefficient. It is assumed that load torque  $T_L$  is a constant during the transient.

$$\omega_m(t) = \left( \frac{T_e - T_L}{J} \right) t + \omega_m^0 \quad (7.2.4.1)$$

#### 7.3 Energy Loss Functions

Power losses inside an IM can be expressed using either current, flux, or voltage variables. For setting up the optimal control problem the losses should be expressed in terms of variables present in the IM model. Hence, we describe the power losses in terms of rotor d-axis flux  $\Psi_{dr}$ , rotor speed  $\omega_r$ , stator d-axis current  $i_{ds}$ , and stator q-axis current  $i_{qs}$  which are all present in the current fed field oriented model of the IM described in section 7.1. The Ohmic losses in the stator and rotor circuits are given by (7.3.1) and (7.3.2) [53].

$$P_{loss}^{stator}(t) = (i_{ds}^2(t) + i_{qs}^2(t)) R_s \quad (7.3.1)$$

$$P_{loss}^{rotor}(t) = (i_{dr}^2(t) + i_{qr}^2(t)) R_r = \frac{R_r}{L_r^2} \left( (\psi_{dr}(t) - L_m i_{ds}(t))^2 + L_m^2 i_{qs}^2(t) \right) \quad (7.3.2)$$

In case of stator iron losses, eddy current losses are proportional to the square of frequency while hysteresis loss is not. Since the IM usually operates in the range of 5 Hz to 60 Hz the hysteresis loss is only a small fraction of eddy current losses, and hence are not part of the loss function. Furthermore, both the hysteresis, and eddy current losses in the rotor circuit are ignored since the frequency of current through the rotor is much lower

than the frequency of current in the stator. Using the equation for eddy current losses given in [53], we get (7.3.3).

$$P_{loss}^{eddy}(t) = \frac{L_m^2 L_{lr}^2}{L_r^2 R_m} \omega_{sync}^2(t) i_{qs}^2(t) + \frac{L_m^2}{R_m} \omega_{sync}^2(t) i_{ds}^2(t) \quad (7.3.3)$$

where  $L_{lr}$  is the rotor leakage inductance and  $R_m$  is the resistance corresponding to the eddy current losses.

$\omega_{sync}$  in (7.3.3) may be replaced by (7.1.1) since we are using a rotor field oriented model of the IM. However, the rotor slip, i.e. the difference between synchronous speed  $\omega_{sync}$  and rotor speed  $\omega_r$  (in electrical rad/s) is very small during most of the transient periods. Hence, this substitution will unnecessarily complicate the loss function in (7.3.3) without significant improvement in the accuracy of power loss calculations. Hence,  $\omega_{sync}$  is instead replaced with  $\omega_r = \frac{p}{2} \omega_m$  in (7.3.3). It can be observed that all loss functions are expressed in terms of either the state variables or control inputs to the IM model.

### 7.3.1 Power loss in terms of rotor d-axis flux at steady state

It is possible to substitute for the d-axis and q-axis currents in terms of rotor flux during steady state using (7.3.1.1) and (7.3.1.2) and express the total loss purely in terms of only rotor flux (7.3.1.3).

$$i_{ds} = \frac{\Psi_{dr}}{L_m} \quad (7.3.1.1)$$

$$i_{qs} = \frac{2L_r T_L}{pL_m \Psi_{dr}} \quad (7.3.1.2)$$

$$P_{loss}^{total} = \left( \left( \frac{\psi_{dr}}{L_m} \right)^2 + \left( \frac{2L_r T_L}{pL_m \psi_{dr}} \right)^2 \right) R_s + R_r \left( \frac{2T_L}{p\psi_{dr}} \right)^2 + \frac{L_{lr}^2 p^2 \omega_m^2}{R_m 4} \left( \frac{2T_L}{p\psi_{dr}} \right)^2 + \frac{1}{R_m} \frac{p^2 \omega_m^2}{4} \psi_{dr}^2 \quad (7.3.1.3)$$

### 7.3.2 Mechanical Power output

The mechanical power produced from a rotating machine is simply the product of speed and torque. The calculation is straight forward if the machine is in steady state since the electromagnetic torque produced by the machine is equal to the load torque (ignoring the rotational torque). However, this is not the case during transients where the electromagnetic torque will be different from the load torque. This is because during transients, a fraction of mechanical power output is stored as kinetic energy in the rotor mass. Hence, (7.3.2.1) gives total mechanical power produced, while (7.3.2.2) gives the mechanical power output available at the shaft of the motor. The relationship between the two is given by (7.3.2.3).

$$P_{mech\_total} = \omega_m(t) T_e(t) \quad (7.3.2.1)$$

$$P_{mech\_out} = \omega_m(t) T_L \quad (7.3.2.2)$$

$$P_{mech\_total} = J \omega_m(t) \frac{d\omega_m}{dt} + P_{mech\_out} \quad (7.3.2.3)$$

### 7.4 Optimal Flux at Steady State

The rotor flux variable provides an additional degree of freedom to produce the necessary torque. Also, the total power loss can be expressed purely in terms of rotor flux, as shown in (7.3.1.3) above. We can utilize these facts to calculate the optimal flux at a steady state speed-torque operating point, i.e. the flux that results in a minimum power loss.

For this, we take the derivative of  $P_{loss}^{total}$  in terms of rotor flux and equate it to 0 (zero) as

shown in (7.4.1). It is possible to arrive at an expression for the optimal value of the steady state flux as in (7.4.2). The full derivation of (7.4.2) is given in Appendix III

$$\frac{\partial P_{loss}^{total}}{\partial \psi_{dr}} = 2R_s \left( \frac{1}{L_m} \right)^2 \psi_{dr} - 8 \left( \frac{L_r T_L}{p L_m} \right)^2 \frac{R_s}{(\psi_{dr})^3} - 8R_r \left( \frac{T_L}{p} \right)^2 \frac{1}{(\psi_{dr})^3} - \quad (7.4.1)$$

$$2 \frac{L_{lr}^2 \omega_m^2}{R_m} \left( \frac{T_L}{p} \right)^2 \frac{1}{(\psi_{dr})^3} + \frac{\omega_m^2}{2R_m} \psi_{dr} = 0$$

$$\psi_{dr}^{opt} = \left( \frac{2T_L}{p} \right)^{\frac{1}{2}} \left( \frac{R_s R_m L_r^2 + R_r R_m L_m^2 + \omega_m^2 L_{lr}^2 L_m^2}{R_s R_m + \omega_m^2 L_m^2} \right)^{\frac{1}{4}} \quad (7.4.2)$$

Note that the optimal steady state flux in (7.4.2) is directly proportional to square root of the load torque  $T_L$  (which is equivalent to the electromagnetic torque produced by the IM), and inversely proportional to the square root of rotor speed  $\omega_m$ . Now if the optimal steady state rotor flux in (7.4.2) were to be used during transients, by replacing  $T_L$  with  $T_{accel}$  and  $\omega_m$  with the current rotor speed, it would certainly give an approximate value of the optimal flux during transients. However, there are two problems with using this value.

- 1) The d-axis stator current needed to generate a specific value of rotor d-axis flux can be calculated using (7.4.3). The magnitude of this required current is directly proportional to the rate of change of rotor flux. This means that trying to change the rotor flux instantaneously will result in a very large d-axis current and the Ohmic losses associated with it. This would negate any decrease in power losses in the IM due to operating at optimal rotor flux.



$$i_{ds}(t) = \frac{1}{L_m} \left( \frac{L_r}{R_r} \left( \frac{d\psi_{dr}}{dt} \right) + \psi_{dr}^0 \right) \quad (7.4.3)$$

2) The rotor speed is continuously changing during transients. Hence, the optimal rotor flux calculated using (7.4.2) for the rotor speed at start of a transient would become sub-optimal as soon as the rotor speed has substantially changed from its initial value.

However, one possible approach to this issue is to start with changing the rotor flux at the beginning of a transient so that it would reach its optimal value soon after the rotor speed has reached a steady state. The approach of changing rotor flux for each change in the speed-torque operating point has already been used in works like [54].

## 7.5 Cost Functional

The energy loss during transient time interval  $t_0$  to  $t_{t_f}$  is represented by the cost functional  $E_{loss}$  in (7.5.1).

$$E_{loss} = \int_{t_0}^{t_f} \left( P_{loss}^{stator}(t) + P_{loss}^{rotor}(t) + P_{loss}^{eddy}(t) \right) dt \quad (7.5.1)$$

where  $P_{loss}^{stator}$  is the stator Ohmic power loss,  $P_{loss}^{rotor}$  is the rotor Ohmic power loss, and  $P_{loss}^{eddy}$  is the eddy current power loss at time  $t$ . Note that the unit for the power loss is in Watts and that of energy loss is in Joules.

It is desired that the rotor speed  $\omega_m$  reaches the reference speed  $\omega_m^{ref}$  within the transient time interval. In addition, it is desirable that the rotor flux,  $\Psi_{dr}$ , converges to the optimal steady state flux,  $\Psi_{dr}^{opt}$ , and the electromagnetic torque,  $T_e$ , converges to load torque,  $T_L$ . These constraints are enforced by assigning a penalty for deviation from the desired steady state operating points using the terminal cost function in (7.5.2).

$$\phi = w_1 \left( \omega_m^{t_f} - \omega_m^{ref} \right)^2 + w_2 \left( T_e^{t_f} - T_L \right)^2 + w_3 \left( \Psi_{dr}^{t_f} - \Psi_{dr}^{opt} \right)^2 \quad (7.5.2)$$

where  $T_e^{t_f}$  is the electromagnetic torque generated at the end of the transient period,  $\omega_m^{t_f}$  is the rotor speed at end of transient period, and  $\Psi_{dr}^{t_f}$  is the rotor d-axis flux at end of the transient period.

Combining (7.5.1) and (7.5.2) results in (7.5.3), which is known as the Bolza form of the cost functional and has to be minimized in the optimal control problem under study. The optimal scenario would be for (7.5.1) to take a non-zero positive value (since a loss free energy conversion is impossible) and for (7.5.2) to become zero.

$$J = E_{loss} + \phi \quad (7.5.3)$$

#### 7.5.1 Reasoning behind setting terminal values of flux, rotor speed, and torque

To solve the IM optimal control problem discussed in this dissertation it is necessary to specify  $\Psi_{dr}^{t_f}$ ,  $\omega_m^{t_f}$ , and  $T_e^{t_f}$ . In case of the  $\omega_m^{t_f}$ , and  $T_e^{t_f}$  the choice is straightforward since the load torque and reference speed constrains them. We want the rotor speed  $\omega_m$  to attain a specific reference speed, and the  $T_e$  to become equal to the load torque at the end of the transient interval. The choice for rotor flux is less obvious since it can take any value between a minimum and maximum limit. However, if the  $\Psi_{dr}^{t_f}$  attains a value that is close to the optimal steady state flux that was calculated by (7.4.2) in section 7.4, the steady state energy losses of the IM would also be minimized. Hence,  $\Psi_{dr}^{t_f}$  may be replaced by  $\Psi_{dr}^{opt}$  of (7.4.2) in the terminal cost function.

## 7.6 Deriving the Necessary Conditions for Optimal Control

To apply Pontryagin's minimum principle we first create the Hamiltonian function in (7.6.1) using (2.3.1) from section 2.3. Here,  $g(x, u, t)$  corresponds to the sum of equations (7.3.1), (7.3.2), and (7.3.3).  $f(x, u, t)$  corresponds to (7.1.2) and (7.1.3).  $\phi(t_f)$  corresponds to (7.5.2).

$$\begin{aligned}
 H(\psi_{dr}, \omega_m, i_{ds}, i_{qs}) = & (i_{ds}^2 + i_{qs}^2)R_s + \frac{R_r}{L_r^2} \left( (\psi_{dr} - L_m i_{ds})^2 + L_m^2 i_{qs}^2 \right) + \\
 & \frac{L_m^2 L_{lr}^2 p^2}{2L_r^2 R_m} \omega_m^2 i_{qs}^2 + \frac{L_m^2 p^2}{2R_m} \omega_m^2 i_{ds}^2 + \\
 & \left( \frac{R_r}{L_r} \right) (L_m i_{ds} - \psi_{dr}) \lambda_1 + \left( \frac{\left( \frac{pL_m}{2L_r} \right) i_{qs} \psi_{dr} - T_L}{J} \right) \lambda_2
 \end{aligned}
 \tag{7.6.1}$$

From the above Hamiltonian, the co-state equations are derived using (2.3.6), from Section 2.3 and given by (7.6.2) and (7.6.3). The terminal conditions for the co-states are found using the transversality conditions from (2.3.7), and they form one set of boundary conditions as shown in (7.6.4) and (7.6.5).

$$\frac{d\lambda_1}{dt} = -\frac{\partial H}{\partial \psi_{dr}} = \frac{2R_r}{L_r^2} (L_m i_{ds} - \psi_{dr}) + \frac{R_r}{L_r} \lambda_1 - \frac{pL_r}{2L_r J} i_{qs} \lambda_2
 \tag{7.6.2}$$

$$\frac{d\lambda_2}{dt} = -\frac{\partial H}{\partial \omega_r} = -\frac{p^2 L_m^2}{R_m} \left( \frac{L_{lr}^2}{L_r^2} \omega_m^2 i_{qs}^2 + \omega_m^2 i_{ds}^2 \right)
 \tag{7.6.3}$$

$$\lambda_1(t_f) = \frac{\partial \phi}{\partial \psi_{dr}^{t_f}} = w_2 \left( \frac{p^2 L_m^2}{2L_r^2} \psi_{dr}^{t_f} (i_{qs}^{t_f})^2 - \frac{pT_L i_{qs}^{t_f} L_m}{2L_r} \right) + 2w_3 (\psi_{dr}^{t_f} - \psi_{dr}^{opt})
 \tag{7.6.4}$$

$$\lambda_2(t_f) = 2w_1(\omega_m^{t_f} - \omega_m^{ref}) \quad (7.6.5)$$

State equations are derived using (2.3.5). However, they are the same as (7.1.2) and (7.1.3), and hence not reproduced here. The initial value for the states in (7.1.4) forms the second set of boundary conditions. Finally, the optimal control equation is derived using (2.3.3). The optimal control equations corresponding to  $i_{ds}$  and  $i_{qs}$  are given by (7.6.6) and (7.6.7), respectively. The second derivative of the Hamiltonian given by (7.6.8) and (7.6.9) is always positive, which guarantees that the optimal trajectories for  $i_{qs}$  and  $i_{ds}$ , which satisfy (7.6.6) and (7.6.7), will cause the Hamiltonian to be a strong local minimum.

$$\frac{\partial H(\psi_{dr}, \omega_m, i_{ds}, i_{qs})}{\partial i_{qs}} = 2 \left( \frac{L_m^2 L_r^2 p^2}{2L_r^2 R_m} \omega_m^2 + \frac{L_m^2}{L_r^2} R_r + R_s \right) i_{qs} + \frac{pL_m}{2L_r J} \psi_{dr} \lambda_2 = 0 \quad (7.6.6)$$

$$\begin{aligned} \frac{\partial H(\psi_{dr}, \omega_m, i_{ds}, i_{qs})}{\partial i_{ds}} &= 2 \left( \frac{L_m^2 p^2}{2R_m} \omega_m^2 + \frac{L_m^2}{L_r^2} R_r + R_s \right) i_{ds} \\ &\quad - \frac{2L_m R_r}{L_r^2} \psi_{dr} + \frac{L_m R_r}{L_r} \lambda_1 = 0 \end{aligned} \quad (7.6.7)$$

$$\frac{\partial H(\psi_{dr}, \omega_m, i_{ds}, i_{qs})}{\partial i_{qs}^2} = 2 \left( \frac{L_m^2 L_r^2 p^2}{2L_r^2 R_m} \omega_m^2 + \frac{L_m^2}{L_r^2} R_r + R_s \right) > 0 \quad (7.6.9)$$

$$\frac{\partial^2 H(\psi_{dr}, \omega_m, i_{ds}, i_{qs})}{\partial i_{ds}^2} = 2 \left( R_s + \frac{L_m^2}{L_r^2} R_r + \frac{L_m^2 p^2}{2R_m} \omega_m^2 \right) > 0 \quad (7.6.8)$$

From (7.6.6) and (7.6.7) it is possible to express the optimal trajectories of  $i_{qs}$  and  $i_{ds}$  as a function of the state and co-state trajectories:

$$i_{qs}^*(t) = \frac{-\frac{pL_m}{2L_r J} \psi_{dr}(t) \lambda_2(t)}{2 \left( \frac{L_m^2 L_r^2 p^2}{2L_r^2 R_m} \omega_m^2(t) + \frac{L_m^2}{L_r^2} R_r + R_s \right)} \quad (7.6.10)$$

$$i_{ds}^*(t) = \frac{\frac{2L_m R_r}{L_r^2} \psi_{dr}(t) - \frac{L_m R_r}{L_r} \lambda_1(t)}{2 \left( \frac{L_m^2 p^2}{2R_m} \omega_m^2(t) + \frac{L_m^2}{L_r^2} R_r + R_s \right)} \quad (7.6.11)$$

To summarize, the necessary conditions for IM transient energy loss minimization problem consists of:

- 1) 4 first order non-linear ODE's (two for states, two for co-states)
- 2) 2 non-linear algebraic equations (one for each control input)
- 3) 4 boundary conditions (two for state, two for co-states).

If we were to substitute (7.6.10) and (7.6.11) into the state and co-state equations it would be possible to get a system of ODE's purely in terms of the state and co-state variables. However, this would also result in the system of ODE's becoming more non-linear. It is not practically possible to find a closed form solution of such a system of equations. Hence, the only recourse is to find a numerical solution for the state and control trajectories that satisfy the necessary conditions, which is the objective of the next chapter.

## 7.7 Summary

This objective of this chapter was to derive the necessary conditions for the transient energy loss optimal control problem of this work using the Pontryagin's minimum principle. For this purpose, the current fed model of the IM was presented. The power

losses in the IM were expressed in terms of the state and control variables of the IM model. This model was analyzed and sub-optimal trajectories for the control inputs were discussed. The expression for optimal rotor flux at steady state was derived. The final section of this chapter derived all the necessary conditions for the optimal control solution.

## 8 NUMERICAL SOLUTION OF INDUCTION MACHINE OPTIMAL CONTROL PROBLEM

The state and co-state equations, along with their four boundary values (two initial and two final) constitute a two-point boundary value problem (TPBVP). A trajectory of the control inputs that solves the TPBVP will also be the optimal control trajectory. There are primarily two iterative methods for solving the TPBVP problem numerically.

- 1) Gradient method
- 2) Shooting method

Gradient method is of two types: Steepest Descent and Conjugate Gradient (CG) [55]. The nonlinear form of CG method is used in this dissertation.

### 8.1 Modified Conjugate Gradient Method

In the gradient method, the state equations are integrated forward through the transient time interval, i.e. from  $t_0$  to  $t_f$ , with the starting point provided by the initial conditions. The co-state equations are integrated backwards, i.e. from  $t_f$  to  $t_0$ , with the starting point provided by the terminal condition of the co-state. For the control input we would begin by assuming an optimal control trajectory for the entire transient time interval. In doing this we are implicitly assuming that the necessary conditions for states and co-states are satisfied while the necessary condition for control inputs, i.e. the optimal control equation, is not satisfied. The control trajectory is then updated in the succeeding iterations so that it would become closer and closer to satisfying the optimal control equation. The direction of the update is found using the gradient of the Hamiltonian w.r.t. the control inputs, and

the magnitude of the update is controlled using a scalar value known as the step length. Also in CG (as opposed to steepest descent), the direction of update is orthogonal to the direction of the gradient. The update rule of the CG algorithm is given by (8.1.1).

$$u^{i+1} = u^i + \tau d^i \quad (8.1.1)$$

$$d^i = \left\{ \begin{array}{l} -\left. \frac{\partial H}{\partial u} \right|^i, i = 1 \\ -\left. \frac{\partial H}{\partial u} \right|^i + \beta^i d^{i-1}, i \geq 2 \end{array} \right\} \quad (8.1.2)$$

where  $u^i$  is the control trajectory at the  $i^{\text{th}}$  iteration,  $\tau$  is the step length,  $d^i$  is the direction of the updates in the control trajectory, and  $\beta^i$  is defined below.

However, the update rule  $d^i$  for the standard CG algorithm is highly sensitive to the step length  $\tau$  which can result in the solution becoming unstable if the step size is not optimal. Instead of calculating the optimal step size in each iteration, the direction  $d^i$  was modified using the coefficient  $\beta$ . The Hestenes-Steifel formula [56] shown in (8.1.3) was used to calculate  $\beta$ .

$$\beta^i = \left[ \frac{dH^i}{dt} \right]^T \left[ \frac{dH^i}{dt} - \frac{dH^{i-1}}{dt} \right] + d^{i-1} \left[ \frac{dH^i}{dt} - \frac{dH^{i-1}}{dt} \right] \quad (8.1.3)$$

Using the above modified CG algorithm made it possible for the solution to converge to the desired control trajectories for the majority of the IM optimal control problems in a reasonable amount of time. The norm of the Hamiltonian gradient given by (8.1.4) was used as a performance measure to determine if the numerical solution was converging.



$$\left| \frac{\partial H^i}{\partial u^i} \right|^2 = \int_{t_0}^{t_f} \left( \frac{\partial H^i}{\partial u^i} \right)^T \frac{\partial H^i}{\partial u^i} dt \quad (8.1.4)$$

A flow chart for the modified CG algorithm to find the numerical solution of the optimal control trajectories is shown in Figure 8.1.

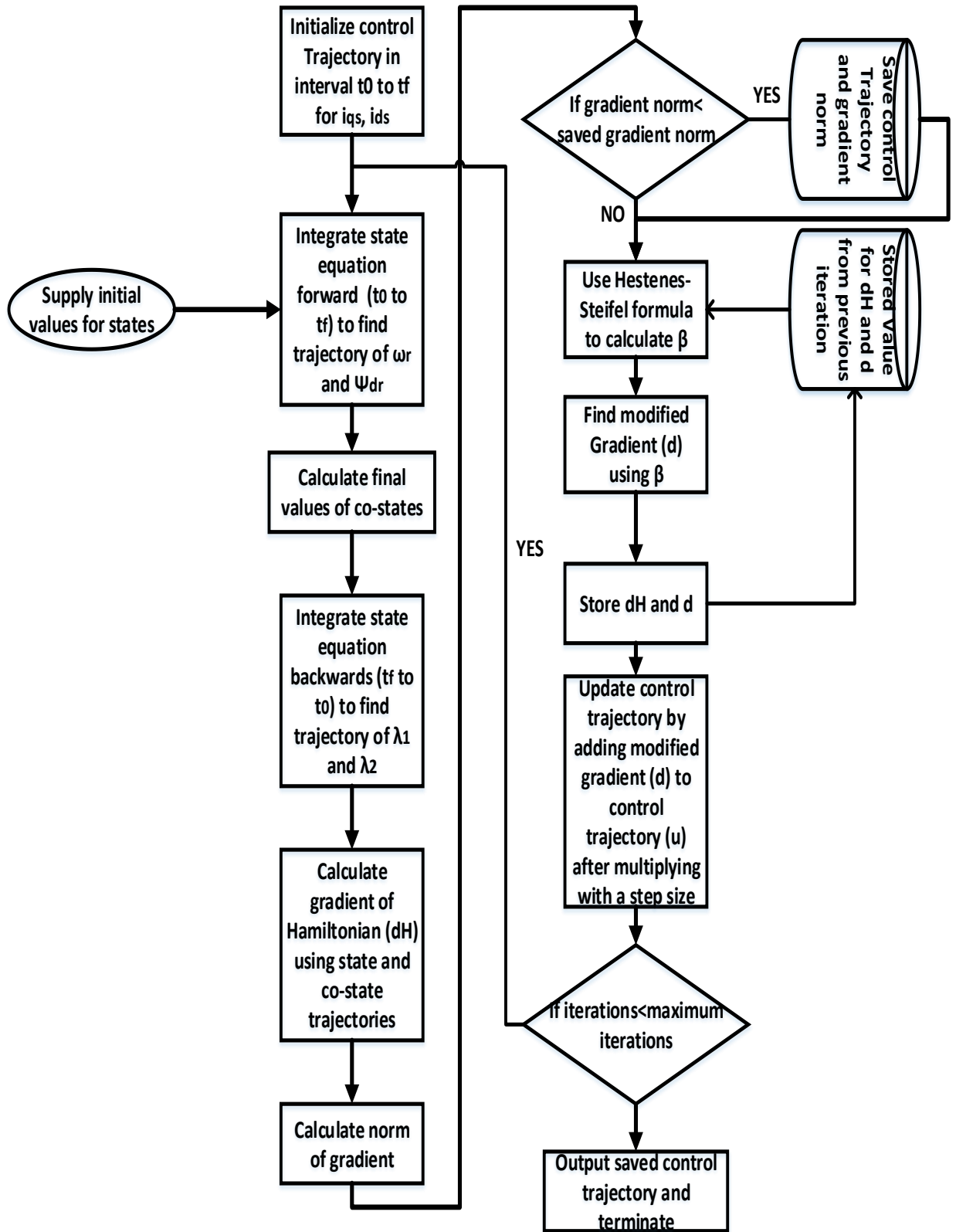


Figure 8.1. Applying the modified CG algorithm to find numerical solution of optimal trajectories

## 8.2 Numerical Solution Example – Scenario 1

In this section, the modified CG algorithm in section 8.1 will be used to solve the TPBVP defined in section 7.6 for different cases and types of IM's. Five parameter values define each of the study cases: initial rotor d-axis flux  $\Psi_{dr}^{opt}$ , initial rotor speed  $\omega_m^0$ , load torque  $T_L$ , reference rotor speed  $\omega_m^{ref}$ , and reference rotor d-axis flux  $\Psi_{dr}^{opt}$ . During this research work the problem has been solved for six different types of IM's. However, only the result for two of the machines are presented here. They are: Type I IM whose parameters were obtained from finite element model in ANSYS Maxwell software and Type II IM from [48]. The parameters of the machines are given in Table I and Table II of Appendix II, respectively. Scenario 1 and scenario 2 correspond to Type I IM and Type II IM, respectively. Each scenario consists of 6 cases as shown in Table 8.1 and Table 8.2. Note that referring to the IM's as Type I and Type II is only for ease of reference and do not correspond to classification provided by NEMA or IEC.

### 8.2.1 Scenario 1 - Optimal

The plots for optimal state trajectories (w.r.t. time) are shown in Figures 8.2 and 8.3. The plots for optimal q- and d-axis stator currents are given by Figures 8.4 and 8.5. The trajectories of co-states are given by Figures 8.6 and 8.7. The electromagnetic torque generated by the IM during transients is shown in Figure 8.8. Finally, the mechanical power produced by the IM is calculated using (7.3.2.1) from the speed and torque trajectories and is given in Figure 8.9. Note that all cases of a similar type of trajectory are shown on the same plot.

Table 8.1. Scenarios for testing IM optimal control problem using Type I IM

Scenario	$\Psi_{dr}^0$ (Wb)	$\omega_r^0$ (rad/s)	$T_L$ (Nm)	$\omega_r^{ref}$ (rad/s)	$\Psi_{dr}^{opt}$ (Wb)	Time interval (s)
1.1	0.5	0	10	90	0.76	0.5
1.2	0.5	0	5	90	0.53	0.5
1.3	0.5	0	1	180	0.3	0.5
1.4	0.5	0	10	50	0.79	0.5
1.5	0.5	0	10	150	0.70	0.5
1.6	0.5	0	15	150	0.86	0.5

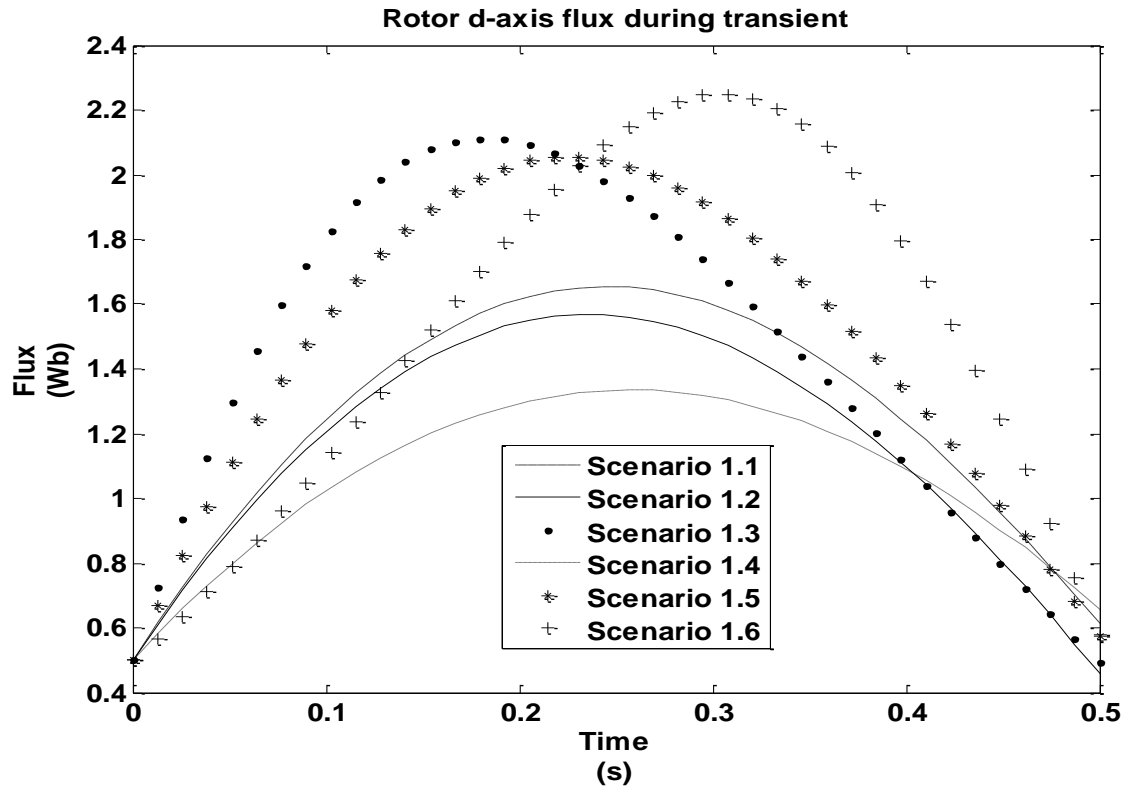


Figure 8.2. Trajectory for rotor d-axis flux (Scenario 1- optimal)

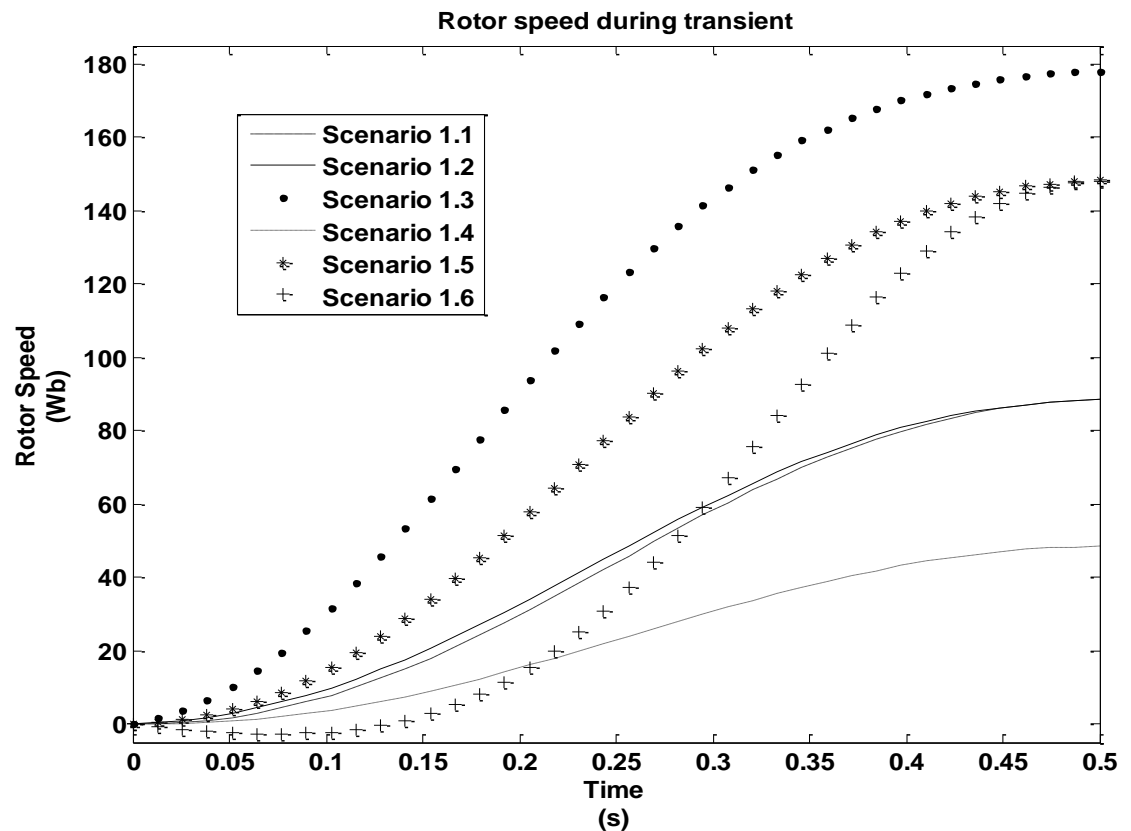


Figure 8.3. Trajectory for rotor speed (Scenario 1 - optimal).

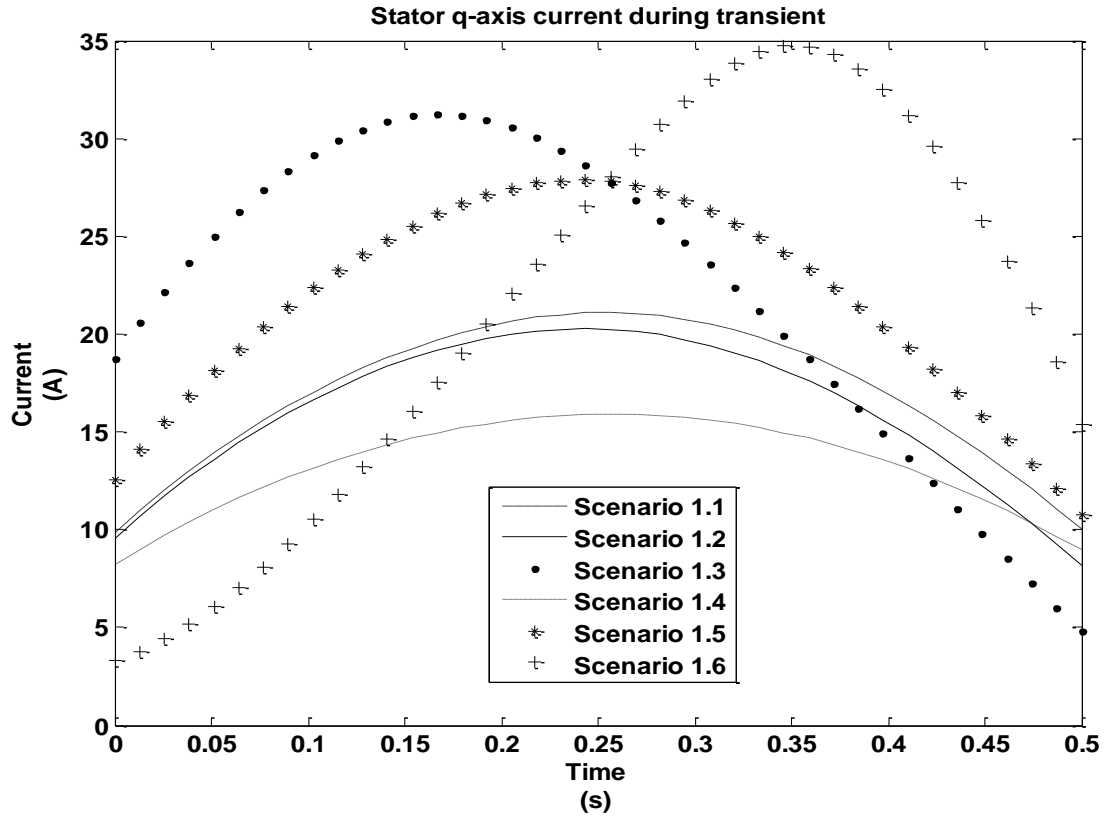


Figure 8.4. Trajectory for q-axis current (Scenario 1- optimal).

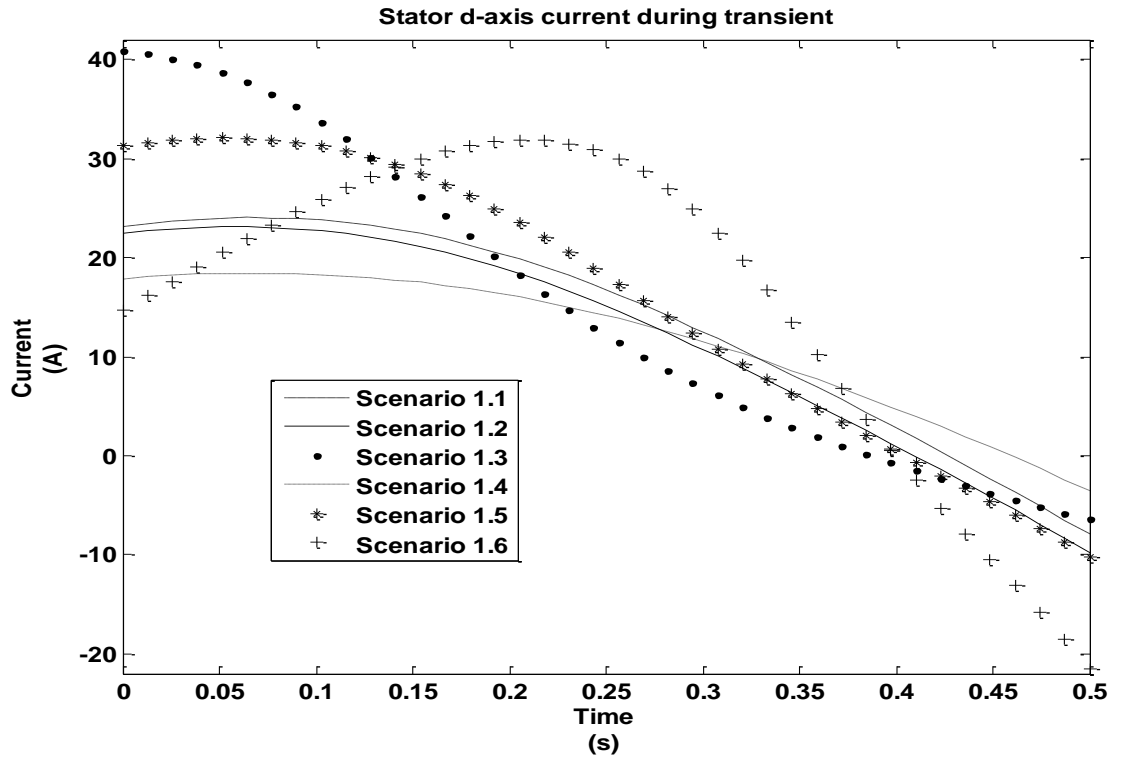


Figure 8.5. Trajectory for d-axis current (Scenario 1- optimal).

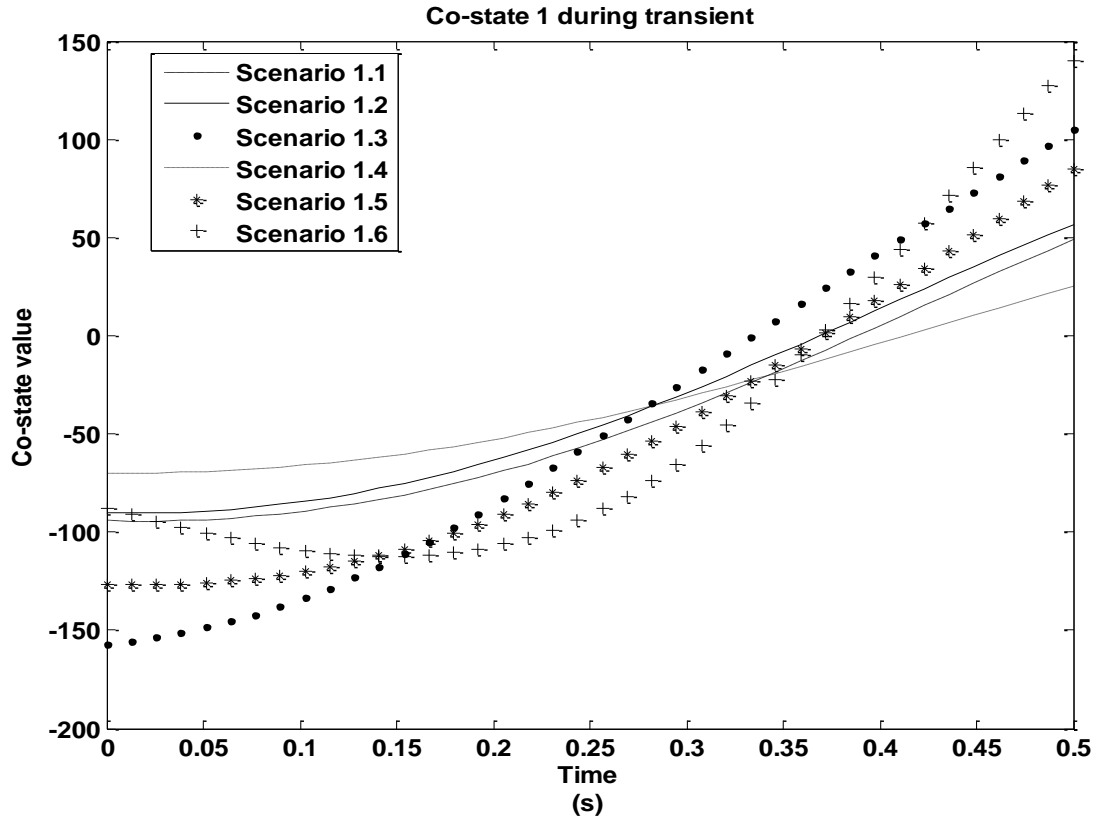


Figure 8.6. Trajectory of co-state 1 (Scenario 1 - optimal).

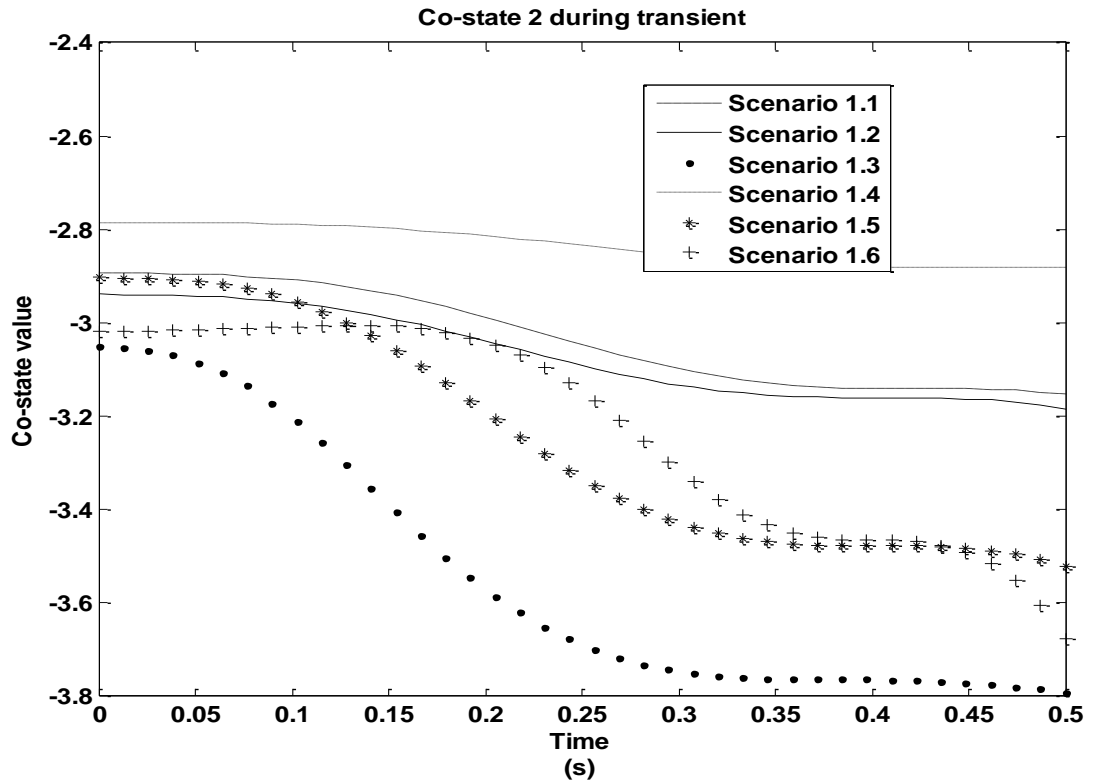


Figure 8.7. Trajectory of co-state 2 (Scenario 1 - optimal).

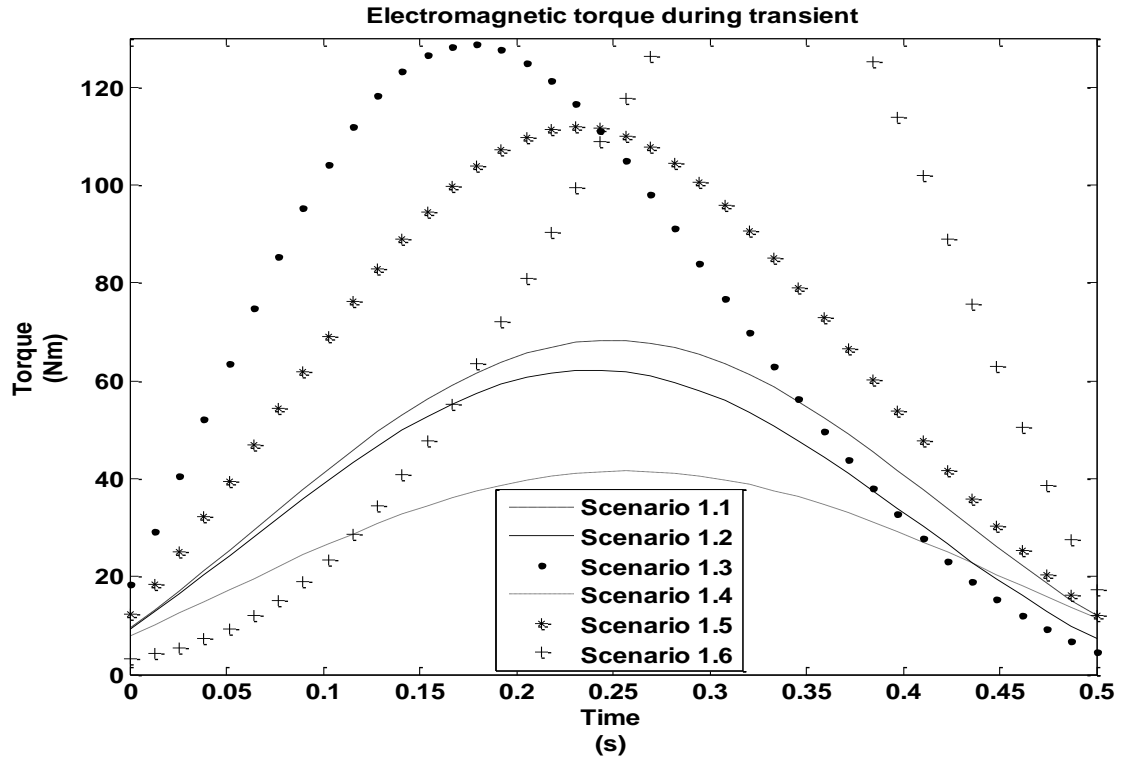


Figure 8.8. Electromagnetic torque trajectory (Scenario 1 - optimal).

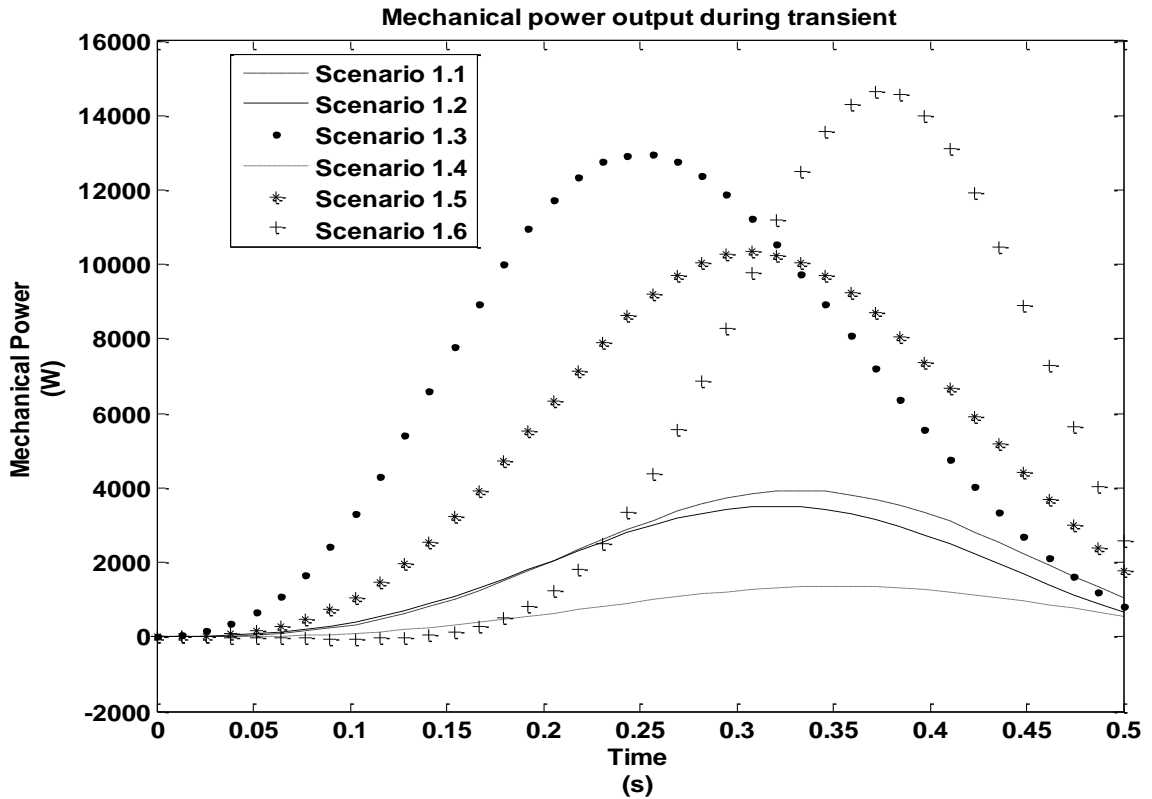


Figure 8.9. Mechanical power corresponding to the rotor speed and torque trajectories (Scenario 1 - optimal).



The value of the Hamiltonian function at each time instant is given in Figure 8.10. The plots for the power losses corresponding to the optimal state and control trajectories are shown in Figures 8.11, 8.12, and 8.13. Figure 8.14 gives the total power losses. The change in energy cost functional and gradient norm (from (8.1.4)) w.r.t. iterations are given in Figures 8.15 and 8.16, respectively.

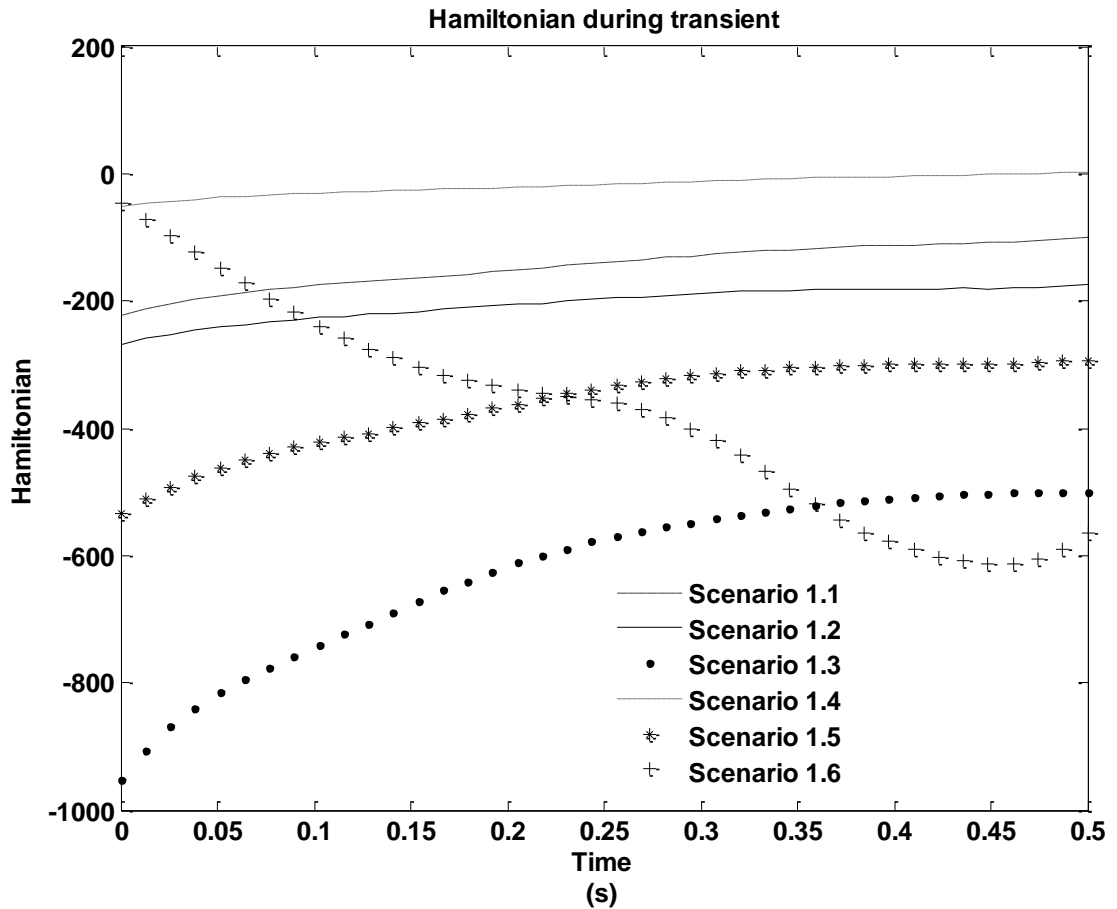


Figure 8.10. Hamiltonian function value during transient (Scenario 1 - optimal).

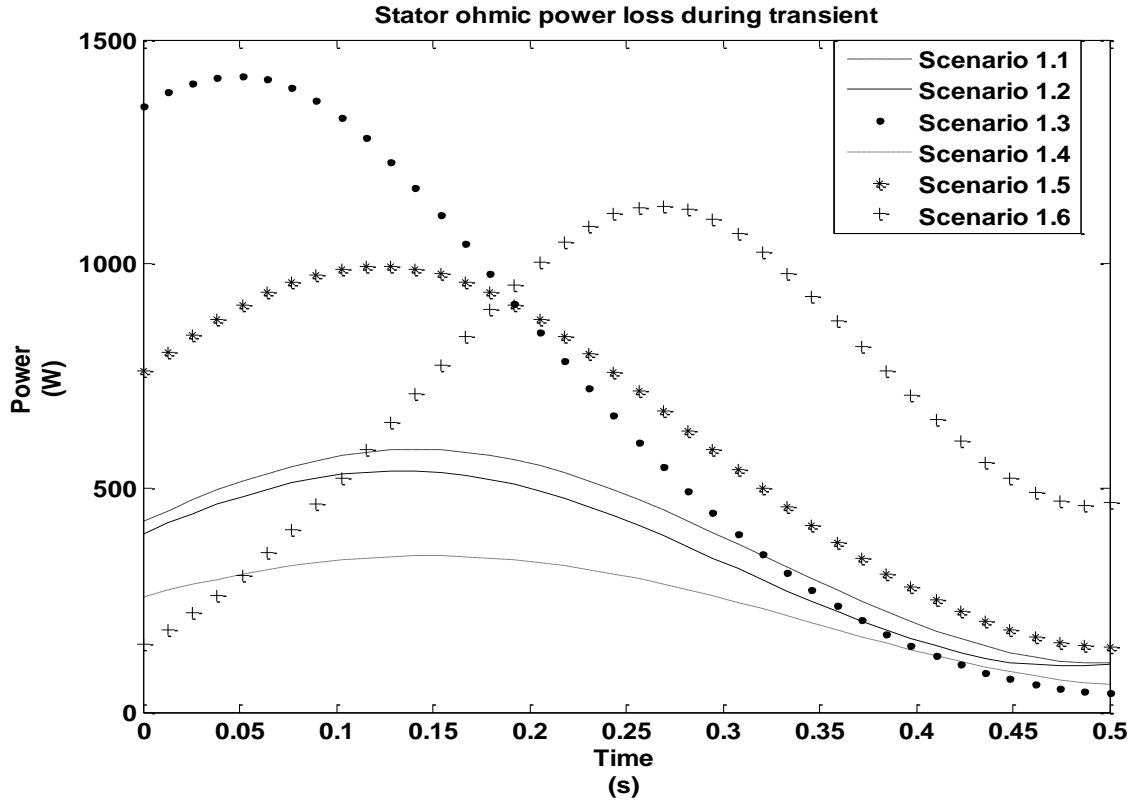


Figure 8.11. Stator Ohmic power losses in IM (Scenario 1 - optimal).

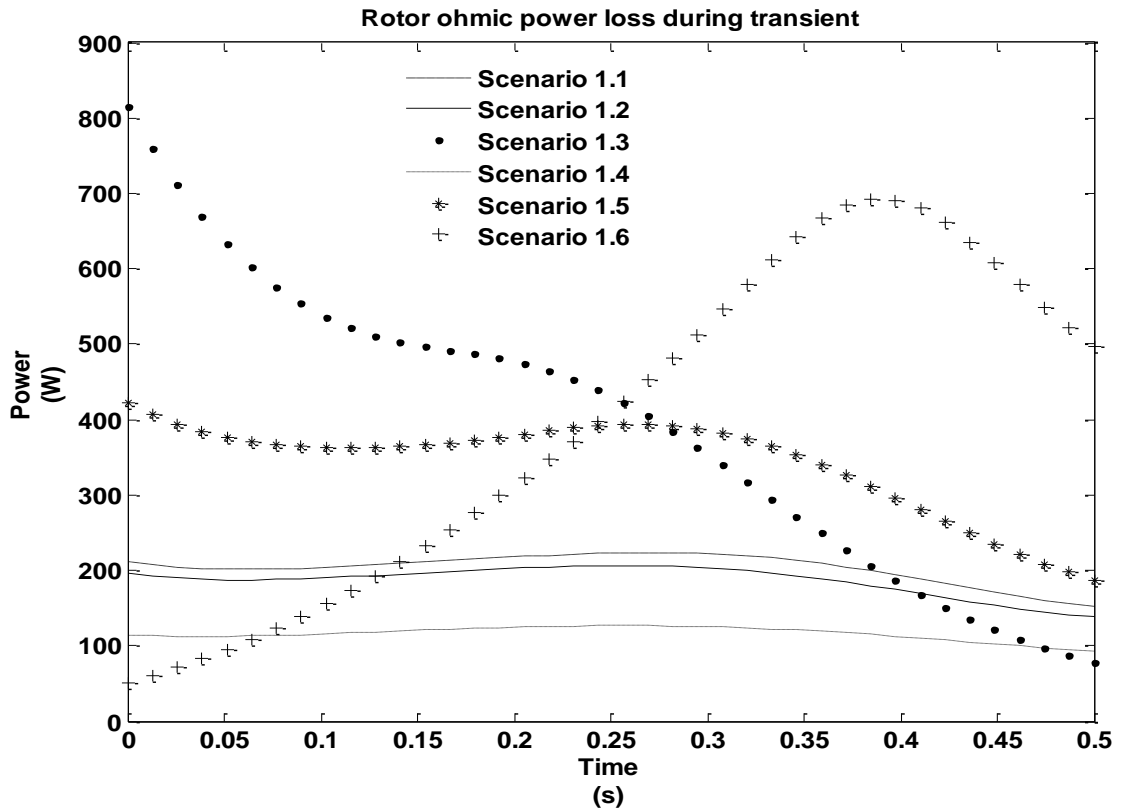


Figure 8.12. Rotor Ohmic power losses in IM (Scenario 1 - optimal).

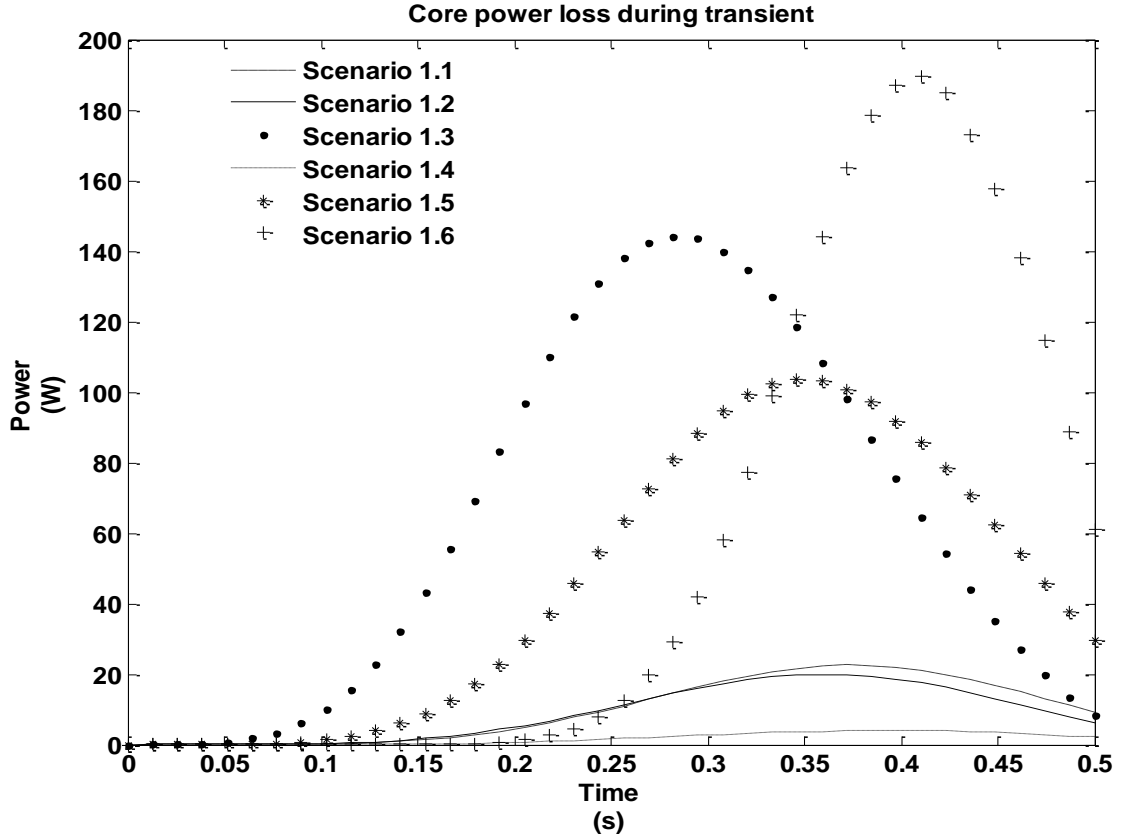


Figure 8.13. Stator core power losses in IM (Scenario 1 - optimal).

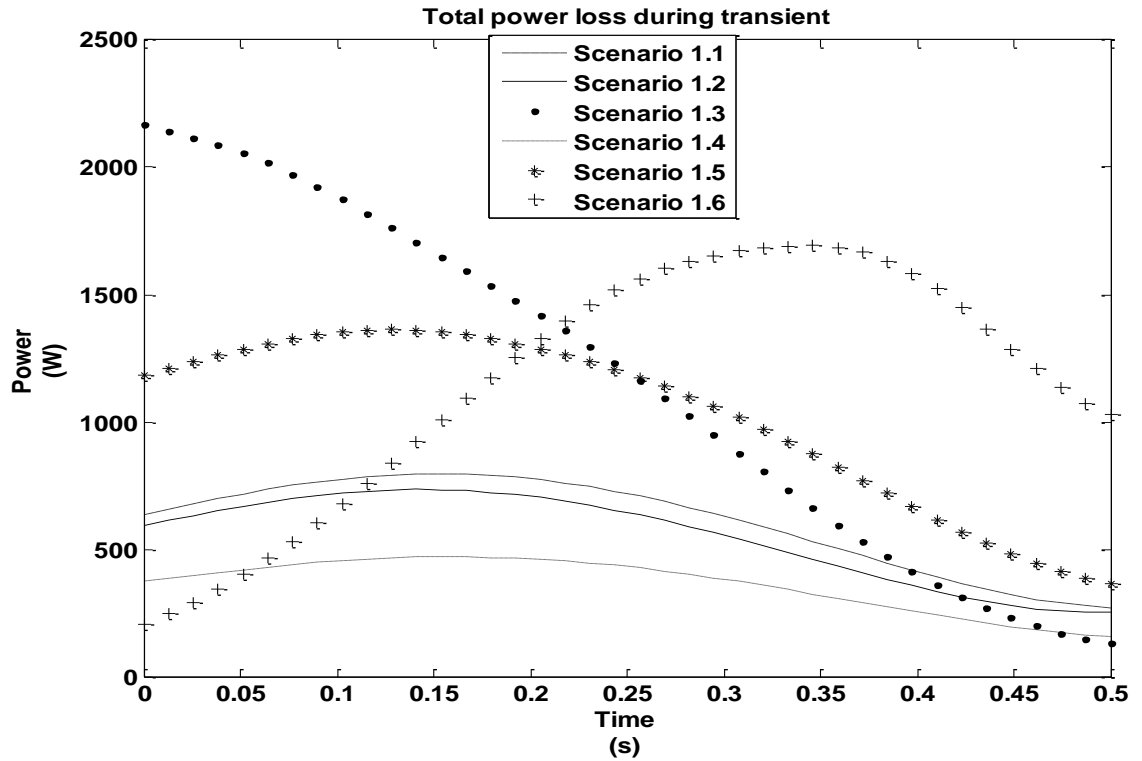


Figure 8.14. Total power losses in IM (Scenario 1 - optimal).

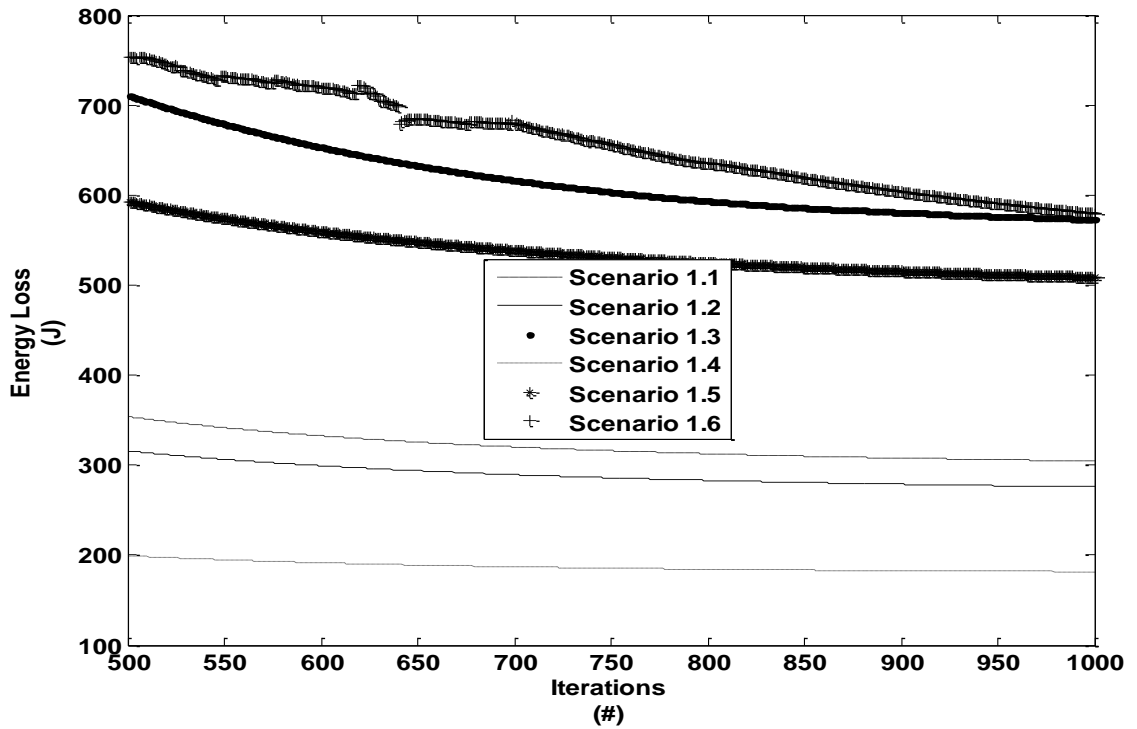


Figure 8.15. Change in the value of the energy loss cost function over iterations (Scenario 1 - optimal)

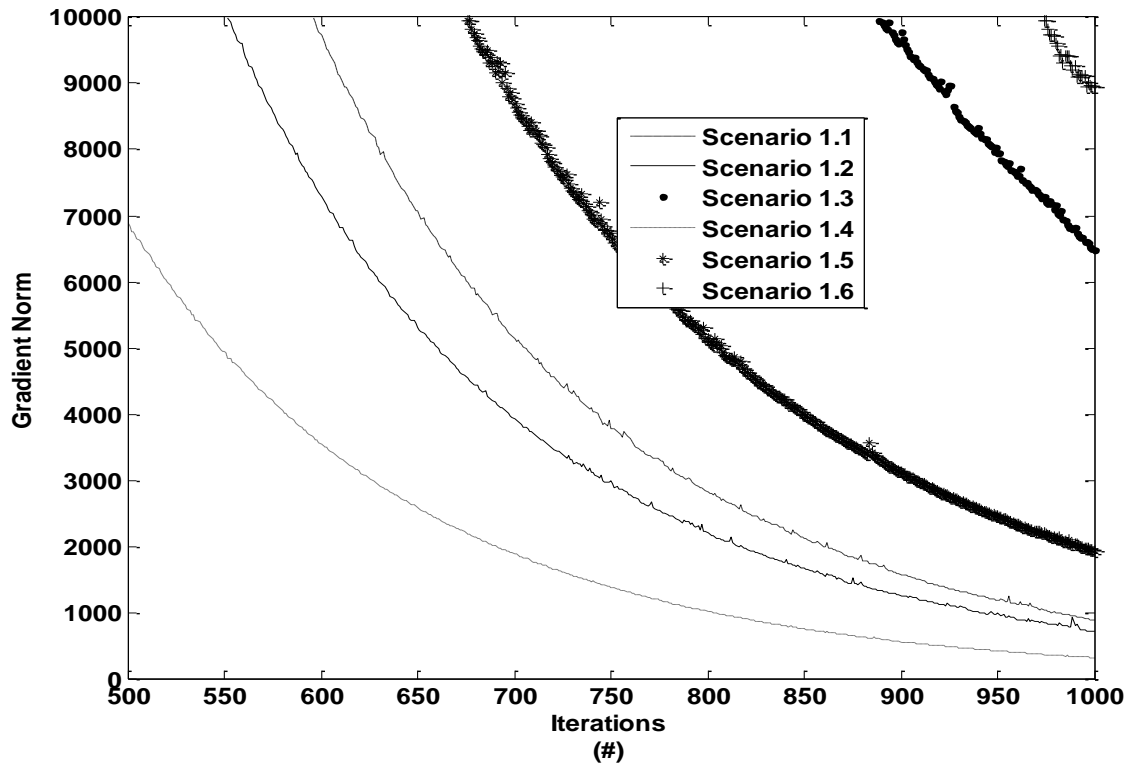


Figure 8.16. Change in the value of the gradient norm over iterations (Scenario 1 - optimal)

### 8.2.2 Scenario 1 - Baseline

It is necessary to compare the optimal trajectories with a baseline in order to determine if the energy efficiency of the IM has improved during transients. For this purpose, we calculate the trajectories of current inputs according to Regime I (from section 7.2.1) using equations (7.2.1.1) to (7.2.1.3) for each case described in Table 8.1. The Regime I trajectories are applied to the IM model (same as the model used in the optimal control problem). The rotor flux and rotor speed are shown in Figures 8.17 and 8.18. The plots for q- and d-axis stator currents are given by Figures 8.19 and 8.20. The electromagnetic torque generated by the IM during transient is shown in Figure 8.21. The mechanical power produced by the IM calculated using (7.3.2.1) from the speed and torque trajectories is given in Figure 8.22. The value of the Hamiltonian function at each time instant is given in Figure 8.23. The plots for the three types of power losses (stator Ohmic, rotor Ohmic, stator core) are given in Figures 8.24, 8.25, and 8.26, respectively. The total power loss is given in Figure 8.27. Note that all cases of a similar type of trajectory are shown on the same plot.

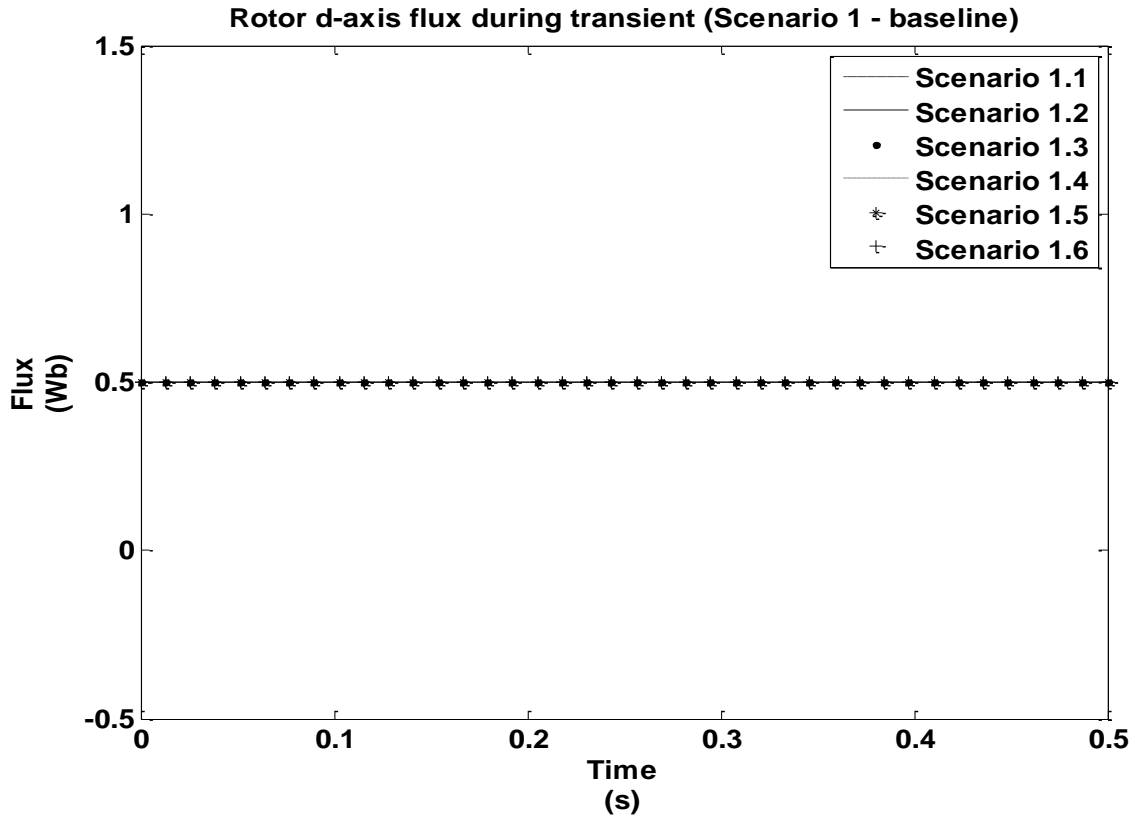


Figure 8.17. Trajectory of rotor d-axis flux (Scenario 1 – baseline)

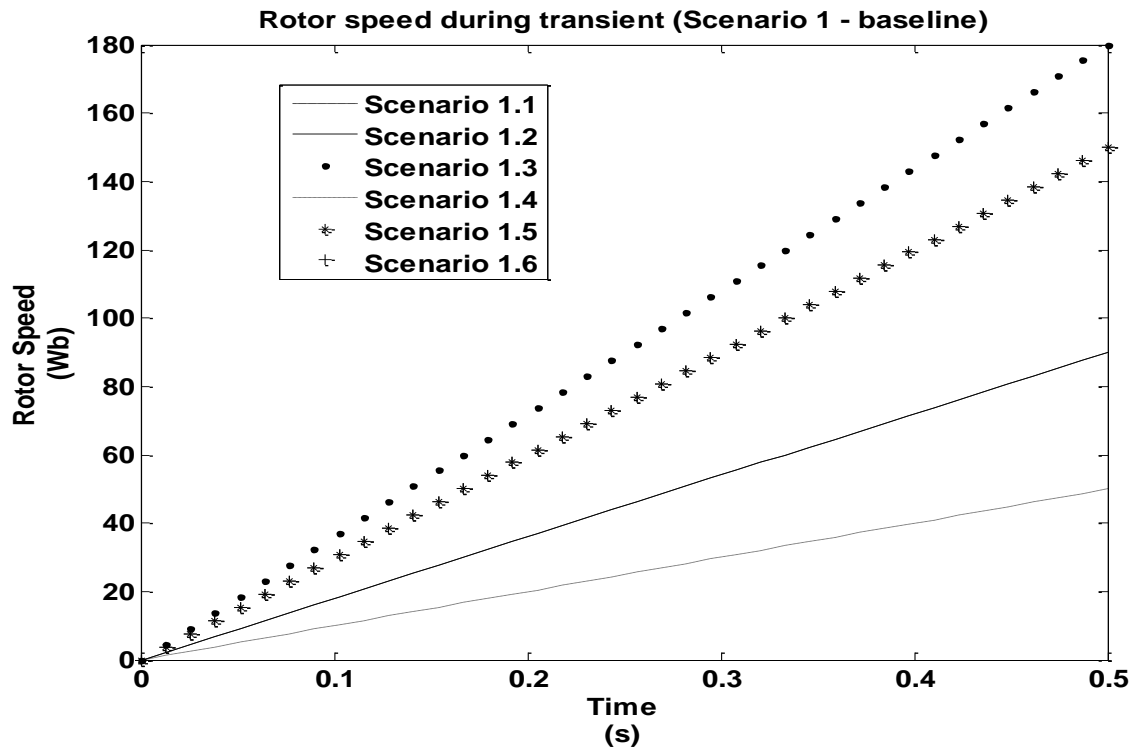


Figure 8.18. Trajectory of rotor speed (Scenario 1 – baseline)

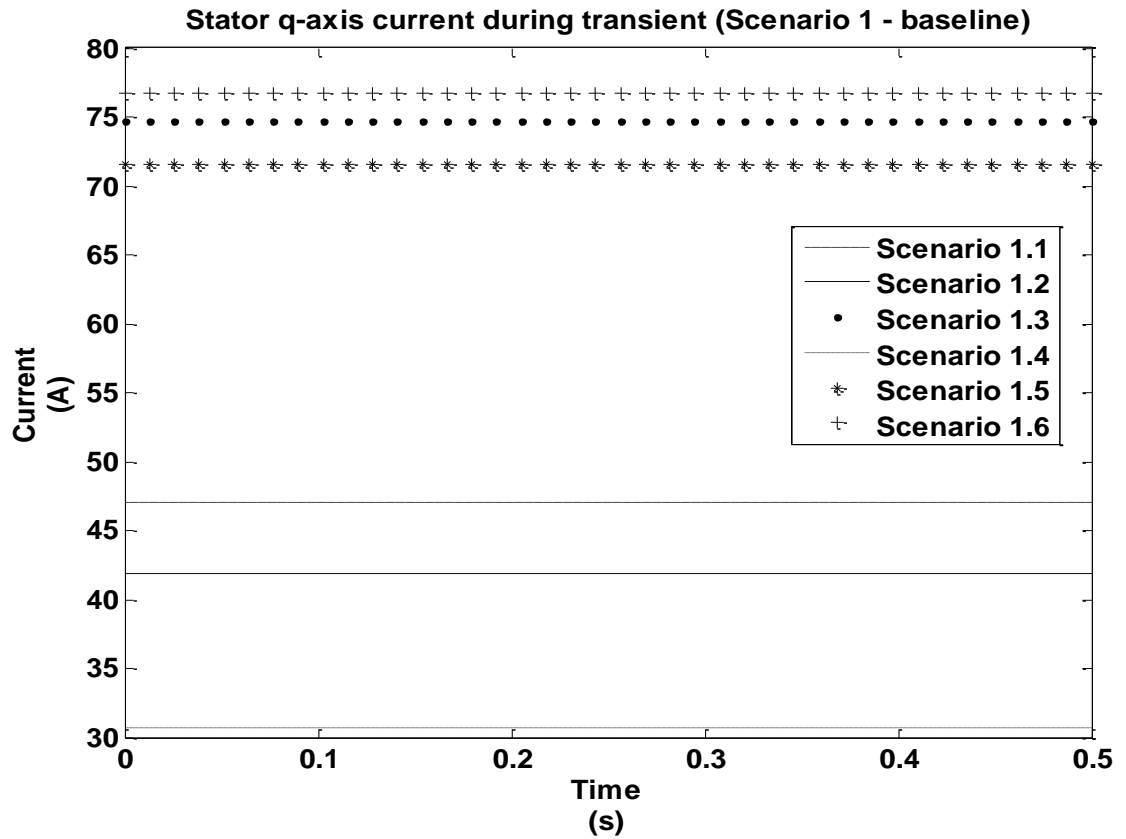


Figure 8.19. Trajectory of stator q-axis current (Scenario 1 – baseline).

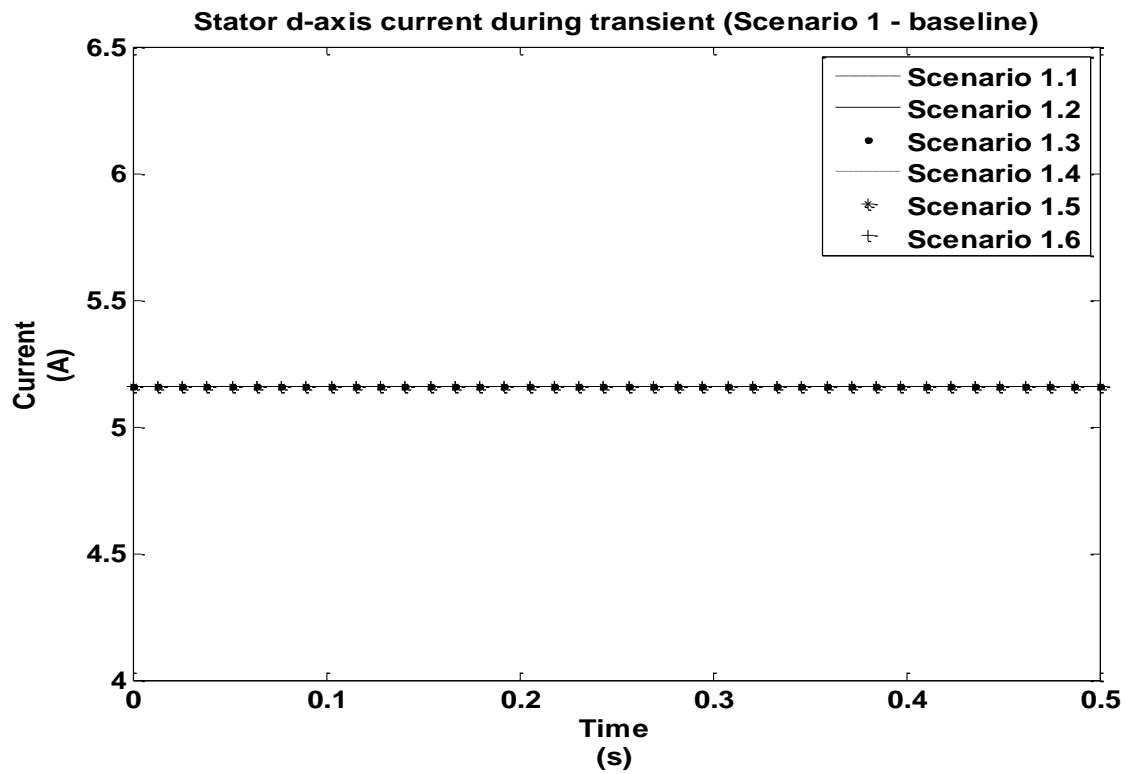


Figure 8.20. Trajectory of stator d-axis current (Scenario 1 – baseline).

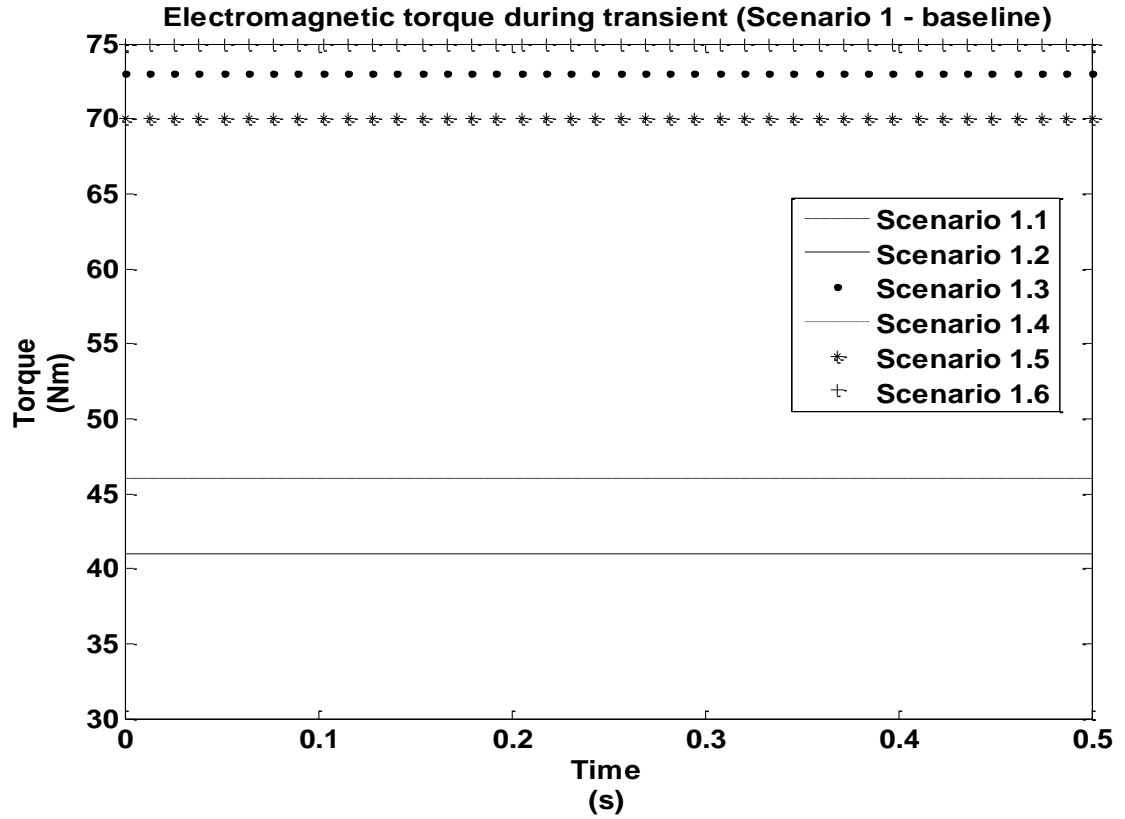


Figure 8.21. Electromagnetic torque produced during transient (Scenario 1 – baseline).

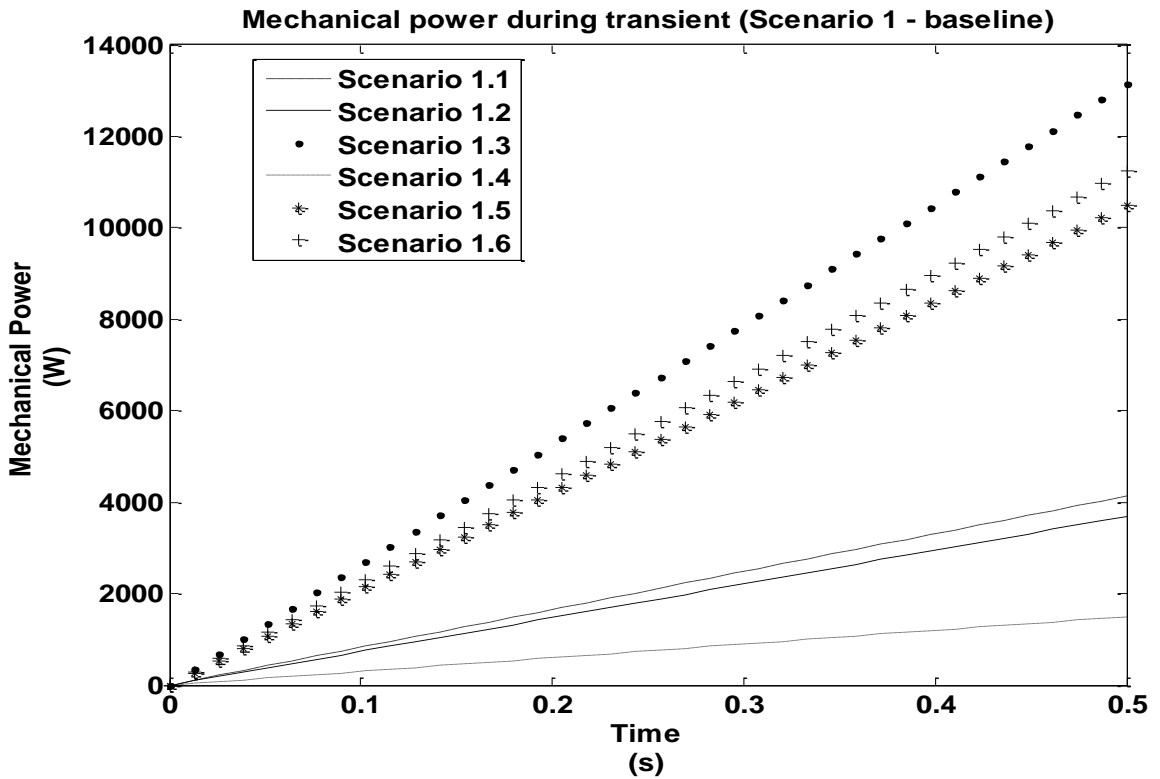


Figure 8.22. Mechanical power produced during transient (Scenario 1 - baseline).



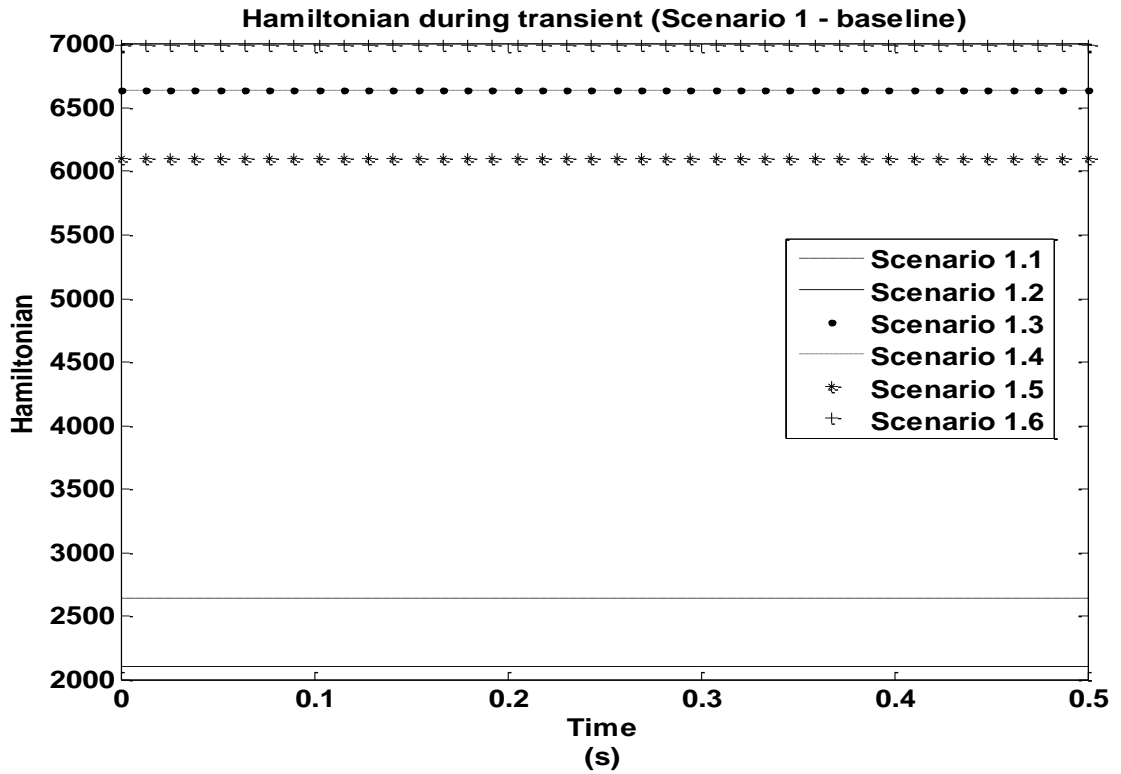


Figure 8.23. Hamiltonian function value (Scenario 1 - baseline).

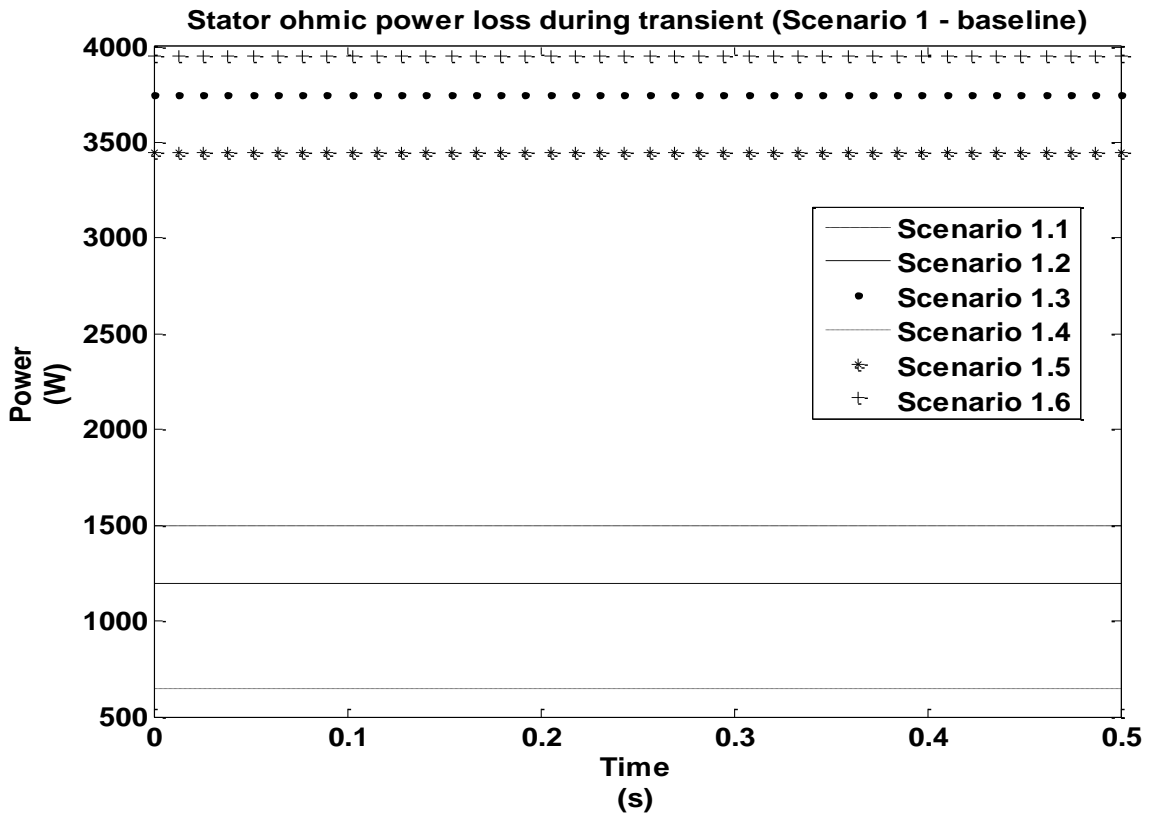


Figure 8.24. Stator Ohmic power losses in IM (Scenario 1 - baseline).

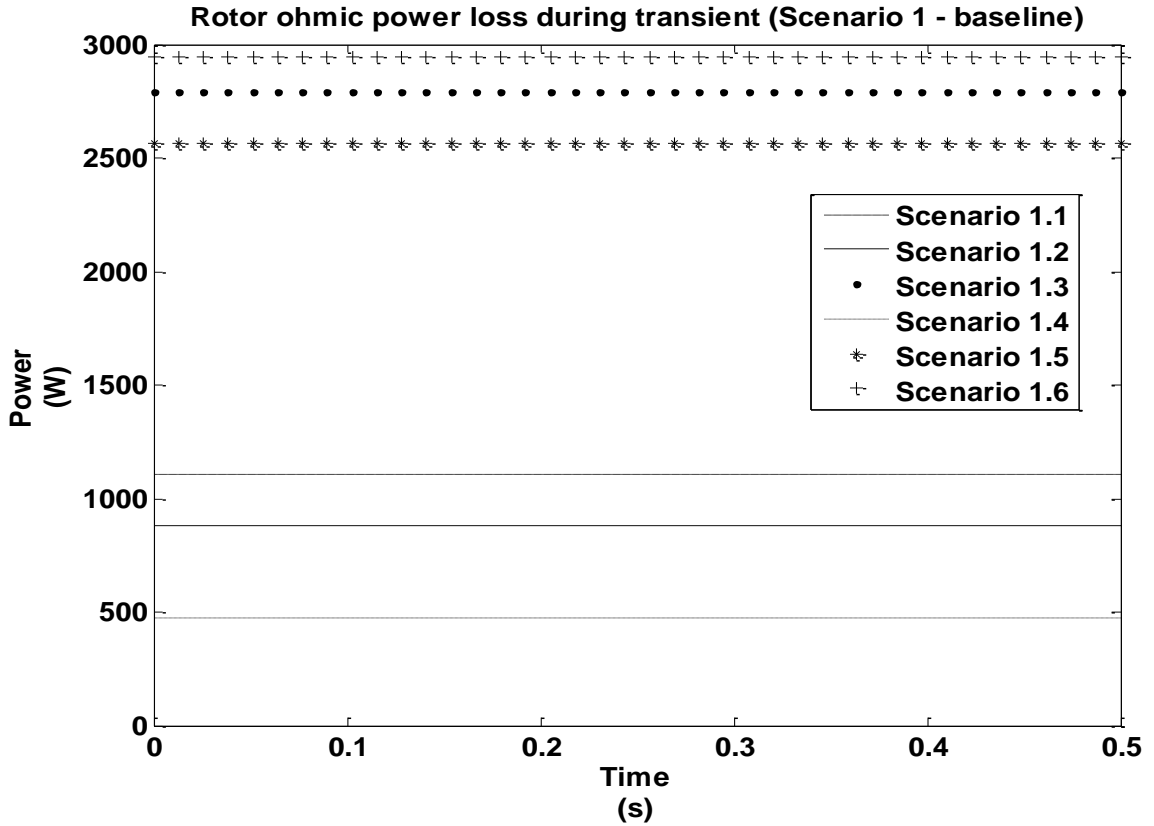


Figure 8.25. Rotor Ohmic power losses in IM (Scenario 1 -baseline).

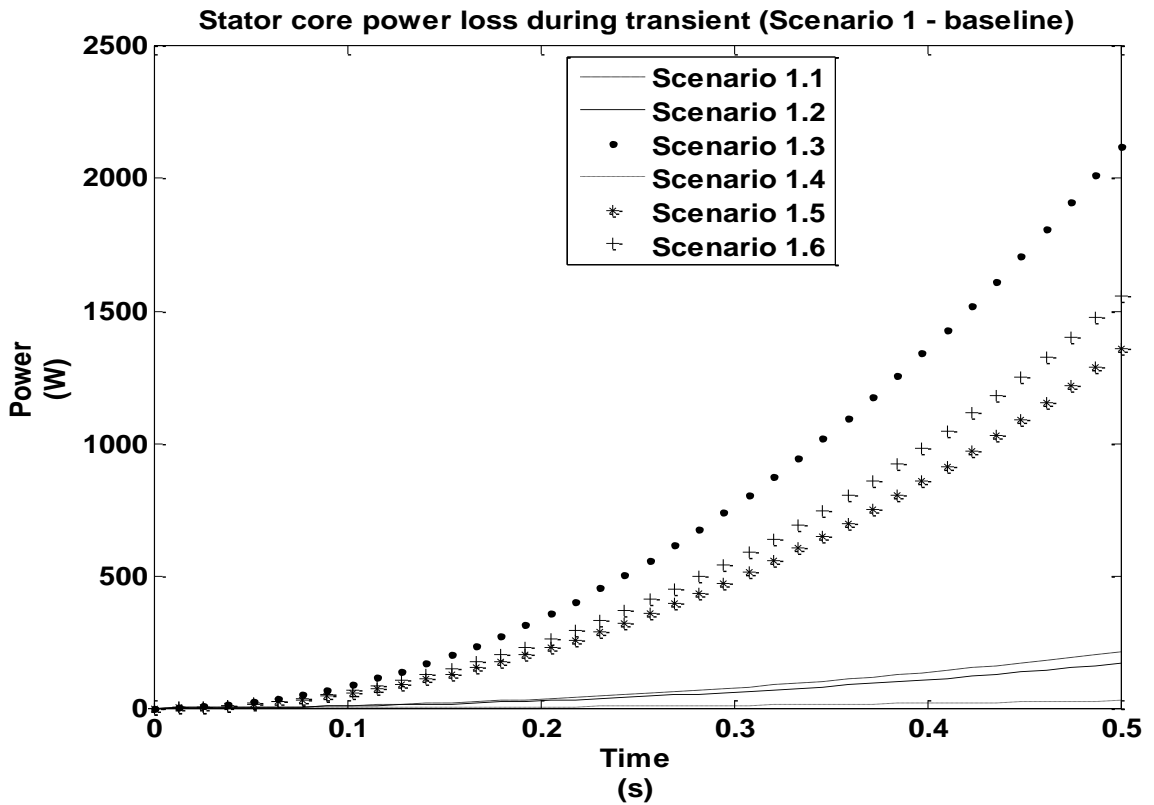


Figure 8.26. Core power losses in IM (Scenario 1 -baseline).

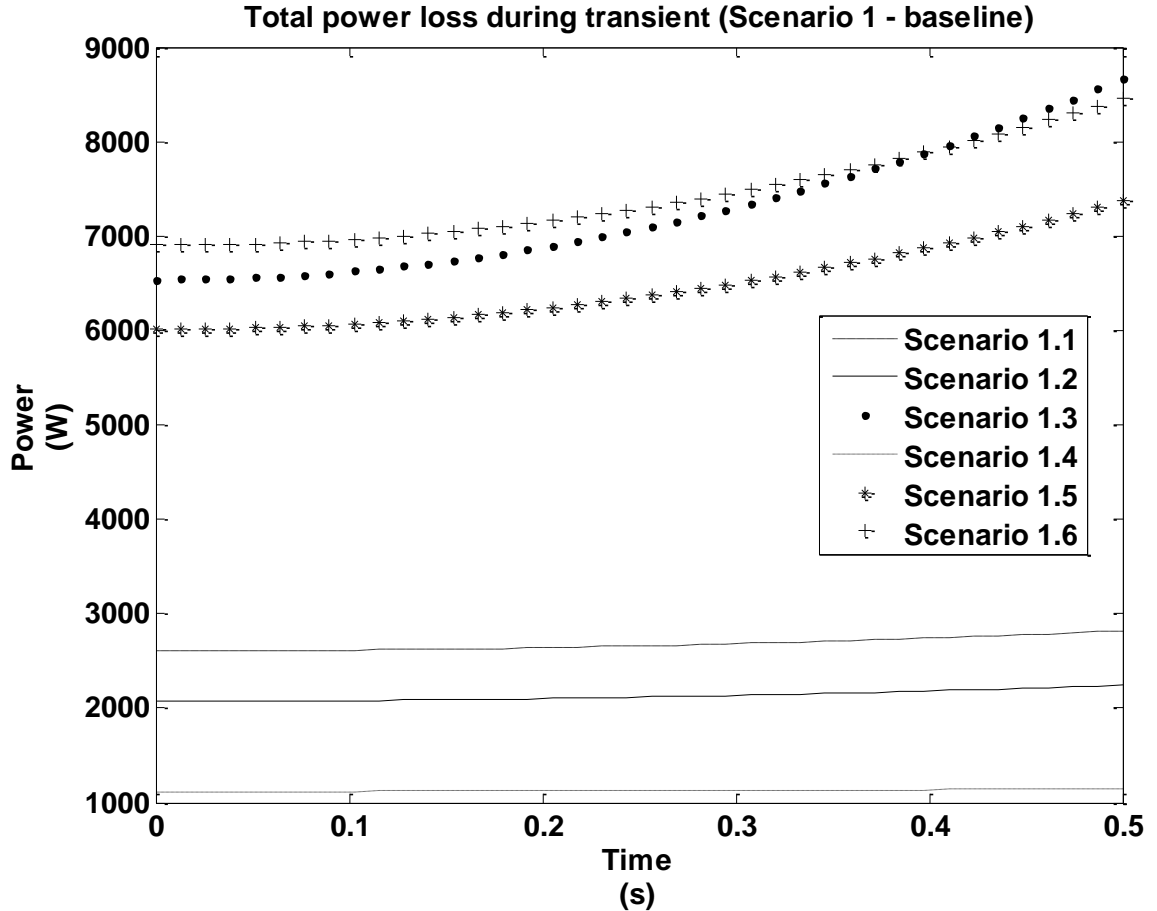


Figure 8.27. Total power losses in IM (Scenario 1 -base case)

### 8.2.3 Comparison of the optimal trajectories vs Regime I trajectories

It can be observed that optimal trajectories for  $i_{qs}$  and  $i_{ds}$  are significantly different from Regime I trajectories. The resulting trajectories for rotor flux and electromagnetic torque also take different shapes when compared to Regime I. Despite that, the rotor speed has attained the desired reference speed at the end of the transient period. Additionally, rotor flux and electromagnetic torque are very close to the specified terminal values. Inspecting the rotor flux trajectories reveals a unique feature: the flux trajectory takes the shape of a conic section. The same is also true for the electromagnetic torque. Using insights obtained from the numerical solution, an analytical expression for the optimal trajectories is derived in Chapter 9.

#### 8.2.4 Comparing energy efficiency for optimal and Regime I in scenario 1

By numerically integrating (using trapezoid rule) the power quantities (mechanical power and total power loss), the total mechanical energy produced and the total energy loss during transient can be found. Then by applying (3.2.2) from section 3.2, the energy efficiency of the machine during transient can be calculated. The calculated values are tabulated in Table 8.2 for both the optimal and for Regime I (baseline) for all six cases in scenario 1.

*Table 8.2. Comparing total energy cost for scenario 1*

Scenario	Energy loss (J)		Mechanical energy output (J)		Energy efficiency (%)		
	Optimal	Regime I	Optimal	Regime I	Optimal	Regime I	Improvement
1.1	305	1300	1000	1035	76.6	44.3	<b>32.2</b>
1.2	275	1050	893	920	76.4	46.7	<b>29.7</b>
1.3	580	3600	3200	3280	84.6	47.7	<b>36.9</b>
1.4	182	560	350	375	65.7	40.1	<b>25.6</b>
1.5	515	3200	2580	2625	83.3	45.0	<b>38.3</b>
1.6	590	3700	2590	2810	81.4	43.1	<b>38.3</b>

It can be observed that there is indeed an improvement in the efficiency averaging around 30% over the baseline when using optimal trajectories during the transient period. It can also be seen that the larger the change in the magnitude of speed, and load torque, the higher is the improvement in efficiency. The relationship between change in magnitude of speed and optimal energy efficiency is derived in the next chapter. The mechanical energy outputs are on an average about 3% lower for optimal when compared to Regime I. However, it will be shown in next section that such large improvements were due to the low value of the initial rotor flux in this scenario.

### 8.3 Numerical Solution - Scenario 2

The procedure in the previous section is now repeated using a Type II IM. The initial and final conditions, in this case, are also different from the previous scenario 1 and are listed in Table 8.3 below. Note that the initial rotor flux is also more than twice that of scenario 1.

*Table 8.3. Scenarios for testing IM optimal control problem using Type II IM*

<b>Scenario</b>	<b><math>\Psi_{dr}^0</math> (Wb)</b>	<b><math>\omega_r^0</math> (rad/s)</b>	<b><math>T_L</math> (Nm)</b>	<b><math>\omega_r^{ref}</math> (rad/s)</b>	<b><math>\Psi_{dr}^{opt}</math> (Wb)</b>	<b>Time interval (s)</b>
2.1	1.1	0	10	100	1.04	0.5
2.2	1.1	0	20	50	1.5	0.5
2.3	1.1	100	3	180	0.5	0.5
2.4	1.1	180	5	50	0.76	0.5
2.5	1.1	100	10	50	1.08	0.5
2.6	1.1	125	0	25	0.3	0.5

#### 8.3.1 Scenario 2 - Optimal

The plots for the optimal state trajectories (w.r.t. time) are shown in Figures 8.28 and 8.29. The plots for optimal q- and d-axis stator currents are given by Figures 8.30 and 8.31, respectively. The electromagnetic torque generated by the IM during transient is shown in Figure 8.32. The mechanical power produced by the IM and calculated using (7.3.2.1) from the speed and torque trajectories is given in Figure 8.33. Figure 8.34 gives the total power losses. The change in energy cost functional and the gradient norm (from (8.1.4)) w.r.t. iterations are given in Figures 8.35 and 8.36, respectively. The plots for co-states, Hamiltonian, and individual power loss components are not included to reduce the number of figures. Note that all cases of a similar type of trajectory are shown on the same plot.

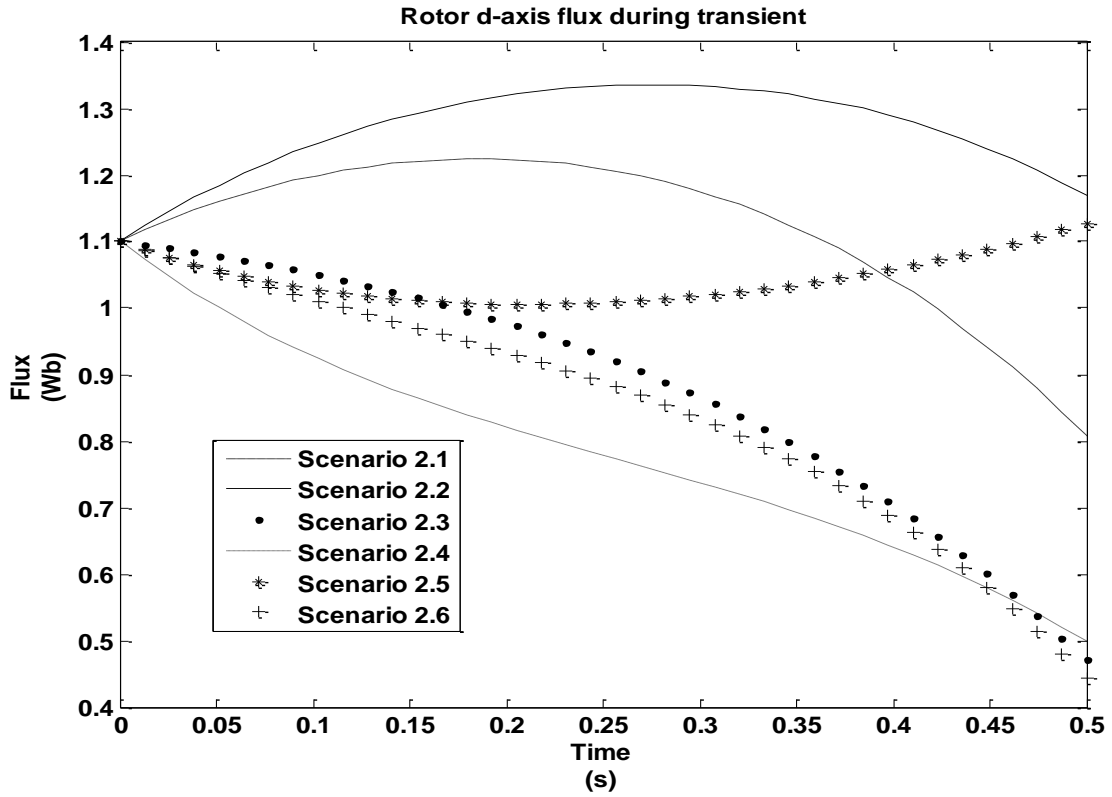


Figure 8.28. Trajectory for rotor d-axis flux (Scenario 2 - optimal).

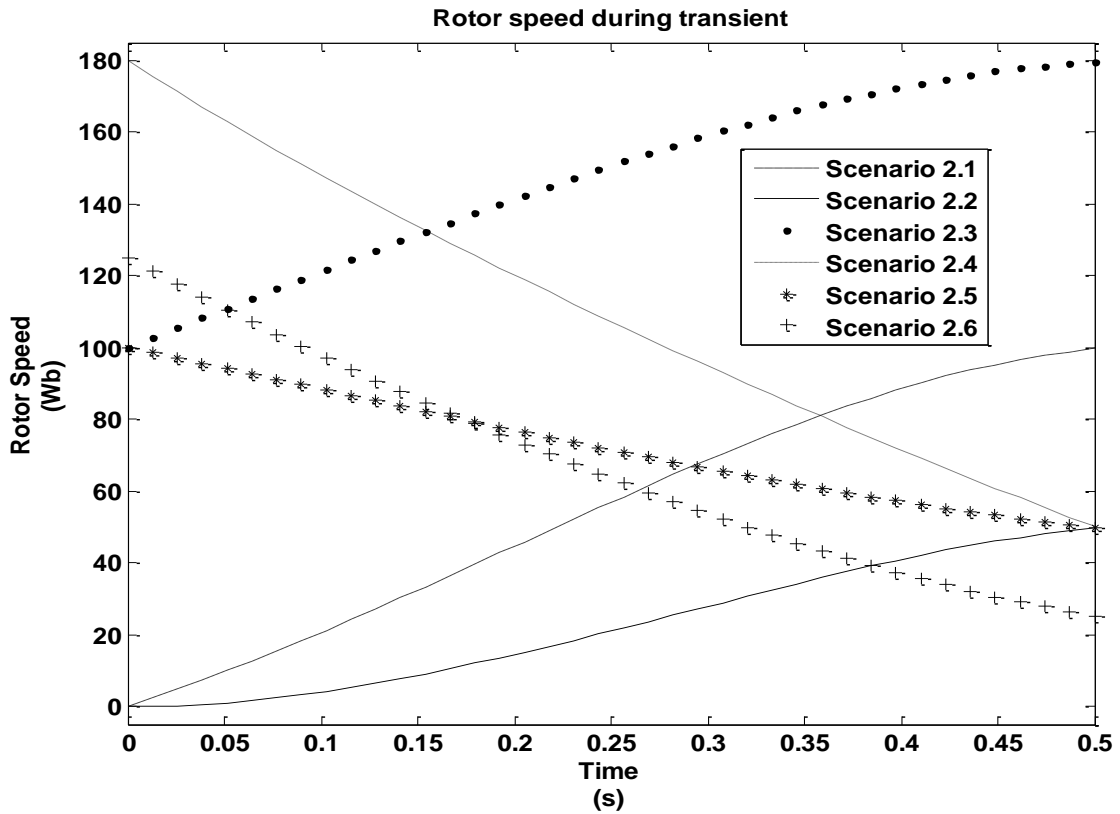


Figure 8.29. Trajectory for rotor speed (Scenario 2 - optimal).

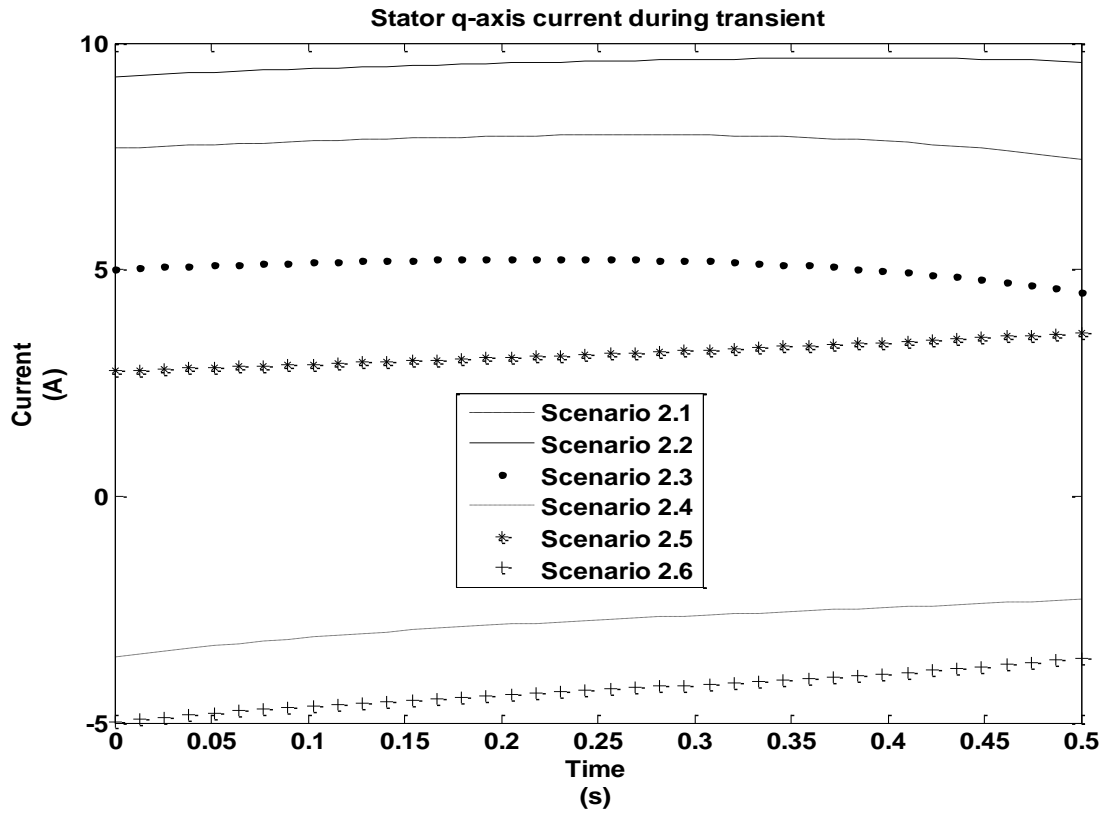


Figure 8.30. Trajectory for q-axis current (Scenario 2- optimal).

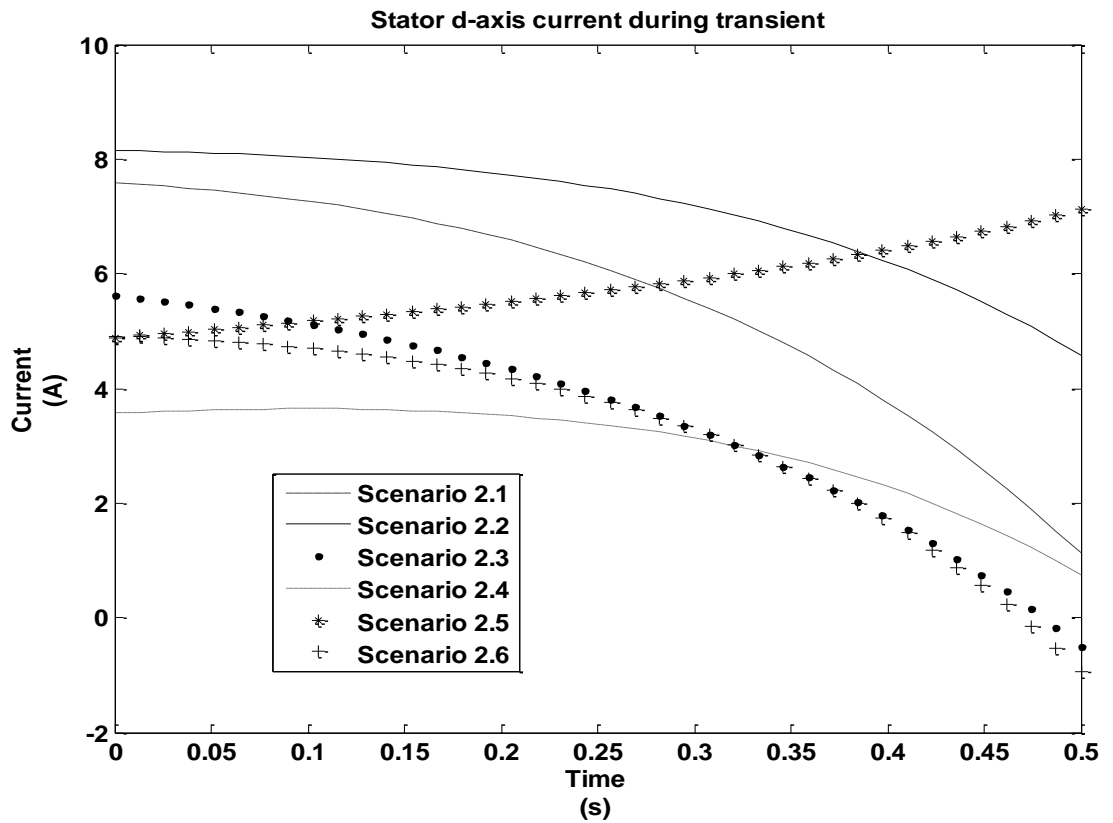


Figure 8.31. Trajectory for d-axis current (Scenario 2- optimal).

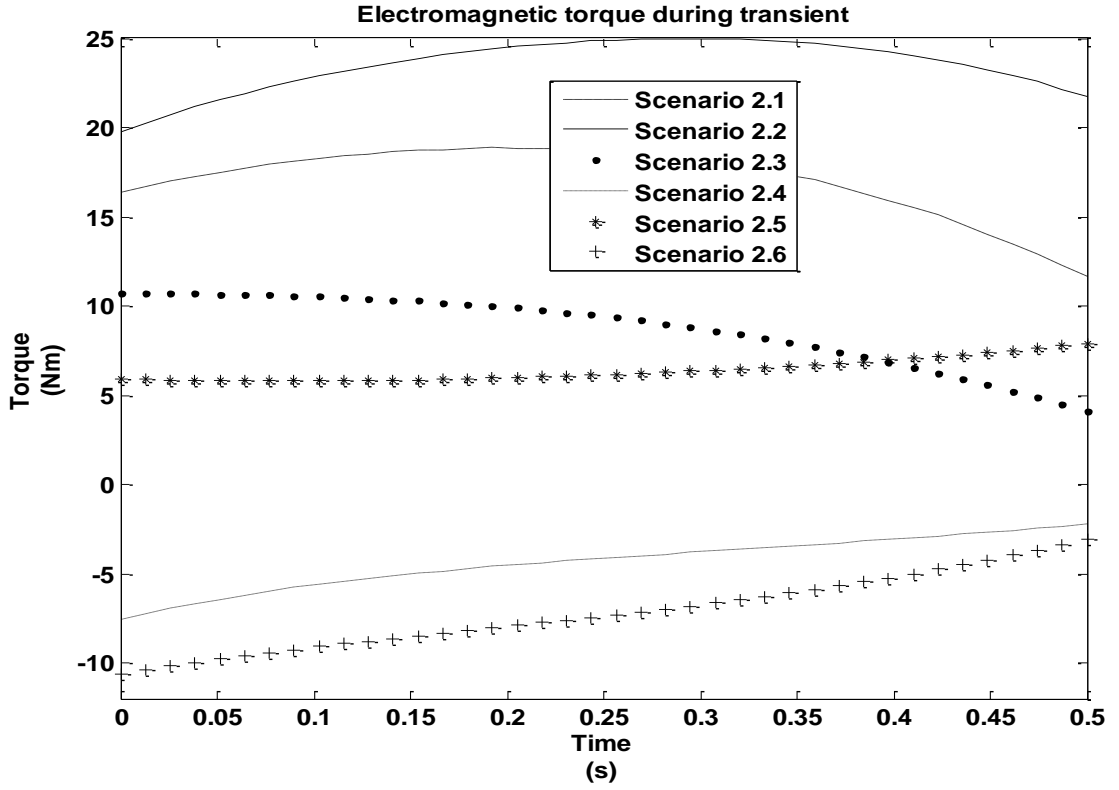


Figure 8.32. Electromagnetic torque trajectory (Scenario 2 - optimal)

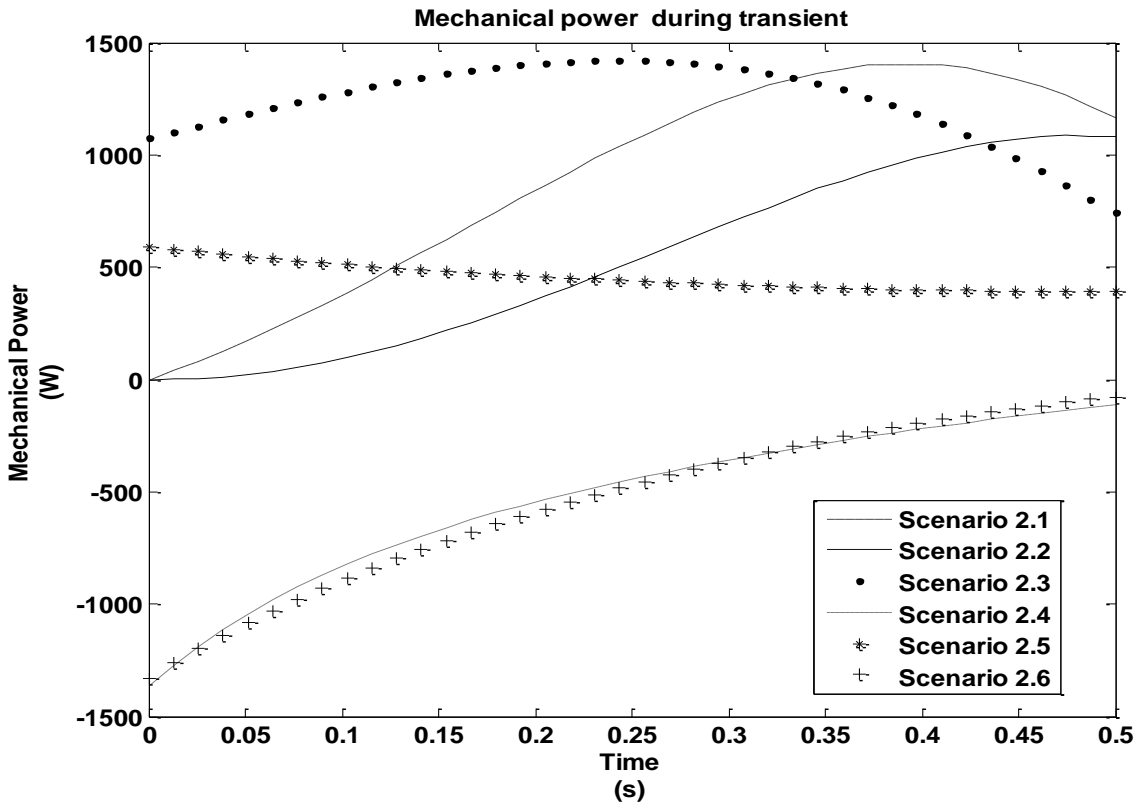


Figure 8.33. Mechanical power corresponding to rotor speed and torque trajectory (Scenario 1 - optimal).



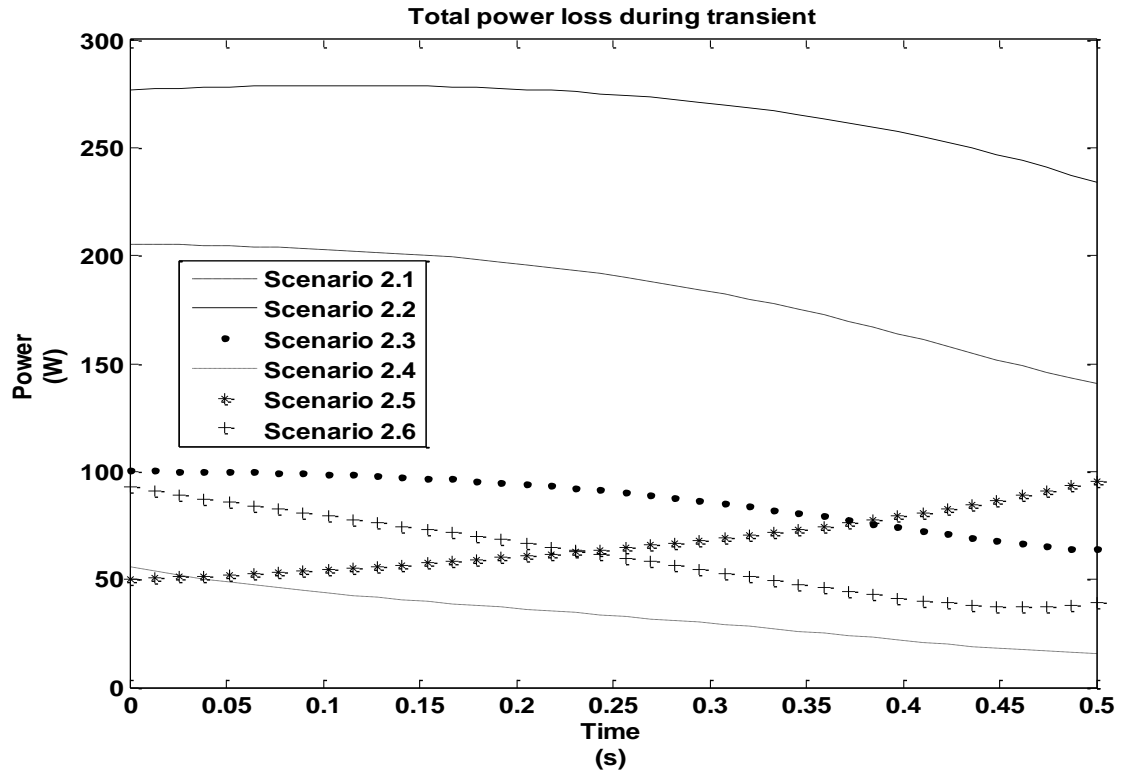


Figure 8.34. Total power losses in IM (Scenario 2 - optimal).

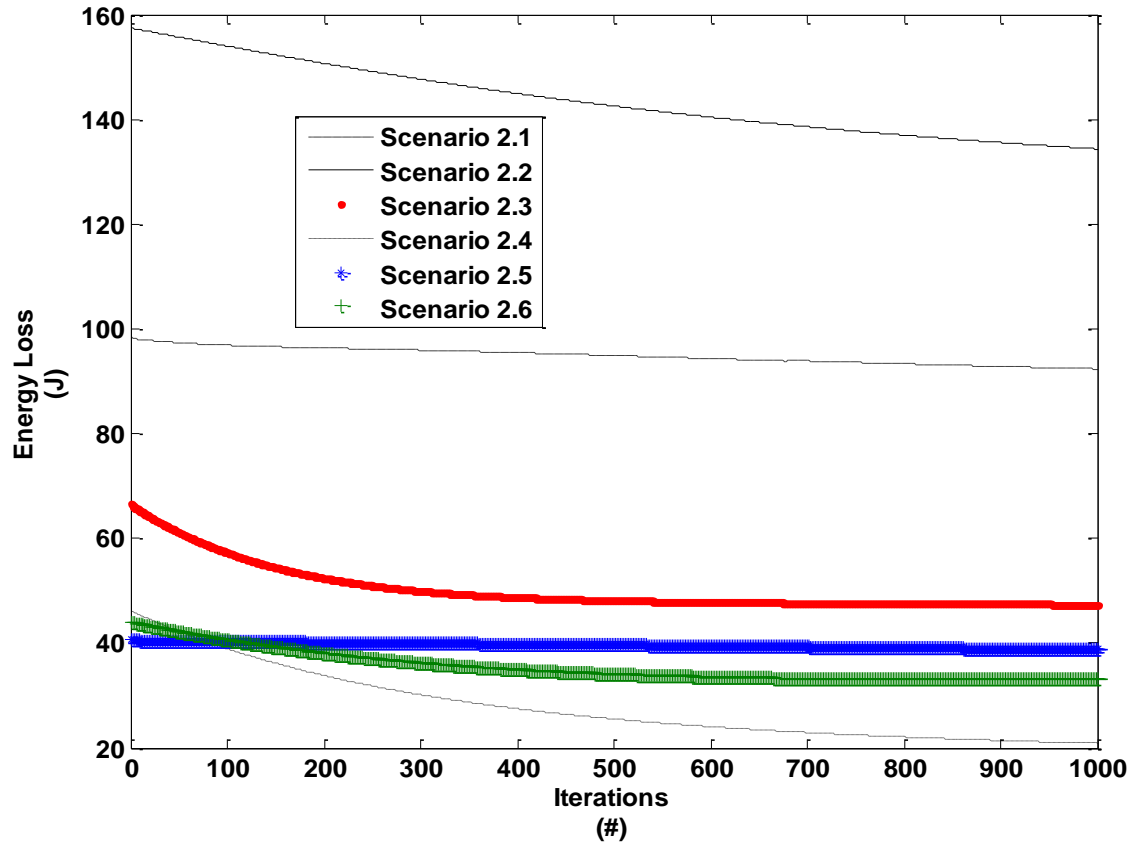


Figure 8.35. Change in value of energy loss cost function over iterations (Scenario 2 - optimal)

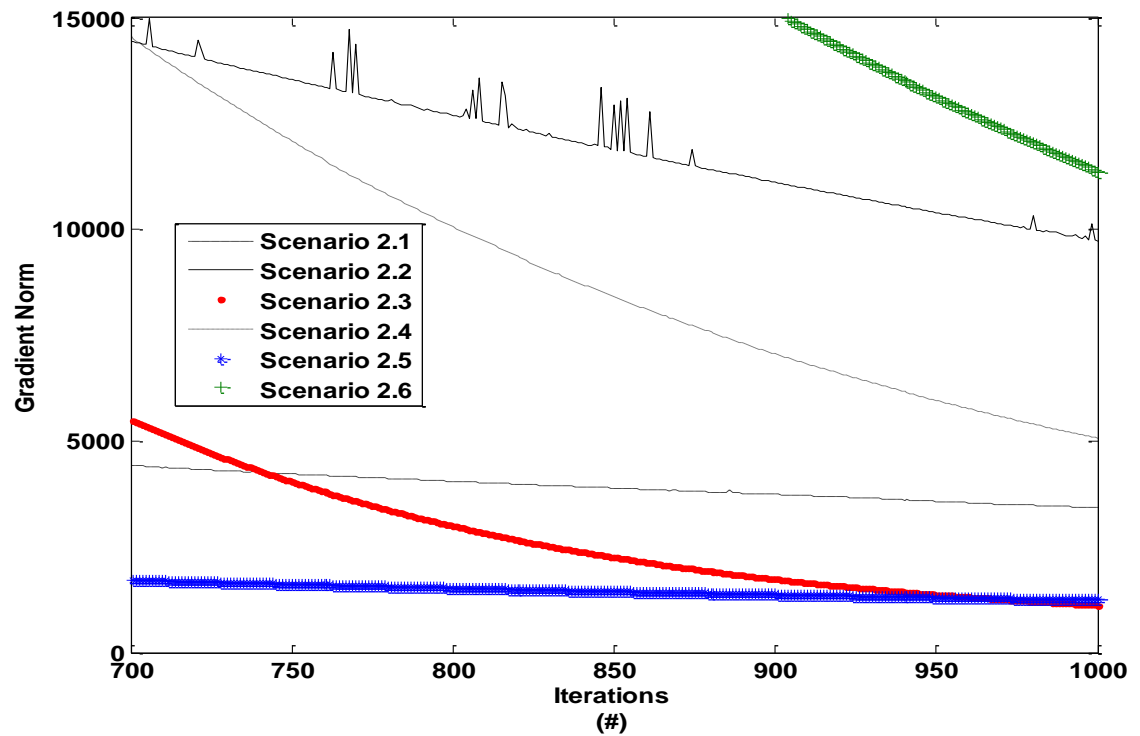


Figure 8.36. Change in value of gradient norm over iterations (Scenario 2 - optimal)

### 8.3.2 Scenario 2 - Baseline

It is necessary to compare the optimal trajectories with a baseline in order to determine if energy efficiency has improved. For this, we calculate the trajectories of current inputs according to Regime I (from section 7.2.1) using equations (7.2.1.1) to (7.2.1.3) for each case described in Table 8.2. The Regime I trajectories are applied to the IM model (same as the model used in the optimal control problem). The rotor flux and rotor speed are shown in Figures 8.37 and, Figures 8.38, respectively. The electromagnetic torque generated by the IM during transient is shown in Figure 8.39. The mechanical power produced by the IM that is calculated using (7.3.2.1) from the speed and the torque trajectories are given in Figure 8.40. The total power loss is given in Figure 8.41. Note that all cases of a similar type of trajectory are shown on the same plot.

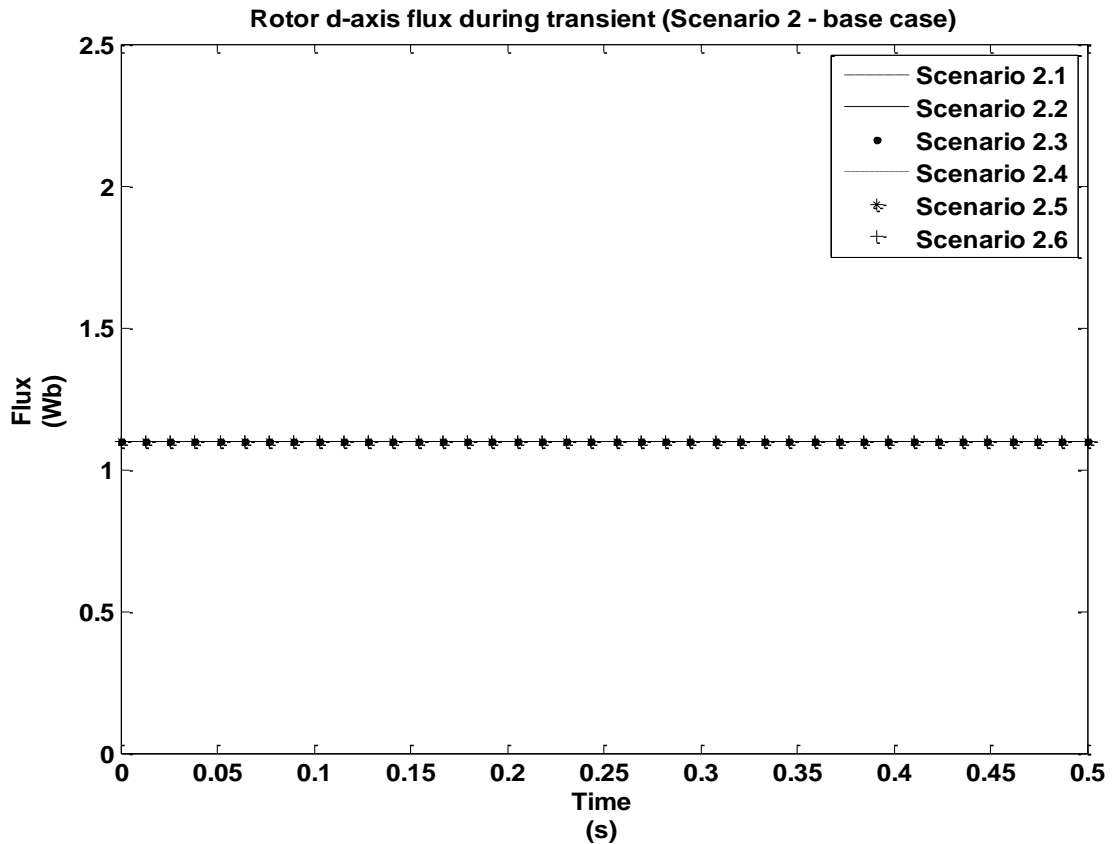


Figure 8.37. Trajectory of d-axis rotor flux (Scenario 2 – baseline)

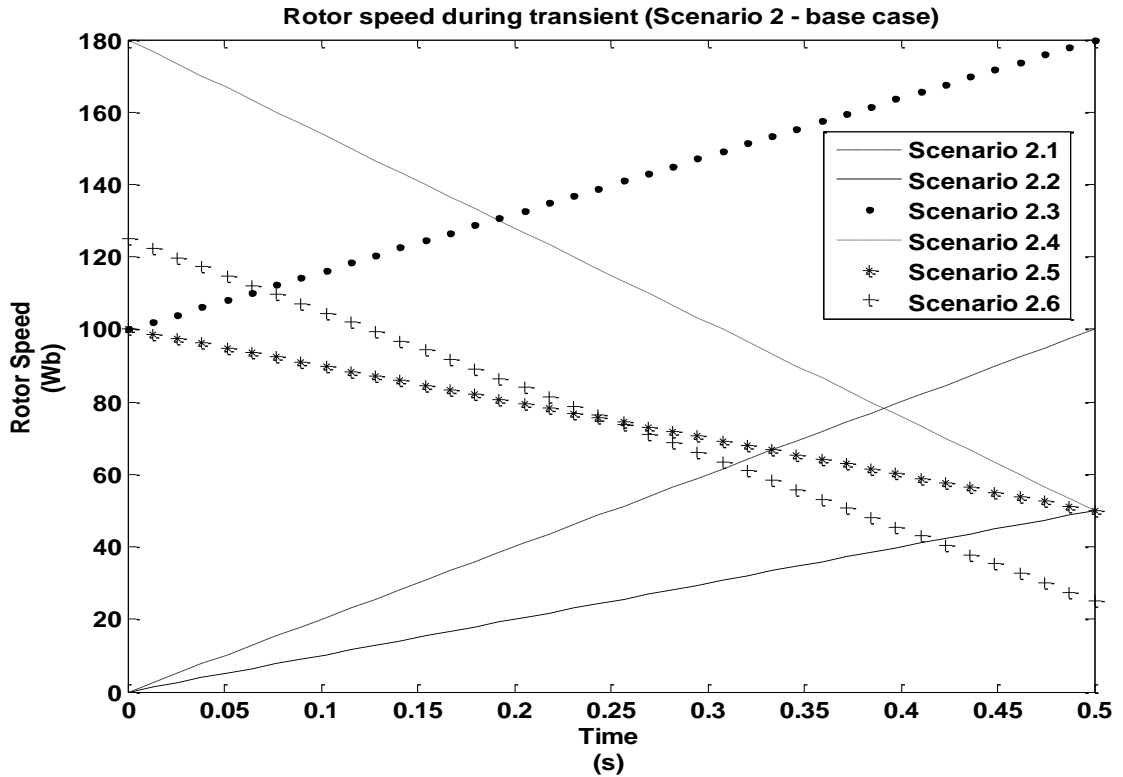


Figure 8.38. Trajectory of rotor speed (Scenario 2 – baseline)

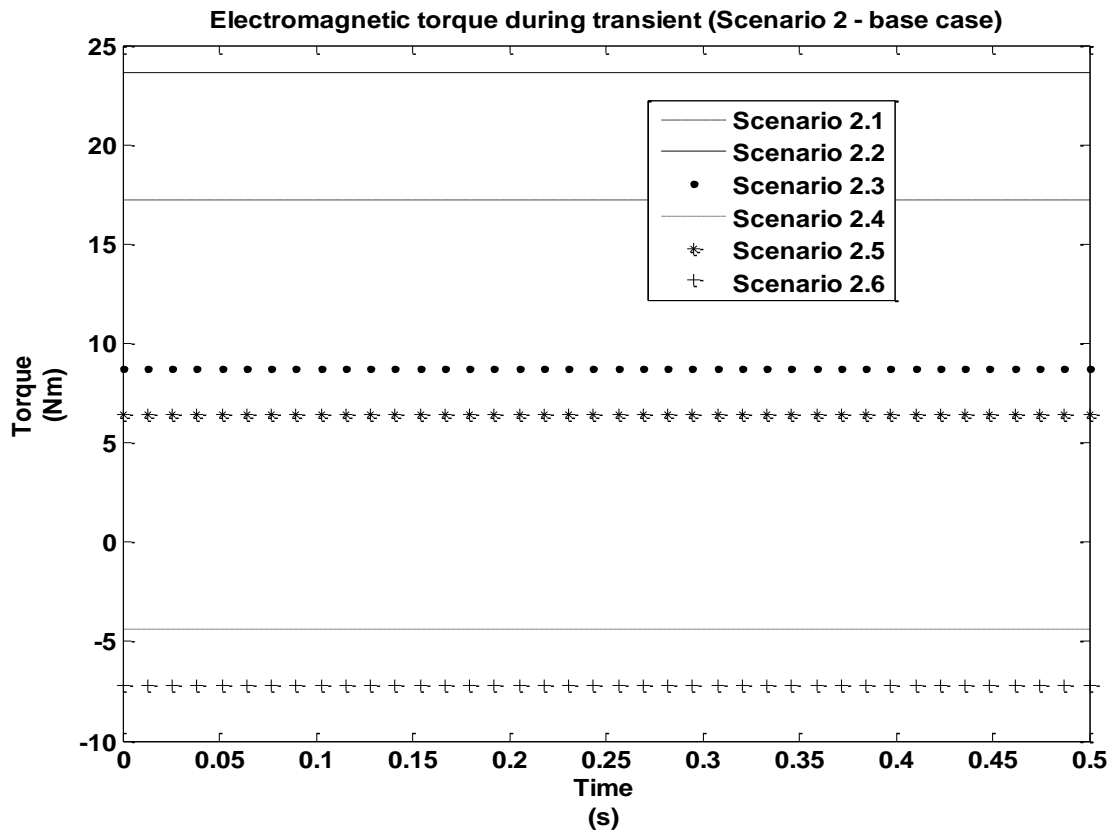


Figure 8.39. Trajectory of electromagnetic torque (Scenario 2 – baseline)

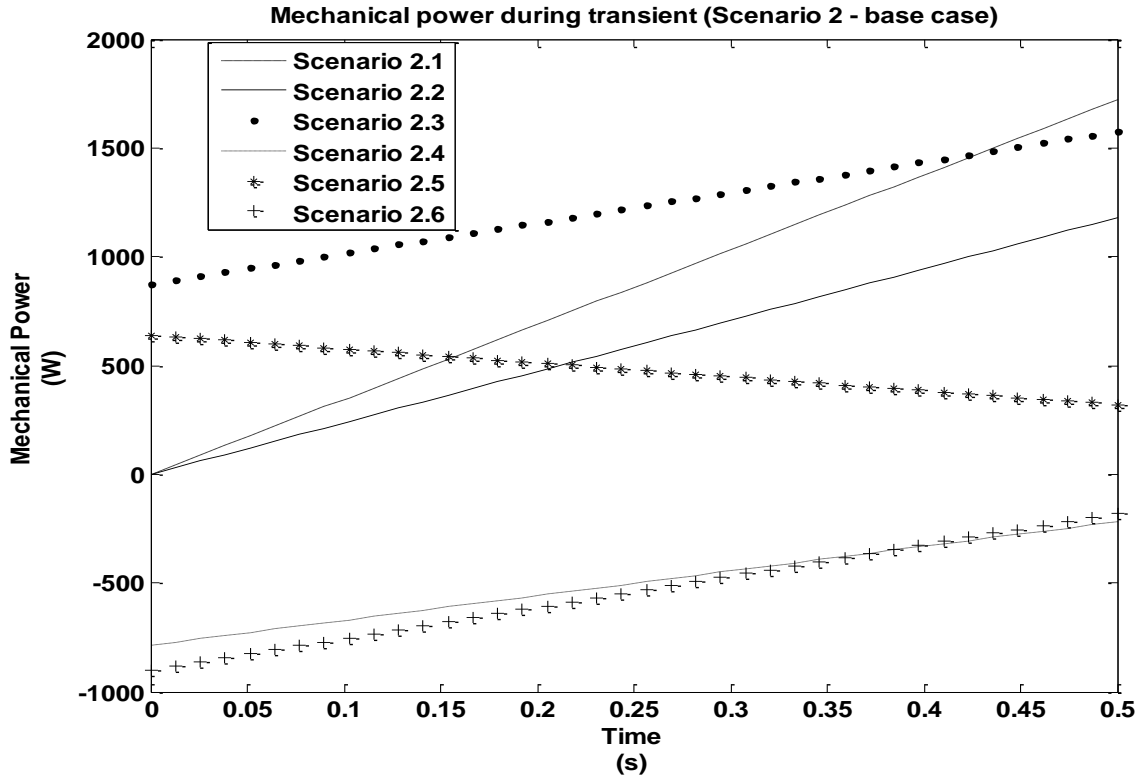


Figure 8.40. Mechanical power produced during transient (Scenario 2 - baseline).

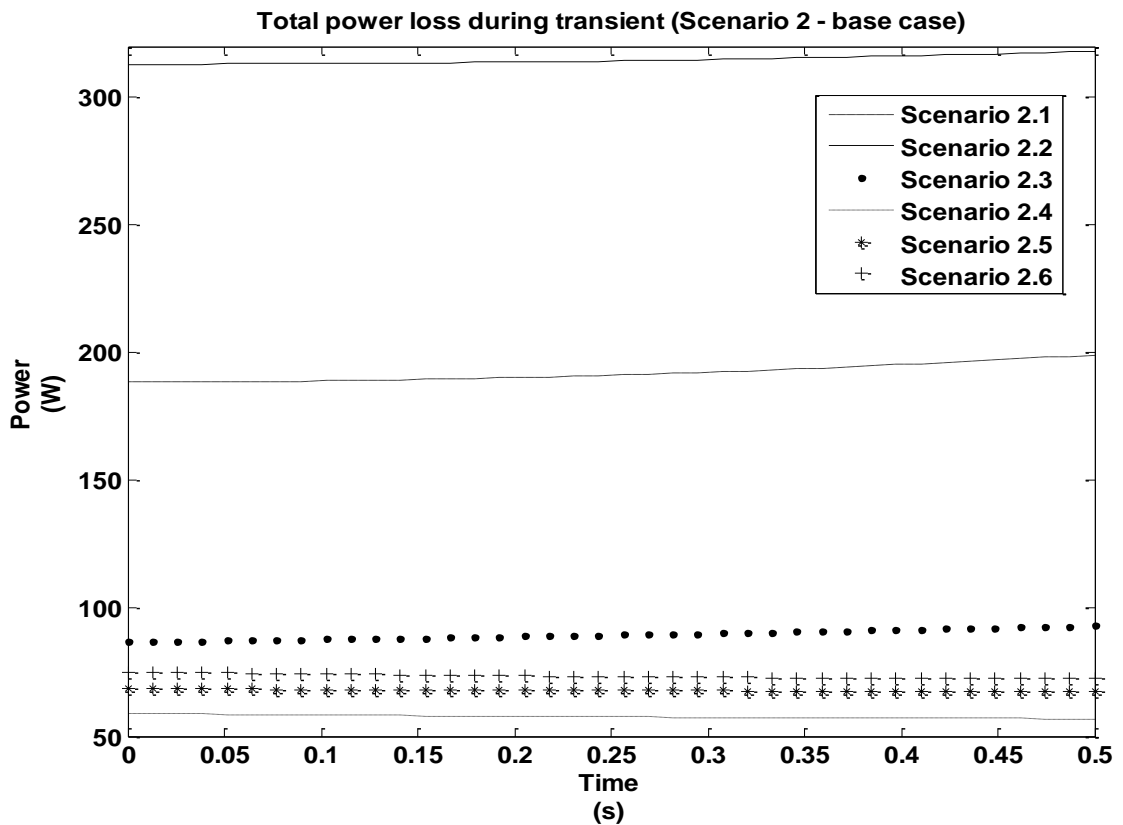


Figure 8.41. Total power losses in IM (Scenario 2 - baseline)

### 8.3.3 Comparison of the optimal trajectories vs Regime I trajectories

It can be observed from the results in above that optimal trajectories for  $i_{qs}$  and  $i_{ds}$  are significantly different from Regime I trajectories. The resulting trajectories for rotor flux and electromagnetic torque take different shapes as well. However, it can be seen that the rotor speed has attained the desired reference speed at the end of the transient period. However, it can be observed that the optimal trajectory of rotor flux takes the shape of a conic section just as it did in Scenario 1. But the optimal electromagnetic torque is found to take on a nearly constant value during the transient period, in contrast to the conic shape it took in Scenario 1. The reasoning behind this becomes clearer in Chapter 9 when the analytic expression for optimal torque is derived.

### 8.3.4 Comparing Energy Efficiencies

By numerically integrating (using trapezoid rule) the power quantities (mechanical power and power losses), the total mechanical energy output and the energy losses during transients can be found. Then by applying (3.2.2) from section 3.2, the energy efficiency of the machine during transients can be calculated. The calculated results are tabulated in Table 8.4 below for both the optimal and the baseline for all the six scenarios.

*Table 8.4. Comparing total energy cost for scenario 2*

Scenario	Energy loss (J)		Mechanical energy produced (J)		Energy efficiency (%)		
	Optimal	Regime I	Optimal	Regime I	Optimal	Regime I	Improvement
2.1	92	96	450	430	<b>83.0</b>	81.7	<b>1.3</b>
2.2	135	157	265	295	<b>66.3</b>	65.3	<b>1</b>
2.3	45	45	620	613	<b>93.2</b>	93.2	<b>0</b>
2.4	20	29	-260	-250	<b>92.3</b>	88.4	<b>3.9</b>
2.5	35	34	225	240	<b>86.5</b>	87.6	<b>-1.1</b>
2.6	30	37	-270	-270	<b>88.9</b>	86.3	<b>2.6</b>

From these results, it can be observed that there is indeed an improvement in the efficiency averaging around 1.5% over the baseline when using optimal trajectories during the transient periods. Note that in cases where the rotor speed is decreased the mechanical energy is negative, i.e. the machine is acting as a generator. In Scenario 2 the improvement in energy efficiency is, however, much lower compared to that in Scenario 1. The reason being that the initial rotor flux was set high at the start of the transient which means it could not be increased to the extent that was possible in Scenario 1. The relationship between initial rotor flux and optimal energy efficiency is derived in the next chapter.

#### 8.4 Summary

This chapter explained the working of an algorithm based on the modified gradient method to numerically solve the TPBVP problem that was developed in Chapter 7 in order to obtain the numerical solution of the optimal control trajectories. The Gradient method involved an initial guessing of a control trajectory and then updating it using the conjugate gradient algorithm. To avoid instability that may occur due to a non-optimal step size, the gradient at each step was modified using the Hestenes-Steifel formula. The algorithm was applied to two IM models (Type I and Type II) having different parameters as well as boundary conditions. All the solutions for the control, state, and co-state trajectories were plotted. A baseline was also established using the Regime I of the control trajectories. The optimal rotor flux trajectories were found to lie on a conic curve in both Scenarios 1 and 2. The optimal electromagnetic torque was found to lie on a conic curve in Scenario 1 but it takes a constant value in Scenario 2. The total energy loss, the total mechanical energy produced and the energy efficiency were tabulated for both machines Type I and Type II.

The results showed that the improvement in energy efficiency due to the optimal trajectory was dependent on the initial rotor flux value and on the magnitude of change in speed.



## 9 ANALYTICAL EXPRESSIONS FOR IM OPTIMAL CONTROL TRAJECTORIES

Numerical solutions of the IM optimal control problem in the previous Chapter showed that it is possible to improve the energy efficiency using optimal control trajectories. However, the numerical solutions were specific to the case studies under investigation and the motor types. Those numerical solutions do not explicitly establish a relationship between the motor operating parameters and the optimal control law. This chapter attempts to do that by proposing prototype analytical expressions to describe the optimal state and control trajectories for an accelerating IM. The expressions for optimal transient energy losses are also derived. The reader of this document should note that while these expressions are inspired by the numerical solutions in Chapter 8 they do not use any data points from them, i.e. this is not a curve fitting exercise specific to the case studies of Chapter 8. The prototype expressions to be derived are generic and are applicable to any type of accelerating/decelerating IM. Hence, this work is in contrast to the other published literature proposing analytical expressions for their specified optimal trajectories. Although the prototype expressions will be in the form of open loop control laws, the objective is not to use them for real-time control of IMs (real-time control is achieved later through the use of neural networks in Chapter 10). Instead, the aim is to study how different IM operating parameters influence the optimal energy efficiency.

A brief overview is provided here to aid in reading the chapter. First, an expression ( a function of time) for the optimal rotor d-axis flux and the stator d-axis current is proposed. Using some assumptions, these expressions are written purely in terms of the initial rotor

flux  $\Psi_{dr}^a$ , and flux ratio,  $x$ . The significance of the flux ratio  $x$  will be discussed later. For optimal stator q-axis current, two types of prototype of expressions (function of time) are proposed and they are expressed in terms of the initial rotor flux  $\Psi_{dr}^a$ , change in speed  $C$ , and flux ratio  $x$ . Hence, we have two sets of prototype expressions which will be referred to as Trajectory A and Trajectory B. The rotor flux expression will be same while the q-axis current expression will be different for A and B. As a baseline, the Regime I trajectory from section 7.2 is used. The displacement in rotor angle due to both optimal and Regime I current trajectories are calculated and equated to each other. To this end, the energy losses for Regime I are first calculated. Then the energy losses for optimal trajectories of the stator q-axis current (both A and B) are expressed in terms of the Regime I energy losses and flux ratio  $x$ . Finally, we find the optimal value of  $x$  which minimizes the energy losses (a one-dimensional static optimization problem), and substitute it in the expressions for the rotor flux and stator current to obtain the optimal trajectories.

### 9.1 Prototype Expression for Optimal Rotor d-axis Flux

As discussed in Chapter 8 the optimal trajectory of the rotor d-axis flux is observed to take the distinctive shape of a conic section. Hence, the optimal rotor flux trajectory can be represented by a generic polynomial function of time as shown in (9.1.1). The rate of change of optimal rotor d-axis flux is found by differentiating (9.1.1) to obtain (9.1.2). The stator d-axis current trajectory necessary to realize this optimal flux trajectory can be obtained by plugging (9.1.2) into (7.4.3) to get (9.1.3).

$$\Psi_{dr}^{opt}(t) = \begin{cases} \Psi_{dr}^{f_1}, & t < t_0 \\ a_1 t^2 + b_1 t + c_1, & t_0 \geq t \leq t_{tf} \\ \Psi_{dr}^{f_2}, & t > t_{tf} \end{cases} \quad (9.1.1)$$

$$\frac{d\psi_{dr}^{opt}}{dt} = 2a_1t + b_1 \quad (9.1.2)$$

$$i_{ds}^{opt}(t) = \frac{1}{L_m} \left( \frac{L_r}{R_r} (2a_1t + b_1) + a_1t^2 + b_1t + c_1 \right) \quad (9.1.3)$$

where  $a_1$ ,  $b_1$ , and  $c_1$  are constants to be determined.

### 9.1.1 Regime I rotor flux trajectory expression

The rotor flux trajectory based on Regime I (from section 7.2.1) will be used as a baseline for comparison and is reproduced in (9.1.1.1). The corresponding rate of change of rotor flux and d-axis current trajectory are given by (9.1.1.2) and (9.1.1.3), respectively. Since the change in flux is zero we can express the stator d-axis current in terms of rotor flux as shown by (9.1.1.3).

$$\psi_{dr}(t) = \psi_{dr}^a, \quad \text{for all } t \quad (9.1.1.1)$$

$$\frac{d\psi_{dr}}{dt} = 0 \quad (9.1.1.2)$$

$$i_{ds}(t) = i_{ds}^a = \frac{\psi_{dr}^a}{L_m} \quad (9.1.1.3)$$

### 9.1.2 Expressing the conic polynomial trajectory in terms of rotor flux values

Assuming that the optimal trajectory of rotor flux (9.1.1) generally takes on the values  $\psi_{dr}^0$ ,  $\psi_{dr}^m$  and  $\psi_{dr}^f$  at  $t = t_0$ ,  $\frac{t_f}{2}$ , and  $t_f$ , respectively as illustrated in Figure 9.1., it is possible to express the parameters  $a_1$ ,  $b_1$ ,  $c_1$  of the generic polynomial of (9.1.1) in terms of these flux values as shown in (9.1.2.1). The derivation of (9.1.2.1) is given in Appendix IV.

$$a_1 = \frac{2\psi_{dr}^a + 2\psi_{dr}^0 - 4\psi_{dr}^m}{t_{f}^2} \quad (9.1.2.1)$$

$$b_1 = \frac{4\psi_{dr}^m - 3\psi_{dr}^0 - \psi_{dr}^f}{t_{tf}}$$

$$c_1 = \psi_{dr}^0$$

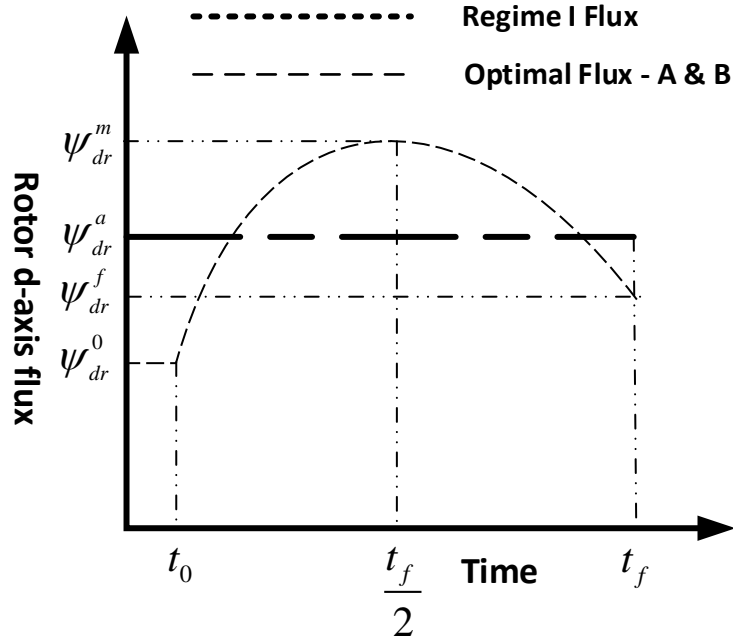


Figure 9.1. Illustration of flux trajectories for baseline (Regime 1) and optimal

## 9.2 Prototype expression for optimal stator q-axis current

The shape of the q-axis current trajectories in the numerical solution (from Chapter 8) varied significantly between the two scenarios that were studied. Hence, two different generic prototype trajectories are considered for the optimal stator q-axis current trajectory. The first prototype optimal trajectory is a conic and will be referred to as Type A. It is represented by a generic polynomial function of time as shown in (9.2.1). An illustration of Type A is depicted in Figure 9.2.

$$i_{qs}^{opt-A}(t) = \begin{cases} i_{qs}^0, & t < t_0 \\ a_2 t^2 + b_2 t + c_2, & t_0 \geq t \leq t_{tf} \\ i_{qs}^f, & t > t_{tf} \end{cases} \quad (9.2.1)$$

where  $a_2, b_2$  and  $c_2$  are constants to be determined.

The second prototype optimal trajectory of the stator q-axis current is a constant value and will be referred to as type B. It is expressed by (9.2.2).

$$i_{qs}^{opt-B}(t) = \begin{cases} i_{qs}^0, & t < t_0 \\ c_3, & t_0 \geq t \leq t_{tf} \\ i_{qs}^f, & t > t_{tf} \end{cases} \quad (9.2.2)$$

### 9.2.1 Regime I q-axis current trajectory

The q-axis current trajectory based on Regime I (from section 7.2.1) will be used as a baseline for comparison and is reproduced in (9.2.1.1).

$$i_{qs}(t) = i_{qs}^a \quad (9.2.1.1)$$

### 9.2.2 Expressing conic trajectory parameters in terms of stator d-axis current

If we assume that the conic optimal Trajectory A of the stator q-axis current passes through the generic points  $i_{qs}^0, i_{qs}^m$  and  $i_{qs}^f$  at  $t = t_0, \frac{t_f}{2}$ , and  $t_f$ , respectively and as illustrated in Figure 9.2, it is possible to express the constants  $a_2, b_2, c_2$  in terms of stator q-axis currents as shown in (9.2.2.1). The derivation is given in Appendix IV. For optimal trajectory B, if the stator q-axis current passes through the point  $i_{qs}^b$  we get (9.2.2.2)

$$b_2 = \frac{4i_{qs}^m - 3i_{qs}^0 - i_{qs}^f}{t_{tf}} \quad (9.2.2.1)$$

$$a_2 = \frac{2i_{qs}^f + 2i_{qs}^0 - 4i_{qs}^m}{t_{tf}^2}$$

$$c_2 = i_{qs}^0$$

$$c_3 = i_{qs}^b$$

(9.2.2.2)

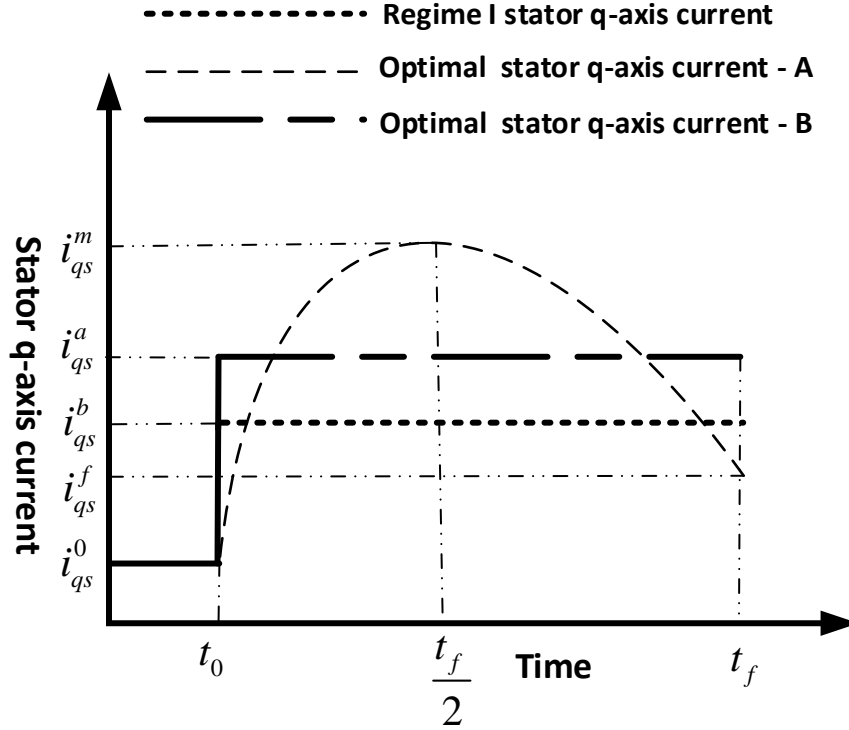


Figure 9.2. Illustrating stator q-axis current for baseline (Regime 1) and optimal

### 9.3 Assumptions to Prove Optimality

In the previous sections, the coefficients  $a_1, b_1, c_1, a_2, b_2, c_2,$  and  $c_3$  of the prototype expressions *were* expressed in terms of currents, rotor fluxes, and time. All except three of these values can be determined using the inputs from the optimal control problem. The unknown in the case of the optimal d-axis flux trajectory is  $\Psi_{dr}^m$ . The unknowns in the case of the optimal q-axis current trajectory are  $i_{qs}^m$  and  $i_{qs}^b$  for both Trajectory A and Trajectory B, respectively. To determine these unknowns, we assume that the IM is running on no-load and maintains a minimum flux during steady state. These assumptions mean that there is no load torque on the IM rotor shaft and all the mechanical energy output from IM is being stored as kinetic energy in the rotor mass. For example, an

IM used in a flywheel application works under these conditions. It must be pointed out these assumptions are there only to alleviate the mathematical effort that is required. They are not a way to force fit a solution. The procedure outlined in the following section can be applied to an IM with a load torque and which operates at different flux levels, depending on the load. However, the mathematical effort would be significantly higher and would require a capable symbolic toolbox. The list of assumptions are:

1. Transient time: The transient time interval is assumed to be normalized so that it starts at 0 and ends at 1. The initial and final times corresponding to this interval are given by (9.3.1).
2. Rotor flux: The initial and final values of the optimal rotor flux trajectory are assumed to be equal as given by (9.3.2) and (9.3.3).
3. Stator q-axis current: The initial and final values of optimal stator q-axis current trajectories A and B are assumed to be equal as given by (9.3.4).
4. Load torque: The load torque is assumed to be zero as shown in (9.3.5).

Note that, the shape of rotor d-axis flux trajectory and the stator q-axis current trajectory corresponding to these assumptions are same as that of Figure 9.1 and Figure 9.2. Only the initial and final values will be changed.

$$t_0 = 0 \tag{9.3.1}$$

$$t_{1f} = 1 \tag{9.3.1}$$

$$\psi_{dr}^f = \psi_{dr}^0 = \psi_{dr}^a \tag{9.3.2}$$

$$i_{qs}^0 = i_{qs}^f = 0 \tag{9.3.4}$$

$$T_L = 0 \tag{9.3.5}$$

Note that  $\Psi_{dr}^a$  is known from the optimal control problem in the form of the initial condition. Hence, the extremum value in the optimum flux trajectory  $\Psi_{dr}^m$  can be expressed in terms of the initial rotor flux  $\Psi_{dr}^a$  as shown in (9.3.3).

$$\Psi_{dr}^m = x\Psi_{dr}^a \quad (9.3.3)$$

where  $x$  is the ratio between  $\Psi_{dr}^m$  and  $\Psi_{dr}^a$ .

Using the above assumptions, it is possible to rewrite the coefficients of the rotor flux expression and the q-axis current expressions (for A and B) as given in (9.3.6) through (9.3.8). Note that even after using the above assumptions we still have the same number of unknowns. However, we have been able to express  $\Psi_{dr}^m$  in terms of the initial flux using the flux ratio  $x$ . This approach will considerably ease the finding of a solution.

$$\begin{aligned} a_1 &= 4\Psi_{dr}^a (1-x) \\ b_1 &= 4\Psi_{dr}^a (x-1) \end{aligned} \quad (9.3.6)$$

$$c_1 = \Psi_{dr}^a$$

$$\begin{aligned} a_2 &= -4i_{qs}^m \\ b_2 &= 4i_{qs}^m \end{aligned} \quad (9.3.7)$$

$$c_2 = 0$$

$$c_3 = i_{qs}^b \quad (9.3.8)$$

Since the load torque is assumed to be zero, the state equation for rotor speed from section 7.1 can be simplified and written as in (9.3.9).



$$\frac{d\omega_m}{dt} = \left( \frac{pL_m}{2JL_r} \right) i_{qs}(t) \psi_{dr}(t) \quad (9.3.9)$$

#### 9.4 Energy Costs and Rotor Angle Displacement for Regime I Trajectories

In this section, we find the energy costs and the rotor angle displacement when the IM is accelerating at a constant rate of  $C$  rad/s during the transient time interval. The state equation for rotor speed (9.3.9) can be equated to  $C$  after substituting for flux and current from Section 9.1.1 and Section 9.2.1 respectively to get (9.4.1). The stator q-axis current can then be found as given by (9.4.2).

$$\frac{d\omega_m}{dt} = K_1 i_{qs}^a \psi_{dr}^a = C \quad (9.4.1)$$

$$i_{qs}^a = \frac{C}{K_1 \psi_{dr}^a} \quad (9.4.2)$$

where,  $K_1 = \left( \frac{pL_m}{2JL_r} \right)$  (from (9.3.9)).

Solving (9.4.1) will give the rotor speed (9.4.3), and integrating the resulting speed within the transient time interval will give the displacement in the rotor angle,  $S_1$ , in radians. The displacement in the rotor angle due to the optimal trajectories should be equal to that due to Regime 1 trajectories to ensure that the mechanical energy produced by the IM in both cases is same.

$$\omega_m = Ct \quad (9.4.3)$$

$$S_1 = \int_0^1 \omega_m dt = \frac{C}{2} \quad (9.4.4)$$

The energy losses for Regime I trajectories provide a baseline for comparing the energy costs due to optimal trajectories. Note that the energy losses can be separated into d-and q-

axis components. The d-axis components of the stator and rotor Ohmic losses can be expressed in terms of d-axis current and d-axis flux as given by (9.4.5) and (9.4.6), respectively. Note that rotor d-axis loss component will be zero for Regime I due to (9.1.1.3)

$$E_{loss}^{stator\_d-axis} = \int_0^1 (i_{ds}^a)^2 R_s dt = \left( \frac{\psi_{dr}^a}{L_m} \right)^2 R_s = E_1 \quad (9.4.5)$$

$$E_{loss}^{rotor\_d-axis} = \int_0^1 \frac{R_r}{L_r^2} L_m^2 (\psi_{dr}^a - L_m i_{ds}^a)^2 dt = 0 = E_2 \quad (9.4.6)$$

Similarly, the q-axis component of the stator and rotor Ohmic losses can be expressed in terms of q-axis current as given by (9.4.7) and (9.4.8), respectively.

$$E_{loss}^{stator\_q-axis} = \int_0^1 (i_{qs}^a)^2 R_s dt = \left( \frac{C}{K_1 \psi_{dr}^a} \right)^2 R_s = E_3 \quad (9.4.7)$$

$$E_{loss}^{rotor\_q-axis}(t) = \int_0^1 \frac{R_r}{L_r^2} L_m^2 (i_{qs}^a)^2 dt = \frac{R_r L_m^2}{L_r^2} \left( \frac{C}{K_1 \psi_{dr}^a} \right)^2 = E_4 \quad (9.4.8)$$

## 9.5 Expressions for Optimal d-axis Rotor Flux, d-axis Current and Transient Energy Loss

In this section, first, the expressions (functions of time) for rotor flux and d-axis current are derived in terms of  $\psi_{dr}^a$ ,  $x$ , and other IM parameters for prototype trajectories A and B. Then using them, the d-axis energy loss components which depend only on the rotor flux and d-axis current are obtained.

First, we substitute the values of  $a_1, b_1, c_1$  from (9.3.6) into (9.1.1) through (9.1.3) to obtain d-axis rotor flux trajectory (9.5.1), rate of change of flux (9.5.2), and stator d-axis current trajectory (9.5.3).

$$\psi_{dr}(t) = \psi_{dr}^a \left( 4(1-x)t^2 - 4(1-x)t + 1 \right) \quad (9.5.1)$$

$$\frac{d\psi_{dr}}{dt} = 4\psi_{dr}^a (1-x)(2t-1) \quad (9.5.2)$$

$$i_{ds}(t) = \frac{\psi_{dr}^a}{L_m} \left( \frac{4L_r}{R_r} (1-x)(2t-1) + 4(1-x)t^2 - 4(1-x)t + 1 \right) \quad (9.5.3)$$

Substituting the above equations in the expressions for stator and rotor Ohmic energy losses during transients gives the d-axis component of the stator energy loss (9.5.4) and rotor energy loss (9.5.5). Note that the intermediate steps involved in deriving the d-axis energy loss components are included in Appendix V for reference.

$$E_{loss}^{stator-d-opt} = \int_0^1 i_{ds}^2(t) R_s dt = R_s \left( \frac{\psi_{dr}^a}{L_m} \right)^2 \left( \frac{\frac{16\tau_r^2}{3}(x-1)^2 + (2(4x^2 + 2x + 1) + 1)}{15} \right) \quad (9.5.4)$$

$$E_{loss}^{stator-d-opt} = \left( \frac{16\tau_r^2}{3}(x-1)^2 + \frac{(2(4x^2 + 2x + 1) + 1)}{15} \right) E_1 \quad (9.5.4)$$

$$E_{loss}^{rotor-d-opt} = \int_0^1 \frac{R_r}{L_r^2} (\psi_{dr}(t) - L_m i_{ds}(t))^2 dt = \left( \frac{16}{3} \right) \frac{(\psi_{dr}^a)^2 (x-1)^2}{R_r} \quad (9.5.5)$$

Note that in above equations, if flux ratio  $x = 1$  then the energy losses for optimal trajectories would be the same as that of the Regime I energy losses.

## 9.6 Stator q-axis Current and Transient Energy Losses for Trajectory A

As stated earlier, based on numerical solutions, the stator q-axis current trajectory is different for both A and B cases, and hence they will have different loss expressions. In this section, the energy losses due to the q-axis current trajectory A is calculated. First, we substitute the values of  $a_2, b_2, c_2$  from (9.3.7) in (9.2.1) to obtain (9.6.1). Then (9.6.1) and

(9.5.1) can be substituted in the state equation for rotor speed (9.3.9) to obtain (9.6.2).

Solving (9.6.2) results in an expression for the rotor speed as in (9.6.3).

$$i_{qs}^{opt-A}(t) = 4i_{qs}^m(t - t^2) \quad (9.6.1)$$

$$\frac{d\omega_m}{dt} = K_1 i_{qs}(t) \psi_{dr}(t) = 4i_{qs}^m \psi_{dr}^a K_1 (t - t^2) (4(1-x)t^2 - 4(1-x)t + 1) \quad (9.6.2)$$

$$\omega_m(t) = 4i_{qs}^m \psi_{dr}^a K_1 \left( \left( \frac{4x}{5} - \frac{4}{5} \right) t^5 + (2 - 2x)t^4 + \left( \frac{4}{3}x - \frac{5}{3} \right) t^3 + \frac{t^2}{2} \right) \quad (9.6.3)$$

Integrating the rotor speed within the transient time interval as shown in (9.6.4) will give the displacement in rotor angle  $S_2$  in terms of radians resulting from the use of the stator q-axis current trajectory A.  $S_2$  must be equal to  $S_1$  (displacement in the rotor angle due to Regime I). Using this equality, then it is possible to solve for  $i_{qs}^m$  as in (9.6.6). Note that the intermediate steps involved in deriving the stator q-axis energy loss components for trajectory A are included in Appendix V for reference.

$$S_2 = \int_0^1 \omega_m dt = 4i_{qs}^m \psi_{dr}^a K_1 \left( \frac{x}{15} + \frac{1}{60} \right) \quad (9.6.4)$$

$$4i_{qs}^m \psi_{dr}^a K_1 \left( \frac{4x+1}{60} \right) = \frac{C}{2} \quad (9.6.5)$$

$$i_{qs}^m = \left( \frac{7.5}{4x+1} \right) \frac{C}{\psi_{dr}^a K_1} \quad (9.6.6)$$

Substituting  $i_{qs}^m$  from (9.6.6) into (9.6.1) will give the expression for stator q-axis current in terms of the flux ratio  $x$  as given by (9.6.7). Now it is possible to obtain an expression for the q-axis component of the stator and rotor Ohmic losses as given by (9.6.8) and (9.6.9), respectively.

$$i_{qs}^{opt-A}(t) = \left( \frac{30}{4x+1} \right) \frac{C}{\psi_{dr}^a K_1} (t - t^2) \quad (9.6.7)$$

$$E_{loss}^{stator-q-optA} = \int_0^1 i_{qs}^2(t) R_s dt = \frac{30}{(4x+1)^2} \left( \frac{C}{K_1 \psi_{dr}^a} \right)^2 R_s = \frac{30}{(4x+1)^2} E_3 \quad (9.6.8)$$

$$\begin{aligned} E_{loss}^{rotor-q-optA} &= \int_0^1 \frac{R_r}{L_r^2} (L_m^2 i_{qs}^2(t)) dt \\ &= \frac{30}{(4x+1)^2} \frac{R_r L_m^2}{L_r^2} \left( \frac{C}{K_1 \psi_{dr}^a} \right)^2 = \frac{30}{(4x+1)^2} E_4 \end{aligned} \quad (9.6.9)$$

### 9.7 Stator q-axis Current Energy Loss for Trajectory B

In this section, the energy losses for stator q-axis current trajectory B are calculated. First, coefficient  $c_3$  from (9.3.8) is substituted into (9.2.2) to obtain (9.7.1). The state equation for rotor speed is obtained by substituting (9.7.1) and (9.5.1) into (9.3.9) to get (9.7.2). Solving (9.7.2) will then result in an expression for the rotor speed as in (9.7.3).

$$i_{qs}^{opt-B}(t) = i_{qs}^b \quad (9.7.1)$$

$$\frac{d\omega_m}{dt} = K_1 i_{qs}^b \psi_{dr}^{opt}(t) \quad (9.7.2)$$

$$\omega_m = K_1 i_{qs}^b \psi_{dr}^a \left( \frac{4(1-x)t^3}{3} - \frac{4(1-x)t^2}{2} + t \right) \quad (9.7.3)$$

Integrating the rotor speed as shown in (9.7.4) within the transient time interval will give the displacement in rotor angle,  $S_3$ , resulting from the use of stator q-axis current trajectory B.  $S_3$  must be equal to  $S_1$  (rotor angle displacement due to Regime I). Then, it is possible to solve for  $i_{qs}^b$  as in (9.7.6). Note that the intermediate steps involved in deriving the q-axis energy loss components for trajectory B are included in Appendix V for reference.

$$S_3 = \int_0^1 \omega_m dt = \left( \frac{2x+1}{6} \right) K_1 i_{qs}^b \psi_{dr}^a \quad (9.7.4)$$

$$\left( \frac{2x+1}{6} \right) K_1 i_{qs}^b \psi_{dr}^a = \frac{C}{2} \quad (9.7.5)$$

$$i_{qs}^b = \frac{3}{(2x+1)} \left( \frac{C}{K_1 \psi_{dr}^a} \right) \quad (9.7.6)$$

The expression for  $i_{qs}^b$  in (9.7.6) can be used to find the stator q-axis and rotor q-axis Ohmic energy losses given by (9.7.7) and (9.7.8), respectively.

$$E_{loss}^{stator-q-optB} = \int_0^1 (i_{qs}^b)^2 R_s dt = \frac{9}{(2x+1)^2} \left( \frac{C}{K_1 \psi_{dr}^a} \right)^2 R_s \quad (9.7.7)$$

$$E_{loss}^{rotor-q-optB} = \int_0^1 \frac{R_r L_m^2}{L_r^2} (i_{qs}^b)^2 dt = \frac{9}{(2x+1)^2} \frac{R_r L_m^2}{L_r^2} \left( \frac{C}{K_1 \psi_{dr}^a} \right)^2 \quad (9.7.8)$$

## 9.8 Determining the Optimal Flux Ratio $x$

In the expressions for energy losses that were obtained in Sections 9.5, 9.6, and 9.7 it can be observed that the only unknown parameter is the flux ratio  $x$ . The parameter  $\Psi_{dr}^a$  can be determined from measuring the flux at the start of the transient interval and by definition  $C$  is the difference between the actual rotor speed at the start of transient and the desired rotor speed at end of the transient interval. It can be noted that  $x$  is inversely related to the q-axis component of the energy losses and directly related to the d-axis component of the energy losses. Hence, there must exist an optimal value of  $x$  that would minimize the total energy losses. From above it can be seen that the problem of finding the optimal trajectory has been reduced to a one-dimensional optimization problem. Taking the first derivative of the total energy losses for Trajectory A w.r.t.  $x$  and equating that to zero gives (9.8.1) which is a 4<sup>th</sup> order polynomial equation in terms of  $x$ . It is possible to solve (9.8.1)

for the  $x$  numerically since the values of the other parameters in the equation are known. Here the ‘solve’ function of MATLAB software was used. Since the second derivative shown by (9.8.2) is found to be always positive, that means  $x$  minimizes the total loss function.

$$\begin{aligned} \frac{dE_{loss}^{total\_optA}}{dx} &= E_1 \left( \frac{16x}{15} + \frac{16\tau_r^2(2x-2)}{3} + \frac{4}{15} \right) + \left( \frac{16}{3} \right) \frac{2(\psi_{dr}^a)^2(x-1)}{R_r} \\ &+ \frac{-240}{(4x+1)^3} (E_3 + E_4) = 0 \end{aligned} \quad (9.8.1)$$

$$\begin{aligned} \frac{d^2E_{loss}^{total\_optB}}{dx^2} &= E_1 \left( \frac{16}{15} + \frac{32\tau_r^2}{3} + \frac{4}{15} \right) + \left( \frac{16}{3} \right) \frac{2(\psi_{dr}^a)^2}{R_r} \\ &+ \frac{2880}{(4x+1)^4} (E_3 + E_4) > 0 \end{aligned} \quad (9.8.2)$$

where,

$$E_1 = \left( \frac{\psi_{dr}^a}{L_m} \right)^2 R_s, E_3 = \left( \frac{C}{K_1 \psi_{dr}^a} \right)^2 R_s, E_4 = \frac{R_r L_m^2}{L_r^2} \left( \frac{C}{K_1 \psi_{dr}^a} \right)^2,$$

The same procedure for calculating the flux ratio  $x$  can be repeated for optimal trajectory B, and can be found in Appendix VI.

The influence that various parameters in the optimal energy loss equation have on the optimal flux ratio  $x$  can be determined by conducting a sensitivity analysis. Parameters from the Type I IM were used in the IM model. The sensitivity of the optimal ratio  $x$  to the initial flux  $\Psi_{dr}^a$  and the moment of inertia  $J$  (which affects  $K_1$ ) is illustrated in Figure 9.3. The sensitivity of the flux ratio  $x$  to initial flux  $\Psi_{dr}^a$  and the change in magnitude of rotor

speed  $C$  (which affects  $K_1$ ) is illustrated in Figure 9.4. The sensitivity of optimal  $x$  to the initial flux  $\Psi_{dr}^a$  and rotor time constant  $\tau_r$  is illustrated in Figure 9.5.

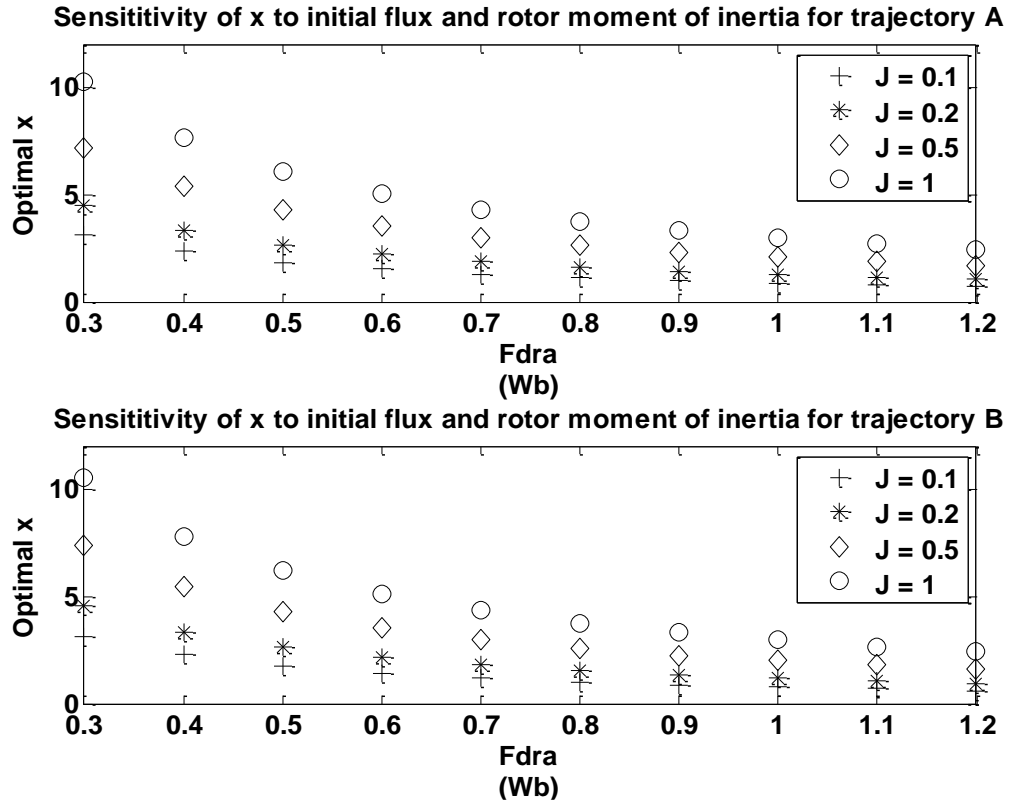


Figure 9.3. Sensitivity of optimal ratio  $x$  to the initial flux and moment of inertia



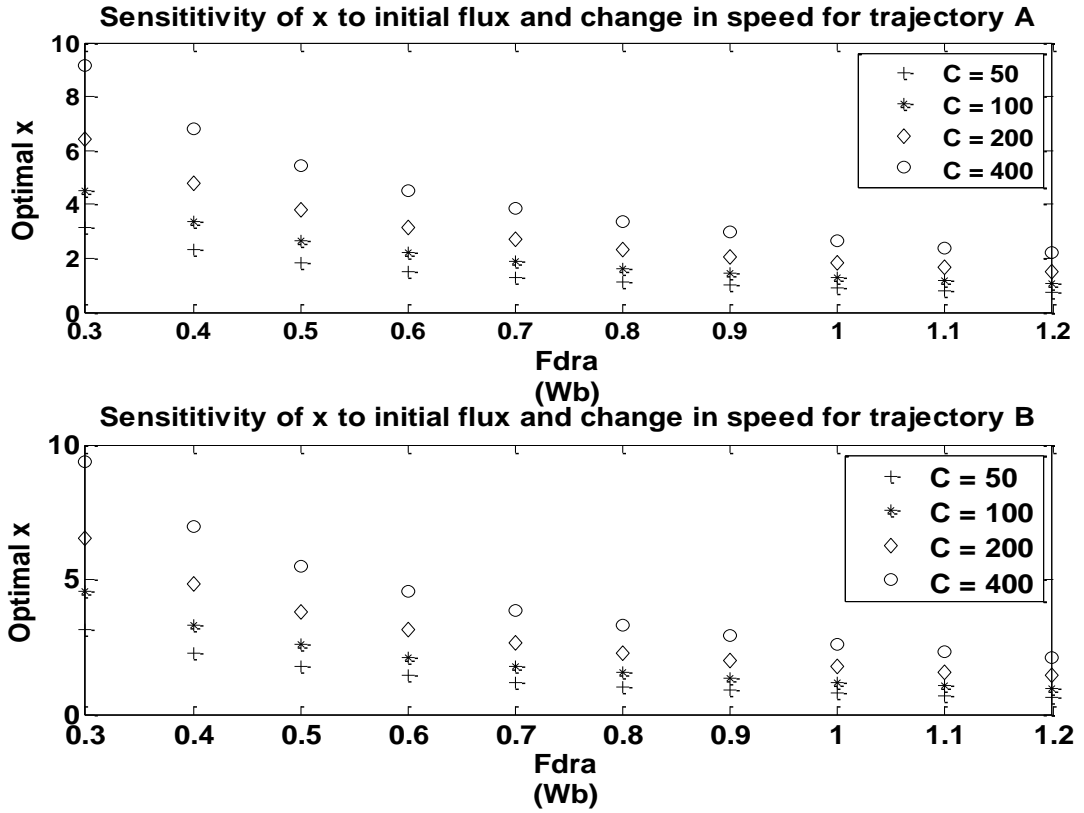


Figure 9.4. Sensitivity of optimal  $x$  to the initial flux and change in speed

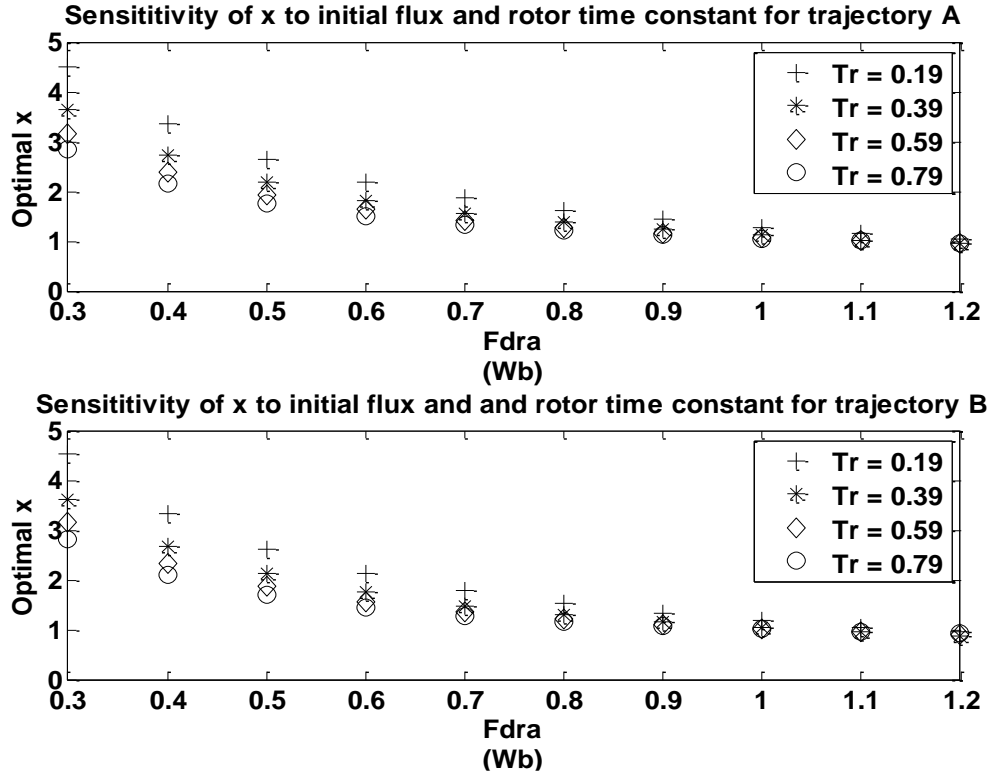


Figure 9.5. Sensitivity of optimal  $x$  to the initial flux and rotor time constant

The above sensitivity analysis shows that a higher initial flux results in a lower value of the optimal flux ratio  $x$ . This is intuitive since it makes no sense for the flux to be increased during the transient interval if it is already high to begin with. Also, if the initial flux is very high, the optimal value of  $x$  would be less than one. Another important observation is that the optimal value of  $x$  increases, corresponding to an increase in the moment of inertia  $J$  and the change in speed  $C$ , while it decreases for an increase in the rotor time constant  $\tau_r$ . Practically, this means that for IM's with heavy rotors, a large change in rotor speed would require a large change in flux to achieve an optimal transient energy efficiency.

#### 9.9 Evaluating improvement in energy efficiency using derived analytical Prototype expressions

The closed form analytical solutions of the optimal control trajectories and the optimal flux ratio  $x$  can be used to calculate the energy efficiency during transients for different scenarios. Parameters from Type I IM were used for this energy efficiency calculation. Regime I is used as a base case for comparison purposes. The test cases for this energy efficiency calculation are given in Table 9.1. In Table 9.1 the first four cases are for positive changes in the reference speed, and next four cases are for negative changes in the reference speed. Note that only  $\Psi_{dr}^a$  is varied across the cases. The calculated energy losses and efficiency for all the cases are tabulated in Table 9.2. The trajectories of rotor d-axis flux, rotor speed, electromagnetic torque, and power losses corresponding to case 1.3 and case 1.7 are given in Figure 9.6, Figure 9.7, Figure 9.8, and Figure 9.9, respectively.

Table 9.1. Optimal  $x$  for different scenarios.

Scenario	$\Psi_{dr}^a$ (Wb)	$C$ (rad/s)	$\omega_r^0$ (rad/s)	Optimal $x$		Time interval (s)
				Trajectory A	Trajectory B	
1.1	0.2	100	0	6.8	6.9	1.0
1.2	0.5	100	0	2.65	2.6	1.0
1.3	1.0	100	0	1.27	1.2	1.0
1.4	1.5	100	0	0.82	0.72	1.0
1.5	0.2	-200	200	9.7	9.9	1.0
1.6	0.5	-200	200	3.8	3.8	1.0
1.7	1.0	-200	200	1.8	1.7	1.0
1.8	1.5	-200	200	1.2	1.1	1.0

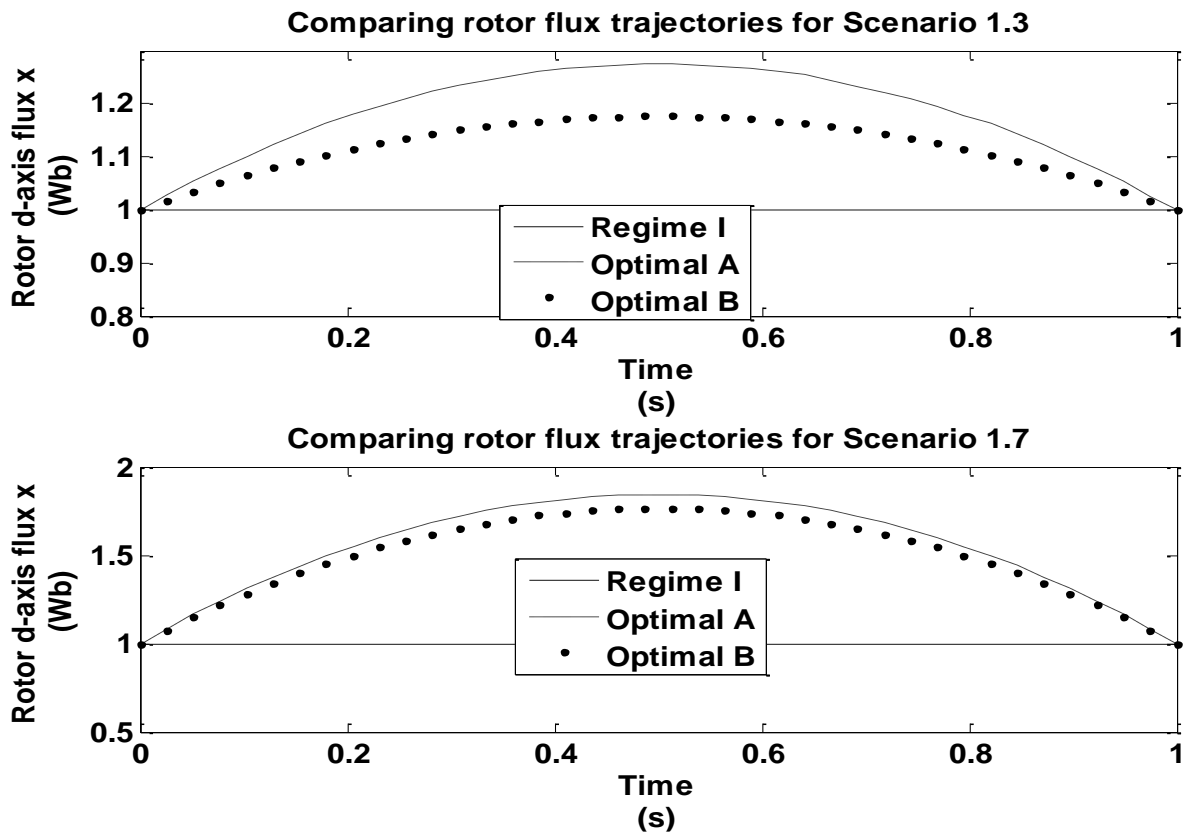


Figure 9.6. Comparison of rotor  $d$ -axis flux trajectories

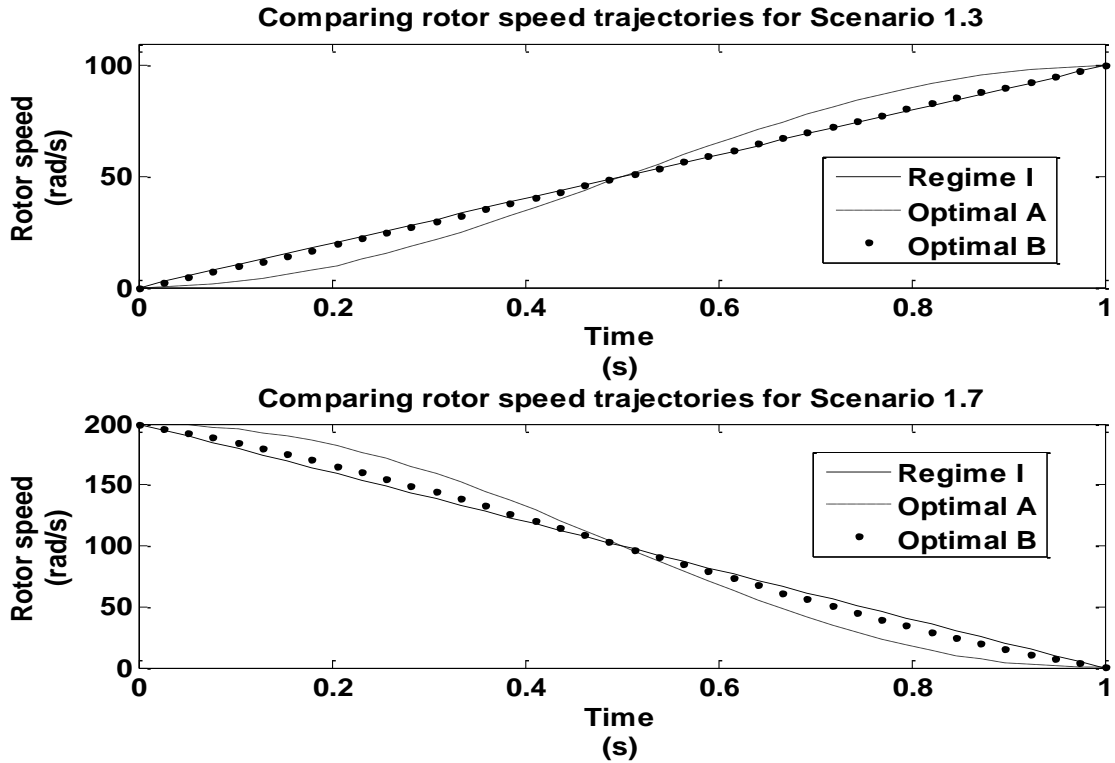


Figure 9.7. Comparison of rotor speed trajectories

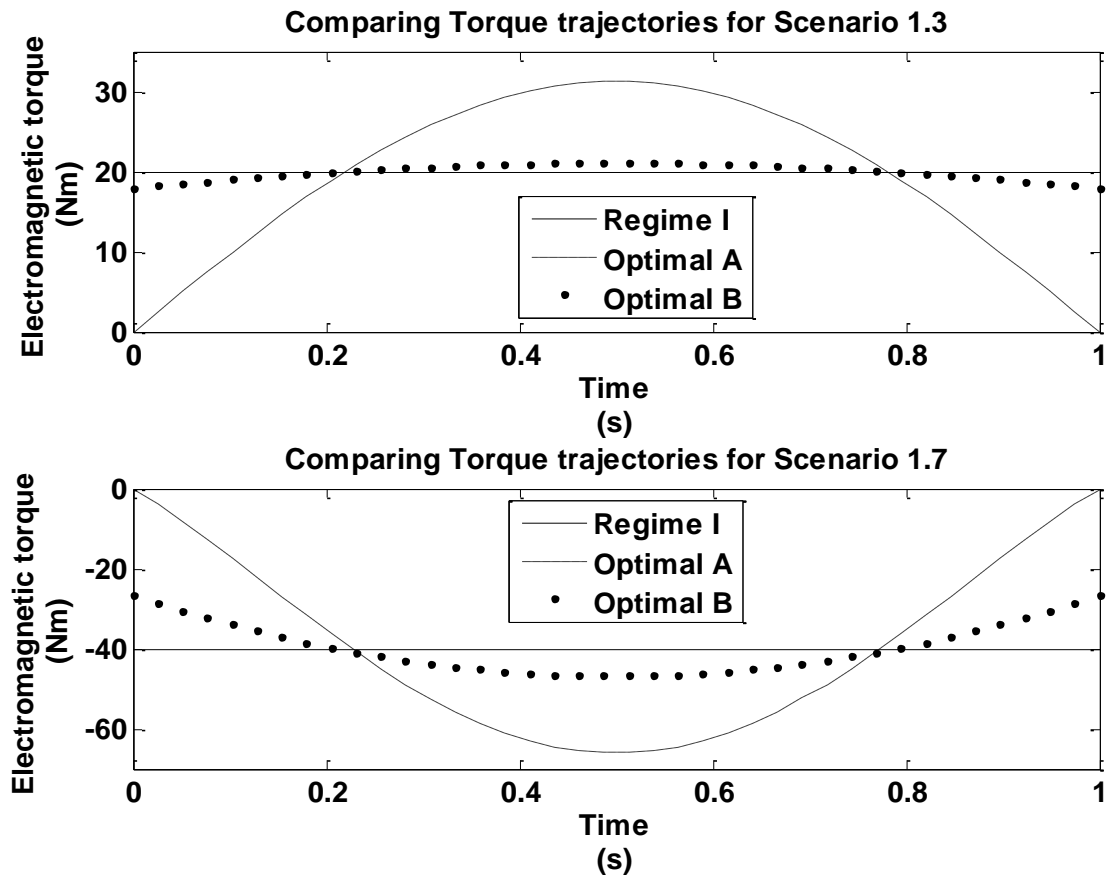


Figure 9.8. Comparison of electromagnetic torque trajectories

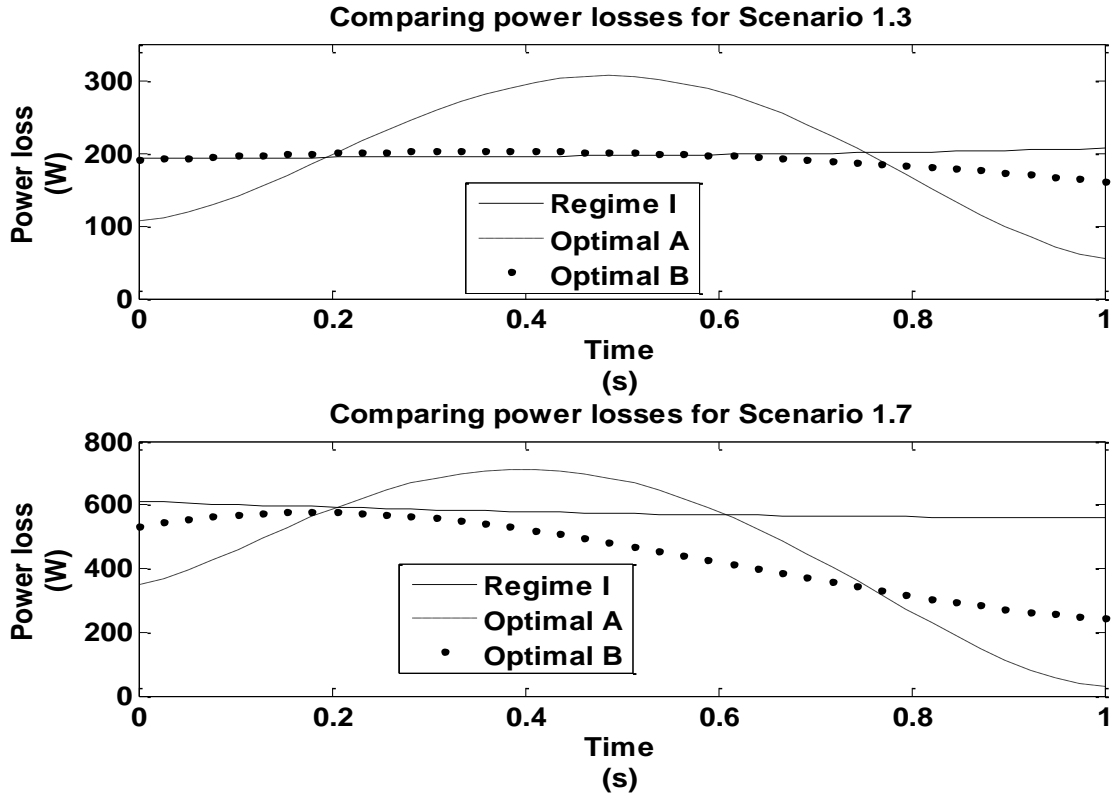


Figure 9.9. Comparison of power losses

As expected the rotor flux trajectory for both optimal trajectory cases A and B of the stator q-axis current are conic shaped and terminal rotor speed attains the specified value. The electromagnetic torque and total power losses for both optimal A and optimal B are time varying unlike Regime I. However, optimal case B has a lower peak torque when compared to optimal case A. The mechanical output power can be found by multiplying the rotor speed and the electromagnetic torque. Integrating this mechanical output power would result in the mechanical energy that is produced. Similarly, the power losses can be integrated to obtain the energy losses. Using these calculated energy values, the energy efficiency during transients can be calculated.

Table 9.2. Comparing energy efficiency for optimal and Regime I (baseline) cases.

Scenario	Mechanical Energy (J)	Total energy losses			Energy efficiency		
		Regime I (J)	Optimal A (J)	Optimal B (J)	Regime I (%)	Optimal A (%)	Optimal B (%)
Motoring							
1.1	1000	3060	226	239	24.6	81.5	80.6
1.2		508	211	213	66.3	82.5	82.4
1.3		197	205	192	83.5	82.9	83.9
1.4		224	225	202	81.7	81.6	83.2
Regenerative Braking							
1.5	-4000	12240	530	560	-206	86.7	85.9
1.6		1980	500	509	50.5	87.5	87.3
1.7		577	470	448	85.5	88.2	88.8
1.8		415	463	419	89.6	88.4	89.5

From above calculations, it can be seen that as the initial flux increases the improvement in the energy efficiency for optimal trajectory over Regime 1 decreases. Similarly, optimal trajectory A is found to have a slightly higher efficiency when compared to optimal trajectory B if the initial flux is low. However, when the value of the initial flux is high the opposite is true. These observations agree with the results of Chapter 8.

#### 9.10 Sensitivity of Energy Efficiency to Parameters

Using the technique of the previous section, the sensitivity of transient energy efficiency to changes in the operating parameters of the IM can be analyzed. The first set of plots in Figure 9.10 shows the sensitivity to the speed change  $C$  and  $\Psi_{dr}^a$  with  $J$  and  $\tau_r$  being constant. Figure 9.11 shows the sensitivity to moment of inertia  $J$  and  $\Psi_{dr}^a$  with speed change  $C$  and  $\tau_r$  being constant. Finally, the sensitivity to  $\tau_r$  and  $\Psi_{dr}^a$ , with  $C$  and  $J$  being constant is shown in Figure 9.12.

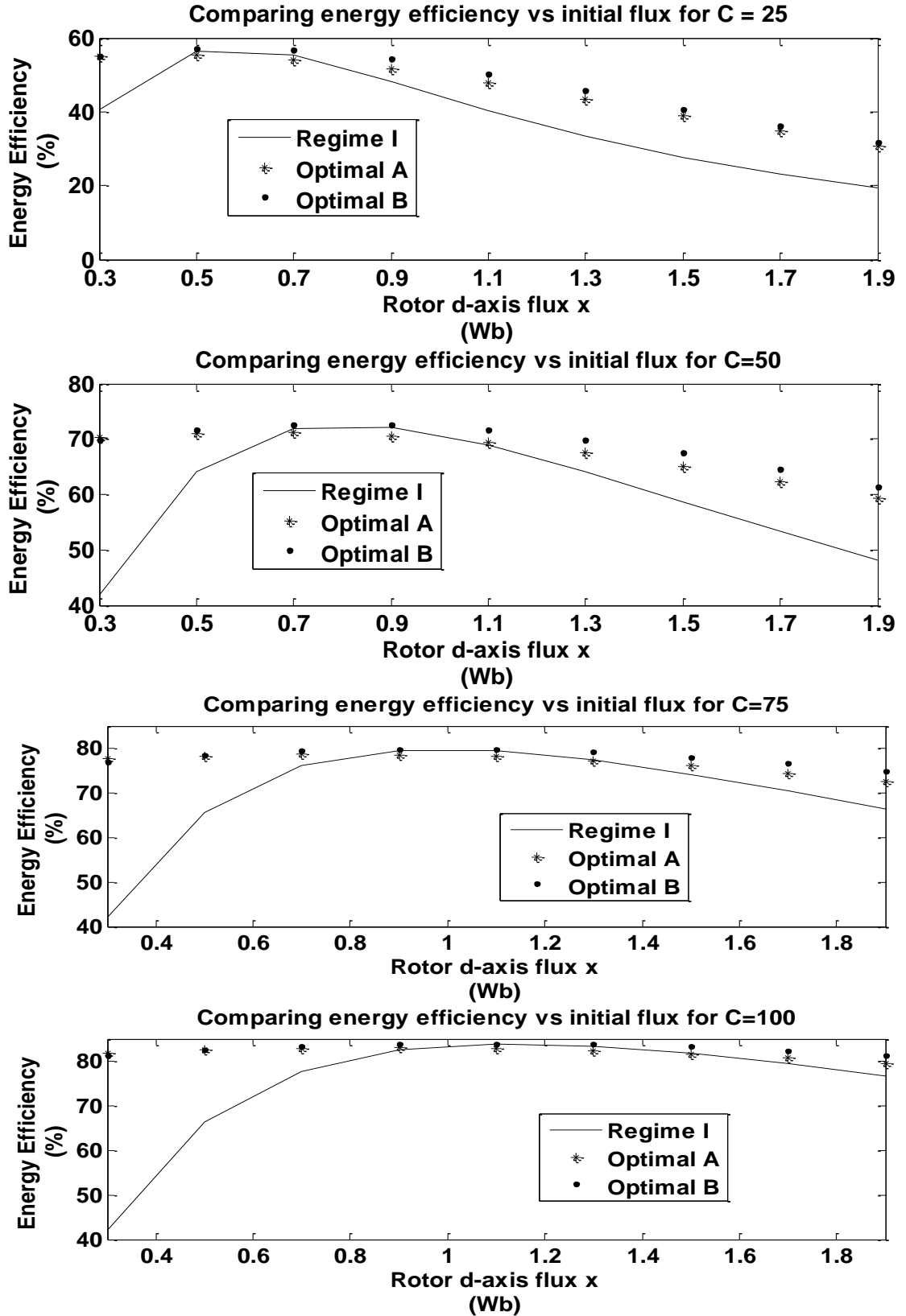


Figure 9.10. Sensitivity of transient energy efficiency to initial flux, and change in rotor speed

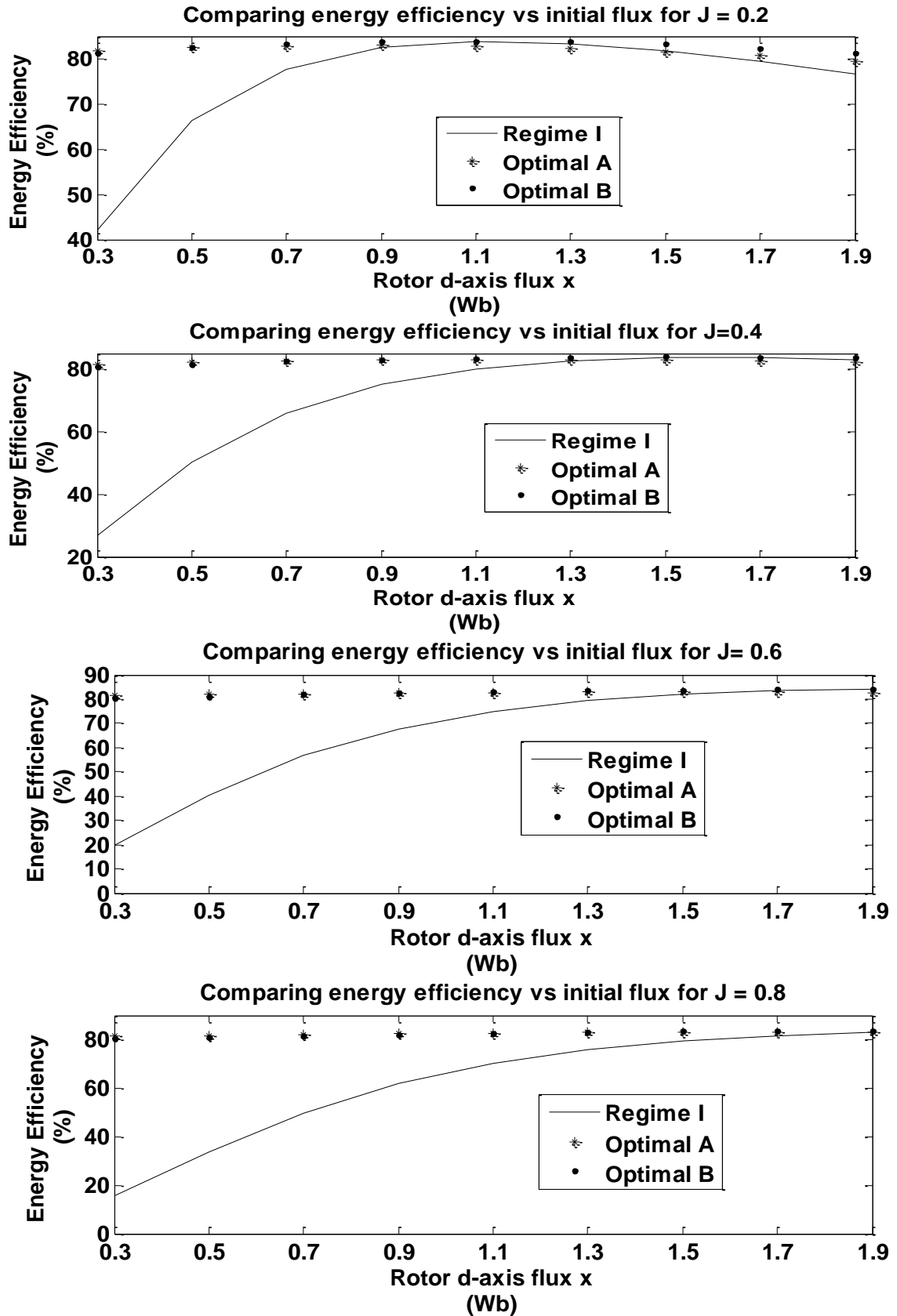


Figure 9.11. Sensitivity of energy efficiency to initial rotor flux and moment of inertia



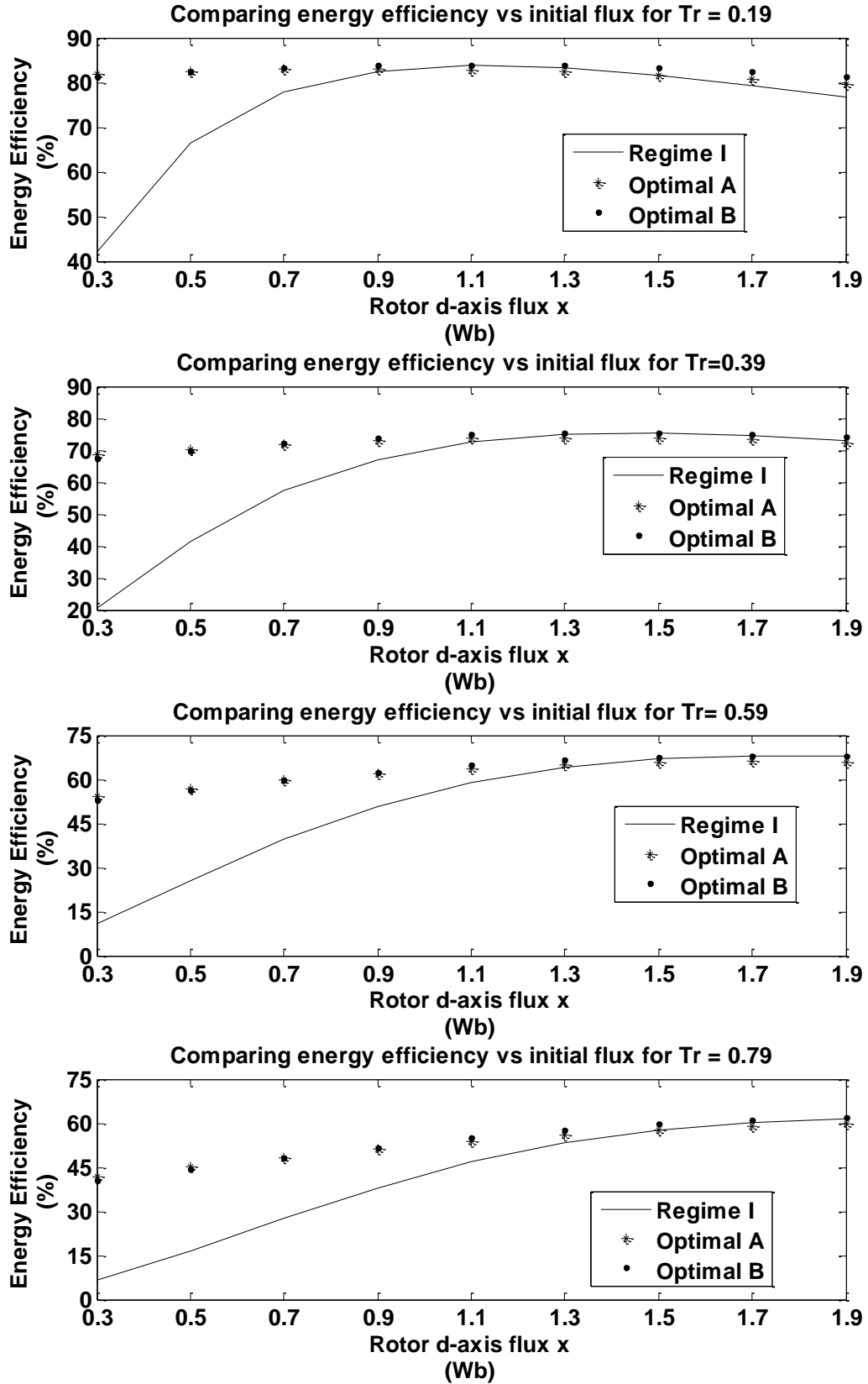


Figure 9.12. Sensitivity of energy efficiency to initial rotor flux and rotor time constant

The observations from the sensitivity plots reveal many interesting features as summarized below:

1. Magnitude of flux ratio  $x$ : The optimal value of  $x$  depends primarily on  $\Psi_{dr}^a$ , i.e. if the initial rotor flux is below a certain threshold,  $x$  is greater than 1 and vice versa. However, the value of the threshold is dependent on speed change  $C$ , and moment of inertia  $J$ .
2. Direction and magnitude of  $i_{qs}^{opt.A}$  and  $i_{qs}^{opt.B}$ : The direction of the q-axis current is dependent solely on the sign of speed change  $C$ . However, the peak current is dependent on both the magnitude of  $C$  and the optimal flux ratio  $x$ .
3. Constant energy efficiency: The optimal trajectories tend to maintain a nearly constant energy efficiency despite changes in  $\Psi_{dr}^a$ ,  $C$ ,  $J$ , and  $\tau_r$ . This contrasts with Regime I whose efficiency increases with increases in  $\Psi_{dr}^a$ , reaches a peak (which is equal to or less than the optimal energy efficiency), and drops off afterwards. The value at which efficiency reaches its peak is dependent upon  $C$  and  $J$ .
4. Stator q-axis current trajectories: Trajectory A of the stator q-axis current provides slightly a higher efficiency when  $\Psi_{dr}^a$  is low. However, the opposite is true when  $\Psi_{dr}^a$  is high.
5. Efficiency improvement: The improvement in energy efficiency over the baseline is directly proportional to  $C$  and  $J$  for the same  $\Psi_{dr}^a$ .
6. Effect of rotor time constant  $\tau_r$ : Decreasing  $\tau_r$  (rotor inductance  $L_r$  decreases constant and rotor resistance  $R_r$  remains constant) increases energy efficiency due to the optimal trajectories, when compared to the baseline for the same  $\Psi_{dr}^a$ .

#### 9.11 Practicality of using the Prototype Analytical Expressions in Real-Time Control

It may seem that it is possible to deploy the above analytical expressions for the optimal trajectories in real-time controllers. However, the following limitations can be identified.

1. Control law is open loop: This means that disturbances that occur during the transient periods will not be reflected in the control trajectory.
2. Solution for flux ratio  $x$  requires an iterative process: The optimal value of  $x$  needs to be calculated at the start of the transient period. This is a static optimization problem

involving a non-linear equation and hence requires more time than what is available during the sampling time of a real-time industrial controller. A potential solution to this is to have a lookup table, which would need to be extensive to account for all possible scenarios. This is not a particularly elegant solution.

To overcome the above limitations, a solution to implement optimal control of IM in real time using Artificial Neural Networks is presented in the next chapter.

### 9.12 Summary

In this chapter, analytical prototype expressions to describe the optimal trajectories for IM control and state variables were developed. The optimal trajectory expressions describe both the rotor flux trajectory and the stator current trajectory. In Trajectory A the rotor d-axis flux was a conic trajectory and the stator q-axis current was also a conic trajectory. In Trajectory B, rotor d-axis flux was a conic trajectory while the stator q-axis current was a constant value trajectory. Trajectory B was found to be best performing in all cases.

## 10 EMULATING OPTIMAL CONTROL OF IM USING ARTIFICIAL NEURAL NETWORKS

The advances made in Artificial intelligence (AI) during the last 5 years have primarily been due to what is called Machine Learning (ML). ML is the “Field of study that gives computers the ability to learn without being explicitly programmed.” This was how Arthur Samuel, one of the pioneers in the field of AI described ML in 1959 [57]. Contemporary ML usually refers to writing programs that learn to perform a task from data rather than being explicitly instructed by the programmer on each step required to perform the task [58]. Data here refers to the information related to the task. There are 3 different approaches to ML, namely supervised learning, unsupervised learning, and reinforcement learning. Each of these approaches has specific strengths and suitability for different tasks. The approach used in this dissertation is supervised learning. The most successful model of ML in recent times has been artificial neural networks (ANN’s) [59].

### 10.1 Neural Network Basics

Generally, ANN’s are computational graphs made up of biologically inspired computational units known as artificial neurons. A simple description of the operation performed by a neuron would be ‘weighted sum of inputs passed through a function’. The process of this operation is illustrated in Figure 10.1.

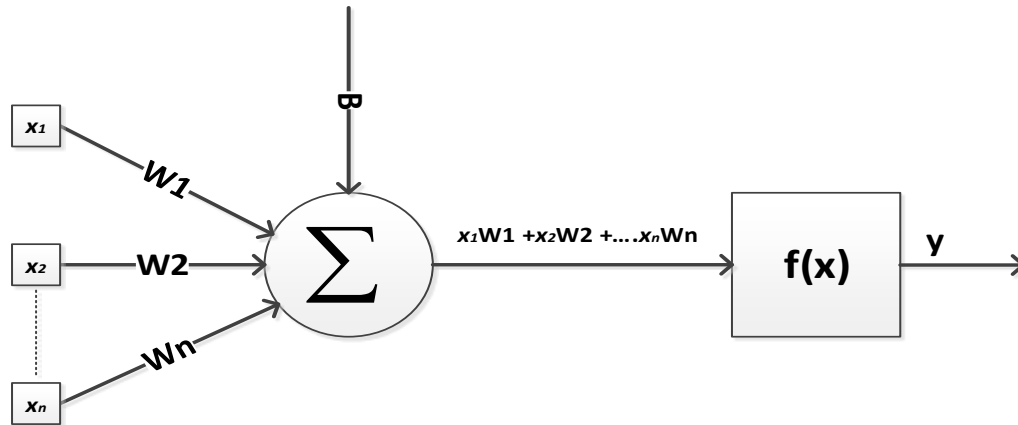


*Figure 10.1. Structure of an Artificial Neuron.*

In Figure 10.1 the inputs to the neuron are represented by  $x_1, x_2, \dots, x_n$ . Each input is multiplied by a corresponding weight  $W_1, W_2, \dots, W_n$ , respectively, before they all enter the summer. Another parameter  $B$  is known as the bias and is added to the sum before being given as input to the activation function  $f(x)$  of the neuron. The activation function  $f(x)$  produces the output of the neuron. All the information in the network is stored in the weights and biases of the neurons. The activation function of each neuron of the network can be generic functions like sigmoid, tanh, or rectified linear, etc. [60].

Taken alone, there is very little that an individual neuron can do. However, many individual neurons arranged in multiple layers with the output of each neuron feeding into other neurons can perform computational tasks which are extremely hard or even impossible with conventional algorithms. An illustration of this concept is shown in Figure 10.2. The phrase ‘The whole is greater than the sum of its parts’ is very true for ANN’s.

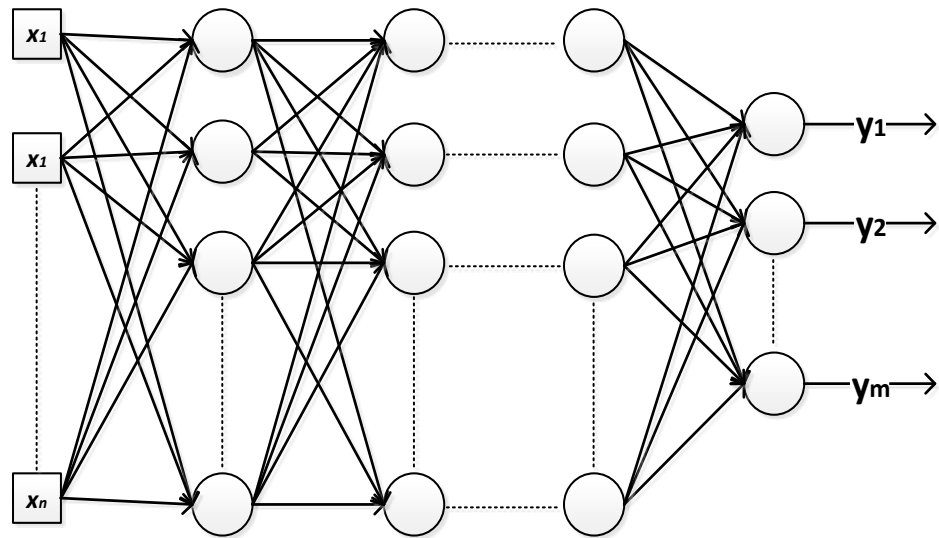


Figure 10.2. Neurons arranged in layers to create a neural network

However, the theory behind how exactly an ANN works is still a topic of debate and active research [61]. Hence, there are only rules of thumb based on empirical results for selecting a specific ANN architecture (how its neurons are arranged) and hyper-parameters that define it for a specific task. The architecture in Figure 10.2 is referred to as the feed forward neural network (FFNN) and is also the simplest and most commonly used architecture.

The process of using information about a problem to adjust the weights of the ANN so that it can produce a meaningful output for a given input is referred to as training. Training is ultimately a static optimization problem, the key ingredients of which are:

- 1) Sufficient samples of inputs/outputs.
- 2) Loss (error) function that measures the difference between the actual ANN output and the desired output.
- 3) An algorithm that would adjust the weights to decrease the loss function value.

The process of feeding a trained ANN with new inputs (similar to those used in its training) and obtaining outputs is known as inference. Discussing more about ANN's would be redundant considering the vast amount of literature available, and hence the reader is referred to [62] for further detail and information.

## 10.2 Using Neural Networks as Controllers

ANN's have been shown to be able to approximate the output of any function provided an appropriate network architecture is chosen and there are sufficient numbers of neurons [63], [64]. Note that one does not need to have any presuppositions regarding the shape of the target function one is trying to approximate when using ANN's. In ML terminology, the task of producing a continuous numeric output for a given continuous numeric input is called regression. This capability can be extended to the control laws, i.e. ANN's can be trained to act like controllers. This concept has been referred to as Neurocontrol in [65]. There are four topologies for Neuro control that have been proposed:

- 1) Template training,
- 2) Learning plant inversion,
- 3) Closed loop optimization, and
- 4) Critic system.

Detailed discussions on these techniques have been provided in [65]. However, only Template training is relevant to the work done in this dissertation. As the name suggests, Template training refers to training an ANN to mimic the output of a control law using a template. Template, in this case, refers to the input presented to the actual control law and its corresponding output. The Template training concept is illustrated in Figure 10.3.

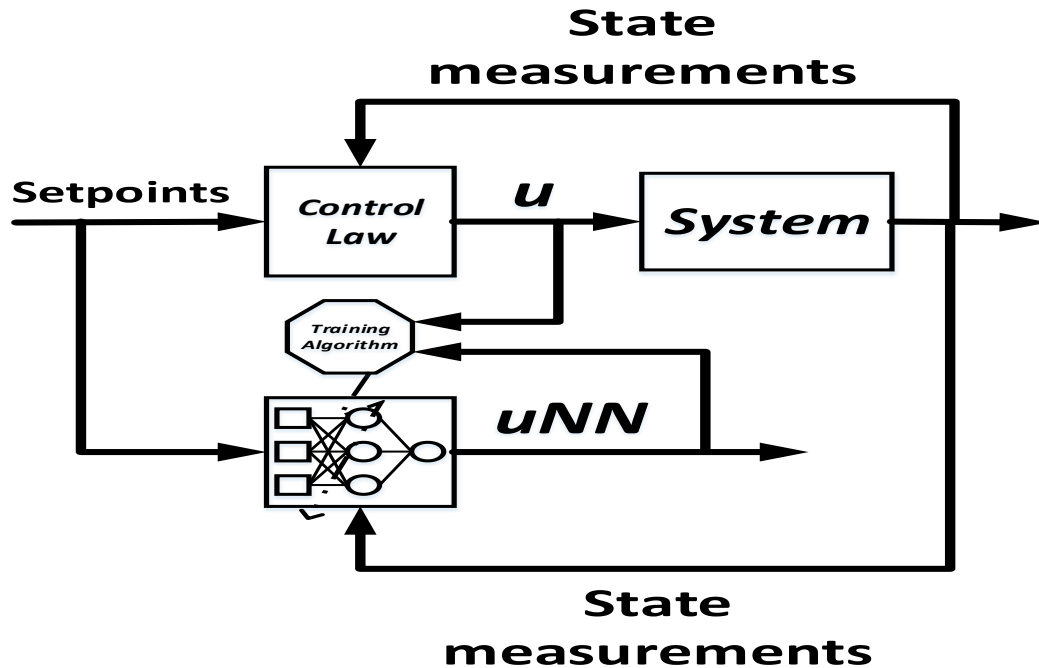


Figure 10.3. Template training an ANN as a controller

A Template trained ANN controller is suitable for solving the IM optimal control problem of this dissertation work because of the following reasons.

- 1) The numerical solutions for the optimal control problem provide a template for training the ANN controller.
- 2) The template trained ANN can instantly generate control outputs in real-time, unlike the conventional numerical solution which is iterative.
- 3) Feedback from the IM can be used as inputs to the ANN controller.

One rule of thumb that can be followed while deciding the number of neurons and the number of hidden layers of the ANN is to get the highest performance using the minimum number of parameters (weights and biases). In this work, through a trial and error process, an ANN with a single hidden layer consisting of 3 neurons was found to give sufficient accuracy.



### 10.3 Training the ANN to Emulate Optimal Control Trajectories

The most important aspect of training an ANN is the availability of good quality training data. A minimum number of samples of training data is required to get acceptable performance. In the case of the IM optimal control problem, the data required for training is available in the form of numerical solutions for optimal state, co-state, torque, and control trajectories from Chapter 8. Each of these numerical solution trajectories represents a potential input to the ANN or an output that must be produced by the ANN. The inputs and the corresponding outputs of the network are referred to as features. It is necessary to select a sub-set of input-output features for the training of the network. The selection of the training features is equivalent to presenting a set of evidence to the ANN based on which it provides an output. The ANN will automatically assign a weight for each piece of evidence that it is provided with during the training process. However, by selecting an optimal set of inputs (through intuition or trial and error) we can help the ANN improve the quality of the result. The features that gave the best results in case of the IM optimal control problem under study are given in Table 10.1. The architecture of the ANN that was chosen and used to generate the optimal control trajectories is given in Figure 10.4.

Table 10.1. Selecting input-output features for ANN to emulate the optimal control trajectory.

ANN input features	Data Type	Source during real-time simulation
Optimal rotor d-axis flux trajectory, $\Psi_{dr}(t)$	Time variant	Feedback from IM
Optimal rotor speed trajectory, $\omega_r(t)$	Time variant	
Initial rotor flux, $\Psi_{dr}^0$	Constant	Generated by supervisory logic
Initial rotor speed, $\omega_r^0$	Constant	
Final rotor flux, $\Psi_{dr}^{tf}$	Constant	
Final rotor speed, $\omega_r^{tf}$	Constant	
Time as a fraction of the transient period ( $t$ )	Varies from 0 to T (where T is the transient time period)	
ANN output features	Data Type	
Optimal d-axis stator current, $i_{ds}(t)$	Time variant	
Optimal q-axis stator current, $i_{qs}(t)$	Time variant	

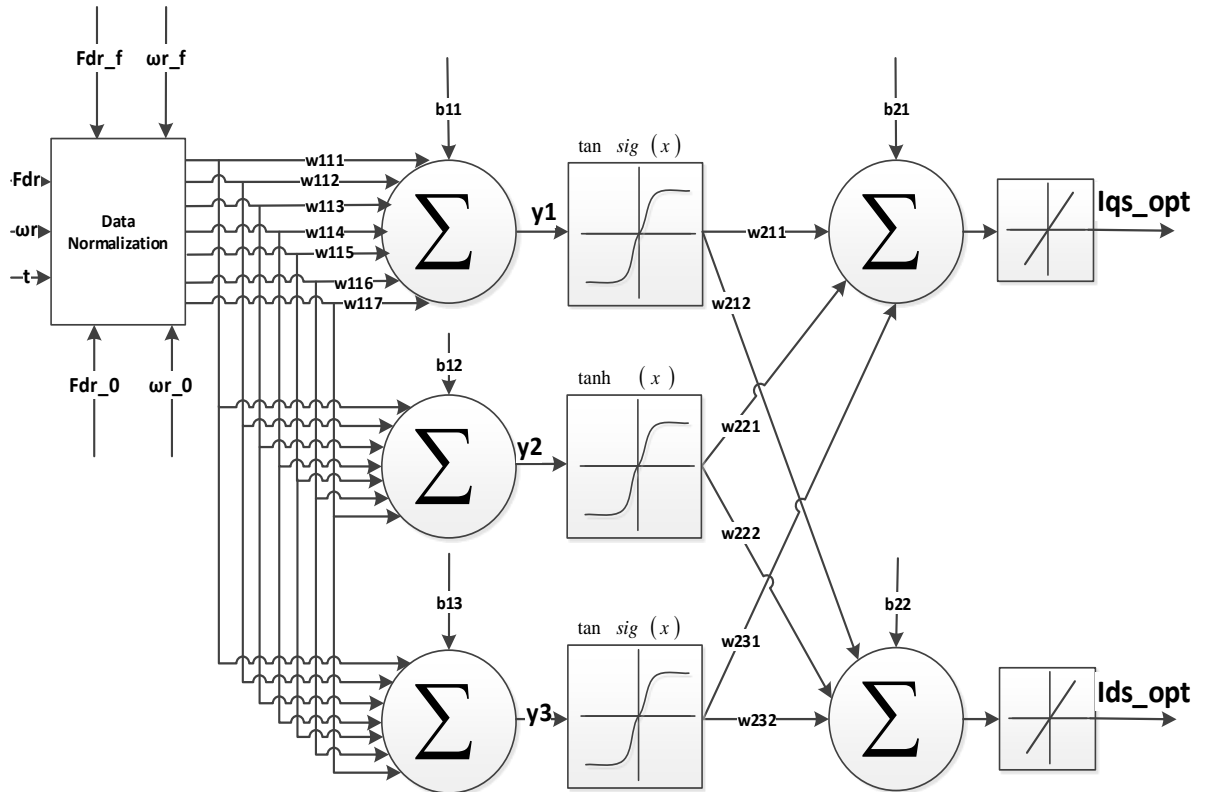


Figure 10.4. Operations in the ANN emulating the IM optimal control solution.

After the features are selected and the data corresponding to those features are available, a training algorithm is chosen. A training data set consisting of 60 trajectories were found to provide acceptable performance. The training algorithm does not have to be implemented from scratch since software toolboxes and libraries for different algorithms are readily available. In this work, the ANN training was done separately using two separate software packages. Firstly, the NN Toolbox available in MATLAB software with the Levenberg-Marquardt training algorithm [66] was used. Then, the open source ML toolkit TensorFlow [67] was used. The computational graph generated by TensorFlow for the ANN is shown in Figure 10.5. The change in the learning error for the training and the validation data set during training when using MATLAB NN toolbox and TensorFlow are shown in Figure 10.6. and Figure 10.7, respectively.

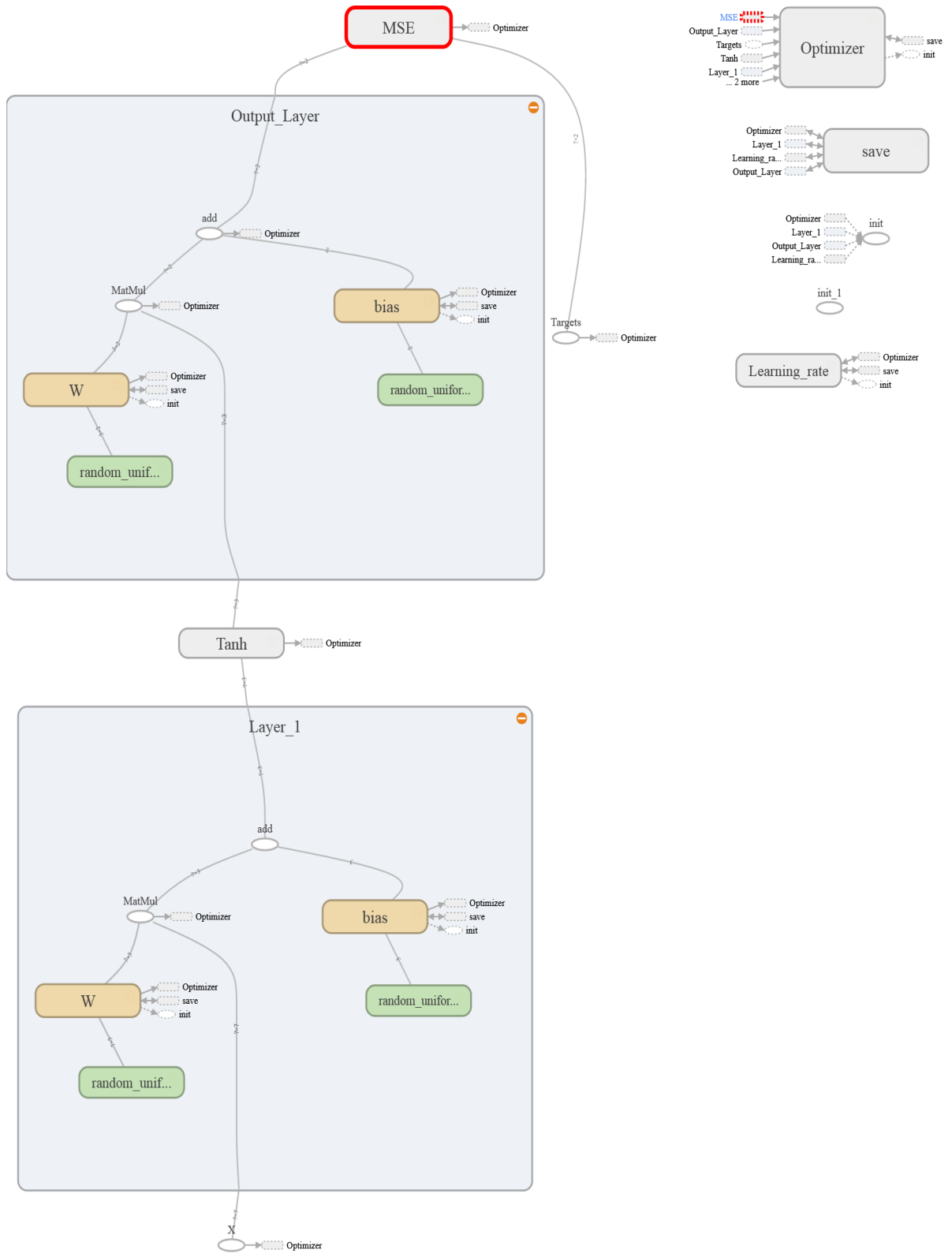


Figure 10.5. TensorFlow computational graph implementing the ANN of the IM Optimal control problem

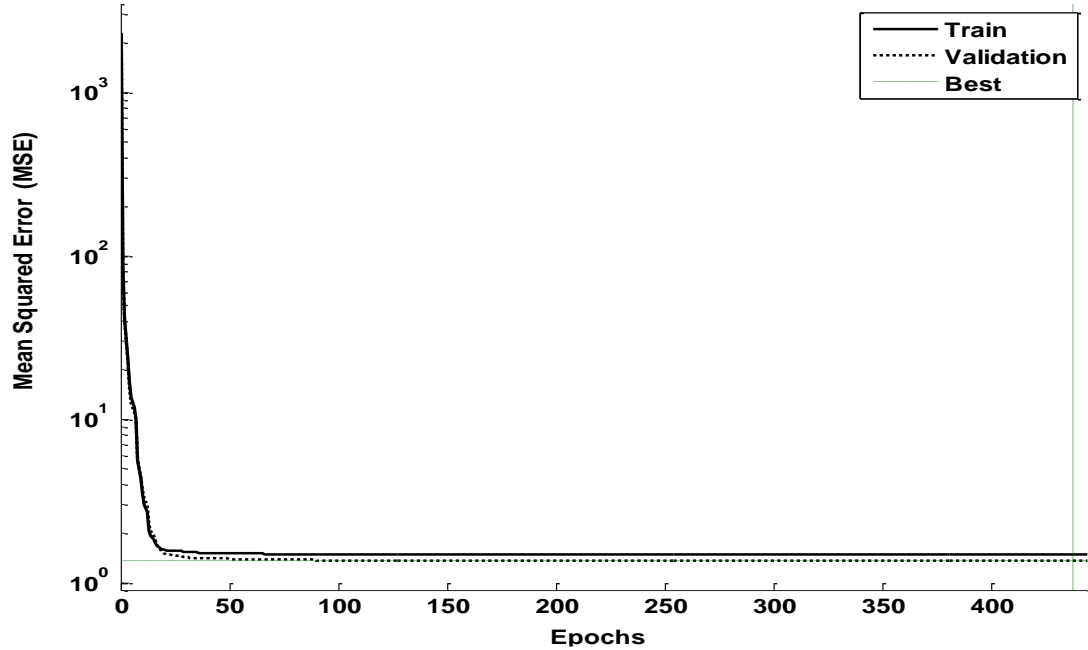


Figure 10.6. Change in the mean square error of training and validation data set during ANN training using Levenberg-Marquardt algorithm in MATLAB

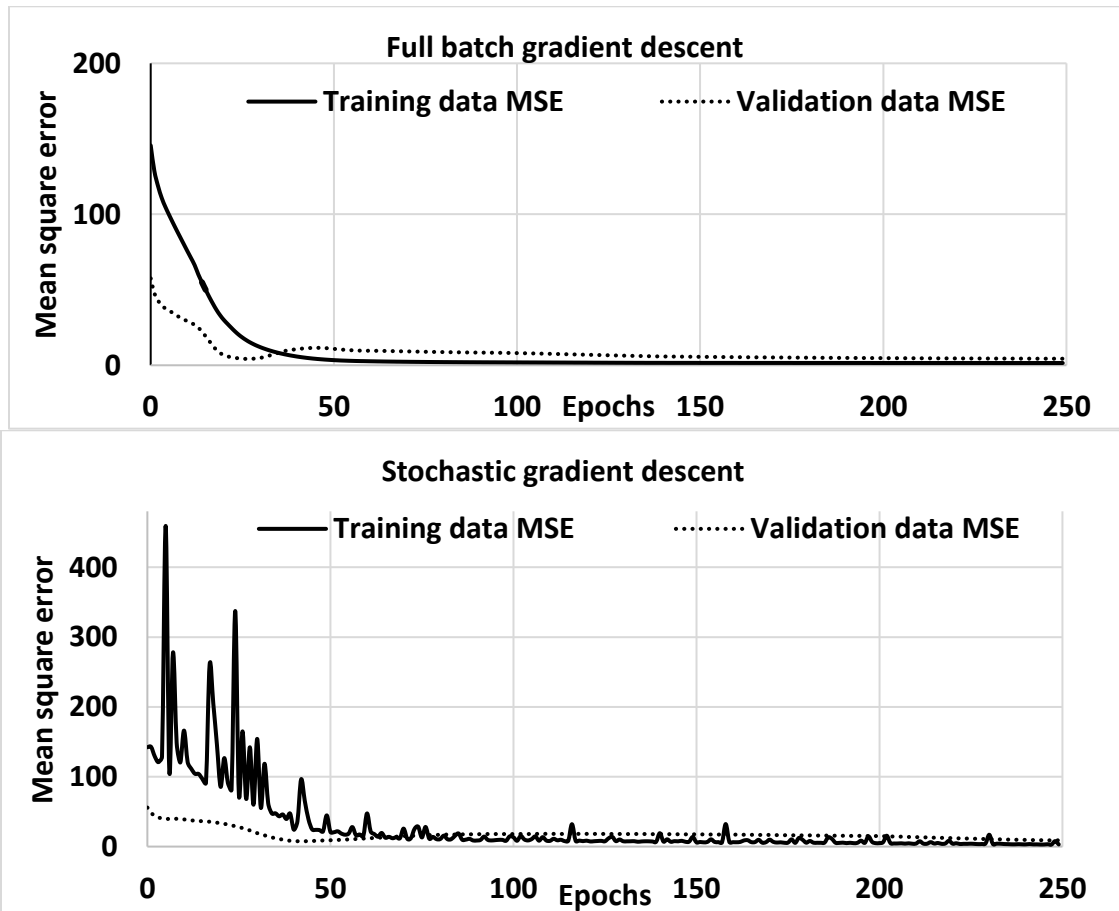


Figure 10.7. Change in the mean square error of training and validation data set during training using ADAM algorithm in TensorFlow

#### 10.4 Incorporating ANN into an IM drive control system

It must be noted that the ANN discussed in the previous section cannot be used alone in an IM drive control system. This is because an IM drive cycle consists of both transients and steady state operating regions. Also, the ANN is only generating the set points for the stator current of the IM. A current controller is required to control the voltage sources so that the stator current takes on that value. Based on this, the integration of the Template trained ANN as part of the IM drive control system is illustrated in Figure. 10.8. The main components of the integrated controller are:

1. ANN block for generating the optimal control trajectories.
2. Feedback controller for motor speed and rotor flux.
3. Supervisory logic to decide when to enable the ANN and provide input data to ANN.
4. Current controllers for the IM d-axis stator currents which can take set points from either the ANN block or the feedback controller.

The optimal trajectories generated by the trained ANN will be referred to as Regime IV.

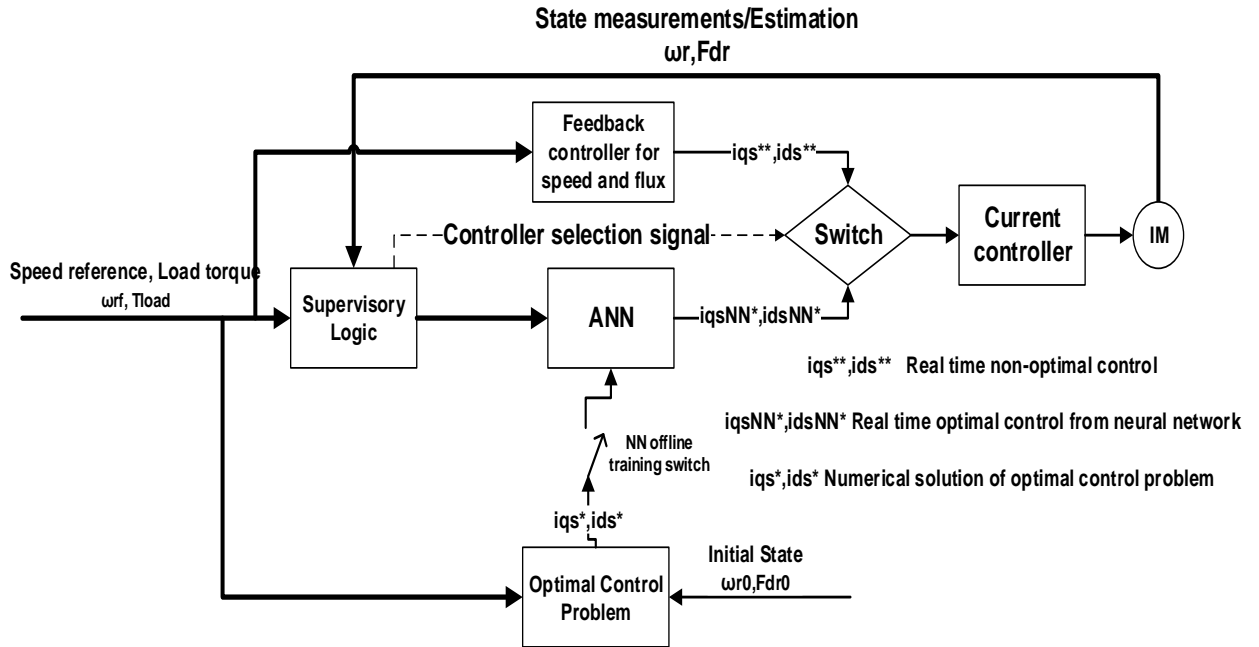


Figure 10.8. Template trained ANN block as a part of the IM drive control system

The operations within the supervisory logic are illustrated in the flowchart diagram shown in Figure 10.9. The ANN's output is enabled when a change in the speed setpoint is detected by the supervisory logic. Once the rotor speed reaches the reference speed, the supervisory logic disables the ANN output and enables the output to the feedback controllers.

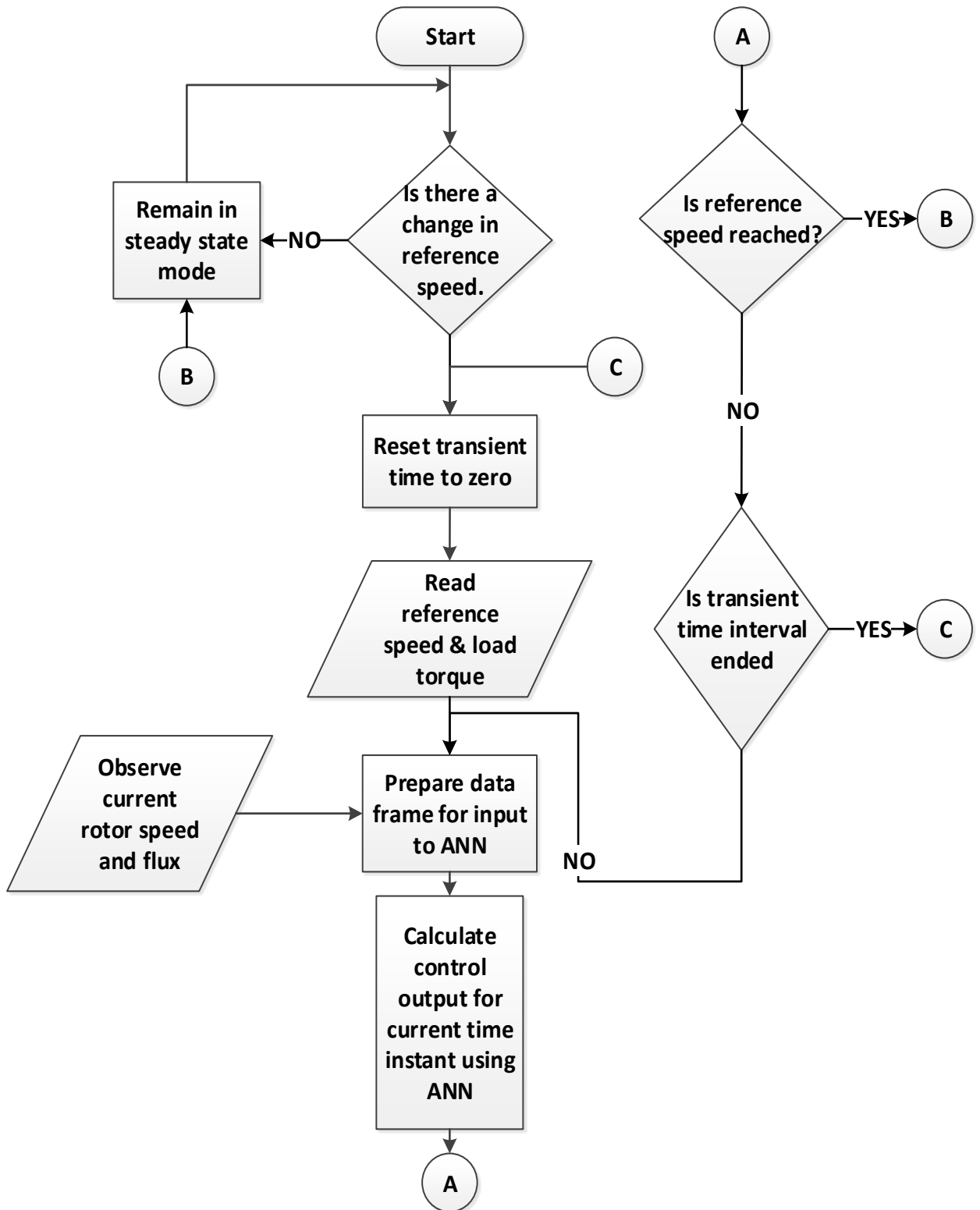


Figure 10.9. Supervisory logic to implement the ANN based IM optimal controller



## 10.5 Performance of the ANN Optimal Control

As stated previously the role of the ANN is to emulate optimal control trajectories. The training is said to be successful when the ANN can generate optimal control trajectories approximating the numerical solution using inputs it has not seen during the training. Fig. 10.10 shows the output produced by a trained ANN compared to the actual control trajectory from the numerical solution. To test the effectiveness of the ANN optimal control system (ANN + supervisory logic), a real-time simulation was performed using a 7<sup>th</sup> order IM model (i.e. IM model with 7 state variables). The inputs (to the ANN) produced by the supervisory control and outputs from the ANN during real-time simulation are shown in Figure. 10.11 and Figure 10.12 respectively. Detailed results can be found in [50].

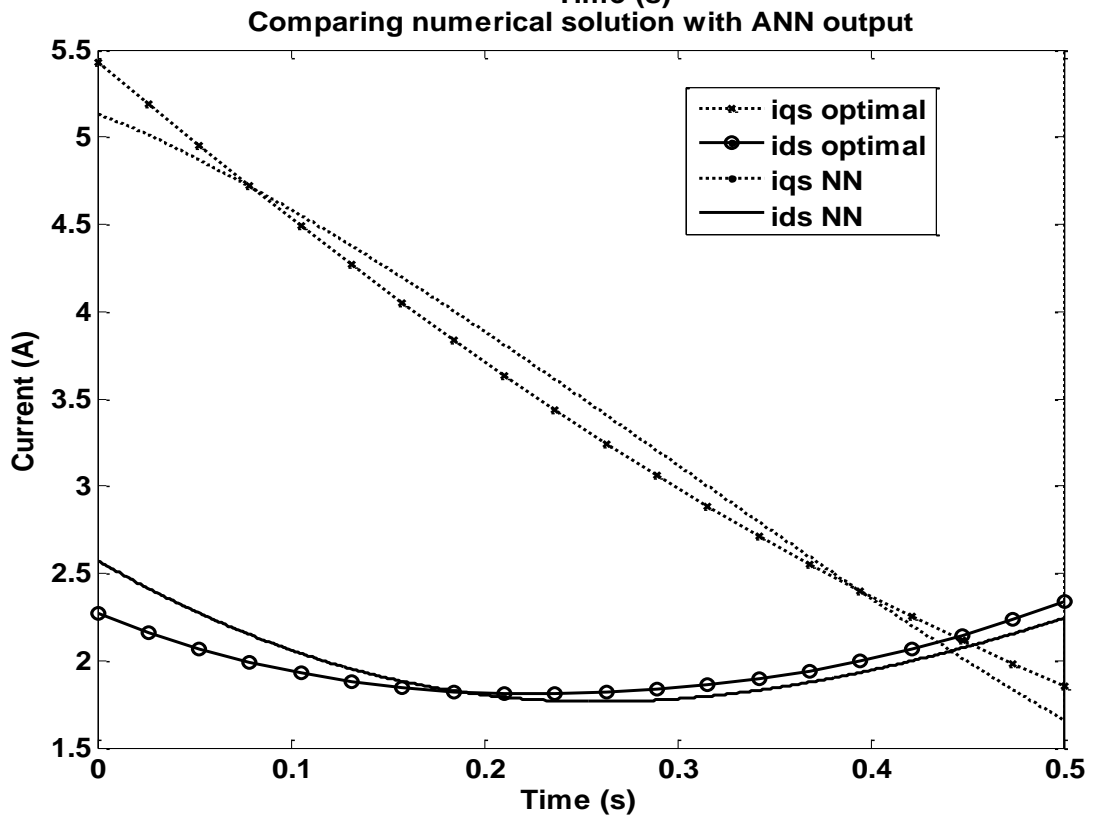
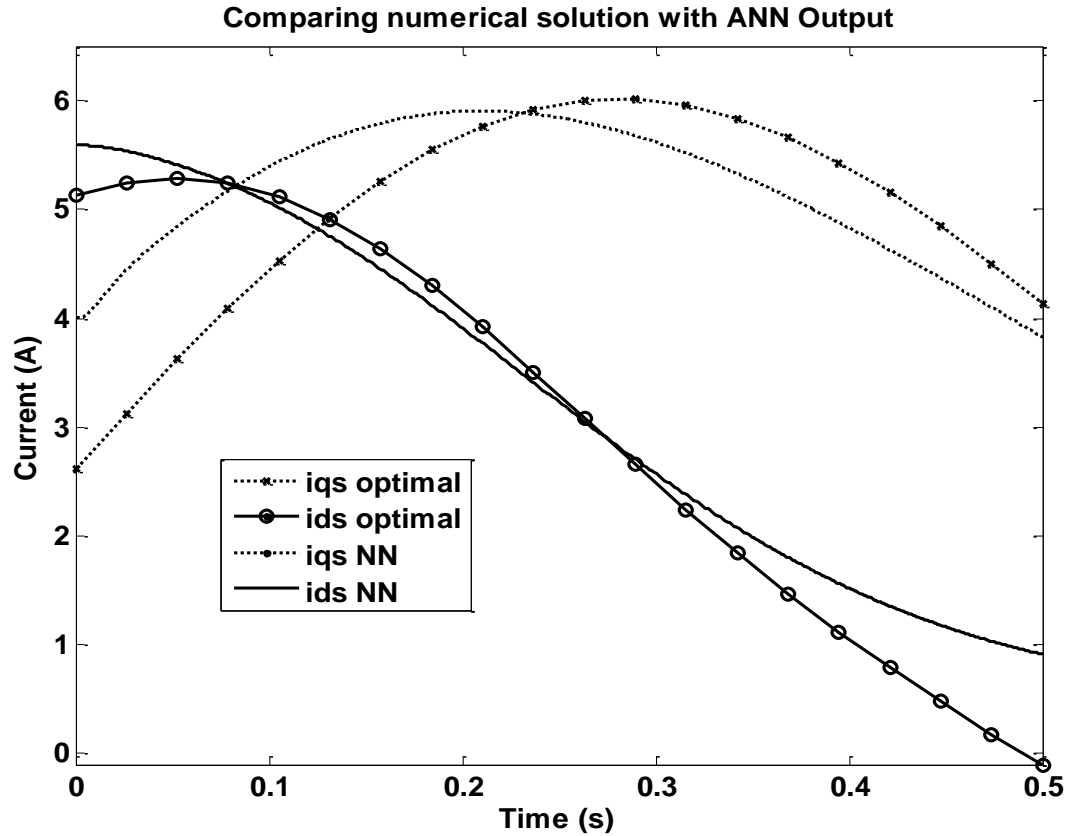


Figure 10.10. ANN output emulating solution of IM optimal control problem

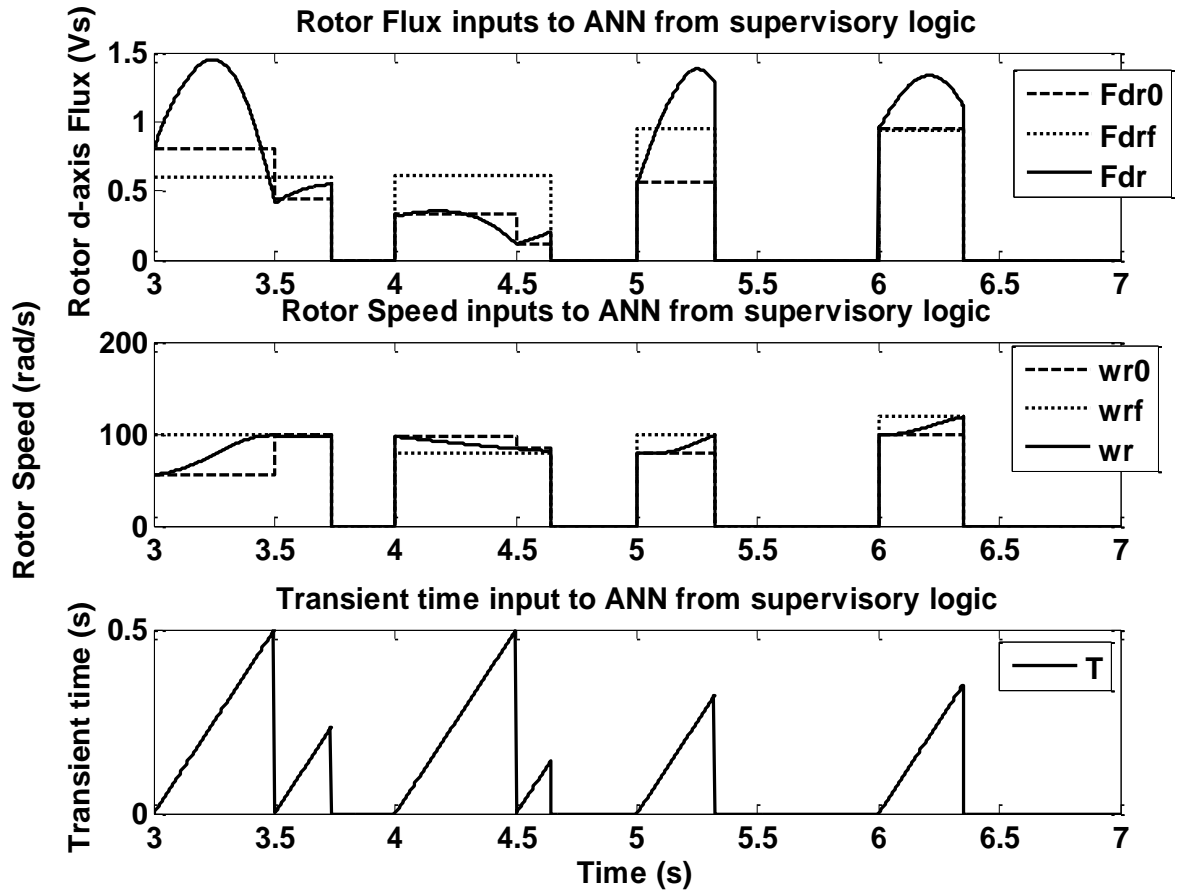


Figure 10.11. Input from supervisory logic to ANN during real-time simulation.

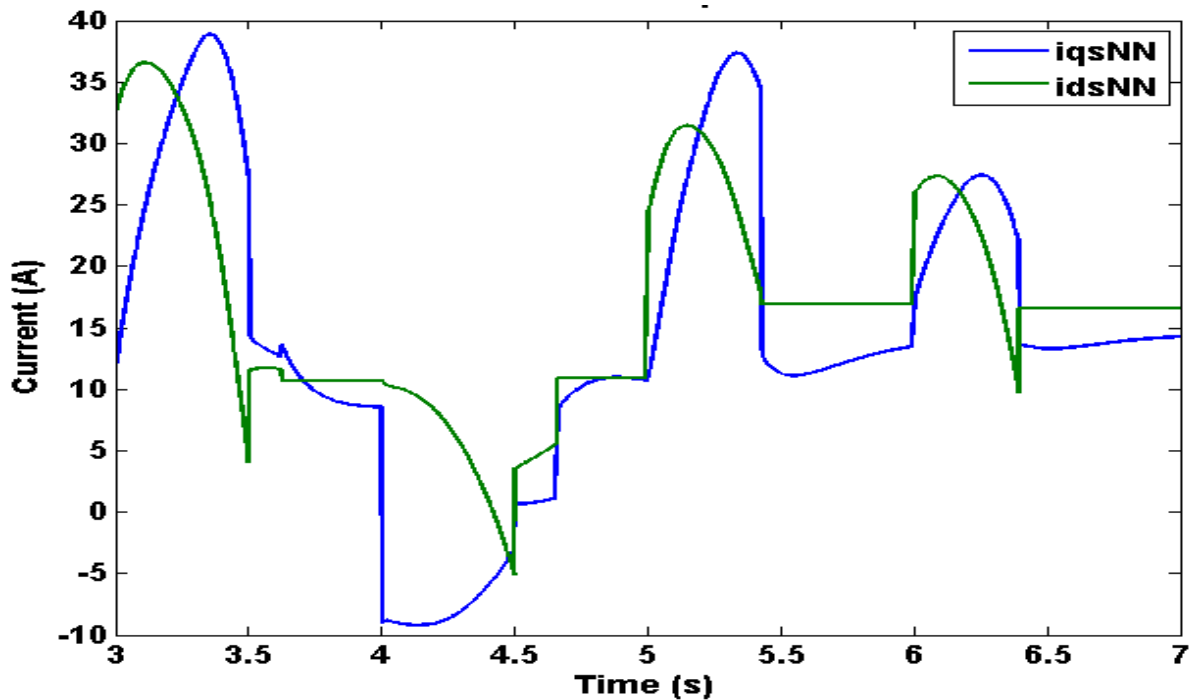


Figure 10.12. Output from ANN during real-time simulation.

It can be observed that the ANN optimal control system is able to reach the setpoint in the specified time. Discontinuities in the current set points occur whenever the changeover from the neural network control to speed feedback control occurs. From Figure. 10.11 input is given to a neural network only during the transient time periods. As soon as the IM achieves its reference speed, the input is switched off.

## 10.6 Summary

In this chapter, the concept of using an ANN for designing control systems was discussed. The use of numerical solutions of optimal control trajectories for training an ANN controller was proposed. MATLAB and TensorFlow based ANN training errors were presented. Finally, incorporating the ANN into the IM drive control scheme was explained. The outputs from the ANN were shown to be emulating the numerical solution of the IM optimal control problem. The ANN Optimal control system was implemented in Simulink/MATLAB will be used in the next chapter to perform real-time control of a finite element method model of the IM.

## 11 REAL-TIME SIMULATION RESULTS USING ANN OPTIMAL CONTROL SYSTEM AND FINITE ELEMENT MODEL OF IM

In this Chapter, real-time simulation results using the ANN optimal control system and the finite element (FE) model of the IM are shown. But first, some experimental results obtained by applying a standard rotor field oriented control (FOC) on IM drive hardware are presented.

### 11.1 Experimental Results of IM Field-oriented Control (FOC)

A schematic of the experimental hardware setup to perform FOC is shown in Figure 11.1. Snapshots of the actual hardware setup available in the Electric Power and Energy System laboratory at UND are shown in Figure 11.2 and Figure 11.3. The experimental measurement results for the rotor speed, input power, rotor flux, and stator d-axis current are shown in Figures 11.4, 11.5, and 11.6.

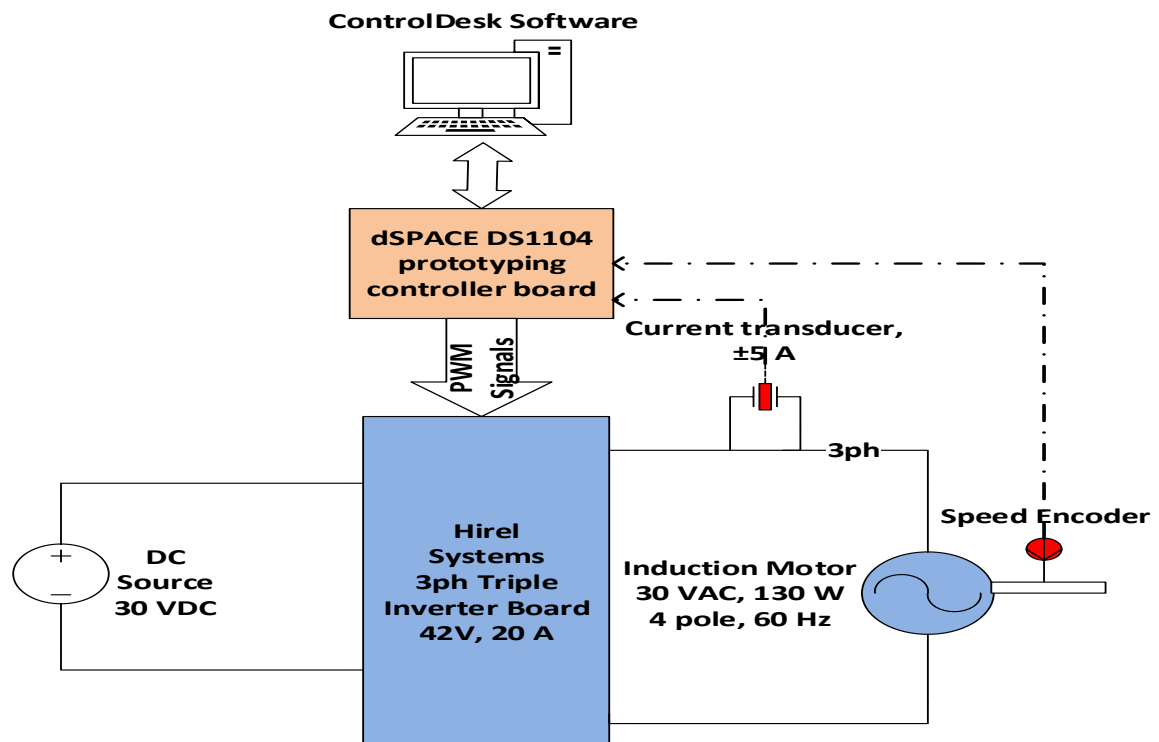


Figure 11.1. IM experimental hardware setup

Encoder feedback      Induction Machine      3ph Inverter (42VDC, 10 A)      dSPACE CP1104 connector panel

130 W, 30VAC

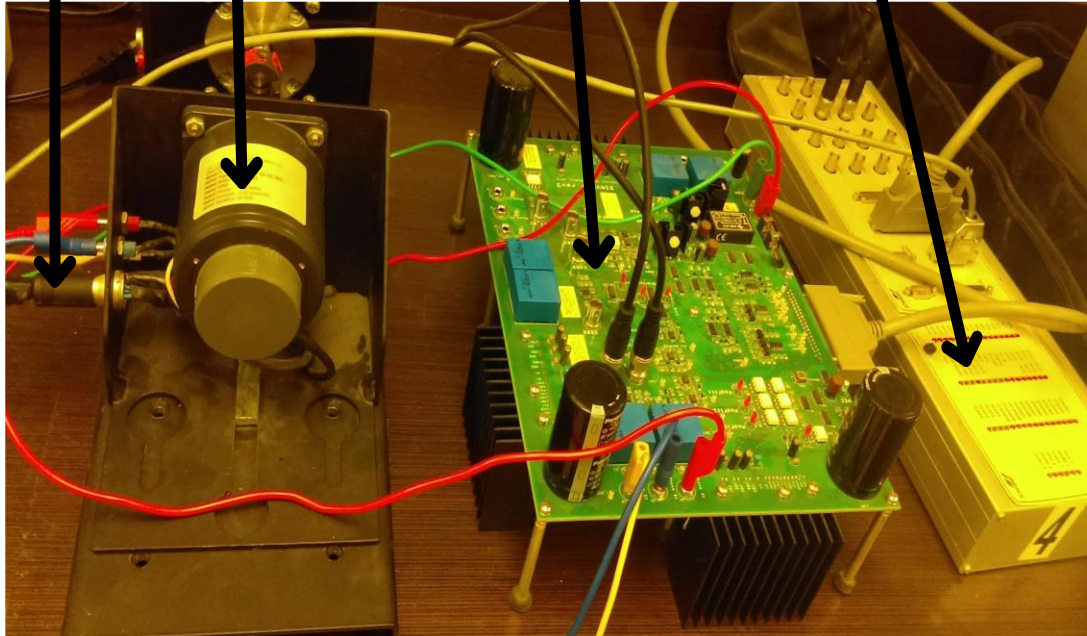


Figure 11.2. IM, 3ph Inverter, and connector hardware

dSPACE DS1104 R&D Controller board + PC      dSPACE ControlDesk user interface

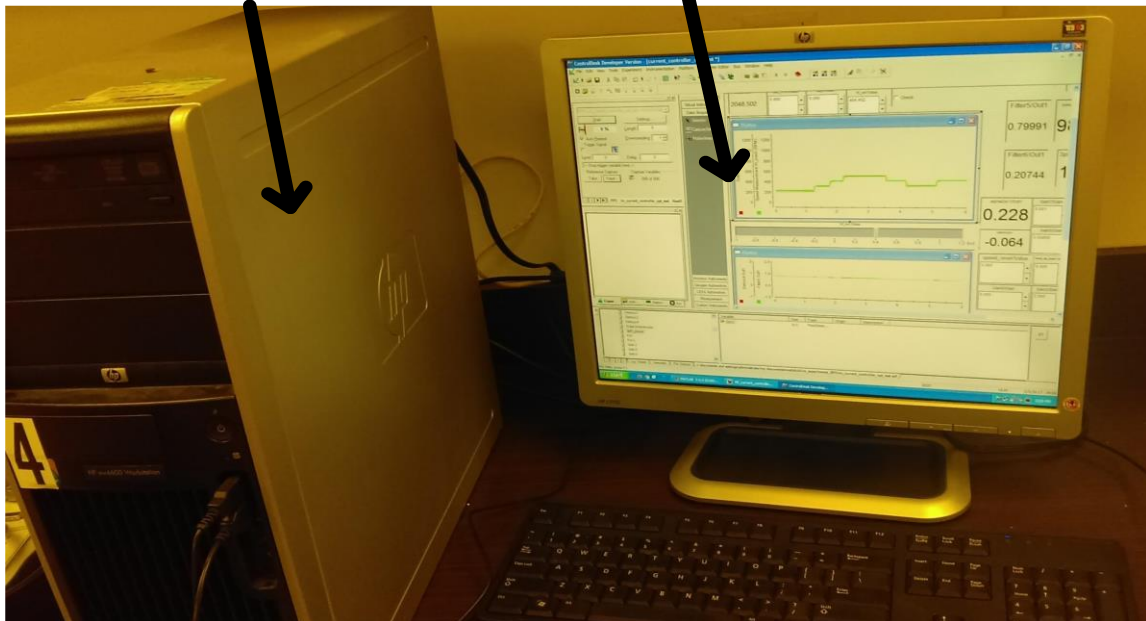


Figure 11.3. dSPACE controller board and ControlDesk UI

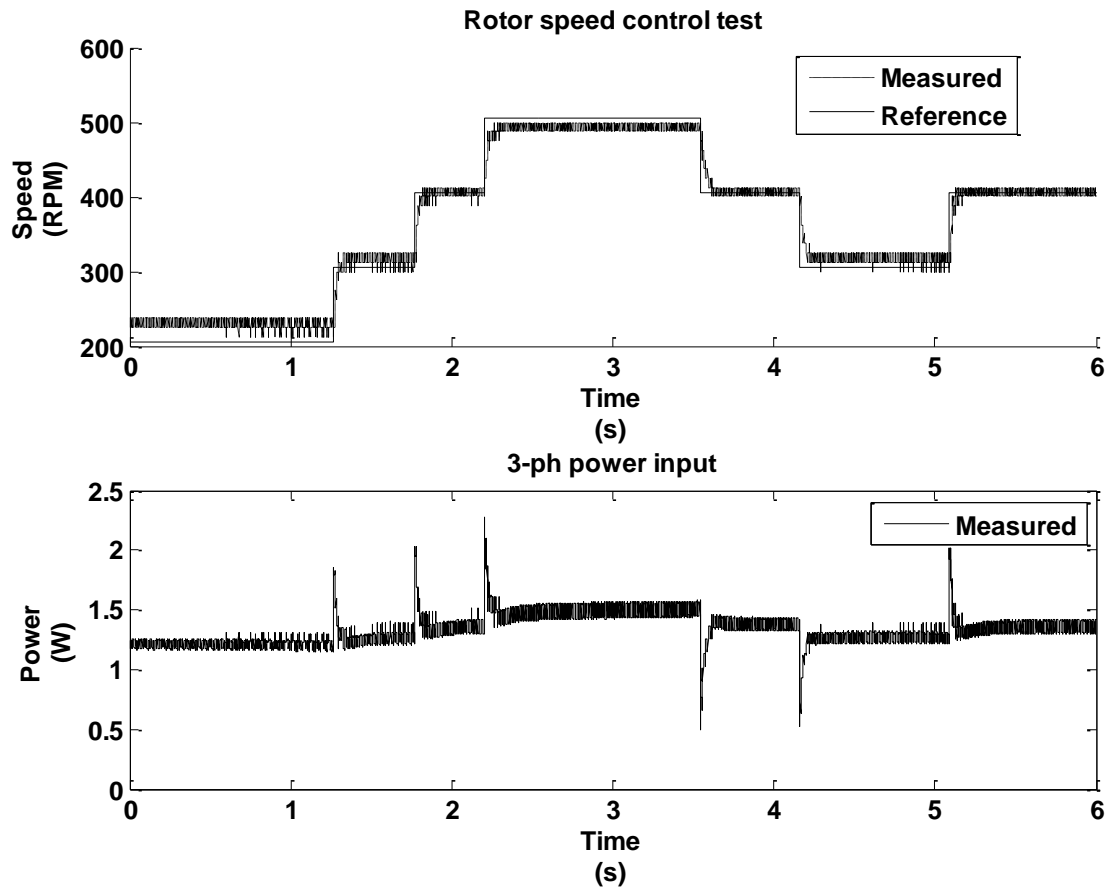


Figure 11.4. Speed and power input.

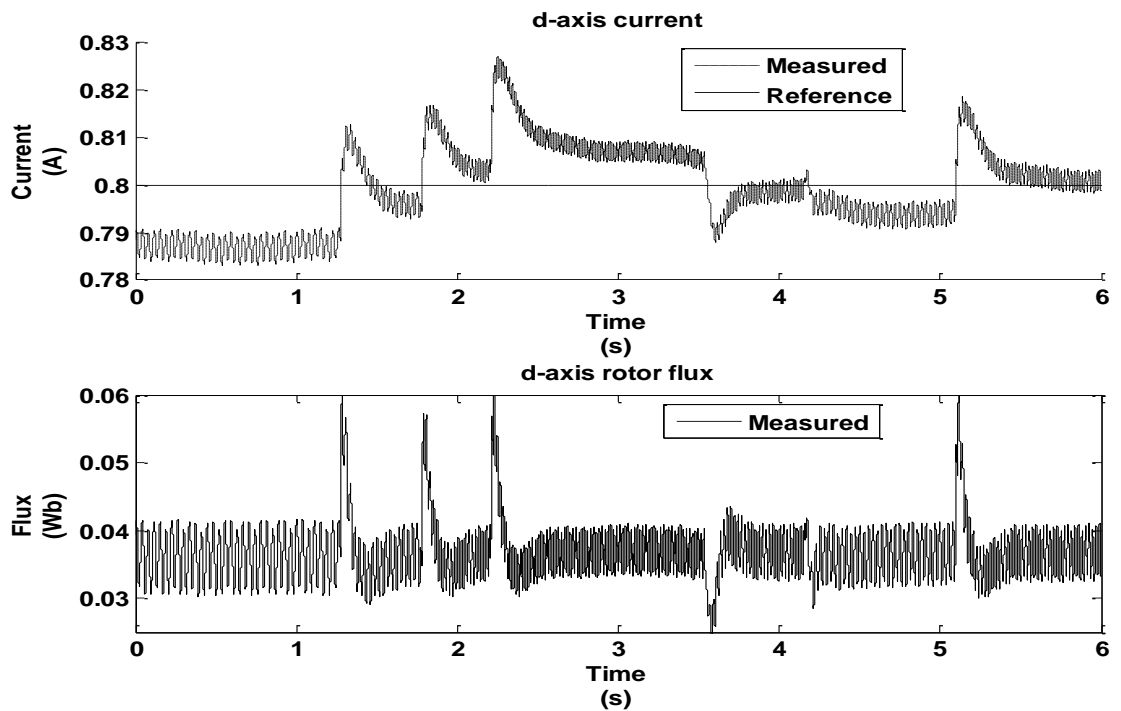


Figure 11.5. Rotor flux and d-axis current corresponding to change in rotor speed.

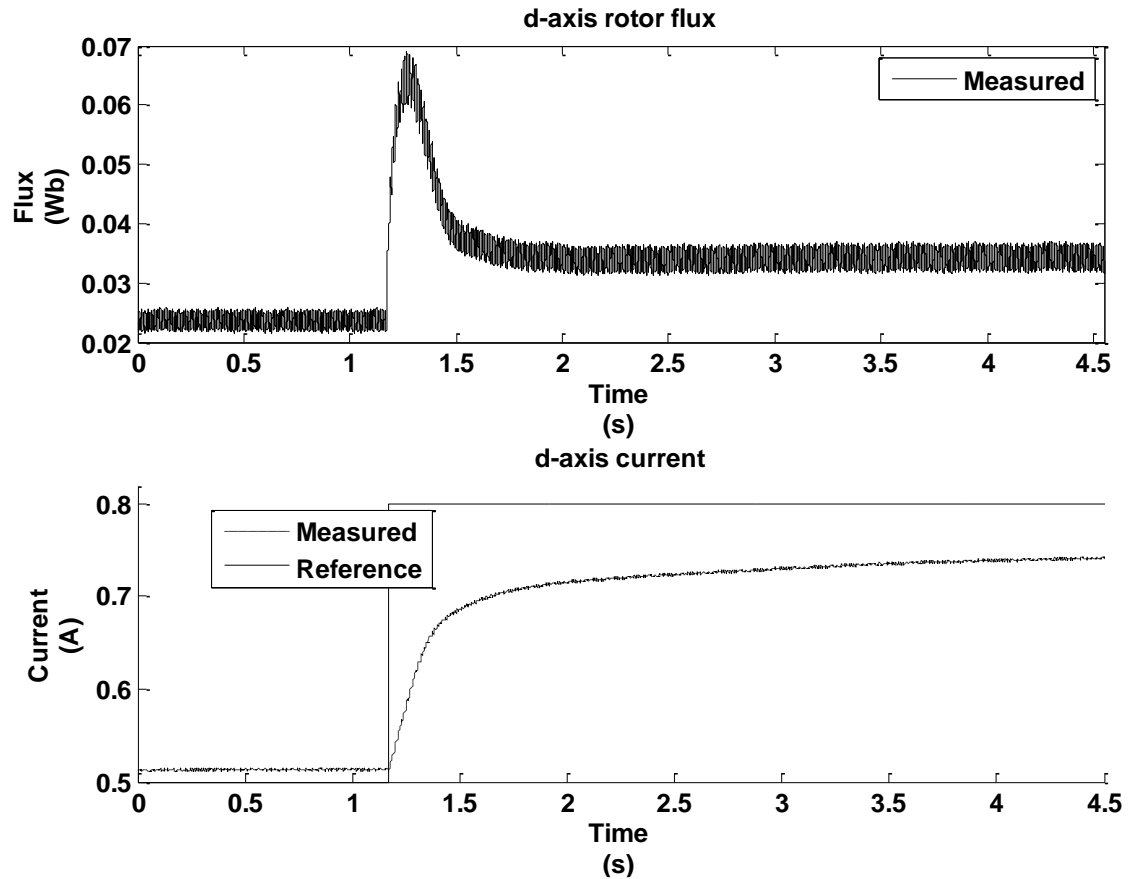


Figure 11.6. Change in rotor flux for change in d-axis current.

In the above figures, it is evident that the FOC is able to maintain a tight control over the rotor speed. The small oscillations at steady state occur because the resolution of the speed encoder is only 12.5 RPM. The change in speed also corresponds to change in the q-axis current as expected. However, there are some disturbances in the d-axis current because in a practical IM (unlike the current fed FOC theoretical model of the IM) a full decoupling of d- and q-axis flux and current components does not exist. The increase in stator current is a first order response rather than a step because the dynamics of the current controller slows down the increase in current. Consequently, the rotor flux response is also not a first order response.



An ideal conclusion to this research work would have been the testing of the developed real-time IM optimal control on a hardware of more than 1 kW rating. However, the power rating of the currently available IM drive hardware in the Electric Power and Energy Systems Laboratory of the Department of Electrical Engineering at UND is much below that. The no-load power consumption rating of the available IM in the laboratory is in the range of 2-3 W. Reliable power measurements are not feasible at this kind of power levels.

### 11.2 ANN Controller deployed on Real-Time Controller Hardware

It is still necessary to verify that the ANN controller and the supervisory logic will work when deployed in a real-time controller hardware. For this, an ANN controller was trained to emulate the output of a PI speed controller for a DC motor. The ANN inputs consisted of reference rotor speed, measured rotor speed, measured armature current, and output was armature voltage. The ANN architecture consisted of a single hidden layer with 3 neurons (same as ANN optimal control). The ANN controller was found to successfully emulate the output of the PI controller and maintain reference speed. A detailed explanation of the training procedure and results can be found in [68].

### 11.3 IM Finite Element Model and Co-simulation using Simulink and ANSYS Maxwell

In this work, the ANSYS Maxwell software [69] is used to develop a Finite Element (FE) model of the IM. The ANN optimal controller that was designed and discussed in Chapter 10 is implemented in the Simulink environment of MATLAB. ANSYS Maxwell software has the capability of performing a transient co-simulation with Simulink of MATLAB [70]. As such, both Maxwell and Simulink programs are run concurrently to perform a co-simulation of the IM FE model and the ANN controller of Chapter 10. [71] and [72] are recent works which take advantage of co-simulation to analyze electric drives.

The RMxprt tool inside ANSYS Maxwell provides some predesigned models of different electric machines. This work used the 4-pole IM model. The spatial dimensions and circuit parameters of the IM are given in Appendix II. It is possible to import the IM design from RMxprt into Maxwell as a 2-dimensional (2D) FE model. An illustration showing a quarter section of the 2D FEM model is shown in in Figure 11.7. Even though the 3D FEM model of the IM gives a more detailed representation of its dynamics, the large computation time needed to complete the simulation on a standard desktop PC made the author of this dissertation choose a 2D model instead. In order to further reduce the computation times, the 2D FEM is further divided into four symmetrical sections, only one of which is used in the simulation.

It is observed from the figure that the geometry of the IM has been discretized into triangles, also known as the finite element meshes of the model. The number of meshes changes depending upon the accuracy of the results required. Usually, the simulation starts with a coarse mesh which is further refined into smaller meshes as the simulation progresses.

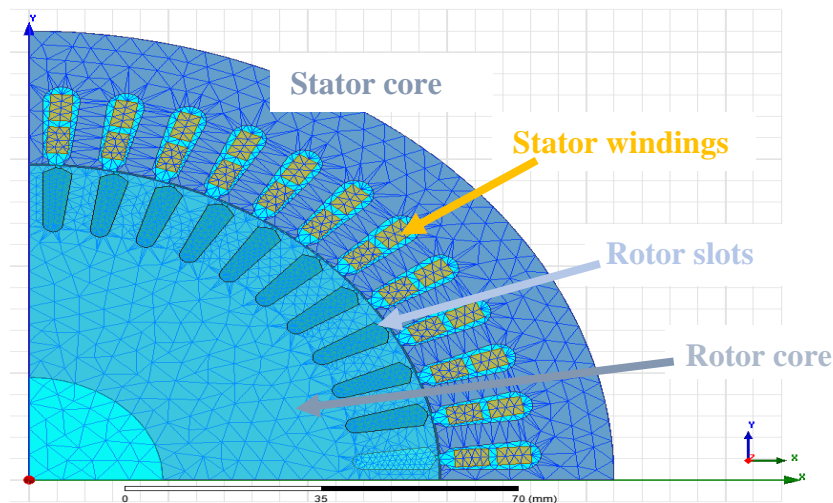
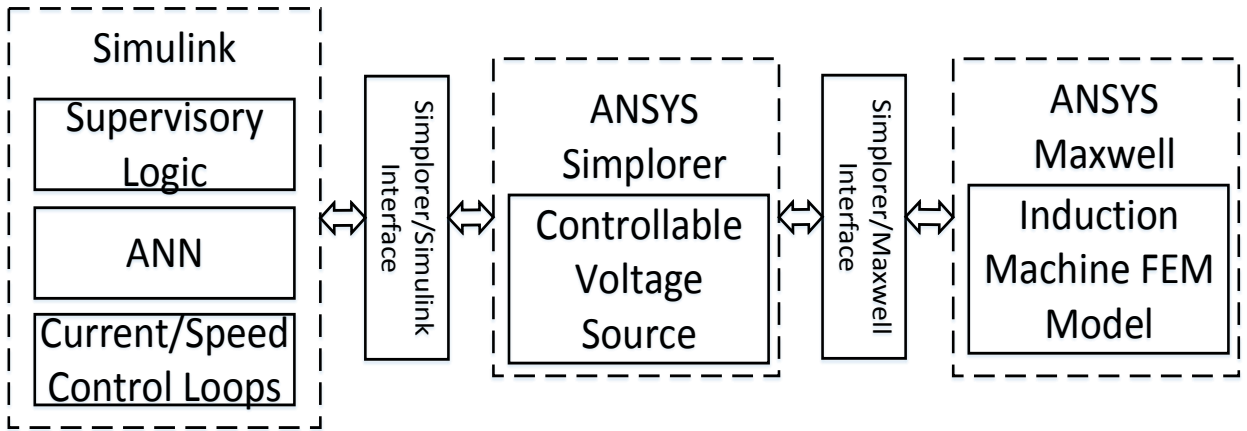


Figure 11.7. Quarter section of IM FEM model simulated in ANSYS Maxwell

It is not possible to directly connect Maxwell to the Simulink tool of MATLAB software where the ANN optimal controller of Chapter 10 is implemented. ANSYS Simplorer, however, provides a common platform for linking the control system in Simulink with the IM model in Maxwell [73] as illustrated in Figure 11.8. It should be noted that all three software programs (Simulink, Maxwell, and Simplorer) were running simultaneously during the simulation.



*Figure 11.8. Co-simulation using Simulink, ANSYS Simplorer, and Maxwell*

#### 11.4 Results

The test drive cycle of this simulation study is 3 seconds long and consists of 2 reference speed-load torque changes. The simulation was done on a PC with Intel Core i7 processor and 8 GB RAM. The complete simulation run took about 4 hours in real-world time. The four control regimes detailed in the previous chapters of this dissertation are applied to each drive cycle of this simulation study. The performance parameters of comparison are: a) settling time, b) peak electromagnetic torque, c) peak rotor flux (estimated), d) integral absolute error (IAE), e) cumulative electrical energy input, f) cumulative mechanical energy output, g) cumulative energy losses, and h) cycle energy efficiency.

The optimal control problem has been designed so as to allow the IM to reach steady state within 0.5 seconds after changing the reference speed. During the first second of simulation, the IM reaches a steady state speed of 50 rad/s and a rotor d-axis flux of 0.5 Wb. Hence, the 1<sup>st</sup> second will be similar for all the regimes. Next, the reference speed is changed from 50 rad/s to 100 rad/s at the end of the 1<sup>st</sup> second and to 150 rad/s at the end of the 2<sup>nd</sup> second. A load with a torque of 10 Nm is applied at the 1s. The input control trajectories were calculated using the expression for Regime I, Regime II, and Regime III. Regime IV refers to the optimal control trajectories generated by ANN optimal control system in Chapter 10. A video of the simulation has been uploaded by the author on YouTube and can be accessed using [74].

The rotor speed and electromagnetic torque profiles for the four control regimes corresponding to the duty cycle explained above are given in Figure 11.9 and Figure 11.10, respectively. The trajectory of rotor d-axis flux w.r.t. time that was estimated using an observer is shown in Figure 11.11. The d- and q-axis current trajectories (control inputs) w.r.t. time for all four regimes are shown in Figure 11.12 and Figure 11.13, respectively. The controllable energy losses and the mechanical energy output w.r.t. time are plotted in Figure 11.14, and Figure 11.15, respectively.

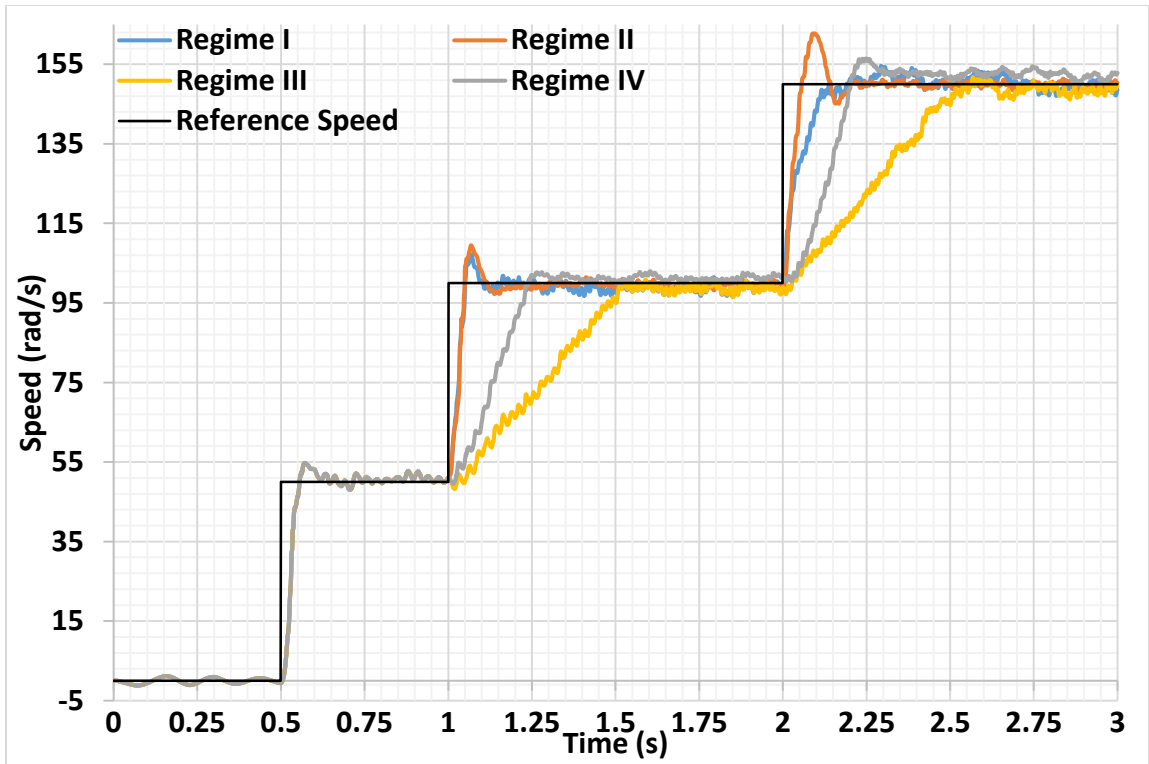


Figure 11.9. IM rotor speed profile corresponding to drive cycle.

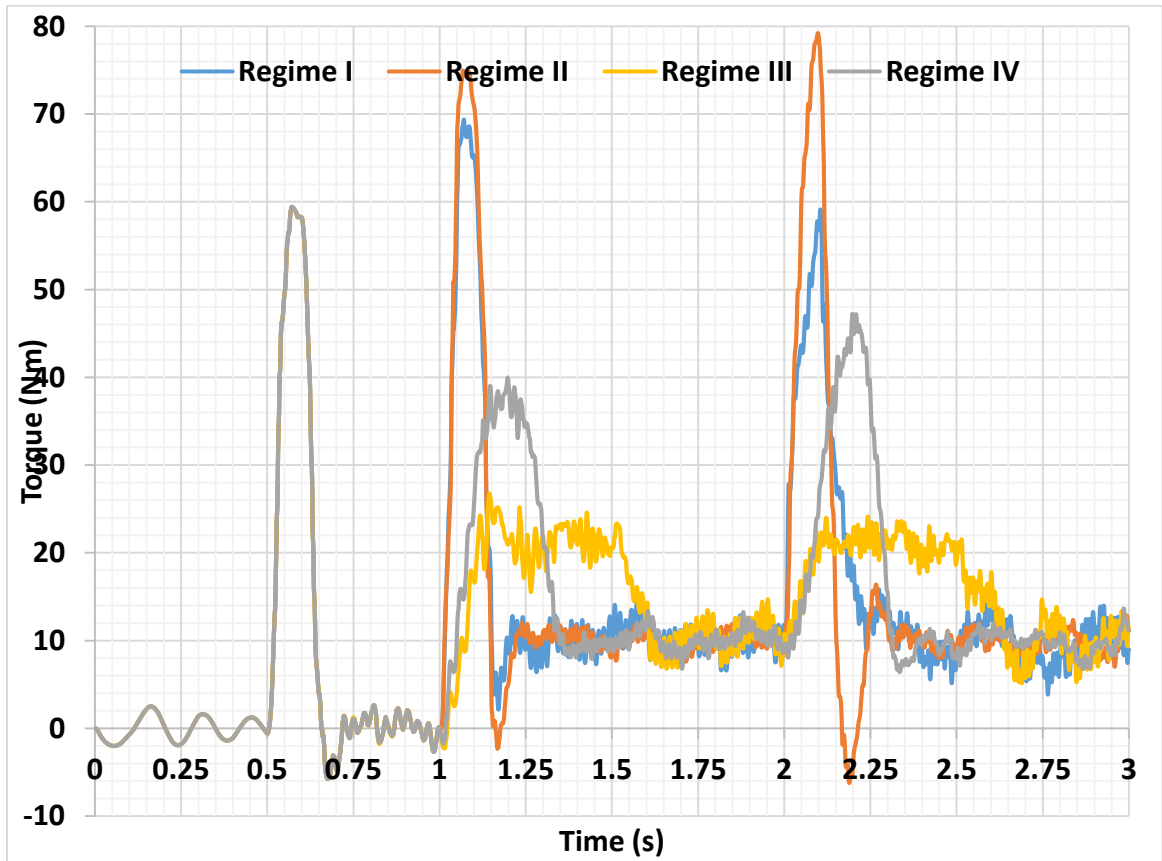


Figure 11.10. IM electromagnetic torque trajectories for given drive cycle

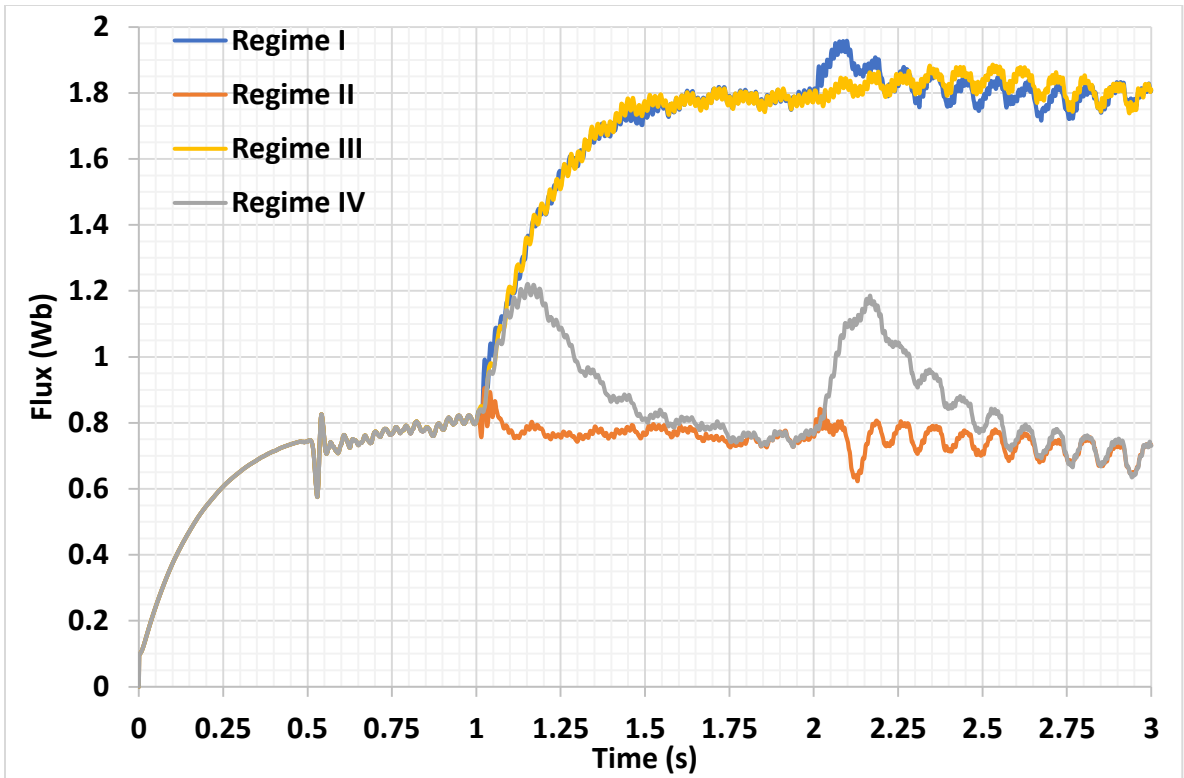


Figure 11.11. IM rotor d-axis flux trajectories for given drive cycle

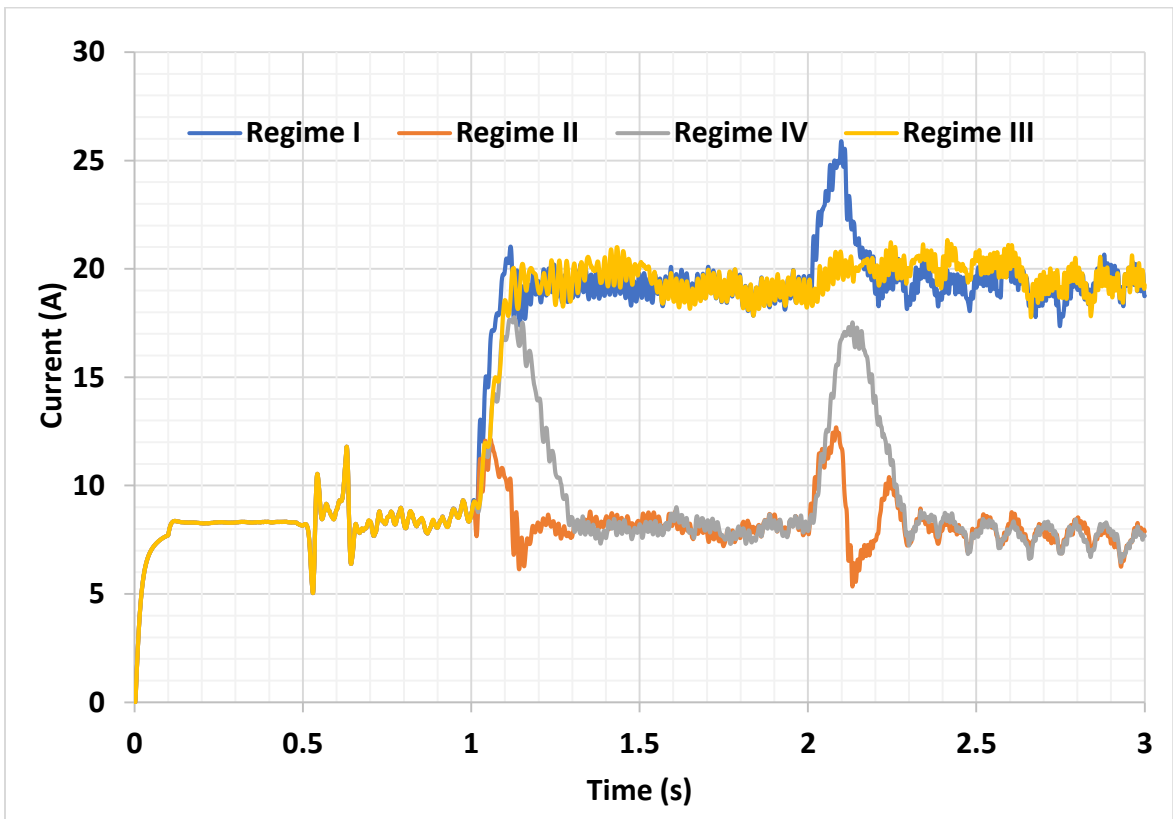


Figure 11.12. Comparing measured stator d-axis current for drive cycle

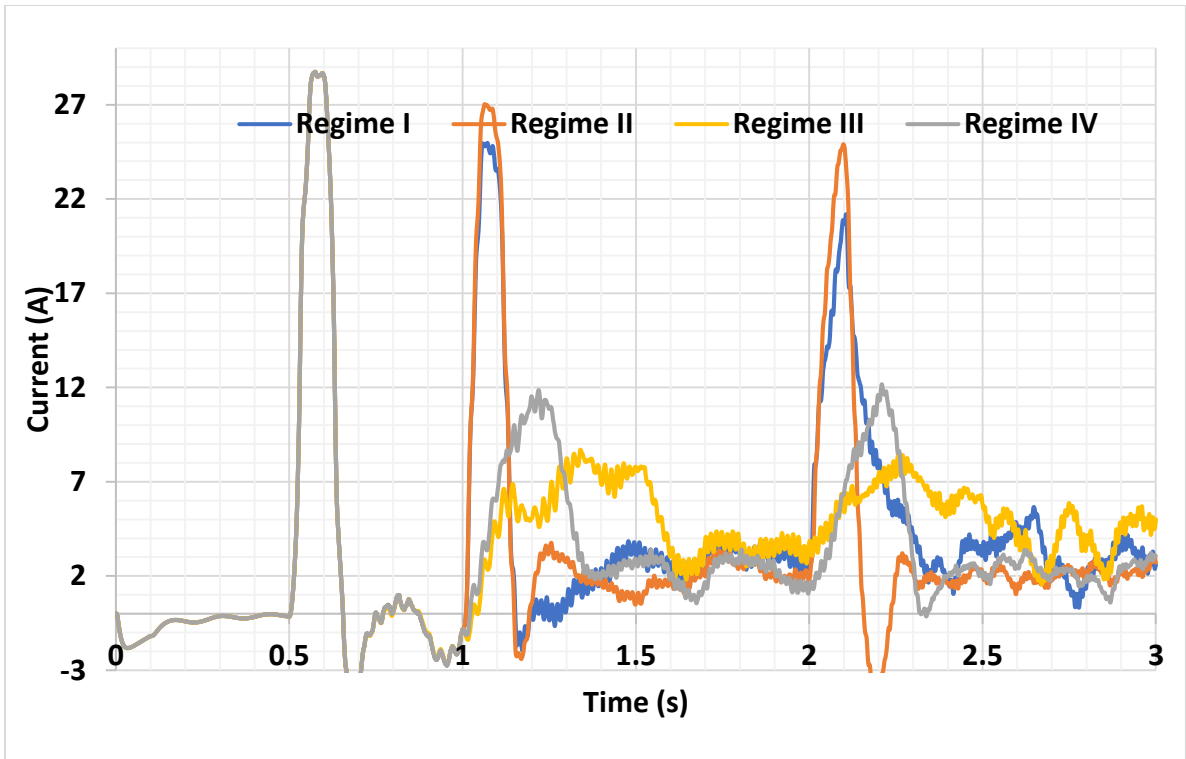


Figure 11.13. Comparing stator q-axis current for drive cycle

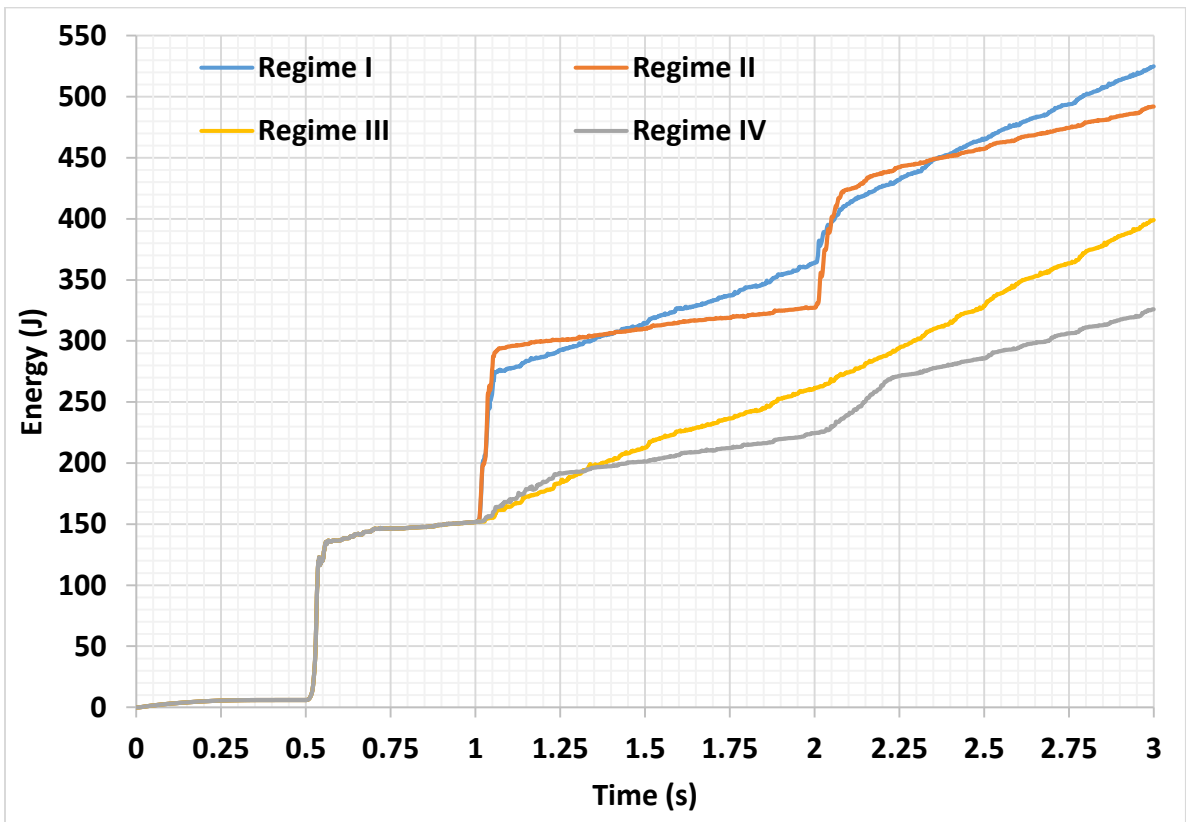


Figure 11.14. Comparing IM energy losses during the drive cycle.

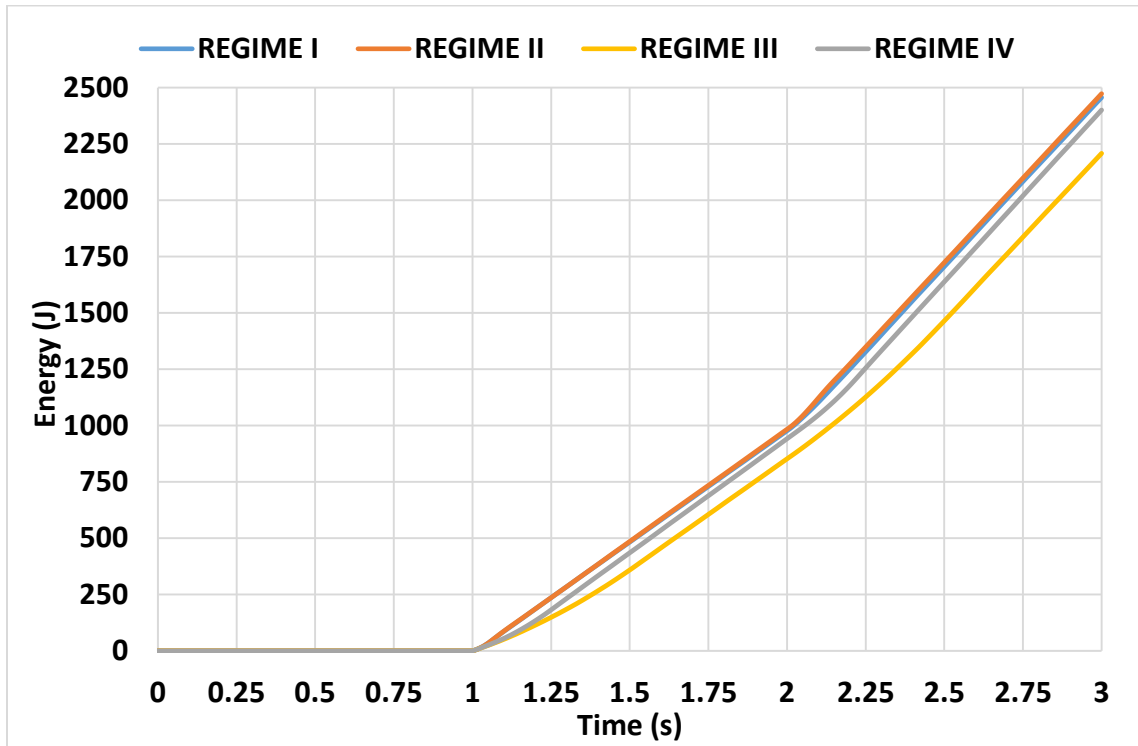


Figure 11.15. Comparing mechanical energy output at shaft during the drive cycle.

The rotor speed trajectories show that the optimal trajectories generated by the ANN could reach the desired speed reference within the time specified by the optimal control problem. The shape of the optimal current trajectories was similar to those obtained from the numerical solution in Chapter 8. The ANN could generate the optimal trajectories even though the rotor speed and the rotor flux feedback from the 2-D FEM model had a small amount of noise.

### 11.5 Summary on Comparing performances for the drive cycle

The performance parameters for the four regimes can be inferred from the plots shown in the previous section and are compiled in Table 11.1 below. As can be seen from this Table, there is a noticeable improvement in the energy efficiency for Regime IV over that for Regime I, Regime II, and Regime III. The results conform with our earlier observations



in Chapter 8 and Chapter 9 of this dissertation, and further validate the utility of the optimal current trajectories.

*Table 11.1. Comparing performance parameters over the drive cycles for all regimes*

<b>Regime</b>	<b>Max Settling Time (s)</b>	<b>Peak Electromagnetic Torque (Nm)</b>	<b>Peak d-axis Flux (Wb)</b>	<b>IAE w.r.t. reference speed</b>	<b>Energy Losses (J)</b>	<b>Mechanical Energy Output (J)</b>	<b>Energy Efficiency (%)</b>
<b>I</b>	0.30	69	1.95	8.6	534	2456	82.4
<b>II</b>	0.25	79	0.91	7.4	491	2472	83.4
<b>III</b>	0.70	26	1.88	31.5	399	2208	84.7
<b>IV</b>	0.46	47	1.22	18.5	325	2400	88

## 11.6 Summary

In this chapter results from a field oriented control experiment using the IM drive hardware and software available in the Electric Power and Energy Systems laboratory at UND was shown. It was shown that the power rating of IM drive hardware was too low to get meaningful results if IM optimal control solutions were applied. Hence a co-simulation using an FE model in ANSYS Maxwell was performed. It was found that the ANN optimal control showed noticeable gains in energy efficiency over a drive cycle when compared to conventional speed control algorithms.

## 12 CONCLUSION AND FURTHER WORK

The goal of this dissertation work was to design an optimal control law for an induction machine to minimize the transient energy losses. The following contributions were made:

1. It was shown that it is possible to incorporate energy losses as well as the terminal costs related to the rotor field oriented induction machine into a single cost functional. Furthermore, it was shown that the necessary conditions arising from Pontryagin's minimum principle can be numerically solved for given set of initial and final conditions (rotor flux, rotor speed, and load torque). From the numerical solutions, it could be noticed that the shape of the optimal flux trajectory (during transient) was a conic section, while the q-axis current trajectory (during transient) could either be a conic section or a constant value function.
2. Prototype analytical expressions to describe the conic and constant value optimal rotor flux and stator current trajectories for a generic rotor field oriented IM were formulated. The parameters related to the expressions were derived as a function of  $x$ , which is defined as the ratio of the rotor flux value at the vertex of the conic section to the rotor flux value at start of transient. It was found that the energy efficiency obtained while accelerating/decelerating an IM using optimal control trajectories remained consistent. Also, the sensitivity of the optimal energy efficiency to parameters like moment of inertia, change in reference rotor speed, and rotor time constant were analyzed.
3. A feedforward neural network was trained using the numerical solutions following the template training concept so that it could emulate the solution of the optimal control

problem. The trained neural network was incorporated into a supervisory control system (ANN optimal control system) that could generate the optimal control trajectories for q-axis and d-axis current IM in real time during transients. Finally, results from a real-time simulation using a finite element model of the IM for a drive cycle was presented which indicated at least 3% improvement in energy efficiency was possible over conventional speed control loops when using the ANN optimal control system.

### 12.1 Further work

The concept of manipulating rotor flux to improve efficiency can be extended to other types of AC machines where rotor flux is controllable, like a wound rotor synchronous machine. Electric vehicle drive train application offers the biggest potential for energy savings due to transient energy loss minimization is probably in electric car drivetrains. The additional dynamics associated with drivetrains can be incorporated into the problem. Also, the ANN optimal control system developed in this dissertation could be modified to work as part of the EV drive train control loops.

## 13 REFERENCES

- [1] D. E. Kirk, *Optimal Control Theory: An Introduction*. New York: Dover Publications, 2004.
- [2] D. Liberzon, *Calculus of Variations and Optimal Control Theory: A Concise Introduction*. Princeton University Press, 2012.
- [3] "Classification of Electric Motors." [Online]. Available: <http://www.electrical-knowhow.com/2012/05/classification-of-electric-motors.html>. [Accessed: 01-Jun-2017].
- [4] W. Rippel, "Induction Versus DC Brushless Motors," *Tesla Blog*, 2007. [Online]. Available: [https://www.tesla.com/blog/induction-versus-dc-brushless-motors?\\_ga=2.124376398.511149995.1497120851-1266924314.1496689154](https://www.tesla.com/blog/induction-versus-dc-brushless-motors?_ga=2.124376398.511149995.1497120851-1266924314.1496689154). [Accessed: 10-Jun-2017].
- [5] S. Muller, M. Deicke, and R. W. De Doncker, "Doubly fed induction generator systems for wind turbines," *IEEE Ind. Appl. Mag.*, vol. 8, no. 3, pp. 26–33, 2002.
- [6] I. Alan and T. A. Lipo, "Induction machine based flywheel energy storage system," *IEEE Trans. Aerosp. Electron. Syst.*, vol. 39, no. 1, pp. 151–163, Jan. 2003.
- [7] US EPA, "Dynamometer Drive Schedules." [Online]. Available: <https://www.epa.gov/vehicle-and-fuel-emissions-testing/dynamometer-drive-schedules>. [Accessed: 20-Oct-2016].
- [8] Z. Shahan, "Tesla's 2016 Deliveries = 76,230+ Vehicles, Production = 83,922 Vehicles," *Clean Technica*, 2017. [Online]. Available: <https://cleantechnica.com/2017/01/03/teslas-2016-deliveries-production/>. [Accessed: 18-Jul-2017].
- [9] C. Thomson, "Tesla will build 500,000 cars per year by 2018," *Buisness Insider*, 2016. [Online]. Available: <http://www.businessinsider.com/tesla-will-build-500000-cars-per-year-by-2018-2016-5>. [Accessed: 18-Jul-2017].
- [10] B. G. Lamme, "The story of the induction motor," *J. Am. Inst. Electr. Eng.*, vol. 40, no. 3, pp. 203–223, Mar. 1921.
- [11] P. L. Alger and R. E. Arnold, "The history of induction motors in America," *Proc. IEEE*, vol. 64, no. 9, pp. 1380–1383, 1976.
- [12] I. Boldea and S. A. Nasar, *Electric drives*. .
- [13] R. J. Lee, P. Pillay, and R. G. Harley, "D,Q reference frames for the simulation of induction motors," *Electr. Power Syst. Res.*, vol. 8, no. 1, pp. 15–26, Oct. 1984.
- [14] P. C. Krause, O. Wasynczuk, S. D. Sudhoff, S. Pekarek, and Institute of Electrical and Electronics Engineers., *Analysis of electric machinery and drive systems*. Wiley-IEEE Press, 2013.
- [15] N. Mohan, *Advanced Electric Drives: Analysis, Control, and Modeling Using MATLAB / Simulink*. Wiley, 2014.
- [16] H. J. Sussmann and J. C. Willems, "300 years of optimal control: from the brachystochrone to the

- maximum principle," *IEEE Control Syst. Mag.*, vol. 17, no. 3, pp. 32–44, Jun. 1997.
- [17] A. E. Bryson, "Optimal control-1950 to 1985," *IEEE Control Syst. Mag.*, vol. 16, no. 3, pp. 26–33, Jun. 1996.
- [18] R. V. Gamkrelidze, "Discovery of the Maximum Principle," *J. Dyn. Control Syst.*, vol. 5, no. 4, pp. 437–451, Oct. 1999.
- [19] H. J. Pesch and M. Plail, "The maximum Principle of optimal control: A history of ingenious ideas and missed opportunities," *Control Cybern.*, vol. 38, no. 4A, pp. 973–995, 2009.
- [20] R. Bellman and R. Ernest, *Dynamic programming*. Dover Publications, 2003.
- [21] R. E. Kalman, "Contributions to the Theory of Optimal Control," in *Bol. Soc. Mat. Mexicana vol. 5*, 1960, pp. 102–119.
- [22] R. E. Kalman, "LQR 2nd paper," in *Mathematical Optimization Techniques*, R. Bellman, Ed. University of California press, 1963, pp. 309–331.
- [23] A. M. Bazzi and P. T. Krein, "Review of Methods for Real-Time Loss Minimization in Induction Machines," *IEEE Trans. Ind. Appl.*, vol. 46, no. 6, pp. 2319–2328, Nov. 2010.
- [24] I. P. Petrov, *Variational Methods in Optimum Control Theory*. New York: Academic Press, 1968.
- [25] G. FIGALLI, M. LA CAVA, and L. TOMASI, "An optimal feedback control for a bilinear model of induction motor drives†," *Int. J. Control*, vol. 39, no. 5, pp. 1007–1016, May 1984.
- [26] R. D. Lorenz and S. M. Yang, "Efficiency-optimized flux trajectories for closed cycle operation of field oriented induction machine drives," in *Conference Record of the 1988 IEEE Industry Applications Society Annual Meeting*, 1988, pp. 457–462.
- [27] R. D. Lorenz and S.-M. Yang, "Efficiency-optimized flux trajectories for closed-cycle operation of field-orientation induction machine drives," *IEEE Trans. Ind. Appl.*, vol. 28, no. 3, pp. 574–580, 1992.
- [28] R. D. Lorenz and S.-M. Yang, "AC induction servo sizing for motion control applications via loss minimizing real-time flux control," *IEEE Trans. Ind. Appl.*, vol. 28, no. 3, pp. 589–593, 1992.
- [29] S. Sangwongwanich, M. Ishida, S. Okuma, Y. Uchikawa, and K. Iwata, "Implementation of a time-optimal single-step velocity response control scheme of field oriented induction machines considering saturation of flux," in *PESC '88 Record., 19th Annual IEEE Power Electronics Specialists Conference*, 1988, pp. 1076–1083.
- [30] S. Sangwongwanich, M. Ishida, S. Okuma, and K. Iwata, "Manipulation of rotor flux for time-optimal single-step velocity response of field-oriented induction machines," *IEEE Trans. Ind. Appl.*, vol. 24, no. 2, pp. 262–270, 1988.
- [31] S. Sangwongwanich, M. Ishida, S. Okuma, Y. Uchikawa, and K. Iwata, "Realization of time-optimal single-step velocity response control of field-oriented induction machines under the condition of nonsaturation of flux," *IEEE Trans. Ind. Appl.*, vol. 27, no. 5, pp. 947–955, 1991.
- [32] S. Sangwongwanich, M. Ishida, S. Okuma, Y. Uchikawa, and K. Iwata, "Time-optimal single-step velocity response control scheme for field-oriented induction machines considering saturation level," *IEEE Trans. Power Electron.*, vol. 6, no. 1, pp. 108–117, 1991.
- [33] T. Murata, T. Tsuchiya, and I. Takeda, "Vector control for induction machine on the application of optimal control theory," *IEEE Trans. Ind. Electron.*, vol. 37, no. 4, pp. 283–290, 1990.
- [34] C. C. De Wit and J. Ramirez, "Optimal torque control for current-fed induction motors," *IEEE*

*Trans. Automat. Contr.*, vol. 44, no. 5, pp. 1084–1089, 1999.

- [35] J. Rodriguez Arribas and C. M. Vega Gonzalez, "Optimal vector control of pumping and ventilation induction motor drives," *IEEE Trans. Ind. Electron.*, vol. 49, no. 4, pp. 889–895, Aug. 2002.
- [36] C. M. Vega Gonzalez, J. Rodriguez Arribas, and D. Ramirez Prieto, "Optimal Regulation of Electric Drives With Constant Load Torque," *IEEE Trans. Ind. Electron.*, vol. 53, no. 6, pp. 1762–1769, Dec. 2006.
- [37] C. Botan, M. Ratoj, and V. Horga, "Optimal control of electrical drives with induction motors for variable torques," in *2008 13th International Power Electronics and Motion Control Conference*, 2008, pp. 1111–1116.
- [38] K. Inoue and T. Kato, "A study of an Optimal torque for Power regeneration of an Induction Motor," in *IEEE Power Electronics Specialists Conference*, 2007, pp. 2108–2122.
- [39] K. Inoue, K. Kotera, and T. Kato, "Optimal torque trajectories minimizing loss of induction motor under given condition of rotational angle," in *2011 IEEE Energy Conversion Congress and Exposition*, 2011, pp. 1734–1738.
- [40] K. Inoue, K. Kotera, and T. Kato, "Optimal motion trajectories minimizing loss of induction motor under amplitude limits," in *2012 IEEE Energy Conversion Congress and Exposition (ECCE)*, 2012, pp. 2576–2581.
- [41] K. Inoue, K. Kotera, Y. Asano, and T. Kato, "Optimal torque and rotating speed trajectories minimizing energy loss of induction motor under both torque and speed limits," in *2013 IEEE 10th International Conference on Power Electronics and Drive Systems (PEDS)*, 2013, pp. 1127–1132.
- [42] M. Gaiceanu, E. Rosu, T. Munteanu, T. Dumitriu, R. Paduraru, and C. Dache, "Optimal control for AC drive with quadratic criteria." pp. 1–10, 2009.
- [43] E. Rosu, T. Munteanu, M. Gaiceanu, T. Dumitriu, R. Paduraru, and C. Dache, "Optimal control using energetic criteria for electric drive systems: Plenary talk," in *2010 3rd International Symposium on Electrical and Electronics Engineering (ISEEE)*, 2010, pp. IV–XV.
- [44] M. Gaiceanu, E. Rosu, R. Paduraru, and T. Munteanu, "Vector-controlled optimal drive system for the induction motor," in *2013 4th International Symposium on Electrical and Electronics Engineering (ISEEE)*, 2013, pp. 1–6.
- [45] A. Ben Ali, R. Abdelati, M. F. Mimouni, and R. Dhifaoui, "Maximum-Torque and Maximum-Efficiency Rotor Flux Selection of an Induction Motor in Transient Regime," *Int. J. Sci. Tech. Autom. Control Comput. Eng.*, vol. 4, no. December, pp. 1370–1387, 2010.
- [46] J.-F. Stumper and R. Kennel, "Real-time dynamic efficiency optimization for induction machines," in *2013 American Control Conference*, 2013, pp. 6589–6594.
- [47] J.-F. Stumper, A. Dotlinger, and R. Kennel, "Loss Minimization of Induction Machines in Dynamic Operation," *IEEE Trans. Energy Convers.*, vol. 28, no. 3, pp. 726–735, Sep. 2013.
- [48] R. Weis and A. Gensior, "A model-based loss-reduction scheme for transient operation of induction machines," in *2016 18th European Conference on Power Electronics and Applications (EPE'16 ECCE Europe)*, 2016, pp. 1–8.
- [49] S. J. Plathottam and H. Salehfar, "Transient loss minimization in induction machine drives using optimal control theory," in *2015 IEEE International Electric Machines & Drives Conference (IEMDC)*, 2015, pp. 1774–1780.
- [50] S. J. Plathottam and H. Salehfar, "Induction machine transient energy loss minimization using

- neural networks,” in *2016 North American Power Symposium (NAPS)*, 2016, pp. 1–5.
- [51] A. Borisevich and G. Schullerus, “Energy Efficient Control of an Induction Machine Under Torque Step Changes,” *IEEE Trans. Energy Convers.*, vol. 31, no. 4, pp. 1295–1303, Dec. 2016.
- [52] ABB, “ABB drives - Technical guide book,” 2013.
- [53] S. Lim and K. Nam, “Loss-minimising control scheme for induction motors,” *IEE Proceedings-Electr. Power Appl.*, vol. 151, no. 4, pp. 385–397, 2004.
- [54] S. N. Vukosavic and E. Levi, “A method for transient torque response improvement in optimum efficiency induction motor drives,” *IEEE Trans. Energy Convers.*, vol. 18, no. 4, pp. 484–493, Dec. 2003.
- [55] L. Lasdon, S. Mitter, and A. Waren, “The conjugate gradient method for optimal control problems,” *IEEE Trans. Automat. Contr.*, vol. 12, no. 2, pp. 132–138, Apr. 1967.
- [56] E. K. P. Chong and S. H. Zak, *An Introduction to Optimization*. Wiley, 2011.
- [57] A. L. Samuel, “Some Studies in Machine Learning Using the Game of Checkers,” *IBM J. Res. Dev.*, vol. 3, no. 3, pp. 210–229, Jul. 1959.
- [58] A. Géron, *Hands-on machine learning with Scikit-Learn and TensorFlow : concepts, tools, and techniques to build intelligent systems*, 1st ed. O’Reilly Media, Inc, 2017.
- [59] Y. LeCun, Y. Bengio, and G. Hinton, “Deep learning,” *Nature*, vol. 521, no. 7553, pp. 436–444, May 2015.
- [60] S. J. Hanson, J. D. Cowan, C. L. Giles, C. . Conference on Neural Information Processing Systems - Natural and Synthetic (6 : 1992 : Denver, and C. . Neural Information Processing Systems Conference (5 : 1992 : Denver, “The power of approximating: a comparison of activation functions,” in *Proceedings of the 5th International Conference on Neural Information Processing Systems*, 1992, pp. 615–622.
- [61] H. W. Lin and M. Tegmark, “Why does deep and cheap learning work so well?,” *arXiv*, Aug. 2016.
- [62] S. S. Haykin and Simon, *Neural networks : a comprehensive foundation*, 2nd ed. Prentice Hall, 1999.
- [63] G. Cybenko, “Approximation by superpositions of a sigmoidal function,” *Math. Control. Signals, Syst.*, vol. 2, no. 4, pp. 303–314, Dec. 1989.
- [64] K. Hornik, “Approximation capabilities of multilayer feedforward networks,” *Neural Networks*, vol. 4, no. 2, pp. 251–257, 1991.
- [65] T. Hrycej, *Neurocontrol : towards an industrial control methodology*. Wiley, 1997.
- [66] H. Yu and B. M. Wilamowski, “Levenberg-Marquardt training,” in *Industrial Electronics Handbook, vol. 5 – Intelligent Systems*, 2nd ed., CRC Press, 2011, pp. 12-1-18.
- [67] J. Dean and R. Monga, “TensorFlow - Google’s latest machine learning system, open sourced for everyone,” *Google Research Blog*, 2015. [Online]. Available: [https://research.googleblog.com/2015/11/tensorflow-googles-latest-machine\\_9.html](https://research.googleblog.com/2015/11/tensorflow-googles-latest-machine_9.html).
- [68] S. J. Plathottam and H. Salehfar, “Trajectory training of feedforward neural networks for DC motor speed control,” in *2017 IEEE Texas Power and Energy Conference (TPEC)*, 2017, pp. 1–5.
- [69] “ANSYS Maxwell.” [Online]. Available: <http://www.ansys.com/Products/Electronics/ANSYS-Maxwell>. [Accessed: 18-Apr-2016].

- [70] ANSYS, "AC Motor Drive Using Cosimulation."
- [71] P. Makolo, "Wind Generator Co-Simulation with Fault Case Analysis," Chalmers University of Technology, 2013.
- [72] C. M. Apostoiaia, "AC machines and drives simulation platform," in *2013 International Electric Machines & Drives Conference*, 2013, pp. 1295–1299.
- [73] "ANSYS Simplorer." [Online]. Available: <http://www.ansys.com/Products/Systems/ANSYS-Simplorer>. [Accessed: 24-Apr-2016].
- [74] S. J. Plathottam, "FEM Simulation of Field Oriented IM using Optimal Transient Flux," *YouTube*, 2016. [Online]. Available: <https://www.youtube.com/watch?v=HYzddL2IFpk>.
- [75] M. A. El-Sharkawi, *Fundamentals of electric drives*. Brooks/Cole, 2000.



## APPENDIX I

Permanent magnet DC motor specifications:

Table I. Parametres of PMDC machine (from [75])

<b>Parameter (unit)</b>	<b>Unit</b>	<b>Value</b>
Armature winding resistance	ohm	2
Torque constant	Vs	3
Terminal voltage	V	600
Rated armature current	A	5
Starting current	A	300

## APPENDIX II

### Induction motor specifications

Table I. Parameters of Type I IM (from ANSYS RMxprt)

<b>Parameter (unit)</b>	<b>Unit</b>	<b>Value</b>
Rated Power	kW	7.5
Terminal voltage	V	400
Rated armature current	A	15
Number of poles		4
Rated frequency	Hz	60
Stator winding resistance	ohm	0.669
Rotor winding resistance	ohm	0.524
Resistance corresponding to core loss	ohm	800
Stator leakage inductance	mH	1.6
Rotor leakage inductance	mH	2.2
Mutual inductance	mH	97
Moment of inertia	kg-m <sup>2</sup>	0.2
Outer Diameter	mm	210
Inner diameter	mm	148
Length	mm	250

Table II. Parameters of Type II IM (from [48])

<b>Parameter (unit)</b>	<b>Unit</b>	<b>Value</b>
Rated Power	kW	4.0
Terminal voltage	V	400
Rated armature current	A	7.5
Number of poles		4
Rated frequency	Hz	50
Stator winding resistance	ohm	1.3
Rotor winding resistance	ohm	0.93
Resistance corresponding to core loss	ohm	2000
Stator leakage inductance	mH	12.6
Rotor leakage inductance	mH	5.3
Mutual inductance	mH	181.8
Moment of inertia	kg-m <sup>2</sup>	0.036

Table III. Parameters of Type C IM (from [15])

<b>Parameter (unit)</b>	<b>Unit</b>	<b>Value</b>
Rated Power	kW	2.4
Terminal voltage	V	460
Rated armature current	A	4
Number of poles		4
Rated frequency	Hz	60
Stator winding resistance	ohm	1.77
Rotor winding resistance	ohm	1.34
Stator leakage inductance	ohm	14
Rotor leakage inductance	mH	12.1
Resistance corresponding to core loss	mH	
Mutual inductance	mH	369
Moment of inertia	kg-m <sup>2</sup>	0.025

### APPENDIX III

The steady state power losses may be written as,

$$i_{ds} = \frac{\psi_{dr}}{L_m}$$

$$i_{qs} = \frac{2L_r T_e}{pL_m \psi_{dr}}$$

$$P_{loss}^{total} = \left( \left( \frac{\psi_{dr}}{L_m} \right)^2 + \left( \frac{2L_r T_e}{pL_m \psi_{dr}} \right)^2 \right) R_s + R_r \left( \frac{2T_e}{p\psi_{dr}} \right)^2 + \frac{L_{lr}^2 \omega_r^2}{R_m} \left( \frac{2T_e}{p\psi_{dr}} \right)^2 + \frac{\omega_r^2 \psi_{dr}^2}{R_m}$$

The first derivation of the power losses with respect to rotor d-axis flux is given by,

$$\begin{aligned} \frac{\partial P_{loss}^{total}}{\partial \psi_{dr}} &= 2R_s \left( \frac{1}{L_m} \right)^2 \psi_{dr} - 8 \left( \frac{L_r T_e}{pL_m} \right)^2 \frac{R_s}{(\psi_{dr})^3} - 8R_r \left( \frac{T_e}{p} \right)^2 \frac{1}{(\psi_{dr})^3} - \\ &8 \frac{L_{lr}^2 \omega_r^2}{R_m} \left( \frac{T_e}{p} \right)^2 \frac{1}{(\psi_{dr})^3} + \frac{2\omega_r^2}{R_m} \psi_{dr} = 0 \end{aligned}$$

Equating to zero, we get,

$$\begin{aligned} R_s \left( \frac{1}{L_m} \right)^2 \psi_{dr} - 4 \left( \frac{L_r T_e}{pL_m} \right)^2 \frac{R_s}{(\psi_{dr})^3} - 4R_r \left( \frac{T_e}{p} \right)^2 \frac{1}{(\psi_{dr})^3} - \\ 4 \frac{L_{lr}^2 \omega_r^2}{R_m} \left( \frac{T_e}{p} \right)^2 \frac{1}{(\psi_{dr})^3} + \frac{\omega_r^2}{R_m} \psi_{dr} = 0 \end{aligned}$$

$$R_s \left( \frac{1}{L_m} \right)^2 \psi_{dr}^4 - 4 \left( \frac{L_r T_e}{p L_m} \right)^2 R_s - 4 R_r \left( \frac{T_e}{p} \right)^2 - 4 \frac{L_{lr}^2 \omega_r^2}{R_m} \left( \frac{T_e}{p} \right)^2 + \frac{\omega_r^2}{R_m} \psi_{dr}^4 = 0$$

$$\left( R_s \left( \frac{1}{L_m} \right)^2 + \frac{\omega_r^2}{R_m} \right) \psi_{dr}^4 = 4 \left( \frac{L_r T_e}{p L_m} \right)^2 R_s + 4 R_r \left( \frac{T_e}{p} \right)^2 + 4 \frac{L_{lr}^2 \omega_r^2}{R_m} \left( \frac{T_e}{p} \right)^2$$

$$\left( R_s \left( \frac{1}{L_m} \right)^2 + \frac{\omega_r^2}{R_m} \right) \psi_{dr}^4 = \frac{4 T_e^2}{p^2} \left( \left( \frac{L_r}{L_m} \right)^2 R_s + R_r + \frac{L_{lr}^2 \omega_r^2}{R_m} \right)$$

$$\psi_{dr}^4 = \left( \frac{2 T_e}{p} \right)^{\frac{1}{2}} \left( \frac{\left( \frac{L_r}{L_m} \right)^2 R_s + R_r + \frac{L_{lr}^2 \omega_r^2}{R_m}}{\frac{R_s}{L_m^2} + \frac{\omega_r^2}{R_m}} \right)^{\frac{1}{4}}$$

Hence the optimal steady state flux is given by,

$$\psi_{dr} = \left( \frac{2 T_e}{p} \right)^{\frac{1}{2}} \left( \frac{R_s R_m L_r^2 + R_r R_m L_m^2 + \omega_r^2 L_{lr}^2 L_m^2}{R_s R_m + \omega_r^2 L_m^2} \right)^{\frac{1}{4}}$$

APPENDIX IV

Expressing parameters in conic equation in terms of flux.

$$\psi_{dr}(t) = \begin{cases} \psi_{dr}^{f_1}, & t < t_0 \\ a_1 t^2 + b_1 t + c_1, & t_0 \geq t \geq t_{tf} \\ \psi_{dr}^{f_2}, & t > t_{tf} \end{cases}$$

$$\frac{d\psi_{dr}}{dt} = 2a_1 t + b_1$$

$$i_{ds}(t) = \frac{1}{L_m} \left( \frac{L_r}{R_r} (2a_1 t + b_1) + a_1 t^2 + b_1 t + c_1 \right)$$

Assuming that trajectory  $\psi_{dr}(t)$  passes through the points  $\psi_{dr}^0$ ,  $\psi_{dr}^e$  and  $\psi_{dr}^{opt}$  at  $t = 0, \frac{t_{tf}}{2}$ , and  $t_{tf}$ ,

$$\psi_{dr}(0) = c_1 = \psi_{dr}^0$$

$$\psi_{dr}\left(\frac{t_{tf}}{2}\right) = \frac{a_1 t_{tf}^2}{4} + \frac{b_1 t_{tf}}{2} + \psi_{dr}^0 = \psi_{dr}^m$$

$$\psi_{dr}(t_{tf}) = a_1 t_{tf}^2 + b_1 t_{tf} + \psi_{dr}^0 = \psi_{dr}^f$$

$$a_1 = \frac{\psi_{dr}^f - b_1 t_{tf} - \psi_{dr}^0}{t_{tf}^2}$$

$$\frac{1}{4}(\psi_{dr}^f - b_1 t_{tf} - \psi_{dr}^0) + \frac{b_1}{2} t_{tf} + \psi_{dr}^0 = \psi_{dr}^m$$

$$\frac{1}{4}(\psi_{dr}^f - b_1 t_{tf} - \psi_{dr}^0) + \frac{b_1}{2} t_{tf} + \psi_{dr}^0 = \psi_{dr}^m$$

$$\psi_{dr}^f + b_1 t_{tf} + 3\psi_{dr}^0 = 4\psi_{dr}^m$$

$$b_1 = \frac{4\psi_{dr}^m - 3\psi_{dr}^0 - \psi_{dr}^f}{t_{tf}}$$

$$a_1 = \frac{\psi_{dr}^f - (4\psi_{dr}^m - 3\psi_{dr}^0 - \psi_{dr}^f) - \psi_{dr}^0}{t_{tf}^2}$$

$$a_1 = \frac{\psi_{dr}^f - 4\psi_{dr}^m + 3\psi_{dr}^0 + \psi_{dr}^f - \psi_{dr}^0}{t_{tf}^2}$$

$$a_1 = \frac{2\psi_{dr}^f + 2\psi_{dr}^0 - 4\psi_{dr}^m}{t_{tf}^2}$$

### Expressing parameters in conic equation in terms of current.

Assuming that the trajectory passes through the points  $i_{qs}^{t_0}$ ,  $i_{qs}^m$  and  $i_{qs}^f$  at  $t = 0$ ,  $\frac{t_{tf}}{2}$  and  $t_{tf}$ , respectively, we can calculate the constants  $a_2$ ,  $b_2$ ,  $c_2$ ..

$$i_{qs} = \begin{cases} i_{qs}^{opt1}, & t < t_0 \\ a_2 t^2 + b_2 t + c_2, & t_0 \geq t \leq t_{tf} \\ i_{qs}^{opt2}, & t > t_{tf} \end{cases}$$

$$i_{qs}(0) = c_2 = i_{qs}^0$$

$$i_{qs}\left(\frac{t_{tf}}{2}\right) = \frac{a_2 t_{tf}^2}{4} + \frac{b_2 t_{tf}}{2} + i_{qs}^0 = i_{qs}^m$$

$$i_{qs}(t_{tf}) = a_2 t_{tf}^2 + b_2 t_{tf} + i_{qs}^0 = i_{qs}^f$$

$$a_2 = \frac{i_{qs}^f - b_2 t_{tf} - i_{qs}^0}{t_{tf}^2}$$

$$\frac{i_{qs}^f - b_2 t_{tf} - i_{qs}^0}{4} + \frac{b_2 t_{tf}}{2} + i_{qs}^0 = i_{qs}^m$$

$$i_{qs}^f + b_2 t_{tf} + 3i_{qs}^0 = 4i_{qs}^m$$

$$b_2 = \frac{4i_{qs}^m - 3i_{qs}^0 - i_{qs}^f}{t_{tf}}$$

$$a_2 = \frac{2i_{qs}^f + 2i_{qs}^0 - 4i_{qs}^m}{t_{tf}^2}$$

## APPENDIX V

### Derivation of d-axis component of losses

Analytical proof of optimality

For simplicity assume,

$$\psi_{dr}^f = \psi_{dr}^0 = \psi_{dr}^a$$

$$i_{qs}^0 = i_{qs}^f = 0$$

$$t_{tf} = 1$$

$$a_1 = \frac{2\psi_{dr}^f + 2\psi_{dr}^0 - 4\psi_{dr}^m}{t_{tf}^2} = 4\psi_{dr}^a - 4\psi_{dr}^m = 4(\psi_{dr}^a - \psi_{dr}^m)$$

$$b_1 = \frac{4\psi_{dr}^m - 3\psi_{dr}^0 - \psi_{dr}^f}{t_{tf}} = 4\psi_{dr}^m - 3\psi_{dr}^a - \psi_{dr}^a = 4(\psi_{dr}^m - \psi_{dr}^a)$$

$$c_1 = \psi_{dr}^0 = \psi_{dr}^a$$

Similarly,

$$a_2 = \frac{2i_{qs}^f + 2i_{qs}^0 - 4i_{qs}^m}{t_{tf}^2} = -4i_{qs}^m$$

$$b_2 = \frac{4i_{qs}^m - 3i_{qs}^0 - i_{qs}^f}{t_{tf}} = 4i_{qs}^m$$

$$c_2 = i_{qs}^0 = 0$$

Hence, we can define,

$$\psi_{dr}(t) = a_1 t^2 + b_1 t + c_1 = 4(\psi_{dr}^a - \psi_{dr}^m) t^2 + 4(\psi_{dr}^m - \psi_{dr}^a) t + \psi_{dr}^a$$

$$\psi_{dr}(t) = 4(\psi_{dr}^a - \psi_{dr}^m) t^2 - 4(\psi_{dr}^a - \psi_{dr}^m) t + \psi_{dr}^a$$

$$\frac{d\psi_{dr}}{dt} = 8(\psi_{dr}^a - \psi_{dr}^m) t - 4(\psi_{dr}^a - \psi_{dr}^m) = 4(\psi_{dr}^a - \psi_{dr}^m)(2t - 1)$$



$$\psi_{dr}^m = x\psi_{dr}^a$$

$$\psi_{dr}(t) = 4(\psi_{dr}^a - x\psi_{dr}^a)t^2 - 4(\psi_{dr}^a - x\psi_{dr}^a)t + \psi_{dr}^a$$

$$\psi_{dr}(t) = \psi_{dr}^a (4(1-x)t^2 - 4(1-x)t + 1)$$

$$i_{ds}(t) = \frac{1}{L_m} \left( \frac{L_r}{R_r} \frac{d\psi_{dr}}{dt} + \psi_{dr}(t) \right)$$

$$i_{ds}(t) = \frac{1}{L_m} \left( \frac{L_r}{R_r} 4(\psi_{dr}^a - \psi_{dr}^m)(2t-1) + 4(\psi_{dr}^a - \psi_{dr}^m)t^2 - 4(\psi_{dr}^a - \psi_{dr}^m)t + \psi_{dr}^a \right)$$

$$i_{ds}(t) = \frac{\psi_{dr}^a}{L_m} \left( \frac{4L_r}{R_r} (1-x)(2t-1) + 4(1-x)t^2 - 4(1-x)t + 1 \right)$$

The stator d-axis current loss for optimal can then be expressed by,

$$P_{loss}^{stator-d-axis}(t) = i_{ds}^2 R_s = \left( \frac{\psi_{dr}^a}{L_m} \left( \frac{4L_r}{R_r} (1-x)(2t-1) + 4(1-x)t^2 - 4(1-x)t + 1 \right) \right)^2 R_s$$

$$P_{loss}^{stator-d-axis}(t) = \left( \frac{\psi_{dr}^a}{L_m} (4\tau_r (1-x)(2t-1) + 4(1-x)t^2 - 4(1-x)t + 1) \right)^2 R_s$$

$$P_{loss}^{stator-d-axis}(t) = \left( \frac{\psi_{dr}^a}{L_m} \right)^2 (4\tau_r (1-x)(2t-1) + 4(1-x)t^2 - 4(1-x)t + 1)^2 R_s$$

$$P_{loss}^{stator-d-axis}(t) = \left( \frac{\psi_{dr}^a}{L_m} \right)^2 (4\tau_r (1-x)(2t-1) + 4(1-x)t^2 - 4(1-x)t + 1)^2 R_s$$

Integrating,

$$E_{loss}^{stator-d-axis} = \int_0^1 i_{ds}^2 R_s dt = R_s \left( \frac{\psi_{dr}^a}{L_m} \right)^2 \int_0^1 (4\tau_r (1-x)(2t-1) + 4(1-x)t^2 - 4(1-x)t + 1)^2 dt$$

$$E_{loss}^{stator-d-axis} = R_s \left( \frac{\psi_{dr}^a}{L_m} \right)^2 \left( 16 \frac{\tau_r^2 x^2}{3} - 32 \frac{\tau_r^2 x}{3} + 16 \frac{\tau_r^2}{3} + \frac{8x^2}{15} + \frac{4x}{15} + \frac{1}{5} \right)$$

$$E_{loss}^{stator\_d-axis} = R_s \left( \frac{\psi_{dr}^a}{L_m} \right)^2 \left( \frac{\tau_r^2}{3} (16x^2 - 32x + 16) + \frac{1}{15} (8x^2 + 4x + 2 + 1) \right)$$

$$E_{loss}^{stator\_d-axis} = R_s \left( \frac{\psi_{dr}^a}{L_m} \right)^2 \left( \frac{\tau_r^2}{3} (4x - 4)^2 + \frac{1}{15} (2(4x^2 + 2x + 1) + 1) \right)$$

$$E_{loss}^{stator\_d-axis} = R_s \left( \frac{\psi_{dr}^a}{L_m} \right)^2 \left( \frac{16\tau_r^2}{3} (x-1)^2 + \frac{(2(4x^2 + 2x + 1) + 1)}{15} \right)$$

The stator d-axis loss for Regime I can then be expressed by

$$P_{loss}^{stator\_d-axis}(t) = i_{ds}^2 R_s = \left( \frac{\psi_{dr}^{rated}}{L_m} \right)^2 R_s$$

Integrating,

$$E_{loss}^{stator\_d-axis}(t) = \int_0^1 i_{qs}^2 R_s dt = \left( \frac{\psi_{dr}^{rated}}{L_m} \right)^2 R_s |t|_0^1 = \left( \frac{\psi_{dr}^{rated}}{L_m} \right)^2 R_s$$

Rotor d-axis loss for optimal,

$$P_{loss}^{rotor\_d-axis}(t) = \frac{R_r}{L_r^2} (\psi_{dr}(t) - L_m i_{ds}(t))^2 \quad (6.3.2)$$

We know that,

$$i_{ds}(t) = \frac{\psi_{dr}^a}{L_m} \left( \frac{4L_r}{R_r} (1-x)(2t-1) + 4(1-x)t^2 - 4(1-x)t + 1 \right)$$

Hence,

$$P_{loss}^{rotor\_d-axis}(t) = \frac{R_r}{L_r^2} \left( \psi_{dr}^a (4(1-x)t^2 - 4(1-x)t + 1) - L_m \frac{\psi_{dr}^a}{L_m} \left( \frac{4L_r}{R_r} (1-x)(2t-1) + 4(1-x)t^2 - 4(1-x)t + 1 \right) \right)^2$$

$$P_{loss}^{rotor\_d-axis}(t) = \frac{R_r (\psi_{dr}^a)^2}{L_r^2} \left( 4(1-x)t^2 - 4(1-x)t + 1 - \frac{4L_r}{R_r} (1-x)(2t-1) - 4(1-x)t^2 + 4(1-x)t - 1 \right)^2$$

$$\begin{aligned}
&= \frac{R_r (\psi_{dr}^a)^2}{L_r^2} \left( -\frac{4L_r}{R_r} (1-x)(2t-1) \right)^2 = 16 \frac{R_r (\psi_{dr}^a)^2}{L_r^2} \left( \frac{L_r}{R_r} \right)^2 ((1-x)(2t-1))^2 \\
&= 16 \frac{(\psi_{dr}^a)^2}{R_r} ((1-x)(2t-1))^2 = 16 \frac{(\psi_{dr}^a)^2 (1-x)^2}{R_r} (2t-1)^2 \\
&= 16 \frac{(\psi_{dr}^a)^2 (x-1)^2}{R_r} (2t-1)^2
\end{aligned}$$

Integrating,

$$E_{loss}^{rotor-d-axis}(t) = 16 \frac{(\psi_{dr}^a)^2 (1-x)^2}{R_r} \int_0^1 (2t-1)^2 dt = 16 \frac{(\psi_{dr}^a)^2 (1-x)^2}{R_r} \int_0^1 (4t^2 - 4t + 1) dt$$

$$E_{loss}^{rotor-d-axis}(t) = 16 \frac{(\psi_{dr}^a)^2 (1-x)^2}{R_r} \int_0^1 (4t^2 - 4t + 1) dt$$

$$E_{loss}^{rotor-d-axis}(t) = \int_0^1 \frac{R_r}{L_r^2} (\psi_{dr}(t) - L_m i_{ds}(t))^2 dt$$

$$= 16 \frac{(\psi_{dr}^a)^2 (1-x)^2}{R_r} \left| \frac{4t^3}{3} - \frac{4t^2}{2} + t \right|_0^1 = 16 \frac{(\psi_{dr}^a)^2 (1-x)^2}{R_r} \left( \frac{4}{3} - \frac{4}{2} + 1 \right)$$

$$= 16 \frac{(\psi_{dr}^a)^2 (1-x)^2}{R_r} \left( \frac{8-12+6}{6} \right) = 16 \frac{(\psi_{dr}^a)^2 (1-x)^2}{R_r} \left( \frac{2}{6} \right) = \left( \frac{16}{3} \right) \frac{(\psi_{dr}^a)^2 (1-x)^2}{R_r}$$

$$E_{loss}^{rotor-d-axis}(t) = \left( \frac{16}{3} \right) \frac{(\psi_{dr}^a)^2 (x-1)^2}{R_r}$$

In case of Regime 1,

$$\frac{d\omega_r}{dt} = K_1 i_{qs}^a \psi_{dr}^a = C$$

$$\omega_r = K_1 i_{qs}^a \psi_{dr}^a t$$

$$S_1 = \int_0^1 K_1 i_{qs}^a \psi_{dr}^a t dt = K_1 i_{qs}^a \psi_{dr}^a \left| \frac{t^2}{2} \right|_0^1 = \frac{K_1 i_{qs}^a \psi_{dr}^a}{2}$$

Also,

$$i_{qs}^a = \frac{C}{K_1 \psi_{dr}^a}$$

For Optimal Trajectory A,

$$i_{qs}(t) = a_2 t^2 + b_2 t + c_2 = -4i_{qs}^m t^2 + 4i_{qs}^m t = 4i_{qs}^m (t - t^2)$$

The state equation for speed can be written as,

$$\frac{d\omega_r}{dt} = K_1 i_{qs}(t) \psi_{dr}(t) = K_1 (4i_{qs}^m (t - t^2)) (\psi_{dr}^a (4(1-x)t^2 - 4(1-x)t + 1))$$

$$\frac{d\omega_r}{dt} = 4i_{qs}^m \psi_{dr}^a K_1 (t - t^2) (4(1-x)t^2 - 4(1-x)t + 1)$$

$$\frac{d\omega_r}{dt} = 4i_{qs}^m \psi_{dr}^a K_1 (t + 4t^2 x - 8t^3 x + 4t^4 x - 5t^2 + 8t^3 - 4t^4)$$

$$\int d\omega_r = 4i_{qs}^m \psi_{dr}^a K_1 \int (t + 4t^2 x - 8t^3 x + 4t^4 x - 5t^2 + 8t^3 - 4t^4) dt$$

$$\omega_r = 4i_{qs}^m \psi_{dr}^a K_1 \left( \left( \frac{4x}{5} - \frac{4}{5} \right) t^5 + (2 - 2x) t^4 + \left( \frac{4}{3} x - \frac{5}{3} \right) t^3 + \frac{t^2}{2} \right)$$

Integrating speed,

$$\int_0^1 \omega_r dt = 4i_{qs}^m \psi_{dr}^a K_1 \int_0^1 \left( \left( \frac{4x}{5} - \frac{4}{5} \right) t^5 + (2 - 2x)t^4 + \left( \frac{4}{3}x - \frac{5}{3} \right) t^3 + \frac{t^2}{2} \right) dt =$$

$$S_2 = \int_0^1 \omega_r dt = 4i_{qs}^m \psi_{dr}^a K_1 \left( \frac{x}{15} + \frac{1}{60} \right)$$

Equating the displacements,

$$S_1 = S_2 = 4i_{qs}^m \psi_{dr}^a K_1 \left( \frac{x}{15} + \frac{1}{60} \right) = \frac{K_1 i_{qs}^a \psi_{dr}^a}{2}$$

$$4i_{qs}^m \left( \frac{x}{15} + \frac{1}{60} \right) = \frac{i_{qs}^a}{2}$$

$$i_{qs}^m \left( \frac{4x+1}{60} \right) = \frac{i_{qs}^a}{8}$$

$$i_{qs}^m = \frac{i_{qs}^a}{8} \left( \frac{60}{4x+1} \right) = \frac{i_{qs}^a}{2} \left( \frac{15}{4x+1} \right) = \left( \frac{7.5}{4x+1} \right) i_{qs}^a$$

Substituting, we can find the expression for optimal q-axis current,

$$i_{qs} = 4i_{qs}^m (t - t^2) = 4 \left( \frac{7.5}{4x+1} \right) i_{qs}^a (t - t^2) = \left( \frac{30}{4x+1} \right) i_{qs}^a (t - t^2)$$

The stator q-axis loss for optimal can then be expressed by

$$P_{loss}^{stator\_q-axis}(t) = i_{qs}^2(t) R_s = \left( \left( \frac{30}{4x+1} \right) i_{qs}^a (t - t^2) \right)^2 R_s$$

Integrating,

$$E_{loss}^{stator-q-axis} = \left( \frac{30i_{qs}^a}{4x+1} \right)^2 R_s \int_0^1 (t-t^2)^2 dt = \left( \frac{30i_{qs}^a}{4x+1} \right)^2 R_s \int_0^1 (t^2 + t^4 - 2t^3) dt$$

$$E_{loss}^{stator-q-axis} = \left( \frac{30i_{qs}^a}{4x+1} \right)^2 R_s \left| \frac{t^3}{3} + \frac{t^5}{5} - \frac{2t^4}{4} \right|_0^1 = \left( \frac{30i_{qs}^a}{4x+1} \right)^2 R_s \left| \frac{10t^3 + 6t^5 - 15t^4}{30} \right|_0^1$$

$$E_{loss}^{stator-q-axis} = \left( \frac{30i_{qs}^a}{4x+1} \right)^2 R_s \frac{1}{30} = \frac{30}{(4x+1)^2} (i_{qs}^a)^2 R_s = \frac{30}{(4x+1)^2} \left( \frac{C}{K_1 \psi_{dr}^a} \right)^2 R_s$$

For q-axis component of rotor losses,

$$P_{loss}^{rotor-q-axis}(t) = \frac{R_r}{L_r^2} (L_m^2 i_{qs}^2(t)) = \frac{R_r L_m^2}{L_r^2} \left( \left( \frac{30}{4x+1} \right) i_{qs}^a (t-t^2) \right)^2$$

$$P_{loss}^{rotor-q-axis}(t) = \frac{R_r L_m^2}{L_r^2} \left( \left( \frac{30}{4x+1} \right) i_{qs}^a \right)^2 (t-t^2)^2$$

Integrating,

$$E_{loss}^{rotor-q-axis}(t) = \frac{R_r L_m^2}{L_r^2} \left( \left( \frac{30}{4x+1} \right) i_{qs}^a \right)^2 \int_0^1 (t-t^2)^2 dt$$

$$E_{loss}^{rotor-q-axis}(t) = \frac{R_r L_m^2}{L_r^2} \left( \left( \frac{30}{4x+1} \right) i_{qs}^a \right)^2 \left( \frac{1}{30} \right) = \frac{30}{(4x+1)^2} \frac{R_r L_m^2}{L_r^2} (i_{qs}^a)^2$$

$$E_{loss}^{rotor-q-axis}(t) = \frac{30}{(4x+1)^2} \frac{R_r L_m^2}{L_r^2} \left( \frac{C}{K_1 \psi_{dr}^a} \right)^2$$

For Optimal Trajectory B,

$$i_{qs}(t) = c_3 = i_{qs}^b$$

$$\frac{d\omega_r}{dt} = K_1 i_{qs}^b \psi_{dr}(t) = C$$

$$\omega_r = Ct$$

$$S_1 = \frac{C}{2}$$

$$\omega_r = K_1 i_{qs}^b \int \psi_{dr}(t) dt = K_1 i_{qs}^b \psi_{dr}^a \int (4(1-x)t^2 - 4(1-x)t + 1) dt$$

$$\omega_r = K_1 i_{qs}^b \psi_{dr}^a \left( \frac{4(1-x)t^3}{3} - \frac{4(1-x)t^2}{2} + t \right)$$

$$S_3 = \int_0^1 \omega_r dt = K_1 i_{qs}^b \psi_{dr}^a \left[ \frac{4(1-x)t^4}{12} - \frac{2(1-x)t^3}{3} + \frac{t^2}{2} \right]_0^1$$

$$S_3 = K_1 i_{qs}^b \psi_{dr}^a \left( \frac{(1-x)}{3} - \frac{2(1-x)}{3} + \frac{1}{2} \right) = K_1 i_{qs}^b \psi_{dr}^a \left( \frac{-1+x}{3} + \frac{1}{2} \right)$$

$$S_3 = K_1 i_{qs}^b \psi_{dr}^a \left( \frac{2x+1}{6} \right)$$

$$S_1 = S_2 = K_1 i_{qs}^b \psi_{dr}^a \left( \frac{2x+1}{6} \right) = \frac{C}{2}$$

$$i_{qs}^b = \frac{3C}{K_1 \psi_{dr}^a (2x+1)} = \frac{3}{(2x+1)} \left( \frac{C}{K_1 \psi_{dr}^a} \right)$$

The stator q-axis power losses can then be written as,

$$P_{loss}^{stator\_q-axis}(t) = (i_{qs}^b)^2 R_s = \left( \frac{3}{(2x+1)} \left( \frac{C}{K_1 \psi_{dr}^a} \right) \right)^2 R_s$$

Integrating to get energy losses,

$$E_{loss}^{stator\_q-axis}(t) = \int_0^1 (i_{qs}^b)^2 R_s dt = \frac{9}{(2x+1)^2} \left( \frac{C}{K_1 \psi_{dr}^a} \right)^2 R_s$$



APPENDIX VI

Finding optimal  $x$  for trajectory A,

$$\begin{aligned}
 E_{loss}^{total} &= E_{loss}^{stator-d-optA} + E_{loss}^{rotor-d-optA} + E_{loss}^{stator-q-optA} + E_{loss}^{rotor-q-optA} \\
 &= E_1 \left( \frac{16\tau_r^2}{3}(x-1)^2 + \frac{(8x^2+4x+3)}{15} \right) + \left( \frac{16}{3} \right) \frac{(\psi_{dr}^a)^2 (x-1)^2}{R_r} \\
 &\quad + \frac{30}{(4x+1)^2} E_3 + \frac{30}{(4x+1)^2} E_4 \\
 \frac{dE_{loss}^{total}}{dx} &= E_1 \left( \frac{16x}{15} + \frac{16\tau_r^2(2x-2)}{3} + \frac{4}{15} \right) + \left( \frac{16}{3} \right) \frac{2(\psi_{dr}^a)^2 (x-1)}{R_r} \\
 &\quad + \frac{-240}{(4x+1)^3} (E_3 + E_4) = 0 \\
 \frac{d^2 E_{loss}^{total}}{dx^2} &= E_1 \left( \frac{16}{15} + \frac{32\tau_r^2}{3} + \frac{4}{15} \right) + \left( \frac{16}{3} \right) \frac{2(\psi_{dr}^a)^2}{R_r} \\
 &\quad + \frac{2880}{(4x+1)^4} (E_3 + E_4) = 0
 \end{aligned}$$

Finding optimal  $x$  for trajectory B,

$$\begin{aligned}
 E_{loss}^{total} &= E_{loss}^{stator-d-optB} + E_{loss}^{rotor-d-optB} + E_{loss}^{stator-q-optB} + E_{loss}^{rotor-q-optB} \\
 E_{loss}^{total} &= E_1 \left( \frac{16\tau_r^2}{3}(x-1)^2 + \frac{(8x^2+4x+3)}{15} \right) + \left( \frac{16}{3} \right) \frac{(\psi_{dr}^a)^2 (x-1)^2}{R_r} \\
 &\quad + \frac{9}{(2x+1)^2} E_3 + \frac{9}{(2x+1)^2} E_4
 \end{aligned}$$

$$\frac{dE_{loss}^{total}}{dx} = E_1 \left( \frac{16x}{15} + \frac{16\tau_r^2(2x-2)}{3} + \frac{4}{15} \right) + \left( \frac{16}{3} \right) \frac{2(\psi_{dr}^a)^2(x-1)}{R_r}$$

$$- \frac{36}{(2x+1)^3} (E_3 + E_4) = 0$$

$$\frac{d^2 E_{loss}^{total}}{dx^2} = E_1 \left( \frac{16}{15} + \frac{32\tau_r^2}{3} + \frac{4}{15} \right) + \left( \frac{16}{3} \right) \frac{2(\psi_{dr}^a)^2}{R_r}$$

$$+ \frac{216}{(4x+1)^4} (E_3 + E_4) = 0$$